# Using pH to Understand Species-Specific Coccolithophore Dynamics: A Multi-Disciplinary Approach

Nishant Chauhan

St. John's College
University of Oxford

**APRIL 18, 2024**

A thesis submitted for the degree of
*Doctor of Philosophy*

## Declaration

I hereby declare that all work presented in this thesis is my own and has been conducted over the course of the past four years (2020-2024). Any contribution by other individuals has been explicitly stated and all information derived from other publications are referenced where due.

**Chapter 1:** Nishant Chauhan and Rosalind Rickaby conceived the study. Nishant Chauhan conducted the culture experiments, and sample preparations. Sample analyses were conducted with the help of Dr Christopher Day (Department of Earth Sciences, University of Oxford) and Dr Bastian Hambach (Department of Earth Sciences, University of Southampton). Nishant Chauhan and Rosalind Rickaby conducted data analysis and Nishant Chauhan wrote the chapter with guidance from Rosalind Rickaby. This chapter is published as an article in Geochimica et Cosmochimica Acta (Volume 373, 15 May 2024, Pages 35-51).

**Chapter 2:** Nishant Chauhan, Craig J. Dedman (Department of Earth Sciences, University of Oxford) and Rosalind Rickaby conceived the study. Nishant Chauhan conducted the culture experiments, and sample preparations. Sample analyses were conducted by the Metabolomics and Proteomics Facility (Baldreki C., Dowle A. A., Larson T. R.) at the University of York. Nishant Chauhan and Craig J. Dedman conducted the data analysis and Nishant Chauhan wrote the chapter with guidance from Craig J. Dedman and Rosalind Rickaby. This chapter has been published as a research article in Marine Pollution Bulletin.

**Chapter 3:** Nishant Chauhan and Rosalind Rickaby conceived the study. Nishant Chauhan conducted the culture experiments, and sample preparations. Sample analyses were conducted with by Nishant Chauhan, with part of the analysis done with the help of Dr Christopher Day (Department of Earth Sciences, University of Oxford) and Dr Bastian Hambach (Department of Earth Sciences, University of Southampton). Nishant Chauhan and Rosalind Rickaby conducted data analysis and Nishant Chauhan wrote the chapter with guidance from Rosalind Rickaby.

**Acknowledgements**

I would like to take this opportunity to express my heartfelt gratitude to all those who have supported and guided me throughout this journey. First and foremost, I am profoundly grateful to Ros for her unwavering support, insightful feedback, and willingness to engage in discussions about ideas and outcomes. Thank you for granting me the freedom to develop my own project and for encouraging me to explore new techniques. While I may not have always been the perfect graduate student, I hope that I have contributed, even in a small way, to your intellectual growth as much as you have to mine.

To Renee, I extend my heartfelt appreciation for being an open and easy-going supervisor. Thank you for imparting new knowledge and skills; I have always been eager to learn, and your guidance has been invaluable. Although the polysaccharide work didn't make it into the thesis, I remain confident that the data will eventually yield something valuable. I am grateful to Chris Day, Luke Williams, and Steve Wyatt for their support during my DPhil. Heather, your unwavering support throughout my DPhil journey has meant the world to me. I am thankful to St. John's College, my time spent at the college has been memorable, and I will always treasure it. Special thanks to Samuel Barton and Craig Dedman for your guidance. Your mentorship has been invaluable to me, and I am forever grateful.

To Toby, William, and Tom, thank you for your friendship and our memorable jam sessions. Every moment spent together has been a joy. To my mom, Anjali, and my brother Shashwat, your love and support have been my pillars of strength. My sincerest thanks to my late grandfather, Mr. M.P. Singh. You have been my role model, and your dedication to your work and love for family have shaped me profoundly. Though you couldn't witness my graduation, your influence remains indelible.

Lastly, to Laura, thank you for rescuing me from chaos and helping me navigate through the completion of my thesis. Your unwavering support during my struggles, whether it was about isotopes or polysaccharides, has been a source of immense comfort. Thank you for accompanying me on this journey, for helping me unwind, and for sharing beautiful moments together. I look forward to many more adventures with you.

**Abstract**

Coccolithophores are fascinating organisms that play crucial roles in marine ecosystems. Their interaction with carbonate chemistry has garnered considerable attention because they act as marine calcifiers and have an impact on primary production. Changes in carbonate chemistry affect $CO_2$ availability for photosynthesis and influence coccolithophore physiology and biochemistry through pH. Moreover, alterations in carbonate chemistry impact calcium carbonate saturation states, thus affecting calcification. This thesis aims to understand species-specific responses through the multifaceted effects of carbonate chemistry. It explores how pH influences molecular processes and how these translate into global impacts through biogeochemical changes. Dilute batch cultures are used to demonstrate how shifts in carbonate chemistry affect the carbon and oxygen isotopic composition of coccolith calcite and organic matter. Additionally, isotopic fractionation is used to understand carbon residence times in the internal carbon pools of coccolithophore species. Proteomic analyses shed light on the cellular mechanisms driving physiological changes in coccolithophores, revealing variations among species from different ecological and geological backgrounds. Moreover, coccolithophore physiology under changing carbonate chemistry is compared to investigate potential impacts on major nutrient cycles. Among all scenarios, *Chrysotila carterae* shows the more unique responses, perhaps due to its characteristic cell biology and habitat. *Coccolithus braarudii* emerges as the most sensitive species among those studied, with pH changes drastically affecting cellular processes and inducing carbon limitation under low $CO_2$ conditions. Stable isotopes of *Gephyrocapsa huxleyi* indicate significant isotopic disequilibrium due to large carbon fluxes in and out of the cell, driven by its high surface area to volume ratio. However, the high adaptability of cellular processes in *G. huxleyi* enables it to acclimate to pH changes, reflected in minor variations in its elemental stoichiometry. This research highlights species-specific responses to changing seawater pH and sets an example for increasing diversity in future coccolithophore research.

# Contents

# Introduction

## The Marine Carbon Cycle

The marine carbon cycle plays a crucial role in the ocean's ecosystem and has significant implications for Earth's climate through its interaction with atmospheric carbon dioxide ($CO_2$; Falkowski et al., 2000). Excluding the relatively stable lithospheric carbon reserves, the ocean stands as the largest carbon reservoir within the atmosphere-terrestrial biosphere-ocean system, holding more than 60 times the amount of carbon compared to the atmosphere before industrialisation (Tanhua *et al.*, 2013). This vast reservoir, with its intricate internal processes, largely influences the concentration of atmospheric $CO_2$ over extended periods (Crowley, 2000; Pagani, 2002). In the last million years, the concentration of carbon in the form of carbon dioxide in the atmosphere has influenced positive feedback mechanisms that have manifested as large-scale climatic changes in the form of glacial-interglacial cycles (Petit *et al.*, 1999). The ocean is a major reservoir of carbon, containing dissolved inorganic carbon (DIC), which includes carbon dioxide ($CO_2$), bicarbonate ($HCO_3^-$), and carbonate ($CO_3^{2-}$) ions (Zeebe & Wolf-Gladrow, 2001). The distribution of these carbonate species is influenced by factors such as temperature, pressure, and pH. On the contrary, the carbonate system in seawater is a buffer that regulates ocean pH (Dickson *et al.*, 2007).

Even minor alterations in natural components of the marine carbon cycle, such as those induced by human activities like ocean warming, eutrophication, acidification, and deoxygenation, can potentially impact Earth's climate system significantly (Doney *et al.*, 2009). Conversely, the ocean's ability to absorb additional $CO_2$ due to its buffering capacity presents an opportunity to mitigate anthropogenic $CO_2$ emissions (Bach *et al.*, 2019). The absorption of $CO_2$ by seawater initiates a complex chemical system known as the seawater $CO_2$–carbonate system,

responsible for maintaining oceanic pH levels and influencing various chemical, biological, and geological processes (Zeebe & Wolf-Gladrow, 2001).

Processes such as photosynthesis, respiration, and the formation/dissolution of calcium carbonate minerals further influence the marine carbon cycle (Falkowski *et al.*, 2000). For instance, photosynthesis in surface waters leads to $CO_2$ uptake, while remineralisation in deeper layers releases $CO_2$ back into the water (Falkowski *et al.*, 1998). Additionally, the formation and sinking of calcium carbonate shells contribute to the transport of carbon from surface to deep ocean layers (Kwon *et al.*, 2024). The seawater $CO_2$–carbonate system undergoes complex interactions driven by physical, biological, and chemical processes, varying across both spatial and temporal scales (Ridgwell & Zeebe, 2005). These interactions are crucial for understanding the marine carbon cycle's dynamics and its impact on anthropogenic $CO_2$ uptake.

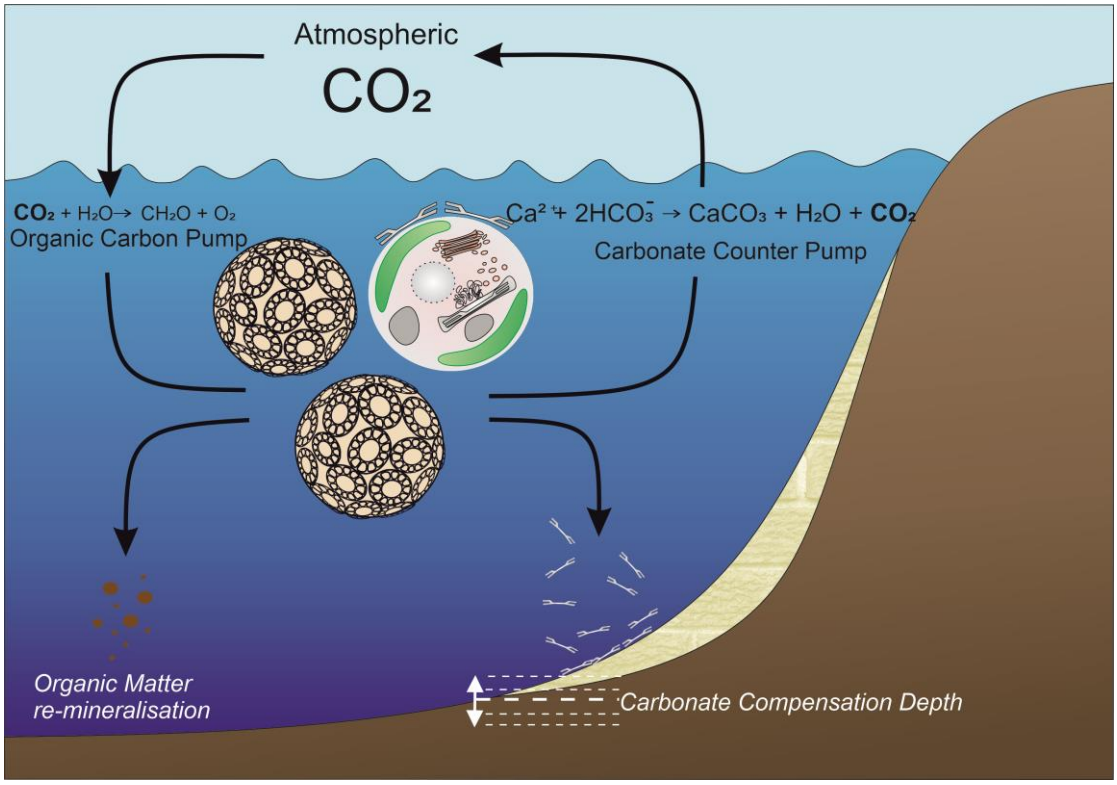


**Figure 1:** The organic carbon pump and the carbonate counter pump, both contributing to the short-term and long-term marine carbon cycle.

The surface ocean is where most of the biological activity occurs, and it interacts directly with the atmosphere, exchanging $CO_2$ (Field *et al.*, 1998). The deep ocean contains the largest pool of DIC, which is transported from the surface via the biological pump and physical processes like thermohaline circulation (Falkowski *et al.*, 2000). The biological pump is a process where carbon is transferred from the surface ocean to the deep sea, primarily through the actions of marine organisms. Photosynthetic organisms, such as phytoplankton, fix carbon from $CO_2$ into organic matter during photosynthesis (Nowicki *et al.*, 2022). When these organisms die, their remains can sink to the ocean floor, effectively sequestering carbon in the deep ocean for extended periods (Tanhua *et al.*, 2013). This process is crucial for regulating atmospheric $CO_2$ levels. Calcifying organisms, such as coccolithophores, play a significant role in the marine carbon cycle (Sheward, 2022). They produce calcium carbonate ($CaCO_3$) structures, which contribute to the ocean's alkalinity and can affect $CO_2$ sequestration. The production, export, and sedimentation of these structures influence the exchange of carbon between the ocean and other reservoirs over various timescales (Rost & Riebesell, 2004a).

**Coccolithophores**

Coccolithophores are single-celled algae belonging to the Haptophyte division of the chromalveolate eukaryotes (Tyrrell & Young, 2009). They secrete calcified scales called “coccoliths” to form their exoskeleton (called a coccosphere) and are one of the most abundant marine phytoplankton groups (Brownlee *et al.*, 2015). Coccolithophores have around 200 extant species in today’s oceans and are known to have occurred since the Triassic period (Bown *et al.*, 2004; Tyrrell & Young, 2009). These small-sized (3 – 40 $\mu$m) organisms live in open ocean environments; they play a key role in the carbonate pump and the ocean carbon cycle (Rost & Riebesell, 2004a).

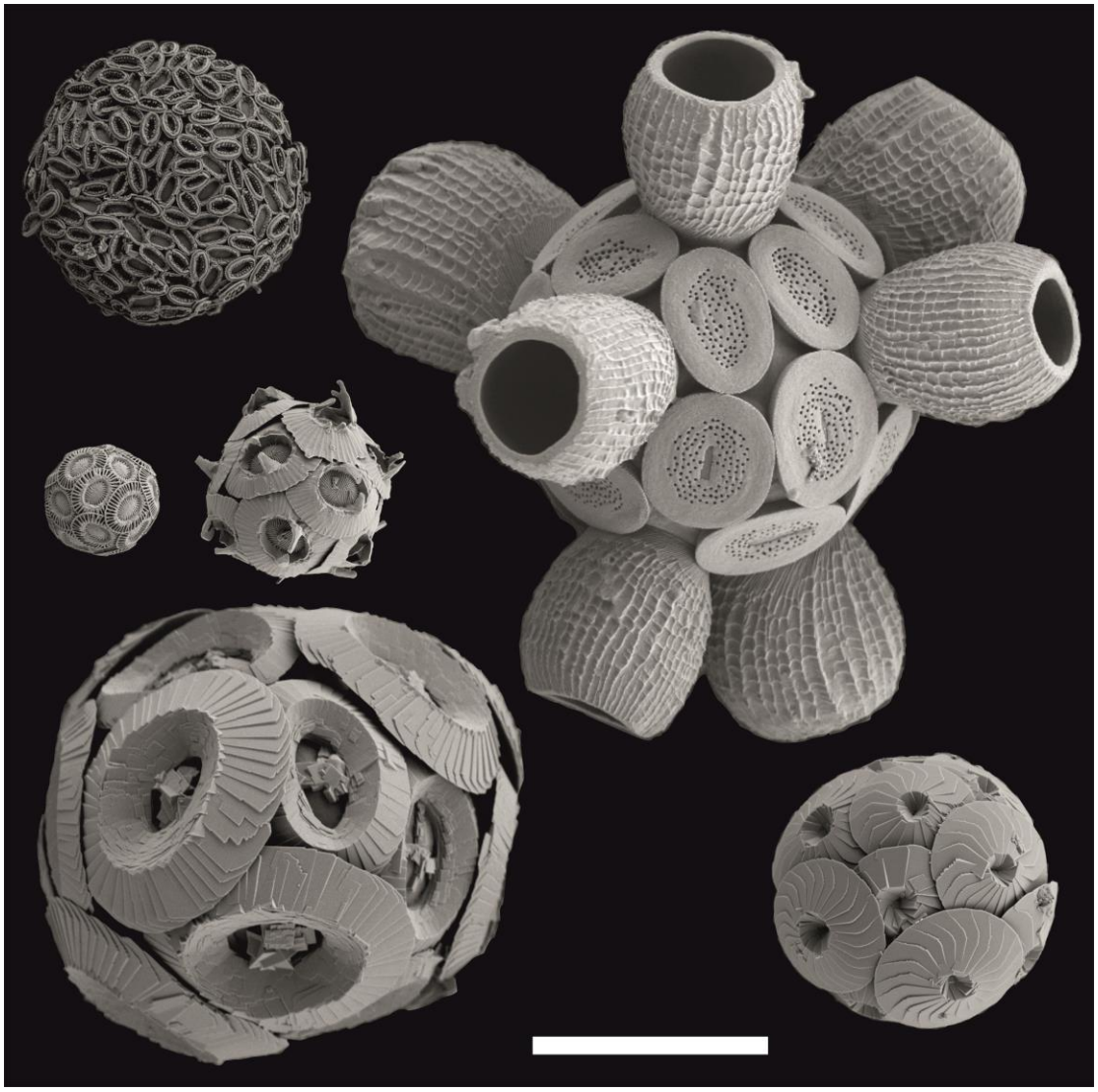

**Figure 2:** Different species of coccolithophores in their diploid stage. The coccoliths that cover the cell in the diploid stage are called heterococcoliths, which show distinct shapes and designs in different species. A prime example is Scyphosphaera apsteinii (top right) that produces two types of coccoliths in its diploid life-cycle stage.

Coccolithophores have two life cycle stages, the diploid (2N) stage, and the haploid (1N) stage, where the N determines the number of chromosome sets (or "ploidy") present inside the cell (De Vries *et al.*, 2021). Cells can divide asexually (mitosis), where one parent cell gives rise to two daughter cells. Additionally, sexual reproduction requires the fusion of two gametes or division of a cell into gametes (via meiosis). Not only can coccolithophores reproduce both sexually and a sexually, but they can also divide asexually in both haploid, and diploid life-cycle

stages. This is called a haplo-diplontic life cycle, which is unique to coccolithophores, and is not reported for diatoms or dinoflagellates (Von Dassow & Montresor, 2011).

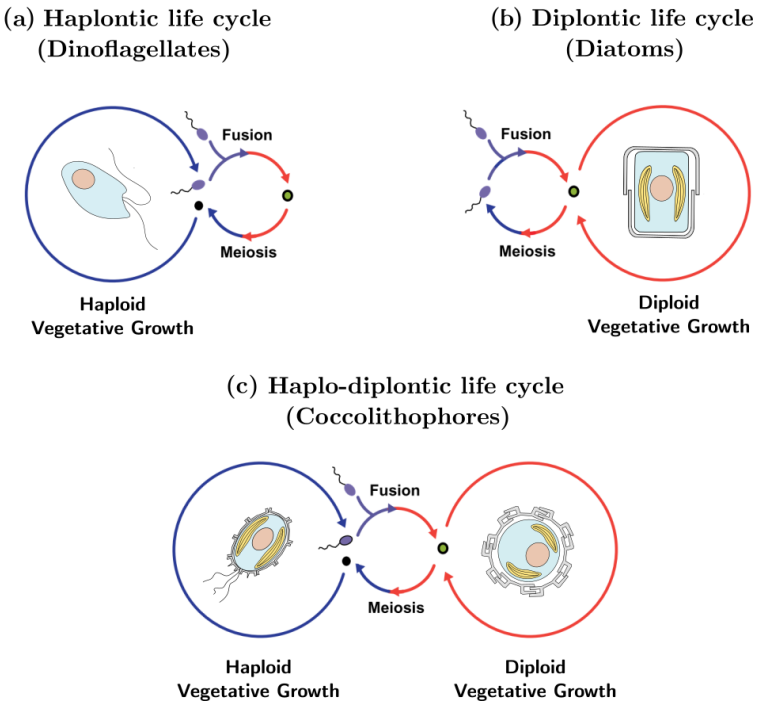


**Figure 3:** The haploid – diploid life-cycle stage in coccolithophores and the interactions between these life-cycle stages. Taken from De Vries et al. (2021).

In some species, even the haploid life-cycle stage bears coccoliths, which are generally simpler in morphology and crystallography. The coccoliths of a haploid life-cycle stage are called holococcolithophores, while those of a diploid life-cycle stage are called heterococcolithophores. Most of the research has focused on the heterococcolith-producing diploid life-cycle stage of coccolithophores (Langer *et al.*, 2006; Rickaby *et al.*, 2016). This may be due to several reasons (Geisen *et al.*, 2002; Billard & Inouye, 2004; Houdan *et al.*, 2006; Cros & Estrada, 2013; De Vries *et al.*, 2021; Ben-Joseph *et al.*, 2023): (1) Heterococcoliths are generally more complex in design and shape than holococcoliths. Therefore, studying the process of biomineralisation in this stage is scientifically more interesting. (2) Most of coccolithophore taxonomy is focused on heterococcolith-bearing cells, which are

used as biomarkers and palaeoceanography. (3) Heterococcoliths are easier to identify during optical measurements (4) Not all species in diploid life-cycle stage have been correlated with their haploid life-cycle stages.

**Cytological characteristics of the Coccolithophore cell**

The cellular structure of a diploid life-cycle stage coccolithophore consists of typical cellular organelles, such as the nucleus, the endoplasmic reticulum, two chloroplasts, mitochondria, a golgi body, and vacuoles. The chloroplasts contain pyrenoids that is a ubiquitous organelle and is used as a carbon concentrating mechanism for RuBisCO in eukaryotes (He *et al.*, 2023). However, there are several unique components in a coccolithophore. For instance, the calcification mechanism, which is completely intracellular in most coccolithophores, uses an organelle called a coccolith vesicle, which is derived from a golgi body. Calcification, therefore, occurs within the trans-golgi network (Young *et al.*, 1999). Several coccolithophore species possess flagella, mostly in their haploid life-cycle stage.

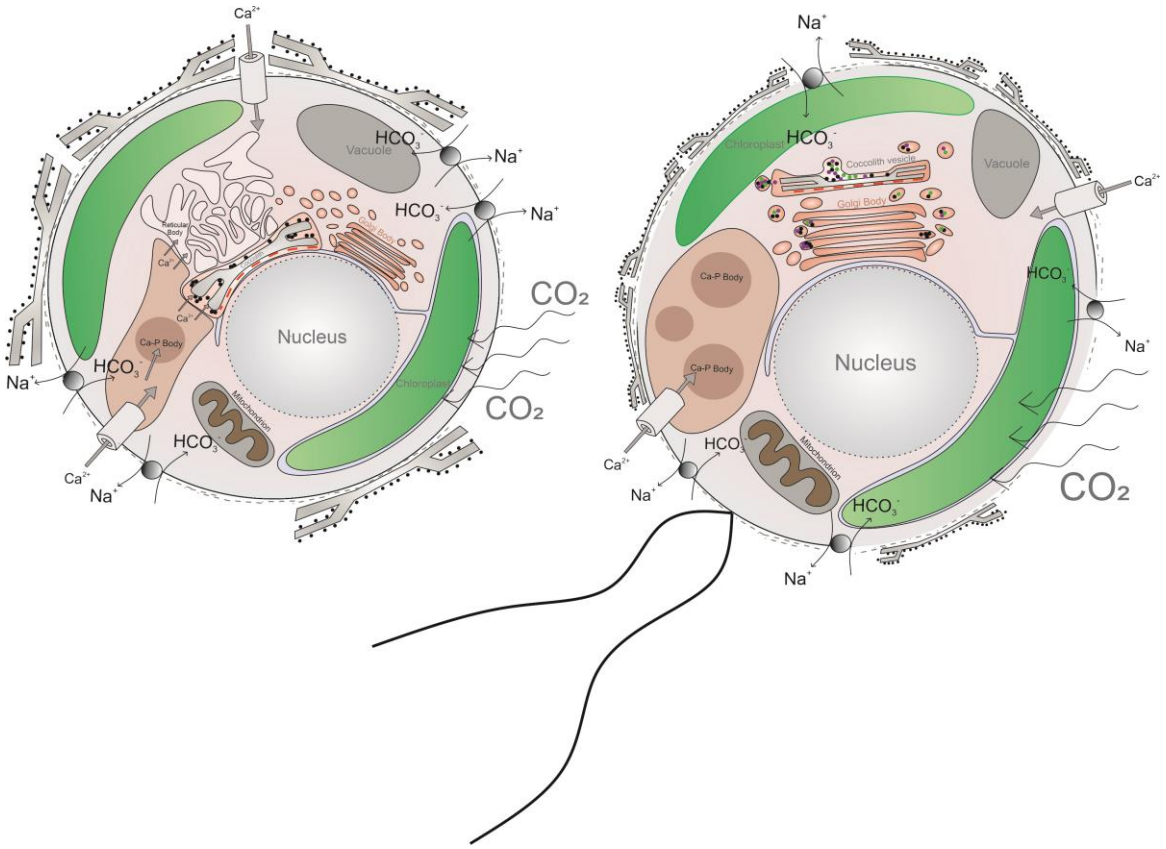


**Figure 4:** Schematic of a coccolithophore cell showing various cellular components in the cell. Most organelles such as the chloroplast, mitochondrion, nucleus, endoplasmic reticulum, and vacuoles are conserved within eukaryotes, and are seen in coccolithophores as well. However, there are several features that are unique to coccolithophores (e.g., coccoliths) and some features that are characteristic of certain species, e.g., flagella. On the left-hand side is a characteristic cell of G. huxleyi, where coccolith calcification takes place right next to the nucleus, where the gap between the CV and the nucleus is called the nuclear envelope. The reticular body is thought to be involved in the transfer of calcium and other ions to the CV, however, the specific role of this organelle is not known. The Ca-P body can be situated adjacent to the CV and is thought to supply Ca to the CV for calcification. On the right is a typical C. carterae cell, where two flagella protrude out of the cell, which can be seen via optical microscopy. This species contains 3 CAPs that are thought to be involved in calcification at various stages of coccolith formation. Moreover, the CV is not situated next to the nucleus in this species and is present within the trans-golgi network as a cisterna.

Coccolithophores typically possess two chloroplasts containing chlorophylls a and c. Presence of a single chloroplast has been observed only in certain holococcolithophores (Billard & Inouye, 2004). The chloroplast typically features thylakoids arranged in stacks of three and often lacks a girdle lamella. It is enveloped by four membranes, with two representing the chloroplast endoplasmic reticulum (Lenning *et al.*, 2004). These additional membranes likely

signify the secondary origin of haptophyte plastids in the endosymbiotic hypothesis of plastid evolution (Whatley & Whatley, 1981). The outer membrane of the nuclear envelope seamlessly connects with the chloroplast endoplasmic reticulum. In coccolithophores, including other haptophytes, chloroplast DNA is dispersed within the stroma (RIS & PLAUT, 1962). Previous investigations into *Ochrosphaera neapolitana* have revealed a significantly larger plastid genome size compared to other chlorophyll a and c-containing algae (Sáez *et al.*, 2001).

Each chloroplast consistently contains a pyrenoid, with distinct characteristics within families (van der Wal *et al.*, 1985). While most coccolithophores are photosynthetic, weakly calcified coccolithophores from the *Papposphaeraceae* family that dwell in the polar region are heterotrophic organisms featuring long, apparently coiling haptonema (Thomasen *et al.*, 2015). These organisms lack chloroplasts and have been verified as such using epifluorescence microscopy. Phagotrophy has been frequently documented in non-mineralized haptophytes with plastids, such as *Chrysochromulina* and *Prymnesium* (Tillmann, 1998; Koppelle *et al.*, 2022). However, information on phagotrophy in coccolithophores is limited, with some studies reporting evidence for phagotrophy or mixotrophy (Kawachi *et al.*, 1991; Houdan *et al.*, 2006; Godrijan *et al.*, 2020). Further investigation into active phagotrophy (or mixotrophy) in coccolithophores is needed due to its potential ecological significance in the microbial food web.

The flagellar apparatus serves as a complex structure crucial for multiple cellular functions, including mitosis and cytoskeleton formation, and its morphological characteristics are considered evolutionarily conserved (Billard & Inouye, 2004). Two flagellar basal bodies and the haptonematal base are arranged in an absolute configuration, which appears to be universal across Haptophyta. In coccolithophores, detailed studies of the flagellar apparatus have primarily

focused on members of the *Pleurochrysidaceae* and *Hymenomonadaceae* families (Green & Hori, 1986; Kawachi & Inouye, 1994). The haptonema, a unique organelle found solely in haptophytes, serves various functions, including substrate adherence, coiling, and uncoiling, and prey capture, notably observed in certain *Chrysochromulina* species (Kawachi *et al.*, 1991). In coccolithophores, the haptonema's structure has been studied in limited genera. Unlike in *Chrysochromulina*, the haptonema's role in substrate adherence is less pronounced in coccolithophores, primarily functioning as an obstacle-sensing device (Billard & Inouye, 2004; Houdan *et al.*, 2006). Reduced or vestigial haptonemas are common in many coccolithophore groups, indicating their lesser importance compared to other prymnesiophytes (Manton & Peterfi, 1969).

**Calcification in Coccolithophores**

The cellular structure relating to calcification has been extensively studied in various species of coccolithophores, notably *G. huxleyi*, *Coccolithus pelagicus*, and *C. carterae* (Manton & Peterfi, 1969; van der Wal *et al.*, 1985; Marsh, 1994). *G. huxleyi* is representative of species producing intricate heterococcolith crystals within intracellular compartments (Young *et al.*, 1999), often dominating modern coccolith populations globally (Tyrrell & Merico, 2004). The process of intracellular coccolith production necessitates significant and sustained influxes of calcium ions ($Ca^{2+}$) and inorganic carbon (DIC) from the external environment into the Golgi-derived calcifying compartment enclosed by membranes, known as the coccolith vesicle (CV). Some species, such as *Coccolithus pelagicus*, produce either heterococcoliths or simpler holococcolith calcite crystals at distinct stages of their life cycle (Ben-Joseph *et al.*, 2023). Although there was speculation that holococcolith production took place on the cell's external surface, more recent studies have now confirmed their calcification in the intracellular space, similar

to heterococcolithophores (Ben-Joseph *et al.*, 2023). The ensuing discussions primarily address the internal production of heterococcoliths.

### *Golgi Apparatus*

The Golgi apparatus forms and secretes the membrane components of a cell. The Golgi-apparatus and trans-Golgi network (TGN) in coccolithophores has some characteristics similar to those of animal cells (Hawkins & Lee, 2001). The stacked membranes (or cisternae) of the TGN are called dictyosome. However, the Golgi body of Prymnesiophytes have a unique feature that the central region of the dictyosome is larger and a dense material is present within these larger regions (Brown *et al.*, 1970). The heterococcoliths and body scales are formed in Golgi-derived vesicles and Golgi apparatus, respectively. The Golgi apparatus is oriented within the cells in a way that the distal (or basal) cisterna faces the cell wall, whereas the proximal cisterna faces the nucleus. (Brown, 1969) discussed the wall-forming functionality of the Golgi apparatus in *Pleurochrysis scherffelii*, which also produces body scales during the haploid phase. They suggested a cisternal progression model for base plate formation (Brown, 1969; Brown *et al.*, 1970). The dilated central region of cisterna function as the "polymerization centre" for cellulosic radial microfibrils (Brown *et al.*, 1973). However, (Hawkins & Lee, 2001) suggested that the cisternal progression model is not valid in the case of body scale formation in *Pleurochrysis*, and the entire basal cisterna does not separate from the Golgi during exocytosis. They argued that fragments of the basal cisterna of the trans-Golgi network gets abstracted into a prosecretory vesicle containing the body scale, which mature into secretory vesicles and fuse to the plasma membrane during exocytosis of scales. They also suggested the involvement of a "Bottlebrush-shaped" macromolecule in scale formation. The hypothesised process of forming body scales is as follows (Hawkins & Lee, 2001): "Bottlebrush-

shaped" macromolecules are first formed in the inner side of (electron-dense) dilations of the cisternae. When the bottlebrush-shaped molecules are fully formed, they get disconnected from the cisternal membrane and polymerise into electron-dense core with branching fibrils. These branching fibrils then nucleate into a fibrillar dilation, which detach from the cisternal inner membrane and form a scale. The cisterna now transforms into a prosecretory vesicle.

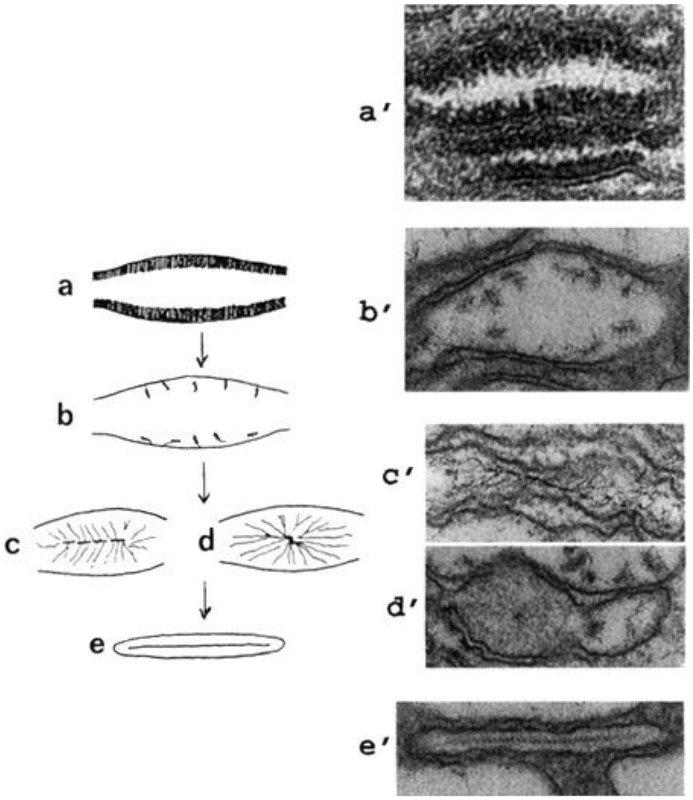


**Figure 5:** A schematic (left) and TEM sections of a coccolithophore cell showing the formation of organic scales and/or base plates within the golgi network. Taken from *(Hawkins & Lee, 2001)*

### Organic Base Plates

### Physical Structure

Calcite nucleates at the rim of organic base plates with the help of organic molecules (polysaccharides and proteins), and the calcite crystals grow in specific directions giving rise to a complex, biologically precipitated coccolith. The base plates are made of pectic polysaccharides and have distinct surficial patterns with

a radial ornamentation on the proximal (bottom) side and discontinuous concentrically-curved ornamentations on the distal (top) side (Pienaar, 1971). This fibrillar material is made of cellulose and form inside the Golgi apparatus (Brown, 1969). (Marzec *et al.*, 2019) used cryoTEM and cryoET microscopy on *C. carterae* base plates to show that they are composed of three layers. The bottom-most layer, which is visible at the "bottom" side is made up of radial fibres, extending to the margin. (Brown *et al.*, 1970) suggested that the organic scales might be interconnected to each other through these outward-extending radial fibrils. The second layer is made of concentric fibres, however, does not extend to the margin. This layer is placed on top of the radial fibres of the bottom layer. The third layer, or that on "top" is composed of disordered, fine fibres in the centre and a 100nm-wide rim made up of globular material. The calcite crystals have been previously shown to nucleate on the base plate rim (Walker *et al.*, 2020).

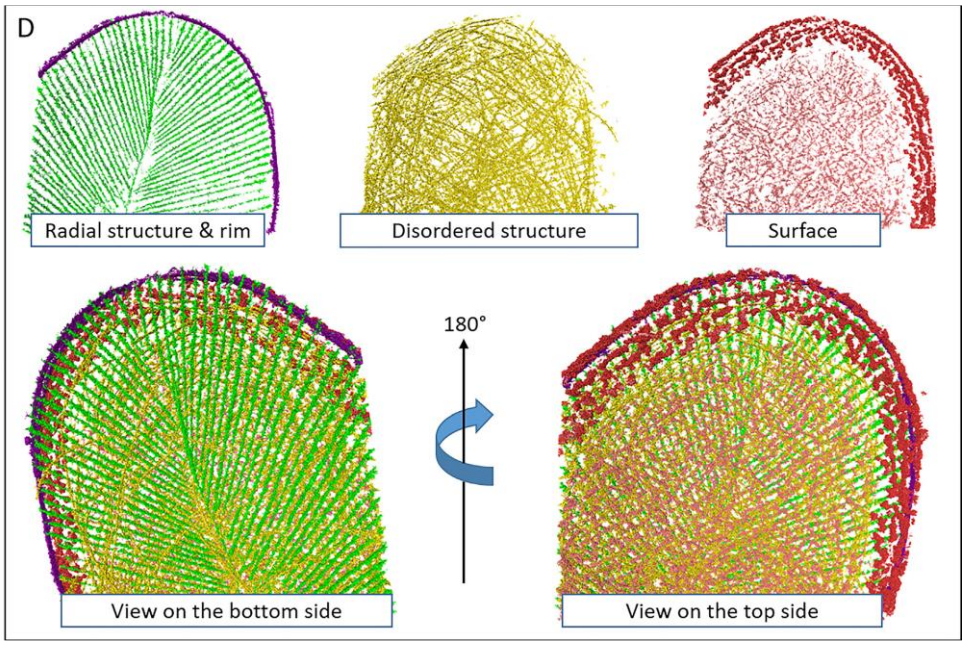


**Figure 6:** A schematic showing the morphology and physical characteristics of an organic base plate from a coccolithophore species. This organic base plate forms a template for calcification within the CV, and calcite is precipitated, initially as a

protococcolith ring on the periphery of the base plate with the help of CAPs. Taken from Marzec et al. (2019).

**Chemical Nature**

The rim of the base plate has been shown to have positive charges, due to the presence of primary amines (Marzec *et al.*, 2019). These potentially attract the negatively charged $Ca^{2+}$-bound polysaccharides during the nucleation (Marzec *et al.*, 2019). In vitro crystal nucleation experiments involving *C. carterae* base plates showed that Ca rich aggregates (organic molecules) precipitate on the top side of the base plate rims only in the presence of both polysaccharides (soluble and insoluble) and $Ca^{2+}$ ions (Gal *et al.*, 2016). (Sakurada *et al.*, 2018) reported comparable results for studies done on *Pleurochrysis haptonemofera* base plates. Experiments involving other ions such as Mg, Sr and Na showed abnormal precipitation (Gal *et al.*, 2016). This suggests a high selectivity for Ca ions by the polysaccharides, and their selectivity towards the base plate rim. Effect of protein-extracted *P. haptonemofera* base plates in the presence of polysaccharides, $Ca^{2+}$ and $CO_3^{2-}$ ions showed no precipitation suggesting a significant role played by unidentified proteins (Sakurada *et al.*, 2018).

**Coccolith Vesicle**

Coccolithophores mineralise their coccoliths intracellularly, within a Golgi-derived body (fig. 1), called the coccolith vesicle (CV). Calcification of a coccolith in the CV is controlled by multiple mechanisms, such as the carbonate chemistry in the CV microenvironment (Brownlee *et al.*, 2015; Lee *et al.*, 2016; Taylor *et al.*, 2017), transport of Ca ions by a membranous organelle called the reticular body (Marsh, 2003) or by Ca-polysaccharide complexes (van der Wal *et al.*, 1983), or calcium channels (Gussone *et al.*, 2006; Mackinder *et al.*, 2010), the spatial constraints from the CV wall (Avrahami *et al.*, 2022, 2023), actin and microtubules in the cytoskeleton (Durak et al., 2017; Langer et al., 2023b), and coccolith associated

polysaccharides (CAPs; (Marsh, 1994; Henriksen & Stipp, 2009; Gal *et al.*, 2016; Lee *et al.*, 2016)). Dense, spherical organic structures, called coccolithosomes have also been reported in *C. carterae* and are thought to carry Ca ions to the CV (van der Wal *et al.*, 1983). The transport of calcium into the CV has also been hypothesized to occur through the calcium-phosphate rich body (Sviben *et al.*, 2016). In this mode of calcium transport, the Ca-P rich body, which is inside a vacuole, is situated directly next to the CV, and transport channels between the Ca-P body and CV move calcium from the Ca-P body to the CV. Although pulse chase experiments have provided evidence towards the movement of calcium from the Ca-P body to the CV (Gal *et al.*, 2017), more recent studies have shown that these vacuoles are present in non-calcifying cells as well, and the size of the Ca-P body does not change during or after calcification (Peled-Zehavi & Gal, 2021).

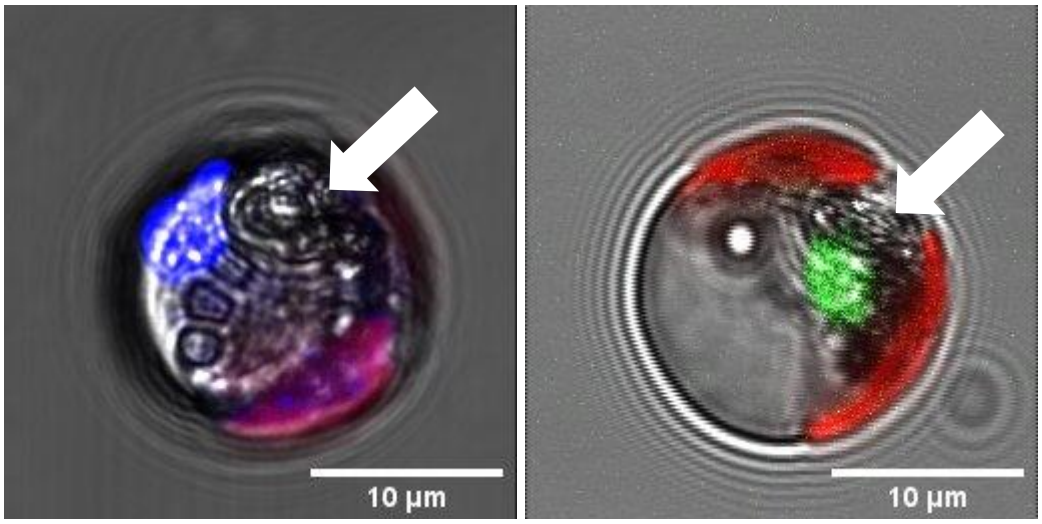


**Figure 7:** A confocal image showing a CA-P rich body stained with DAPI (left; blue) and SNARF (right; green). The association with the coccolith vesicle (white arrows) is clearly observed in both images, providing evidence towards their function in coccolith calcification. Images were obtained during preliminary studies conducted by the author.

The formation of coccolith occurs in the trans-Golgi cisternae, where multiple coccoliths at various stages of formation have been seen within a single cell (van der Wal *et al.*, 1983; Young *et al.*, 1999). Small crystals nucleate at the edge of an organic base plate, forming the protococcolith ring (Young *et al.*, 1999) nucleation

and growth of $CaCO_3$, where the $CaCO_3$ crystals attach to the organic base plate (Gal *et al.*, 2016; Marzec *et al.*, 2019; Walker *et al.*, 2020). CAPs are responsible for regulating the crystal morphology of the coccoliths. They favourably attach to specific surfaces of the calcite crystal and block further growth of that specific crystal face (Henriksen *et al.*, 2004). CAPs are made up of neutral monosaccharides with acidic moieties, sulphate esters and uronic acids (Fichtinger-Schepman *et al.*, 1980). However, they differ in structure as well as chemistry within species thereby affecting the morphology of the coccosphere (Lee *et al.*, 2016). The calcification process within the CV is also governed by the carbonate chemistry conditions within the CV (Giuffre *et al.*, 2013). The uronic acid moieties in CAPs govern the calcification rate within the CV (Fichtinger-Schepman et al., 1981). High uronic acid content in CAPs leads to a high calcite nucleation rate when the saturation state for calcite inside the CV is high. On the other hand, when the calcite saturation state is low, CAPs with a lower uronic acid content encourage faster nucleation rates (Giuffre *et al.*, 2013; Lee *et al.*, 2016). For a more detailed understanding of coccolith biomineralisation, see reviews (Marsh *et al.*, 1992; Marsh, 1996; Young *et al.*, 1999; Brownlee *et al.*, 2021).

**The benefit of calcification in coccolithophores**

Numerous arguments have been made in the past regarding the benefit of having a calcite shell, and most of the arguments are discussed in (Monteiro *et al.*, 2016). Briefly, the most plausible arguments include, (1) enhancing the rate of photosynthesis by supplying the cell with $CO_2$ either directly through carbon uptake, or indirectly via $H^+$ expulsion from the cell. (2) Photosynthetic rate can also be accelerated by concentrating the light falling on to the coccosphere towards the chloroplasts. This could be done by either taking advantage of the optical properties of calcite, or using the complex design of coccolith, or both. (3) The

coccosphere provides protection from high light intensity, which can cause photoinhibition and photodamage. Thus, coccoliths can be used to provide cover from light, or the calcification rate can be increased as a means of energy dissipation. The coccosphere can also protect the cells from UV light. (4) The coccosphere can also be used as protection against viruses and predators.

Another popular hypothesis is that the benefit of calcification in coccolithophores relates to its origin and that coccolithophores started calcifying in order to expel calcium from the cell as high concentration can be toxic (Müller, 2019). Accordingly, coccolithophores could be producing coccoliths as a means of getting rid of extra Ca inside the cell and they have found ways to make use of the coccoliths for more than expelling Ca. Although all of the above arguments have strong points and substantial evidence to support each hypothesis, there have been multiple studies that suggest otherwise. For instance, non-calcifying strains of *G. huxleyi* are able to grow in normal seawater and do not show any signs of calcium toxicity (Paasche, 2001). Furthermore, strains of *C. carterae* and *G. huxleyi* were able to grow in seawater with 0.1 mM Ca without calcification, albeit, at a slightly reduced growth rate. This suggests that photosynthesis is not dependant on carbon provided by calcification, although might still benefit from it, if available (Trimborn *et al.*, 2007; Leonardos *et al.*, 2009; Sviben *et al.*, 2016).

On the other hand, (Trimborn *et al.*, 2007; Sviben *et al.*, 2016) showed that coccolithophores grown in low Ca concentrations (0.1 mM) calcify abnormally, or not at all; and the growth rate is also affected. Even though Ca is thought to be toxic to eukaryotic phytoplankton, at low Ca concentrations, where it is adequate for cellular biochemical purposes, but not enough for calcification to take place, the growth rate is affected. This means that calcification must have a part to play in cell growth. However, as discussed above, this in direct contradiction to studies

that reported no correlation between calcification and photosynthesis.

The argument that suggests that the coccosphere can protect the cell from photodamage contradicts the hypothesis that coccoliths concentrate the light towards the chloroplasts. Moreover, *G. huxleyi* is a dominant calcifying species in the modern ocean, but is not photo-inhibited when calcifying, even at 1600 $\mu$mols $m^{-1}s^{-1}$, however, the non-calcifying haploid *G. huxleyi* did suffer from photoinhibition at 400-500 $\mu$mols $m^{-1}$ $s^{-1}$ (Balch *et al.*, 1992; Nanninga & Tyrrell, 1996). Although these results might suggest that calcification indeed plays a role in protecting the cell from photoinhibition, it is to be noted that this study was performed on a haploid versus a diploid strain. According to (Nanninga & Tyrrell, 1996), calcifying, decalcified, as well as naked *G. huxleyi* cells were resistant to photoinhibition up to at least 1000 $\mu$mols $m^{-1}$ $s^{-1}$. The hypothesis that a calcite shell provides protection against grazers is a plausible one, there has been no conclusive evidence to confirm this (see (Monteiro *et al.*, 2016). This hypothesis also does not justify the complex design of individual coccoliths. Although it is essential to scrutinise each hypothesis individually, it is highly plausible that coccoliths provide multiple benefits to the cell.

**Photosynthesis and Carbon fixation in Coccolithophores**

Coccolithophores are major drivers in the global biogeochemical carbon cycle since they photosynthesise as well as form scales made of calcite. The main $CO_2$-fixing enzyme of the Calvin-Benson-Bassham ($C_3$) cycle is RuBisCO (ribulose 1,5-bisphosphate carboxylase/oxygenase), which functions as a carboxylase to produce 3-phosphoglycerate that gets converted into stable organic compounds. Or as an oxygenase to catalyse oxygenic reactions to give 2-phosphoglycolate. The ratio of carboxylation/oxygenation depends on the respective concentrations of $CO_2$ and $O_2$, and the specificity factor ($\tau$; Berry et al., 2002). This is defined as:

$$\tau = (K_o/K_c)(V_c/V_o)$$

Where $K_o$ and $K_c$ are concentrations of $O_2$ and $CO_2$, respectively, at half-saturated rates of carboxylase activity ($V_c$), and oxygenase activity ($V_o$). The low affinity towards $CO_2$ ($K_m$ of 20-70 µmol $L^{-1}$; Badger et al., 1998), and the low catalytic turnover per active site are the two main catalytic imperfections of RuBisCO. Since the enzyme evolved early in a high $CO_2$ environment, the efficiency of the enzyme has been shown to have gone down considerably due to a global increase in atmospheric $O_2$ levels and a significant decrease in the $CO_2$ levels up to the Holocene.

Organisms have applied various strategies to overcome the catalytic inefficiency of RuBisCO (Badger *et al.*, 1998). Some organisms have improved catalytic activity through evolution. The specificity factor, τ, has evolved to a higher affinity towards $CO_2$ over geological time, as a response to decreasing $CO_2$ concentrations (Tortell, 2000). Therefore, RuBisCO varies phylogenetically in structure and efficiency and therefore, has been divided into subfamilies. RuBisCO in coccolithophores classifies under the subform ID (Lenning *et al.*, 2004). τ for coccolithophores falls somewhere between the more recent diatoms and the more ancient green algae. Moreover, an inverse relation between τ and the measured ratio of internal to external $C_i$ has been found (Tortell, 2000).

The other tactic has been to supply RuBisCO with considerable amounts of $CO_2$ substrate by adapting carbon concentrating mechanisms (CCMs). The dominating carbonate species among $CO_2$, $HCO_3^-$, and $CO_3^{2-}$ depends on the seawater pH and concentration of DIC. It also depends on the temperature and salinity of the seawater but to a lesser extent. In the modern ocean, the dominant carbonate species is $HCO_3^-$ while the primary substrate for RuBisCO is $CO_2$ (Badger *et al.*, 1998; Zeebe & Wolf-Gladrow, 2001). The diffusive supply of $CO_2$ is insufficient to

meet the demands required by photosynthesis. Therefore, the cell also utilizes $HCO_3^-$ as a carbon source for photosynthesis and calcification (Paasche, 1964; Sikes *et al.*, 1980; Nimer & Merrett, 1992; Buitenhuis *et al.*, 1999). The algae use internal (pyrenoid) and/or external carbonic anhydrase (CA) to increase the amount of $CO_2$ substrate available to the cell. CA is an enzyme that catalyses the conversion of $HCO_3^-$ into $CO_2$ (Nimer *et al.*, 1994b). An internal CA, or pyrenoid, will catalyse the conversion of $HCO_3^-$ taken up by the algae into $CO_2$ which gets concentrated around the fixation site.

An external CA would convert the $HCO_3^-$ in the surrounding medium into $CO_2$ to be taken up through the plasmalemma (Elzenga *et al.*, 2000). However, there are other lines of evidence-based studies done on diatoms that showed that external CA and $HCO_3^-$ uptake are positively correlated (Rost *et al.*, 2003; Chrachri *et al.*, 2018). Such results have encouraged new thoughts about external CA. A higher $CO_2$ concentration inside the cell can result in higher diffusive $CO_2$ leakage. An external CA could thus reduce the $CO_2$ leakage by converting the $CO_2$ efflux into $HCO_3^-$ which the cell can take up again (Martin & Tortell, 2008; Trimborn *et al.*, 2009; Chrachri *et al.*, 2018). However, compelling evidence is lacking to support this hypothesis, specifically for *G. huxleyi*, which has been reported to have a high $CO_2$ leakage (Rost *et al.*, 2006). Moreover, (Chrachri *et al.*, 2018) reported opposing results and reports that external CA in their studies was not being used for refixing the $CO_2$ efflux.

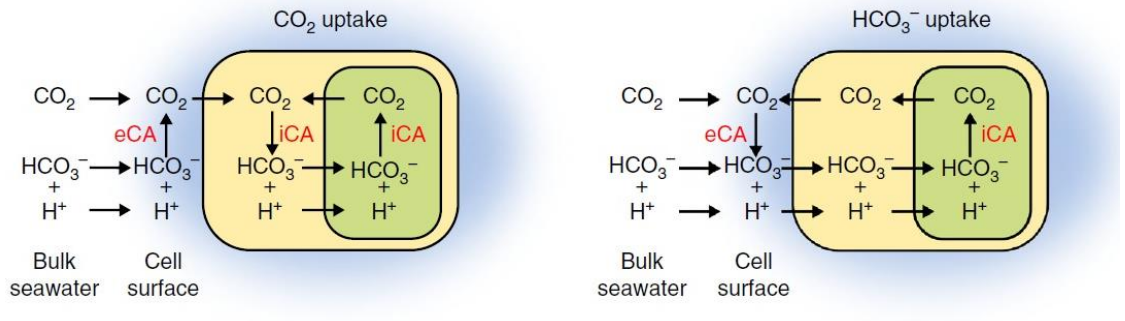

**Figure 8:** Two models for eCA activity based on the carbonate species being taken up by the cell. Taken from Chrachri et al. (2018).

The utilisation of external CA has been shown to vary among species; for instance, many studies suggest that *G. huxleyi* does not show any external EA activity (Sikes & Wheeler, 1982; Sekino & Shiraiwa, 1994; Elzenga *et al.*, 2000; Rost *et al.*, 2003, 2006), while a more recent study by (Stojkovic *et al.*, 2013) suggested that external CA activity in *G. huxleyi* is present and depends on the calcification rate. Lack of external CA would mean that $HCO_3^-$ is the carbon source for calcification rather than CA-catalysed conversion of $HCO_3^-$ into $CO_2$ and its uptake (Sekino & Shiraiwa, 1994; Nimer *et al.*, 1997). The absence of external CA, and therefore, lack of $CO_2$ scavenging could explain the high diffusive $CO_2$ leakage in *G. huxleyi* compared to diatoms, which increases with decreasing ambient $CO_2$ concentration (Rost *et al.*, 2006).

However, some studies show that *G. huxleyi* shows biphasic kinetics with varying DIC concentrations indicating that *G. huxleyi* acquires DIC by at least two mechanisms (Paasche, 1964; Herfort *et al.*, 2002). This would mean that *G. huxleyi* (and potentially other coccolithophore species) can switch from diffusive $CO_2$ uptake to active bicarbonate uptake (or a combination of both) depending on the ambient DIC concentration.

Calcification in coccolithophores is also considered an energy-efficient CCM, apart from other suggested benefits (Monteiro *et al.*, 2016; Müller, 2019), since calcification of coccoliths generates protons, which are suggested to act as a substrate in the conversion of $HCO_3^-$ to $CO_2$ to be used by RuBisCO by the following reaction (Anning *et al.*, 1996; Buitenhuis *et al.*, 1999):

$$2HCO_3^- + Ca^{2+} \rightarrow CaCO_3 + CO_2 + H_2O$$

Alternatively, the $H^+$ produced can be used to balance any cytoplasmic alkalinisation resulting from the use of $HCO_3^-$ for carbon fixation with the help of an internal CA (Nimer *et al.*, 1994b; Berry *et al.*, 2002). Numerous studies have supported the inverse relationship between CCMs and calcification rate in coccolithophores (Nimer *et al.*, 1994a; Herfort *et al.*, 2002; Stojkovic *et al.*, 2013). For calcification to be beneficial for photosynthesis through the uptake of $HCO_3^-$, coccolithophores must (1) use $HCO_3^-$ as their primary carbon species, rather than $CO_2$ or $CO_3^{2-}$, (2) grow better in comparison to non-calcifying cells when $CO_2$ is limiting, (3) show variability in calcification rates with varying $CO_2$ concentrations (Berry *et al.*, 2002).

There have been some studies that support the hypothesis that calcification benefits photosynthesis (Sikes *et al.*, 1980; Anning *et al.*, 1996; Hoppe *et al.*, 2011). (Nimer & Merrett, 1992) reported that calcifying cells grow better than non-calcifying cells at high pH or low $CO_2$ concentrations. (Walker *et al.*, 2018) showed that although there is no evidence of calcification supporting photosynthesis, but disruption in calcification did lead to cell cycle arrest in *C. braarudii*. However, the evidence suggesting that calcification aids photosynthesis is not clear (Herfort *et al.*, 2004; Trimborn *et al.*, 2007; Leonardos *et al.*, 2009; Bach *et al.*, 2013). For instance, species like *G. huxleyi* and *Chrysotila carterae* are able to grow without calcifying coccoliths (Paasche, 2001; Marsh, 2003). Contradictory evidence includes the fact that calcification in most species stops after one layer of coccoliths, or a complete coccosphere is produced to cover the cell surface entirely (Billard & Inouye, 2004). *G. huxleyi* has been reported to stop calcifying but continue photosynthetic carbon fixation under DIC limiting conditions (Mackinder *et al.*, 2010; Bach *et al.*, 2013). This could indicate that photosynthesis and calcification compete for carbon from the $C_i$ pool under DIC-limiting conditions (Bach *et al.*, 2013; Bolton & Stoll, 2013). Alternatively, it could also be

argued that calcification is switched off to preserve the energetic costs involved with calcification and allocate the energy and substrate to photosynthesis.

There have been some reports on the ability of coccolithophores to obtain carbon (and other nutrients) via mixotrophy. Early reports from Houdan et al. (2006) showed that some coccolithophore species could switch to phagotrophy in their haploid life-cycle stage. More recent study from Godrijan et al. (2020) showed evidence of uptake of organic carbon compounds. However, the concentration of organic carbon uptake in their study was significantly lower than standard dissolved organic carbon uptake. While more research is clearly needed to understand mixotrophy in coccolithophores, there is insufficient evidence to consider organic carbon sources as significant.

## The role of carbonate chemistry in Coccolithophore Ecology and Biogeochemistry

Carbonate chemistry plays a key role in the physiology and calcification of coccolithophores in the modern ocean (Riebesell *et al.*, 2000; Bach *et al.*, 2015). Studies in the past have reported contradictory results on the effect of ocean acidification on calcification and growth (Riebesell et al., 2000; Iglesias-Rodriguez et al., 2008b; Beaufort et al., 2011; Hoppe et al., 2011). Species such as *G. huxleyi* and *G. oceanica* showed a reduction in calcification rate with increasing $CO_2$ concentration in some studies (Riebesell *et al.*, 2000; Zondervan *et al.*, 2002; Sciandra *et al.*, 2003; Barcelos E Ramos *et al.*, 2010), while in other studies, they showed an increase in photosynthetic carbon fixation rate and calcification rate (Iglesias-Rodriguez et al., 2008b). A study was done on *Chrysotila carterae* (earlier known as *Pleurochrysis carterae*) reported an increase in net photosynthetic carbon uptake and calcification rates with increasing $CO_2$ concentrations over long incubations compared to short incubations (Casareto *et al.*, 2009). A study using *Calcidiscus*

*leptoporus* showed an optimum growth response of calcification to increasing $CO_2$ concentration, while photosynthetic carbon uptake did not change. On the other hand, *Coccolithus pelagicus* did not show any response to changing $CO_2$ concentrations (Langer *et al.*, 2006).

Contradictory results are reported by (Krug *et al.*, 2011) who reported that *Coccolithus braarudii* showed a decrease in calcification and growth rate with increasing $CO_2$ concentration. Moreover, there are variations within strains of a single species, as reported by (Langer *et al.*, 2009) in *G. huxleyi*, where four different strains responded differently to changing $CO_2$ concentration in their POC and PIC production rates. Such varied responses to different carbonate chemistries have been hypothesised to be a result of adaptation to different carbonate chemistry conditions of different strains in their local environment (at the point of isolation, Rickaby et al., 2016). Moreover, $H^+$-removing capabilities of distinct species from their calcifying vesicle and maintaining a suitable calcium carbonate saturation state may play a role in species-specific sensitivities to changes in pH (Ω; Allison & Finch, 2010; Trotter et al., 2011; Ries, 2011).

According to the substrate-inhibitor concept, calcification is positively correlated with $CO_2$, and $HCO_3^-$, but negatively correlated with $H^+$ (Bach et al., 2011b, 2015). This is important because several experimental studies have reported $HCO_3^-$ as the primary substrate for calcification (Sekino & Shiraiwa, 1994; Nimer *et al.*, 1997; Buitenhuis *et al.*, 1999; Rickaby *et al.*, 2010; Bach *et al.*, 2013), and $CO_2$ as the primary substrate for photosynthesis (Paasche, 1964; Rost et al., 2003; Bach et al., 2011b). However, contradicting evidence arises from isotopic data, where $CO_2$ has been suggested to be the key carbonate species involved in calcification (Hermoso, 2015).

## Thesis Aims and Objectives

Coccolithophores are one of the key phytoplankton groups that contribute significantly to the global carbon cycle (Rost & Riebesell, 2004a). Consequently, tremendous research has focused on understanding the genesis, and function of calcification in coccolithophores (Monteiro *et al.*, 2016; Müller, 2019). Due to their key role in marine biogeochemical cycles, coccolithophore ecology and physiology has received significant attention in the past century (Hay, 2004). However, most of the work has focused on the ubiquitous species *G. huxleyi*, where this species is regarded as a model coccolithophore species (Wheeler *et al.*, 2023). *G. huxleyi* is the only coccolithophore species at this point, which has a complete reference genome (Skeffington *et al.*, 2023). Previous studies have emphasised on the importance of other coccolithophore species, such as *C. braarudii* (Daniels *et al.*, 2016; Kottmeier *et al.*, 2022), however, this has not translated into improved representation of coccolithophore species other than *G. huxleyi* in the research literature.

The discussion in the previous section has shown that our fundamental knowledge about coccolithophore biogeochemistry is incomplete, with limited knowledge of the presence of an internal carbon pool in coccolithophores (Hermoso, 2015), or the mode of carbon uptake in coccolithophores (Herfort *et al.*, 2002). Although calcification has been considered as a key characteristic in determining the importance of Coccolithophores in global biogeochemical cycles, the cellular processes related to calcification are not clear. Recent studies have highlighted the importance of cellular proteins in calcification (Skeffington et al., 2023), the biological importance of calcification in coccolithophores is yet unknown.

Due to the diverse range of culturing conditions that are applied to study the

response of coccolithophore species to changing environmental conditions, it is difficult to compare between studies, as temperature, light and nutrients may dictate the sensitivity of a species to pH and $CO_2$ related changes (Bach *et al.*, 2015). Therefore, a comparative study of coccolithophore species under similar culturing conditions is needed to properly quantify species-specific effects. Although the real-world ecological conditions for different coccolithophore species may differ, due to for example, either a coastal or oligotrophic habitat, establishing physiological responses under constant condition allows for quantitative comparison between species. It has been shown many times that PIC:POC ratios change with changing pH and $CO_2$, but little is known about the cellular processes that are activated/upregulated during stressed conditions in coccolithophores that give rise to these changes. This knowledge is even more depleted in species other than *G. huxleyi*.

Stable isotopes in the coccolith calcite have been shown to change with changing $CO_2$ levels, but there have been discrepancies between studies. The method of carbonate chemistry manipulation, for instance, has been proposed as a reason for the observed differences in responses. Moreover, isotopic studies have primarily focused on the paleoclimatic implications of changing $CO_2$. Whereas isotopes are able to provide an insight into the chemical behaviour of carbon in a given coccolithophore cell. Stable isotopes of both calcite and organic matter have never been utilised together to understand the dynamics of carbon regulation in coccolithophores. Lastly, we lack a holistic understanding of the biological and chemical processes that dictate isotopic, and physiological changes in coccolithophores. With the recent technological advancement in omics, an increasing number of studies are employing this methodology to gain further insights into the molecular mechanisms responsible for the physiological and biogeochemical responses observed on a macro scale. Proteomics enables the

investigation of changes in abundance of specific proteins and can be utilised to study the effects of environmental changes on organismal biology (Tomanek, 2010). Therefore, the key aim of this thesis is to advance our understanding of the chemistry, biology, and physiology of coccolithophores through a comprehensive set of experiments that test a wide range of parameters.

More specifically, this thesis aims to:

1. Understand the dynamics of the internal carbon pool in coccolithophores, and how this translates into coccolith "vital effects" in different coccolithophore species. To understand the dynamics of carbon regulation, this thesis used stable isotopes of carbon and oxygen in the coccolith calcite, along with carbon isotopes in the organic matter.
2. Improve our knowledge of the cellular mechanisms that drive physiological and chemical changes in coccolithophores under environmental change. Investigate the difference in sensitivity to pH stress in different species and to put these findings in an ecological context.
3. Bring together our understanding of chemical and molecular changes to investigate coccolithophore physiology and species-specific behaviour. To utilise changes in cellular elemental composition to understand potential changes in global biogeochemical cycles. An attempt to compare the physiological findings from this study with previous literature has also been made.

# Chapter 1: Size-Dependent Dynamics of the Internal Carbon Pool Drive Isotopic Vital Effects in Calcifying Phytoplankton

## Foreword

This chapter has been published in Geochimica et Cosmochimica Acta (Volume 373, 15 May 2024, Pages 35-51) by the same title. To maintain consistency, no changes have been made to the chapter and the supplementary information of the article has been presented as supplementary information to the chapter.

## Abstract

Isotopic offsets in biogenic calcite from equilibrium values can provide unique insights into the physiology and mechanisms of carbon regulation in calcifying phytoplankton. This study examines the impact of varying $CO_2$ (controlled via pH) on five coccolithophore species chosen for varied cell sizes, physiology, and calcification. The study investigates isotopic offsets in coccolith calcite and organic matter, in relation to carbon demand and supply ($\mu/CO_2$). Species-specific $CO_2$ and/or pH optima for growth ($\mu_{opt}$) were derived from variations in growth rates with varying $CO_2$ concentrations. Growth rates for all species declined with rising $CO_2$ (decreasing pH) due to $H^+$-driven inhibition. *C. braarudii* and *C. leptoporus* exhibited $\mu_{opt}$ at high $CO_2$ concentrations (suggesting high carbon-demand) and limited growth under low $CO_2$ (high pH) suggesting carbon limitation. Under low $CO_2$ supply, when growth rates were $CO_2$-limited, both species exhibited coincident isotopic depletion in calcite and organic matter as a consequence of $CO_2$ diffusion into the cell that experienced no equilibration as a result of a highly depleted internal carbon pool. In these two species, isotopic values in calcite remained unaffected by growth rates and $CO_2$ concentration

($\mu/CO_2$) when $CO_2$ was sufficient for optimal growth. *G. huxleyi* and *G. oceanica* displayed optima for growth ($\mu_{opt}$) at low $CO_2$ concentrations and showed no growth limitation under low $CO_2$ (indicating low carbon-demand). Both species experienced depleted (negative) vital effects caused by an excess of $CO_2$ diffusion into the small internal carbon pool of the cell when diffusive carbon supply outpaced low demand (low $\mu/CO_2$). Enriched (positive) vital effects were observed under low carbon supply and high demand, likely due to increased $HCO_3^-$ uptake and diffusive $CO_2$ loss from the intracellular carbon pool due to a lower intracellular pH than the seawater pH. *C. carterae* exhibited a $\mu_{opt}$ at intermediate $CO_2$ concentrations and isotopically equilibrated intracellular carbon pool such that $\delta^{13}C$ values in calcite and organic matter suggested a shared carbon pool. This study illustrates that pH and $CO_2$ driven vital effects and fractionation into organic matter indicate the residence time for carbon in the intracellular carbon pool, where the size of the pool is proportional to cell size. Due to the increased buffering afforded by a larger pool, *C. leptoporus* and *C. carterae* may have elevated intracellular pH which minimises $CO_2$ leakage, whereas vital effects in *G. huxleyi* and *G. oceanica* are caused by $CO_2$ diffusion in or out of their small internal carbon pool with limited buffering capacity owing to its small size.

## Introduction

Stable isotopes in biogenic calcite offer insights into paleoclimate reconstructions spanning a sizeable portion of Earth's geological history and enhance our understanding of Biosphere-Geosphere interactions. However, "vital effects", the isotopic offset from calcite precipitated in equilibrium, due to factors within the biomineralizing organism, often complicate the interpretation of climate signals in biologically mediated carbonate precipitation. These “vital effects” are caused by a multitude of chemical, physical, and biological processes,

which introduce deviations in the biogenic calcite from equilibrium and calculated inorganic compositions.

Purely inorganic calcite precipitation causes equilibrium fractionation effects, inducing isotopic fractionation between the solution and calcite due to differences in the strength of molecular bonding (Zeebe & Wolf-Gladrow, 2001). Additionally, thermodynamic factors stemming from environmental variables such as temperature can also contribute to the differences in molecular energies and impact equilibrium fractionation. Urey (1947) first demonstrated the utility of temperature-related fractionation in foraminiferal calcite for paleotemperature reconstruction.

McCrea (1950) established the relationship between solution pH and the isotopic composition of precipitating calcite. The study revealed the dependence of the calcite oxygen isotopic composition (referred to as $\delta^{18}O$) on the concentration of $CO_3^{2-}$ ions, which is proportional to pH. They showed that with increasing pH, as the abundance of $CO_3^{2-}$ ion increases, the $\delta^{18}O$ of the precipitating calcite becomes more depleted. This is because the $\delta^{18}O$ of $CO_3^{2-}$ is isotopically depleted compared to the other carbonate species and the proportion of $CO_3^{2-}$ ion within the DIC increases with rising pH (Zeebe, 1999).

The $\delta^{18}O$ – pH relationship has since gained significance as the isotopic composition of temperature-corrected calcite could function as a proxy for seawater pH or carbonate ion (Spero *et al.*, 1997). Conversely, pH-mediated effects on the isotopic composition of calcite could interfere with the temperature signal. Subsequent advancements unveiled the mechanism of isotopic equilibration in the $H_2O$-DIC-$CaCO_3$ system for the carbon and oxygen isotopes which have been explained here briefly (referred to as $\delta^{13}C$ and $\delta^{18}O$ respectively; Zeebe and Wolf-Gladrow 2001).

Isotopic equilibration in $\delta^{13}C$ is controlled by interconversion reactions between $CO_2$, $HCO_3^-$, and $CO_3^{2-}$ driven by the different binding strengths of the carbon in each molecule. Among these reactions is the hydration/hydroxylation of $CO_2$ to $HCO_3^-$ and its reverse, which is the rate limiting step in carbon isotopic equilibration. The hydration reaction can cause the $HCO_3^-$ to be (-)13 ‰ more depleted in $\delta^{13}C$ than $CO_2$, whereas the dehydration reaction can cause the $CO_2$ to be about (-)22 ‰ more depleted in $\delta^{13}C$ than $HCO_3^-$ (O'Leary *et al.*, 1992; Zeebe & Wolf-Gladrow, 2001). The slow carbon isotopic equilibration rate between $CO_2$ and $HCO_3^-$ can cause a significant depletion in the isotopic composition of the precipitating calcite. A depletion of (-)10 – 15 ‰ in the $\delta^{13}C$ and (-)4 ‰ in $\delta^{18}O$ of corals was reported to be caused by such a mechanism (McConnaughey, 1989a).

Carbonic anhydrase (CA) is suggested to significantly influence the rate of hydration/hydroxylation between $CO_2$ and $HCO_3^-$ (the rate limiting step) by catalysing this reaction, therefore, allowing faster equilibration in both $\delta^{13}C$ and $\delta^{18}O$ and alleviating kinetic fractionation effects caused by hydration/hydroxylation of $CO_2$ to $HCO_3^-$ (Chen et al., 2018; Thaler et al., 2017; Uchikawa and Zeebe, 2012).

Isotopic equilibration in $\delta^{18}O$ occurs through the equilibration between $CO_2$ – $HCO_3^-$ – $CO_3^{2-}$ (DIC) through interconversion reactions described above and equilibration between $H_2O$ and $CO_2$ and occurs more slowly than that for carbon isotopes. $\delta^{18}O$ isotopic equilibration needs to take place between one oxygen atom in $H_2O$ and three atoms in each carbonate and bicarbonate molecule ($HO\text{-}COO^-$ and $COOO^{2-}$), and two atoms in the $CO_2$ molecule. Isotopic equilibration between $H_2O$ and DIC is also influenced by pH, as the proportion of DIC present as $CO_2$ becomes significantly low at high pH. For instance, the time required for 99% isotopic equilibration in the carbonate system of seawater can take about 12.4 hours at pH 8 at 19˚C (Zeebe & Wolf-Gladrow, 2001). Under alkaline conditions (common

during calcite precipitation), isotopic equilibration is even slower, and can cause significant deviations in the calcite isotopes from equilibrium values, causing kinetic isotopic effects (McConnaughey, 1989a,b, 2003; Adkins *et al.*, 2003).

Kinetic isotope effects in $\delta^{13}C$ and $\delta^{18}O$ caused by disequilibrium in the DIC-$H_2O$ system have also spurred investigations into kinetic fractionation in inorganic $CaCO_3$ due to calcite crystal growth rate, where a high calcite-crystal growth rate causes isotopic depletion in the $\delta^{13}C$ and $\delta^{18}O$ of calcite due to non-equilibrium fractionation factors (Watkins *et al.*, 2013). Additionally, $CO_2$ diffusion to the site of precipitation in an organism can lead to mass-dependent kinetic isotope effects (Schauble, 2004; Eiler, 2007). According to the kinetic diffusion model, lighter isotopes (e.g., $^{12}C^{16}O^{16}O$) diffuse more rapidly than their heavier counterparts (e.g., $^{13}C^{16}O^{16}O$ and $^{12}C^{18}O^{16}O$; Wanner & Hunkeler, 2019). Although a limited number of studies have attempted to quantify the extent of isotopic depletion caused by aqueous-phase $CO_2$ diffusion, experimental evidence suggests a potential depletion of (-)0.7 to (-)0.87 ‰ in $\delta^{13}C$ (O'Leary, 1984; Jähne *et al.*, 1987) and (-)1.6 ‰ in $\delta^{18}O$ (Thiagarajan *et al.*, 2011).

Furthermore, biogenic calcite can also be influenced by metabolic processes such as respiration and photosynthesis. Isotopic changes due to the preferential uptake of depleted $CO_2$ by RuBisCO, the key enzyme in photosynthesis have been highlighted in $\delta^{13}C$ (McConnaughey, 1989a; McClelland *et al.*, 2017). However, it is worth noting that fractionation by RuBisCO is recognised in both $\delta^{13}C$ and $\delta^{18}O$ (Guy *et al.*, 1993; Tcherkez *et al.*, 2006).

Understanding the variability of vital effects with environmental factors can provide significant additional information about the physiology of biomineralizing organisms. Noteworthy candidate organisms are coccolithophores, offering a promising avenue for paleoenvironmental

reconstruction owing to their geological history spanning over 200 Ma (Bown *et al.*, 2004). Much like foraminifera, stable isotopes in different species of coccolith calcite are known to display distinct offsets from equilibrium which have been used for the reconstruction of past environments (Dudley *et al.*, 1986; Bolton & Stoll, 2013; Hermoso *et al.*, 2020; Claxton *et al.*, 2022).

Prior studies have suggested that vital effects in coccolithophores diminish as carbon supply increases, but species-specific deviations from abiogenic calcite occur at low DIC/$CO_2$ concentrations (Rickaby *et al.*, 2010; Hermoso *et al.*, 2016a; McClelland *et al.*, 2017). These studies simulated an increase in $CO_2$ by increasing DIC concentrations at a constant pH. Moreover, they suggested a mechanistic link between the magnitude of coccolith vital effects and the species-specific ratio of particulate inorganic carbon (PIC) to particulate organic carbon (POC) and carbon demand vs supply (analogous to $\mu/CO_2$).

It remains unclear whether the physiological and isotopic effects observed stem from an increase in $CO_2$, from changes in DIC concentration, or from an interplay of both factors. This is because vital effects in coccolithophore calcite were reported to become increasingly depleted with increasing $CO_2$ (Hermoso, 2015), where $CO_2$ was modified through pH manipulation at constant DIC concentration. This discrepancy indicates that the isotopic response of coccolithophores may vary depending on the specific parameters of the manipulated carbonate chemistry and on the effect of those chemical manipulations on their physiology.

In the diffusive model for organic isotopic fractionation, isotopic fractionation in organic matter increases with $CO_2$ concentration but can be affected by growth rate (Laws *et al.*, 1995; Rau *et al.*, 1996). Accordingly, carbon demand to supply (denoted by $\mu/CO_2$) has been correlated with isotopic fractionation in the organic matter and attributed to Rayleigh fractionation of an

internal pool of carbon and used as a proxy for past $pCO_2$ (Pagani, 2002; Henderiks & Pagani, 2008). This correlation comes with limitations due to factors that impact the relationship between isotopic fractionation and $\mu/CO_2$, such as active carbon uptake (Keller & Morel, 1999; Tchernov *et al.*, 2014; Stoll *et al.*, 2019).

There have been few studies reporting isotopic fractionation in both calcite and organic matter, and in $\delta^{13}C$ and $\delta^{18}O$ simultaneously. The carbon demand to supply models in coccolith calcite (McClelland *et al.*, 2017) and organic matter (Rau *et al.*, 1996) suggest that this parameter, possibly with active bicarbonate uptake, plays a crucial role in understanding vital effects and their relationship with species-specific coccolithophore physiology. Further investigation is needed to understand the relationship between isotopic fractionation in the calcite and organic matter of coccolithophores and seawater carbonate chemistry.

This study delves into the effects of pH and $CO_2$ variations on isotopic signatures within coccoliths and organic matter. Through dilute batch cultures, stable isotopes in calcite and organic matter of five coccolithophore species of varying cell sizes, carbon demands, and PIC:POC ratios were investigated to understand the mechanisms of carbon regulation and isotopic fractionation in calcifying phytoplankton. The results obtained from this study will provide a context within which size-separated coccolith fractions can be interpreted during paleoclimate reconstructions that use coccolithophore calcite and organic matter isotopes specifically pointing to periods when carbon limitation of different size fractions emerged (e.g., González-Lanchas et al., 2021; Bolton et al., 2016). Moreover, the broader application of the findings of this study will be useful in constructing numerical cell models to quantify the fluxes of carbon and calcium, and intracellular reservoirs, involved in coccolithophore calcification (Holtz *et al.*, 2015, 2017).

## Methodology

### Coccolithophore Culturing

Live coccolithophore monocultures were sourced from the Roscoff Culture Collection (www.roscoff-culturecollection.org) and the Marine Biological Association (MBA, www.mba.ac.uk). Strains RCC 1198 (*Coccolithus braarudii*), RCC 1130 (*Calcidiscus leptoporus*), RCC 1314 (*Gephyrocapsa oceanica*), PLY 837 (*Gephyrocapsa huxleyi*, morphotype A; Bendif et al., 2019), and PLY 406 (*Chrysotila carterae*) were grown in filter-sterilised artificial seawater prepared using the Synthetic Ocean Water (SOW) recipe from Aquil* synthetic medium (Price *et al.*, 1989), modified from Morel et al. (1979) with a starting constant DIC concentration of ~2100 μmol $KgSW^{-1}$. These species were selected based on their unique physiological characteristics. For instance, *C. carterae* is a coastal species with a large cell size and small PIC:POC ratio (Houdan *et al.*, 2004). PIC:POC ratios were taken from previously published data (Table S1, Supplementary Information; Gafar et al., 2019; McClelland et al., 2017). *G. huxleyi* and *G. oceanica* are ubiquitous bloom forming species that are widely studied in the paleoclimatic records and the modern ocean (Paasche, 1964; González-Lanchas *et al.*, 2021; Wheeler *et al.*, 2023). These species have small cell sizes and intermediate PIC:POC ratios. *C. leptoporus* and *C. braarudii* have long ancestral lineages and are key calcifiers in the modern ocean (Backman, 1980; Young, 1998; Ridgwell, 2005; Agnini *et al.*, 2014). These species have large cell sizes, and relatively higher PIC:POC ratios (Table S1). The SOW was enriched with 100 μmol $kg^{-1}$ nitrate, 6.25 μmol $kg^{-1}$ phosphate, and 27 μmol $kg^{-1}$ silicate, supplemented with vitamins based on the *f*/2 protocol (Guillard & Ryther, 1962) and trace metals according to the K/2 protocol (Keller & Guillard, 1985; Keller *et al.*, 1987), with modifications according to (Rickaby et al. 2010, Supplementary Material). pH was adjusted using

1N NaCl and 1N HCl and measured with a 3-point calibrated benchtop pH meter (Mettler Toledo SevenEasy). The seawater was filtered through a sterile 0.22 μm Merck Steritop® bottle top filter, UV sterilized, and filled into acid-clean, sterile 2.3L polycarbonate bottles with no headspace.

Dilute batch cultures were employed, with a maximum 5 % change in [DIC] as recommended by (Langer et al. 2006; LaRoche et al. 2010; Rickaby et al. 2010; Hermoso 2015; Supplementary Material). Cultures were grown in triplicate within a PHCbi MLR-352 Climate Chamber at 17 ± 0.1˚C. A 14-hour light:10-hour dark cycle was maintained, with the photon flux density ranging between 55 and 80 $\mu$mol $m^{-2}$ $s^{-1}$ during the light phase, depending on the position relative to the light source, which was randomised during the acclimatisation and experiment incubation phase. The strains were acclimated in the experimental media for a minimum of 14 generations (2 subsequent batch cultures of ~7 generations each, transferred at mid-exponential growth) prior to their use as initial inoculates for the main experiment. Culture bottles were gently shaken daily and opened for less than a minute each to measure growth. Only 600 μL of culture was extracted at once yielding a negligible effect on gas exchange and headspace.

Cell counts were measured using a Beckman Coulter Counter Z2 analyser. Isotopic measurements were conducted on the day of optimal cell density. All measurements were taken at the same time of day, starting 6 hours after the beginning of the light phase, and lasting approximately 2 hours. Coccosphere sizes were measured using SEM images obtained on a Zeiss Sigma 300 FEG-SEM.

**Measurement of Growth**

Specific growth rates were calculated based on in vivo log change in chlorophyll fluorescence per day using a TECAN Spark® Multimode Microplate

Reader (excitation = 485 ± 20 nm, emission = 680 ± 30 nm; Andersen, 2005). The specific growth rate (μ) was determined using the following equation:

$$\mu = \frac{\ln Chl\ flo_f - \ln Chl\ flo_i}{\Delta t}$$

Here, $Chl\ flo_f$ represents the blank-corrected chlorophyll fluorescence of the cell culture on the harvest day, $Chl\ flo_i$ represents the blank-corrected chlorophyll fluorescence one or two days before cell harvest, and $\Delta t$ is the difference in days between the two measurements. Sterile culturing media was used as blanks. See Methods (Supplementary Material) for an overview of the challenges faced in this study with traditional cell counting methods at such dilute concentrations to justify *in vivo* log change in chlorophyll fluorescence per unit time being used for measuring specific growth rates.

**Calculation of Carbonate Chemistry Parameters**

To determine pH, alkalinity, and DIC drift, approximately 12 mL of seawater sample was collected on the day of inoculation and at harvest after filtering through a 0.22 μm syringe filter unit and stored in Labco Exetainer® vials with no headspace. The seawater samples were titrated in technical duplicates with a 0.01N HCl standardized solution on a Metrohm 916 Ti-Touch titrator to determine Total Alkalinity (TA) and pH. The pH probe was calibrated daily using NIST standard reference material (Thermo Scientific), and the precision and accuracy of the machine were assessed using Dickson $CO_2$ in seawater reference material (Batch 126, 197) provided by A. Dickson, Scripps Institution of Oceanography, La Jolla, CA. See Methods (Supplementary Material) for an overview of the precision and accuracy of the Dickson standards. Carbonate chemistry parameters were calculated using CO2Sys v2.1 (Pierrot *et al.*, 2006) with the measured pH, TA, temperature, and calculated initial phosphate and silicate

concentrations. The $K_1$ and $K_2$ constants were obtained from Mehrbach et al. (1973) and refit by Dickson & Millero (1987).

**Isotopic Measurements**

For the analysis of $\delta^{13}C$ of organic matter ($\delta^{13}C_{ORG}$), 200 mL (per technical replicate) of culture was filtered through pre-combusted (450˚C, overnight) GF/F filters, washed with sterile seawater, acidified using 230 µL of 0.1N HCl and oven-dried overnight at 40˚C. Samples were analysed on an Elementar Vario Isotope Select Elemental Analyser linked to an Isoprime 100 continuous flow IRMS at the Stable Isotope Ratio Mass Spectrometry Laboratory, School of Ocean and Earth Science, University of Southampton, National Oceanography Centre in Southampton, UK.

To measure $\delta^{13}C$ and $\delta^{18}O$ of coccolith calcite ($\delta^{13}C_{Coccolith}$, $\delta^{18}O_{Coccolith}$), approximately 600 mL of culture was filtered on a polycarbonate filter with a 0.8 µm pore size. The collected material was cleaned according to (Lee et al., 2016, Supplementary Material). Internal standards were treated in the same manner as samples to evaluate the isotopic offset from absolute values due to cleaning.

For $\delta^{13}C$ and $\delta^{18}O$ of DIC ($\delta^{13}C_{DIC}$ and $\delta^{18}O_{DIC}$), culturing media was collected on the harvest day in the same way as the alkalinity samples. All calcite and DIC samples were analysed on a Thermo Delta V Advantage at the Stable Isotope Laboratory, Department of Earth Sciences, University of Oxford.

$\delta^{13}C$ of $CO_2$ was calculated from $\delta^{13}C_{DIC}$ and the absolute temperature ($T_K$) according to (Mook *et al.*, 1974) and the following equation taken from Rau et al. (1996)

$$\delta^{13}C_{CO_2} = \delta^{13}C_{DIC} + 23.644 - (9701.5/T_K)$$

$\delta^{13}C$ of inorganic calcite ($\delta^{13}C_{INORG}$) was calculated as $\delta^{13}C_{DIC}$ +1 (Romanek *et al.*, 1992) and $\delta^{18}O_{INORG}$ was calculated to be –0.72 ‰ V-PDB, based on the equation from Kim & O'Neil (1997) and Watkins et al. (2013) for a temperature of 17˚C and the $\delta^{18}O$ of the seawater of 0 ‰ V-SMOW (Table S2, Supplementary Material). The effect of pH was considered from Zeebe (1999), where the $\delta^{18}O$ of the precipitating calcite becomes lighter (depleted) with increasing pH as a consequence of the increasing proportion of the isotopically depleted $CO_3^{2-}$.

Reproducibility of replicated standards (NBS 18 and NBS 19) was always better than 0.07 ‰ VPDB for $\delta^{13}C_{Calcite}$ and better than 0.11 ‰ VPDB for $\delta^{18}O_{Calcite}$. In addressing the impact of the cleaning process on isotopic values, an internal calcite standard was employed to account for offsets. The cleaning process resulted in a depletion of (-)0.13 ‰ in $\delta^{13}C_{Calcite}$ values relative to the expected absolute values, while $\delta^{18}O_{Calcite}$ values exhibited a corresponding enrichment of (+)0.04 ‰. The standard error associated with isotopic analysis using external standards found from the influence of the cleaning process on the absolute isotopic values of the internal standard was non-significant. The influence of sample treatment with similar magnitudes has been documented in prior studies (McConnaughey, 1989a). A comprehensive examination using Scanning Electron Microscopy did not reveal any indications of inorganic $CaCO_3$ overgrowth or coccolith dissolution after cleaning. For $\delta^{13}C$ values of cellular organic matter ($\delta^{13}C_{ORG}$), reproducibility on replicated standards (USGS 40 and 41a) was 0.00 – 0.04 ‰ VPDB for USGS 40 and 0.05 – 0.43 ‰ VPDB for USGS 41a.

## Results

### Carbonate Chemistry

During the dilute batch culture experiments, the average change in dissolved inorganic carbon concentration, [DIC], was approximately 4.7%, with an

average pH drift of 0.04 units. We used the initial alkalinity and pH values to compute and visualise other carbonate chemistry parameters, such as $CO_2$ concentration (hereafter [$CO_2$]). It is noted that the method of altering carbonate chemistry (through acid/base addition, $CO_2$ bubbling, or changing DIC concentration) can impact species–specific responses to varying carbonate conditions (Iglesias-Rodriguez et al., 2008b; Hoppe et al., 2011; Bach et al., 2013; Kottmeier et al., 2016a). The observed responses in this study are a consequence of modifications in both [$CO_2$] and [$H^+$].

**Effect of [$CO_2$] and pH on growth rates**

All species consistently exhibited a decrease in growth rate (minimum of ~0.2 $day^{-1}$) when exposed to high [$CO_2$] and low pH ( $CO_2 \geq 40$ μmol $kg^{-1}$, pH < 7.75), while species–specific effects were observed at low [$CO_2$] (high pH; Fig. 1). These observed changes in growth rates are in line with previous research findings, as all species exhibited an optimum growth curve in response to variable [$CO_2$] and/or pH (Gafar *et al.*, 2019a; Kottmeier *et al.*, 2022).

The estimates for growth rate optimum ($\mu_{opt}$) for $CO_2$ and/or pH differed among species: *C. leptoporus* exhibited a modelled $\mu_{opt}$ at 16.3 μmol $kg^{-1}$ (pH 8.1), *C. braarudii* at 21.05 μmol $kg^{-1}$ (pH 8.02), *C. carterae* at 13.5 μmol $kg^{-1}$ (pH 8.22), and *G. oceanica* at 3.5 μmol $kg^{-1}$ (pH 8.7). *G. huxleyi* did not reach a $CO_2$ optimum for growth (< 5 μmol $kg^{-1}$, pH >8.8).

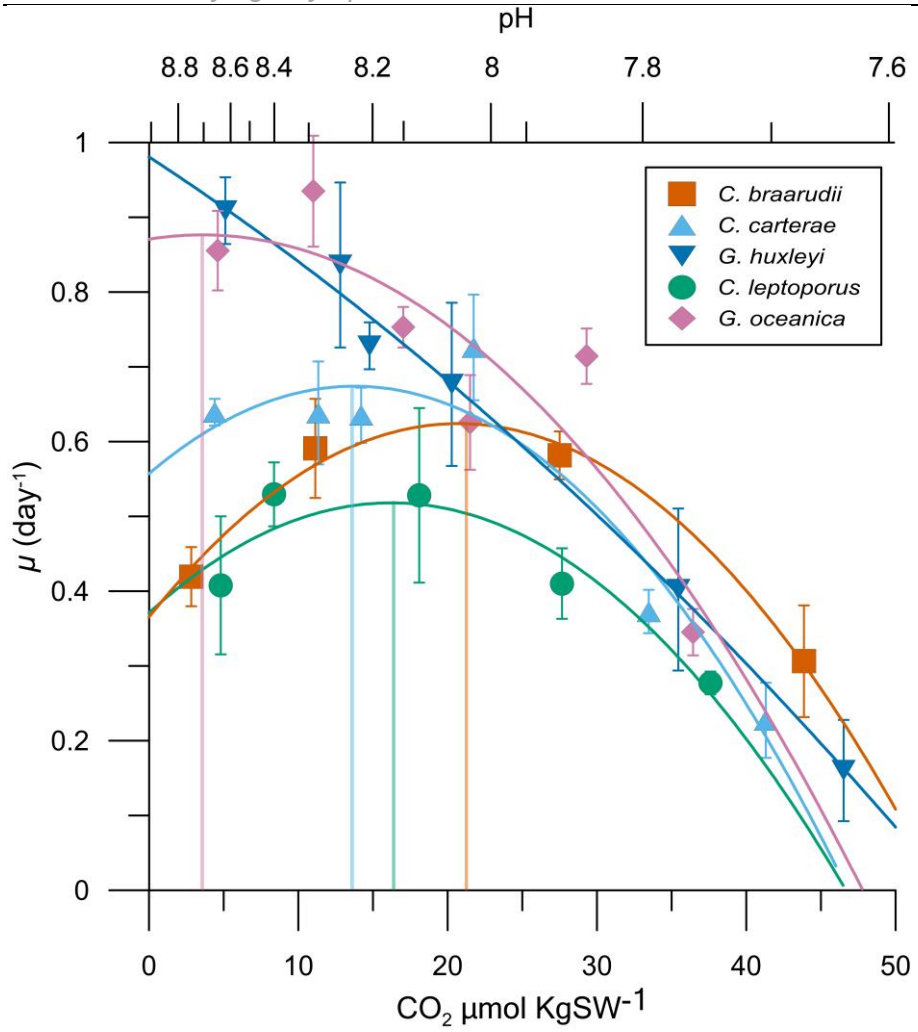


**Figure 1:** Growth rates (day$^{-1}$) for *C. braarudii* (■), *C. leptoporus* (●), *C. carterae* (▲), *G. huxleyi* (▼), and *G. oceanica* (◆). Each point is an average of 3 biological replicates. The curved lines represent 2$^{nd}$–degree polynomial fits. Vertical bars indicate maximum growth rates ($\mu_{opt}$), defined as the maximum of the polynomial fit curve. A plot of growth rates of all biological replicates can be found in the Supplementary Material (Fig. S3).

*G. huxleyi* exhibited the highest growth rate of 0.91 d$^{-1}$ at [$CO_2$] of 5.1 µmol kg$^{-1}$ (pH 8.6) and continually declined with increasing [$CO_2$] (Fig. 1). Similarly, maximum $\mu$ for *G. oceanica* was 0.94 d$^{-1}$ at [$CO_2$] 11 µmol kg$^{-1}$ (pH 8.3) and growth rates declined with increasing $CO_2$ (decreasing pH). Growth rates for *C. carterae* plateaued for [$CO_2$] below 22 µmol kg$^{-1}$ (pH 8.05). *C. braarudii* showed maximum $\mu$ between [$CO_2$] 10–30 µmol kg$^{-1}$ (pH 7.9 – 8.3) of ~ 0.58 d$^{-1}$ and showed declining $\mu$ at higher and lower [$CO_2$]. Overall, *C. leptoporus* showed the lowest $\mu$ in comparison to other species at all [$CO_2$] conditions and we observed significant

cell clumping at $[CO_2]$ ~ 40 μmol $kg^{-1}$ (pH 7.7). Similar observations have previously been reported for *C. leptoporus* (Langer & Bode, 2011).

Declining growth rates with increasing $[CO_2]$ (decreasing pH) align with some studies (e.g., Gafar et al., 2019; Kottmeier et al., 2022; Krug et al., 2011), but differ from others (e.g., Langer et al. 2009; Rickaby et al. 2010; Hermoso et al. 2016) where growth rates did not change significantly with increasing $[CO_2]$. This may be owing to carbonate chemistry parameters in these studies being manipulated through either $CO_2$ bubbling or DIC addition, instead of pH manipulation as in this study. Culture conditions, such as temperature, light intensity, nutrient concentration, seawater composition and irradiance cycles can also affect coccolithophore sensitivity to changing carbonate chemistry (Zondervan et al., 2002; Rokitta & Rost, 2012a; Sett et al., 2014; Bach et al., 2015; Zhang & Gao, 2021). Growth rates can be compared between experiments within this study to understand species-specific and interspecific responses. Significant changes in coccosphere size were only observed in *C. carterae,* where coccosphere diameter increased from ~12 μm to ~19 μm with increasing $[CO_2]$ (Fig. S6, Supplementary Material).`

**Stable isotopes**

The carbon and oxygen isotopic composition of the coccolith calcite, denoted as $\Delta^{13}C_{Coccolith}$ and $\Delta^{18}O_{Coccolith}$ were plotted in the form of $\delta^{13}C_{Coccolith} - \delta^{13}C_{CO2}$ and $\delta^{18}O_{Coccolith} - \delta^{18}O_{DIC}$ values, respectively (Fig. 2a,b). carbon isotopes of the organic matter are represented as $\Delta^{13}C_{ORG} = \delta^{13}C_{ORG} - \delta^{13}C_{CO2}$, ‰ VPDB. This allowed the quantification of the true isotopic fractionation relative to DIC, e.g., $\Delta^{13}C_{Coccolith} = \delta^{13}C_{Coccolith} - \delta^{13}C_{CO2}$, ‰ VPDB (Zeebe & Wolf-Gladrow, 2001; Hermoso *et al.*, 2016a; McClelland *et al.*, 2017). We assume that the DIC species and their respective isotopic compositions ($\delta^{13}C$ and $\delta^{18}O$) were in isotopic equilibrium with $H_2O$ and

other ions in the seawater when the experiment commenced. The magnitude of isotopic offset from calculated inorganic calcite values (Table S2, Supplementary Material), deemed the vital effect, were derived as $\delta^{13}C_{Coccolith} - \delta^{13}C_{Inorganic\ calcite}$ and $\delta^{18}O_{Coccolith} - \delta^{18}O_{Inorganic\ calcite}$ (Fig. 3). The $\Delta^{13}C_{Coccolith}$ and $\Delta^{18}O_{Coccolith}$ values aligned with previous studies (see Results: Supplementary Material).

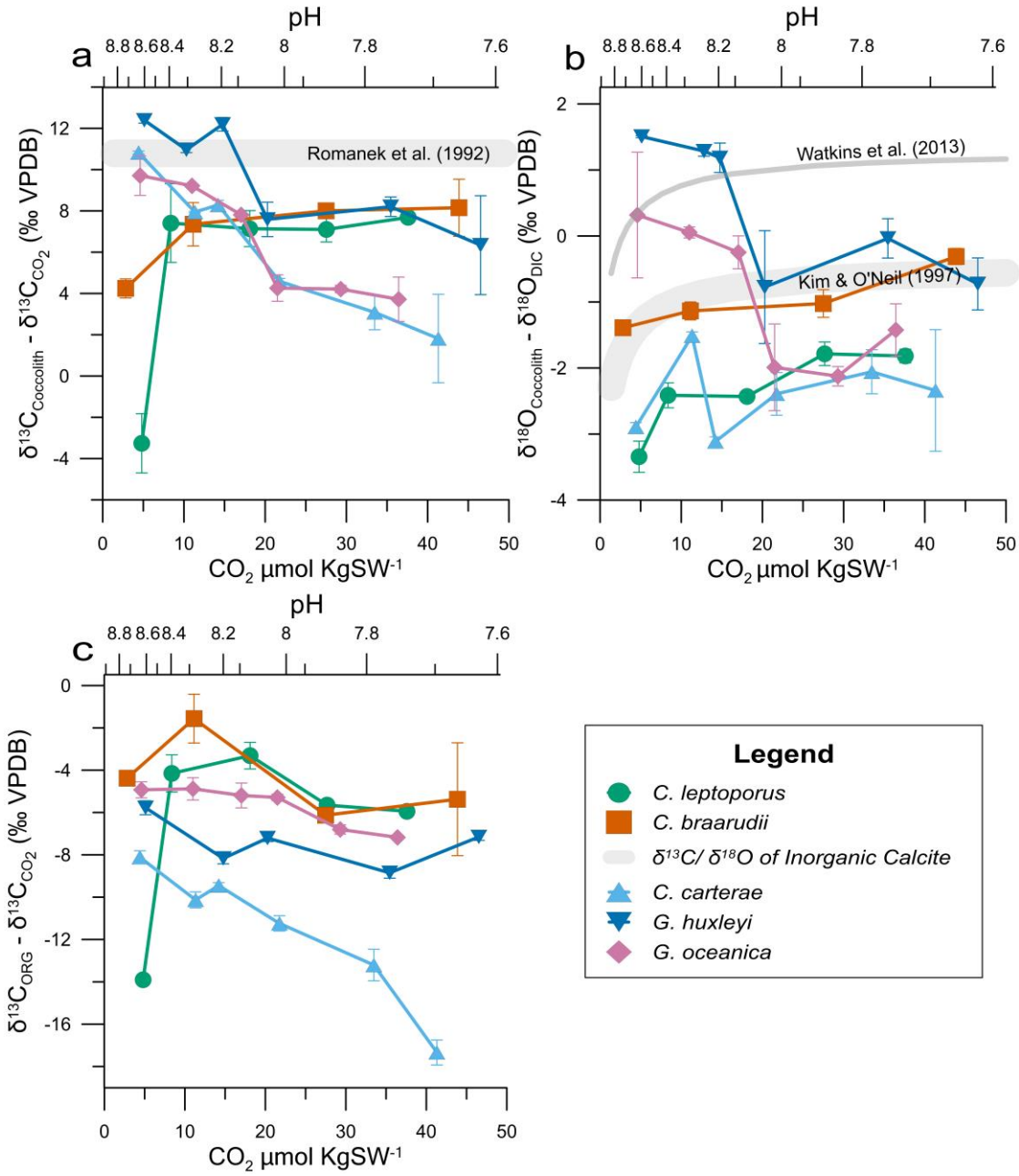


**Figure 2: (a)** $\Delta^{13}C_{Coccolith}$ ($\delta^{13}C_{Coccolith} - \delta^{13}C_{CO2}$), **(b)** $\Delta^{18}O_{Coccolith}$ ($\delta^{18}O_{Coccolith} - \delta^{18}O_{DIC}$), **(c)** $\Delta^{13}C_{ORG}$ values ($\delta^{13}C_{ORG} - \delta^{13}C_{CO2}$) for *C. braarudii* (■), *C. leptoporus* (●), *C. carterae* (▲), *G. huxleyi* (▼), and *G. oceanica* (◆). Note the change in y-axes. Each data point signifies an average of 3 biological replicates, each with 3 replicate measurements.

Measurements for each biological replicate can be found in the Supplementary Material (Fig. S4). Error bars represent one standard deviation. The grey line in (a) and (b) represents isotope values for inorganic calcite derived from *(Romanek* et al., *1992; Kim & O'Neil, 1997; Watkins* et al., *2013)*. $\delta^{18}O_{Inorganic\ Calcite}$ values are adjusted for pH according to (Zeebe, 1999). $\delta^{18}O$ values for Inorganic Calcite from Watkins et al. (2013) represent closest $\delta^{18}O$ values to thermodynamic equilibrium, while $\delta^{18}O$ values for Inorganic Calcite from Kim and O'Neil (1997) represent inorganic $\delta^{18}O$ values influenced by kinetic isotope effects. Note that although the relationship between $\delta^{18}O$ and pH is linear, between $\delta^{18}O$ and $CO_2$, it is logarithmic.

**Species-specific coccolith vital effects**

A crucial reference point to infer species-specific offsets is the isotopic composition of inorganic calcite, which is affected by both equilibrium and thermodynamic fractionation effects due to pH. At a given temperature, the $\delta^{13}C$ and $\delta^{18}O$ values of inorganic calcite are determined by the speciation of carbon species in the DIC according to the pH (Zeebe, 1999). With increasing pH, the $\delta^{18}O$ value of the inorganic calcite will become more depleted due to the increasing proportion of isotopically depleted $CO_3^{2-}$ ions, referred to as the "carbonate ion effect" (Zeebe, 1999; Ziveri *et al.*, 2012).

Although the $\delta^{13}C$ of carbonate species varies within the carbonate system, with the $\delta^{13}C$ of $CO_2$ being (-)9 ‰ more depleted, and $\delta^{13}C$ of $CO_3^{2-}$ (-)2 ‰ more depleted compared to that of $HCO_3^-$ (Zeebe & Wolf-Gladrow, 2001), the $\delta^{13}C$ of the calculated inorganic calcite should exhibit no change at equilibrium. This is because if the inorganic calcite is precipitated with all DIC species, the $\delta^{13}C$ of the inorganic calcite should only show a consistent 1‰ enrichment in the solid irrespective of the pH (Romanek *et al.*, 1992).

*G. huxleyi* displays slightly positive $\Delta^{13}C_{Coccolith}$ values (up to (+)2 ‰ enrichment than $\delta^{13}C_{Inorganic\ Calcite}$) when $CO_2$ levels are below ~17 µmol $kg^{-1}$ (below pH 8.1; Fig. 3a). However, when $CO_2$ levels go above this threshold, *G. huxleyi* exhibits negative vital effects in $\Delta^{13}C_{Coccolith}$ (Fig. 3a). A similar shift in vital effects is observed in *G. oceanica* at 17 µmol $kg^{-1}$ $CO_2$. However, *G. oceanica* shows near-inorganic

$\Delta^{13}C_{Coccolith}$ values (< (-)2 ‰ depletion than $\delta^{13}C_{Inorganic\ Calcite}$) at $CO_2$ levels below 17 µmol $kg^{-1}$ in $\Delta^{13}C_{Coccolith}$. Moreover, $\Delta^{13}C_{Coccolith}$ values for *G. oceanica* above 17 µmol $kg^{-1}$ $CO_2$ are more negative compared to *G. huxleyi*. These observations suggest that both *G. huxleyi* and *G. oceanica* exhibit near-inorganic vital effects below ~17 µmol $kg^{-1}$ $CO_2$ (corresponding to a pH of 8.1), while above this $CO_2$ concentration, *G. huxleyi* and *G. oceanica* display negative vital effects in $\Delta^{13}C_{Coccolith}$. $\Delta^{18}O_{Coccolith}$ values exhibit similar trends to $\Delta^{13}C_{Coccolith}$ (Fig. 3b). When compared to the inorganic calcite by Kim and O'Neil (1997), *G. huxleyi* and *G. oceanica* display positive vital effects in $\Delta^{18}O_{Coccolith}$ values below ~17 µmol $kg^{-1}$ $CO_2$. While above this threshold, *G. huxleyi* exhibits near-inorganic $\Delta^{18}O_{Coccolith}$ values, and *G. oceanica* exhibits negative $\Delta^{18}O_{Coccolith}$ values.

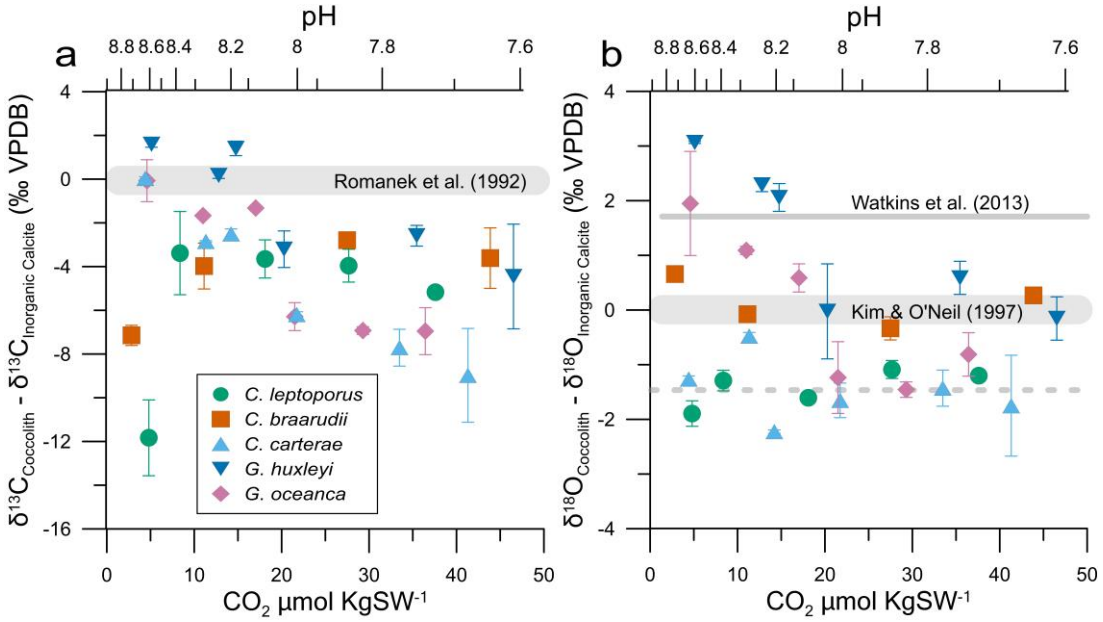


**Figure 3: (a)** Vital effects in $\Delta^{13}C_{Coccolith}$ ($\delta^{13}C_{Coccolith}$ - $\delta^{13}C_{Inorganic\ Calcite}$). 0 ‰ (grey line) signifies $\delta^{13}C_{Inorganic\ Calcite}$ based on Romanek et al. (1992). **(b)** Vital effects in $\Delta^{18}O_{Coccolith}$ ($\delta^{18}O_{Coccolith}$ - $\delta^{18}O_{Inorganic\ Calcite}$) using $\delta^{18}O$ of pH-corrected inorganic calcite. The $\Delta^{18}O_{Coccolith}$ values for *C. carterae* and *C. leptoporus* can be compared to the dashed line due to their elevated intracellular pH causing depleted $\Delta^{18}O_{Coccolith}$ values. The grey line at 0 ‰ signifies $\delta^{18}O_{Inorganic\ calcite}$ based on Kim and O'Neil (1997), and at 1.79 ‰ based on *(Watkins* et al.*, 2013)*. The thickness of grey lines accounts for the standard deviation in the isotopic composition of the inorganic calcite. Each data point signifies an average of ≥3 biological replicates, each with ≥3 replicate measurements.

Vital effects in $\Delta^{13}C_{Coccolith}$ of *C. braarudii* and *C. leptoporus* show a consistent depletion of ~4 ‰ compared to the inorganic value, except when $CO_2$ falls below 10 µmol $kg^{-1}$, at which point these species display large negative vital effects (Fig. 3a). Regarding $\Delta^{18}O_{Coccolith}$, *C. braarudii* only exhibits minor deviations from the inorganic values, while *C. leptoporus* consistently departs from the inorganic value by a constant offset (Fig. 3b). Finally, *C. carterae* demonstrates that $\Delta^{13}C_{Coccolith}$ values become progressively depleted as $CO_2$ concentrations rise (due to lowering pH), while $\Delta^{18}O_{Coccolith}$ values consistently exhibit negative vital effects under all $CO_2$ and/or pH conditions, similar to *C. leptoporus*.

## Discussion

### Growth rate: effect of species-specific [$CO_2$] and/or pH optima.

We found distinct growth rate optima ($\mu_{opt}$) for $CO_2$ and/or pH among various coccolithophore species. Notably, *C. braarudii* and *C. leptoporus* exhibited $\mu_{opt}$ values at 21.05 (pH 8.02) and 16.3 µmol $kg^{-1}$ $CO_2$ (pH 8.1) respectively (Fig. 1). *C. carterae* demonstrated a $\mu_{opt}$ value at 13.5 µmol $kg^{-1}$ $CO_2$ (pH 8.22), while *G. oceanica* displayed a $\mu_{opt}$ value at 3.5 µmol $kg^{-1}$ $CO_2$ (pH 8.7). *G. huxleyi* did not exhibit an upper $\mu_{opt}$ limit (< 5 µmol $kg^{-1}$, pH >8.8). A growth optimum likely sits at the intersection of $H^+$-induced growth inhibition and $CO_2$ fertilisation at low pH, and alleviation of $H^+$-related inhibition, high pH-related cellular stress, and $CO_2$ limitation at high pH. Moreover, species-specific optima exist due to the contrasting physiologies and carbon requirements of the species studied here.

The $\mu_{opt}$ values at high $CO_2$ (and low pH), for larger-sized, heavily calcifying species such as *C. braarudii,* and *C. leptoporus* is due to their high carbon demand (see Table S1 for species-specific PIC and POC quotas, Supplementary Material). Moreover, the ancestral lineages to these species existed in more acidic, $CO_2$-rich waters during the Paleogene (Young, 1998; Ridgwell, 2005; Agnini *et al.*, 2014). A

significant growth rate decline in both *C. braarudii* and *C. leptoporus* is observed below 10 μmol $kg^{-1}$ $[CO_2]$, when approaching the lower limit of their optimum curve (Fig. 1). The decline suggests a $CO_2$ limitation at lower $[CO_2]$ (Bach et al., 2011b, 2013). Signs of carbon starvation are also evident in the coccolith malformations of *C. braarudii* under low $CO_2$ conditions (Fig. S6, Supplementary Material). The declining growth rates suggests that these species rely predominantly on passive $CO_2$ diffusion as their carbon source and are less able to use $HCO_3^-$, which is abundant at the higher pH conditions (Zeebe & Wolf-Gladrow, 2001). At lower $CO_2$ levels, diffusive and active carbon uptake may be insufficient or have too low affinity to meet the carbon demands of these two species.

The notion of active carbon uptake has been primarily explored in the context of *G. huxleyi* (Sikes et al., 1980; Mackinder et al., 2010; Rokitta & Rost, 2012a). Therefore, it is plausible that the active carbon uptake capabilities might explain the absence of a lower limit for a growth optimum for *G. huxleyi*, which also has a comparably low carbon demand due to its small size and low PIC quotas (Table S1). Similar mechanisms probably exist in the case of the small sized and lightly calcifying *G. oceanica*, as it exhibits a similar trend to *G. huxleyi* in its growth rates (Fig. 1). *G. huxleyi* exhibits high affinity for $CO_2$ and/or an effective active carbon uptake mechanism as suggested by the reported half-saturation rate ($K_c$) for growth at 1.7 μmol $kg^{-1}$ $CO_2$ (Feng *et al.*, 2017), which aligns with its $\mu_{opt}$ value at low $CO_2$ concentrations. This is noteworthy, given the high half-saturation rates for RuBisCO in *G. huxleyi,* reportedly at 39 – 41 μmol $kg^{-1}$ $CO_2$ (Heureux 2016; note the difference between half-saturation rates for growth and RuBisCO). These findings further support the presence of an active carbon concentrating mechanism (CCM) in *G. huxleyi*, particularly under low $CO_2$ conditions (Reinfelder, 2010; Kottmeier et al., 2014; Zhang et al., 2021a). Given the predominant focus on the active carbon uptake mechanisms in *G. huxleyi,* it is important to determine

the extent of this mechanism in other species, particularly those which exhibit $\mu_{opt}$ values at high $CO_2$ concentrations due to their larger size and/or higher calcification requirements as highlighted in previous studies (Daniels *et al.*, 2014; Bach *et al.*, 2015).

The $\mu_{opt}$ value for *C. carterae* at a relatively higher $CO_2$ concentration is possibly due to its large cell size, despite being the lowest PIC:POC species (Table S1, Supplementary Material). $\mu_{opt}$ values at a higher $CO_2$ concentration may be due to the large internal carbon pool of *C. carterae* (also *C. braarudii* and *C. leptoporus*), which requires higher carbon fluxes into the cell for its replenishment or due to their higher internal pH buffering capacities. A decrease in coccosphere size for *C. carterae* was observed with decreasing $[CO_2]$/increasing pH, resulting in a ~60% increase in Surface Area to Volume (SA:V) ratio (Fig. S2, Supplementary Material). An increase in the SA:V ratio may potentially aid $CO_2$ diffusion into the cell under reduced $CO_2$ availability. Alternatively, cell size may increase under low pH due to elevated $[H^+]$-driven reduced cellular division rates (inferred from reduced growth rates at low pH in Fig. 1). Nonetheless, the flexibility in cell size and the plateau in growth rates at a wide pH range (pH 8 – 8.7) can be a trait related to the dynamic coastal habitat of *C. carterae* (Houdan *et al.*, 2004).

Increased carbon supply at higher $CO_2$ concentrations has been shown to enhance growth due to its fertilizing effect on phytoplankton, as the enzyme RuBisCO utilizes $CO_2$ for carbon fixation (Iglesias-Rodriguez et al., 2008b; Fiorini et al., 2011). This phenomenon has been previously demonstrated in the case of *C. braarudii* (Langer *et al.*, 2006; Halloran *et al.*, 2008), which is consistent with our findings of $\mu_{opt}$ values at high $CO_2$ concentrations for the same species.

Our study reveals a consistent decline in growth rates for all species, especially at $[CO_2]$ greater than 30 μmol $kg^{-1}$ (below pH 7.9). This observation

coincides with increased malformation in the coccolith calcite (Fig. S6, Supplementary Material) suggesting the inhibitory effect of increased [$H^+$] associated with decreasing pH is experienced universally (Suffrian *et al.*, 2011a; Taylor *et al.*, 2011; Bach *et al.*, 2015). In terms of pH sensitivity, the inhibitory effect of pH in *G. huxleyi* and *G. oceanica* is observed as a continuous decline in growth rates starting from pH 8.4 and progressing to lower pH values. However, the inhibitory effect of low pH on the growth rates of *C. braarudii, C. leptoporus and C. carterae* is observed only at pH levels below 7.9. This implies that the larger species (*C. braarudii, C. leptoporus and C. carterae*) display a stronger threshold towards sensitivity to declining pH which may be attributed to their stronger intracellular pH buffering capacity due to their comparatively large size and small SA:V ratio (Table S1). $H^+$ efflux during calcification through membrane channels has been previously documented as the mechanism responsible for pH homeostasis in *C. braarudii* (Taylor *et al.*, 2011; Kottmeier *et al.*, 2022). It is plausible that this mechanism is also operative in *C. leptoporus and C. carterae,* contributing to their higher tolerance to variable pH.

**The relationship between vital effects and carbon demand to supply ratio.**

Species-specific growth rates at varying $CO_2$ and pH levels allows the investigation of vital effects to the carbon demand to supply ratio (represented as $\mu/CO_2$) and often used to describe the sensitivity of carbon isotopic fractionation into organic matter (e.g., Keller and Morel, 1999). While previous research has examined the relationship between $\mu/CO_2$ and vital effects in coccolith calcite (e.g., Hermoso 2015) and isotopic fractionation in organic matter (e.g., Tchernov et al. 2014), studies rarely address both the organic and inorganic systems simultaneously.

Although the parameter $\mu/CO_2$, as a measure of the carbon demand versus supply, may not incorporate factors such as the additional carbon demand imposed by a calcifying cell for biomineralisation, or carbon supply through active $HCO_3^-$ uptake, it does offer a framework for interpretation (Hermoso *et al.*, 2016b). This significance is magnified as the portion of carbon supply via active $HCO_3^-$ uptake has only been quantified in one coccolithophore species (Kottmeier et al., 2014; Kottmeier et al., 2016a). According to Kottmeier et al. (2014), *G. huxleyi* used >90 % $CO_2$ below pH of 8.1 ([$CO_2$] greater than 17 µmol $kg^{-1}$ for this study) and the proportion of active $HCO_3^-$ uptake progressively increased above pH 8.1, with ~55 % $HCO_3^-$ at pH 8.7. The current study did not measure calcification rates so these cannot be factored into the carbon demand calculation. SA:V ratio is included to get a better estimate of carbon demand through organic carbon fixation and diffusive supply of $CO_2$, especially with changing cell sizes. In this study, SA:V calculations were based on coccosphere diameters rather than naked cell sizes, as measuring the latter resulted in higher inaccuracies.

Vital effects in Figure 3 suggest that large-sized and heavily calcifying species such as *C. braarudii* and *C. leptoporus* that show $\mu_{opt}$ values at high $CO_2$ concentrations, show a consistent depletion of ~ (-)4 ‰ from inorganic calcite under most scenarios, and only exhibit significant offsets in $\Delta^{13}C_{Coccolith}$ under the lowest $CO_2$ concentrations. Small-sized and lightly calcifying species such as *G. huxleyi* and *G. oceanica* that show a $\mu_{opt}$ value at low $CO_2$ concentrations, show a shift towards more depleted values at 17 µmol $kg^{-1}$ $CO_2$ but display a constant offset from each other across the conditions. Finally, *C. carterae* that exhibit $\mu_{opt}$ values at intermediate $CO_2$ concentrations, display progressively depleted $\Delta^{13}C_{Coccolith}$ values with increasing $CO_2$ while $\Delta^{18}O_{Coccolith}$ values show minimal changes. In the following section, we investigate the relationship between vital effects and carbon demand to supply ratio in these three groups, and provide insights into

the observed trends in $\Delta^{13}C_{Coccolith}$, $\Delta^{18}O_{Coccolith}$ , and $\Delta^{13}C_{ORG}$ across varying growth rates, $CO_2$, and pH levels.

**Long carbon residence times in *C. braarudii* and *C. leptoporus* allow isotopic equilibration of their internal pool: vital effects emerge during lowest carbon supply and high carbon demand.**

Above [$CO_2$] of 10 μmol $kg^{-1}$, growth rates decrease at high $CO_2$, and coccoliths show malformations with increasing $CO_2$ (Fig. S6, Supplementary Material) for *C. braarudii* and *C. leptoporus*. Moreover, their $\Delta^{13}C_{Coccolith}$ values show a consistent offset from the $\delta^{13}C$ of inorganic calcite (grey line, Fig. 4a), with minor variations in isotopic values with increasing $CO_2$ (Fig. 4a), and minimal changes with $\mu/CO_2$ ([$CO_2$] >10 μmol $kg^{-1}$; Fig. 4c). Similar offsets at high [$CO_2$] have been reported previously (Hermoso, 2015; Wilkes *et al.*, 2018). At [$CO_2$] above 10 μmol $kg^{-1}$, $\Delta^{13}C_{ORG}$ values become more depleted with increasing $CO_2$ and decreasing growth rates (Fig. 2c, 4b). This observation is consistent with previous studies that report a depletion in $\Delta^{13}C_{ORG}$ values with increasing diffusive $CO_2$ supply due to increasing ambient $CO_2$ concentration (e.g., Burkhardt et al. 1999a).

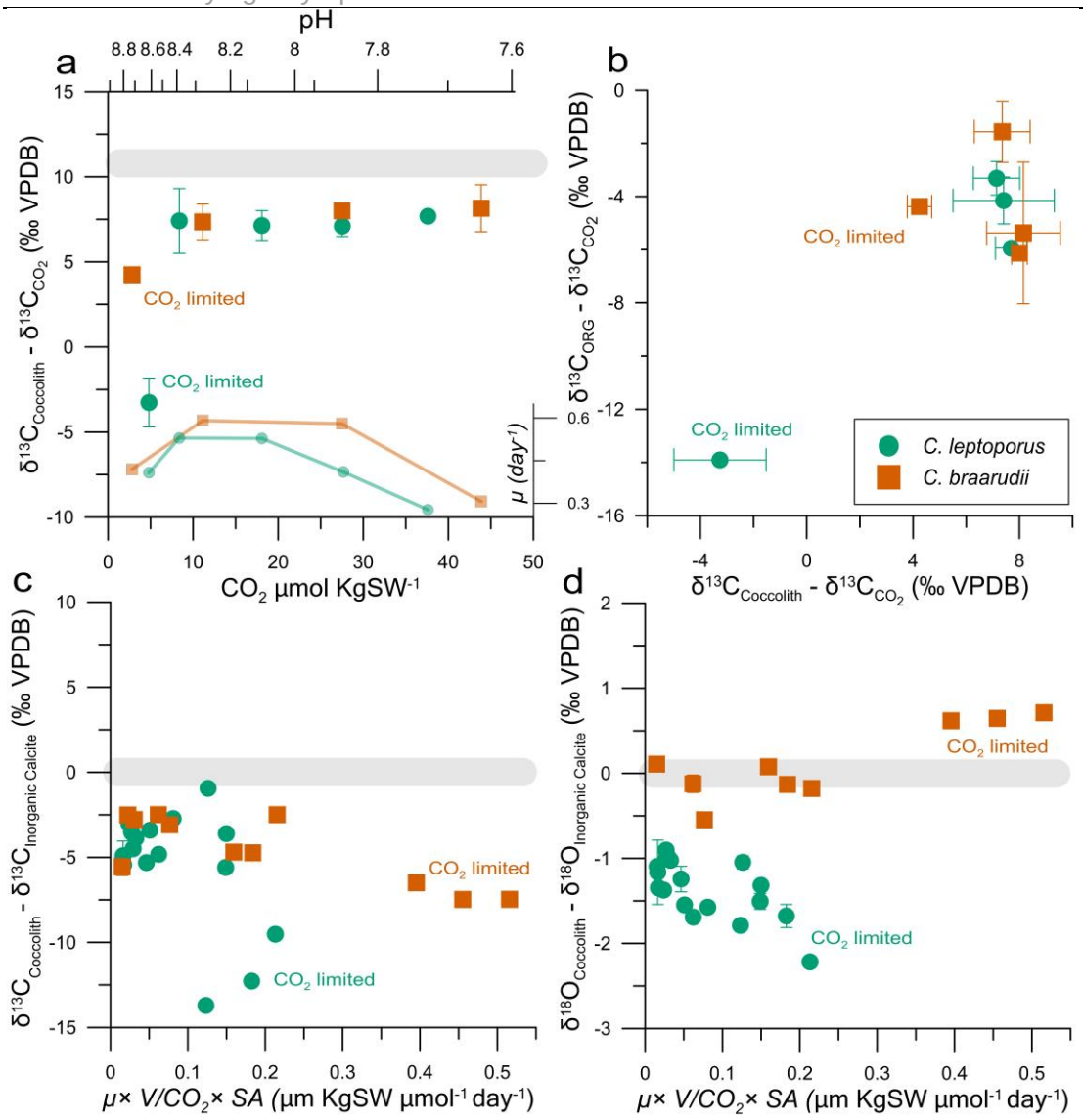


**Figure 4: (a)** $\delta^{13}C_{Coccolith} - \delta^{13}C_{CO2}$ for *C. braarudii* (▪) *and C. leptoporus* (●) with growth rate ($\mu$, day$^{-1}$) plotted as a subset. Grey line denotes inorganic calcite. **(b)** $\Delta^{13}C_{Coccolith}$ vs. $\Delta^{13}C_{ORG}$ **(c)** $\delta^{13}C_{Coccolith} - \delta^{13}C_{Inorganic\ Calcite}$ vs. $\mu \times V/CO_2 \times SA$ **(d)** $\delta^{18}O_{Coccolith} - \delta^{18}O_{Inorganic\ Calcite}$ vs. $\mu \times V/CO_2 \times SA$. The line thickness at 0 ‰ accounts for the standard deviation in the isotopic composition of the inorganic calcite. Note that in (a) and (b), the replicates are averaged, while in (c) and (d), they are not averaged. $\delta^{13}C_{ORG} - \delta^{13}C_{DIC}$ vs $\mu \times V/CO_2 \times SA$ can be found in the Supplementary Material (Fig. S5).

Regarding $\Delta^{18}O_{Coccolith}$ values, *C. braarudii* exhibits minor offsets from inorganic calcite, while $\Delta^{18}O_{Coccolith}$ values for *C. leptoporus* show a consistent offset towards depleted values from the inorganic value under all $CO_2$ conditions (Fig. 2b, 3b). The lack of changes in $\Delta^{18}O_{Coccolith}$ with $\mu/CO_2$ suggest that carbon residence times are long enough to allow isotopic equilibration of the oxygen isotopes with intracellular $H_2O$ (Fig. 4d). The offset in $\Delta^{18}O_{Coccolith}$ towards depleted values in *C.*

*leptoporus* can be attributed to the pH of the calcifying fluid within the coccolith vesicle (described hereafter as intracellular pH) being higher than the ambient pH, as reported previously (Liu *et al.*, 2021). Specifically, under high intracellular pH, $\Delta^{18}O_{Coccolith}$ becomes depleted due to the increased proportion of the (isotopically depleted) $CO_3^{2-}$ ions. Although intracellular pH may increase proportionally with ambient pH (Suffrian *et al.*, 2011a), active $Ca^{2+}/H^+$ exchangers can raise the pH of the calcifying fluid to increase the calcite saturation state, therefore, affecting the $CO_3^{2-}/HCO_3^-$ ratio (Anning *et al.*, 1996; Mackinder *et al.*, 2010; Chen *et al.*, 2018). It is worth noting that the $\delta^{18}O$ value of $CO_3^{2-}$ itself becomes more depleted with rising pH (Fig. 4 in Zeebe 1999). Similar mechanisms of elevating intracellular pH to promote calcification have been observed in corals (Venn *et al.*, 2011).

Below $[CO_2]$ of 10 μmol $kg^{-1}$, $\Delta^{13}C_{Coccolith}$, $\Delta^{13}C_{ORG}$, and growth rates for *C. braarudii* and *C. leptoporus* show a consistent decline (Fig. 1, 2a,c, 4a,b). This observation points to a unifying factor driving the concurrent isotopic depletion in the calcite and organic matter, which is a consequence of alterations in the isotopic composition of the shared internal pool (Fig. 2a,c, 4b). Under $CO_2$-limiting conditions, where growth rates are $CO_2$-limited and imply a diminished internal carbon pool, a strong $CO_2$ gradient is established between the highly utilised (and therefore low concentration) intracellular carbon pool and the ambient seawater that facilitates high rates of passive diffusion of isotopically depleted $CO_2$ (~9 ‰ depleted compared to DIC, for $\delta^{13}C$) into the coccolithophore cell. Within the carbon depleted internal pool, there is very little carbon for isotopic exchange, such that the carbon isotopes of the internal pool tend towards that of the carbon supply. The calcite and organic matter then reflect the $CO_2$-induced depletion in isotopic values of the starved carbon pool, which has allowed no carbon isotopic equilibration as both calcification and organic matter fixation draw carbon from

the same intracellular carbon pool (Tchernov *et al.*, 2001; Kaplan & Reinhold, 2003; Holtz *et al.*, 2017). A strong coupling between $\Delta^{13}C_{Coccolith}$ and $\Delta^{13}C_{ORG}$ suggest that the primary substrate for the internal carbon pool is $CO_2$ (Hermoso, 2015) and that a mechanistic relationship exists between the cell cycle and calcification, which has previously been suggested for *C. braarudii* (Walker *et al.*, 2018).

The internal carbon pool represents carbon dissolved in a water media such that there are sufficient oxygen atoms available from $H_2O$ to equilibrate the oxygen isotopes given sufficient residence time, which dilutes the heavy oxygen isotopic signal of the diffusing $CO_2$ (Hermoso et al., 2016). An aggravated $CO_2$ gradient stems from the extremely high carbon demands ($\mu_{opt}$ at high $CO_2$ concentrations, high PIC, large cell size) for these species and severely starved intracellular carbon concentrations at low [$CO_2$]. Moreover, passive $CO_2$ diffusion can be enhanced under low [$CO_2$] through $H^+$ efflux to maintain pH homeostasis during calcification or during $Ca^{2+}/H^+$ exchange (Mackinder *et al.*, 2010; Taylor *et al.*, 2011).

The difference in $\Delta^{18}O_{Coccolith}$ offsets for *C. braarudii* and *C. leptoporus* suggest contrasting mechanisms for intracellular pool equilibration, where *C. braarudii* possesses a large intracellular pool with long carbon residence times, allowing isotopic equilibration and $\mu_{opt}$ values at higher $CO_2$ concentrations. Moreover, $\Delta^{18}O_{Coccolith}$ values similar to those of inorganic calcite suggest high intracellular pH buffering capacity in *C. braarudii* (Fig. 2b, 3b). Whereas *C. leptoporus* possesses a smaller intracellular carbon pool (compared to *C. braarudii*), which is more susceptible to depletion, but higher intracellular pH and long residence times for carbon causing an isotopic offset in $\Delta^{18}O_{Coccolith}$ values and $\mu_{opt}$ values at higher $CO_2$ concentrations. The size of the internal carbon pool can be said to be proportional to the size of the cell (Fig. S2). Moreover, the contrasting

size of their intracellular carbon pool is marked by the magnitude of isotopic change under $CO_2$-limiting conditions where *C. braarudii* exhibits small offsets in $\delta^{13}C$ due to a large intracellular carbon pool but *C. leptoporus* displays large depletion in $\delta^{13}C$ due to a comparatively smaller internal pool.

Observations reported here are unlikely to be caused by hydroxylation/hydration of $CO_2$ to $HCO_3^-$ as changes in $\Delta^{18}O_{Coccolith}$ values with changing $CO_2$ are negligible (Fig. 2b, 3b, 4d). Moreover, the depletion in $\Delta^{13}C_{ORG}$ as observed at $CO_2$ below 10 μmol $kg^{-1}$ should not occur during hydration/hydroxylation of $CO_2$ into $HCO_3^-$ because $CO_2$ serves as the primary substrate for RuBisCO and therefore should not be affected by hydration/hydroxylation reactions. Also, the likely presence of carbonic anhydrase in coccolithophores would catalyse this reaction (Reinfelder, 2010).

**Vital effects for *G. huxleyi* and *G. oceanica* show greatest change during low carbon demand and high carbon supply due to the short carbon residence times in their internal carbon pools.**

The isotopic shift in $\Delta^{13}C_{Coccolith}$ values for *G. huxleyi* and *G. oceanica* at ~ 17 μmol $kg^{-1}$ (pH 8.1) is caused by changes in the mode of carbon uptake (Kottmeier *et al.*, 2014). $CO_2$ diffusion driven carbon uptake is prominent at high [$CO_2$], causing isotopic depletion in the $\delta^{13}C$ of the carbon pool, while active uptake of isotopically heavy ($\delta^{13}C$) $HCO_3^-$ brings the pool closer to inorganic values at low [$CO_2$] (Fig. 5a). Active carbon uptake is also evident as growth rates are not limited under low $CO_2$ conditions. Indeed, the best growth conditions for these species appear to be at low $CO_2$ (Fig. 1; 5a-inset). Alternatively, heavier $\Delta^{13}C_{Coccolith}$ values at low $CO_2$/high pH can also be attributed to preferential leakage of lighter $CO_2$ from the internal carbon pool. $CO_2$ leakage was previously suggested to be prominent in *G. huxleyi* at low [$CO_2$] (Rost *et al.*, 2006). Under low $CO_2$, the intracellular carbon

pool has a higher carbon concentration than ambient seawater, causing $CO_2$ leakage, while at high $CO_2$ (>17 µmol $kg^{-1}$, pH < 8.1), diffusion of lighter $CO_2$ into the cell causes isotopic depletion of the intracellular carbon pool, and consequently, the coccolith calcite. This indicates that the intracellular carbon concentration in these species is ≥ 17 µmol $kg^{-1}$ (Liu *et al.*, 2021).

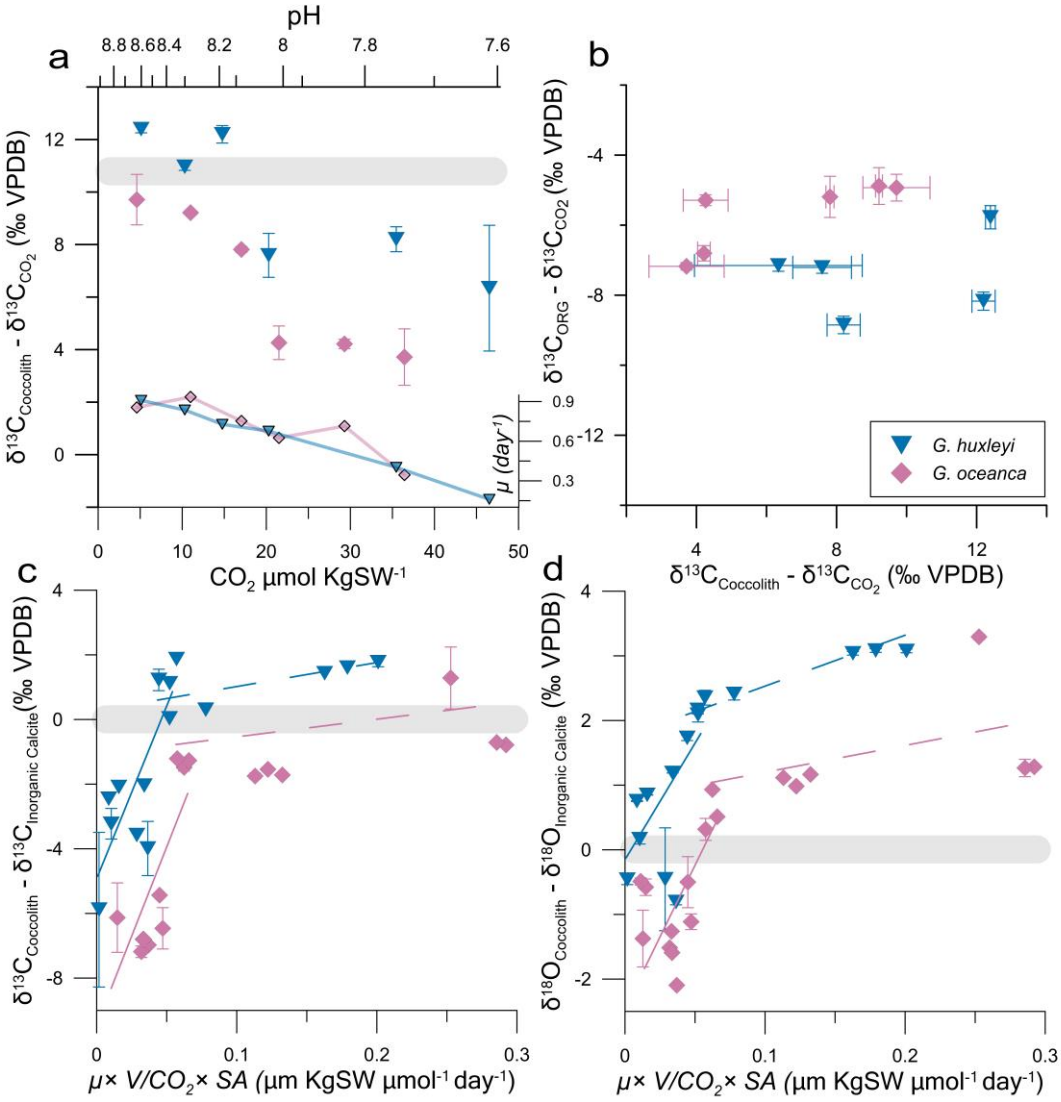


**Figure 5: (a)** $\delta^{13}C_{Coccolith} - \delta^{13}C_{CO2}$ for *G. huxleyi* (▼) and *G. oceanica* (◆) with growth rate ($\mu$, $day^{-1}$) plotted as a subset. Grey line denotes inorganic calcite. **(b)** $\Delta^{13}C_{Coccolith}$ vs. $\Delta^{13}C_{ORG}$ **(c)** $\delta^{13}C_{Coccolith} - \delta^{13}C_{Inorganic\ Calcite}$ vs. $\mu \times V/CO_2 \times SA$ (d) $\delta^{18}O_{Coccolith} - \delta^{18}O_{Inorganic\ Calcite}$ vs. $\mu \times V/CO_2 \times SA$. The line thickness at 0 ‰ accounts for the standard deviation in the isotopic composition of the inorganic calcite. Note that in (a) and (b), the replicates are averaged, while in (c) and (d), they are not averaged. $\delta^{13}C_{ORG} - \delta^{13}C_{DIC}$ vs $\mu \times V/CO_2 \times SA$ can be found in the Supplementary Material (Fig. S5).

Although shifts in carbon uptake mechanism have been documented through $\Delta^{13}C_{ORG}$ (as $\varepsilon_p$) at [$CO_2$] of ~13 μmol $kg^{-1}$ (Laws *et al.*, 1998; Keller & Morel, 1999; Burkhardt *et al.*, 1999a; Tchernov *et al.*, 2014), in this study, *G. huxleyi* and *G. oceanica* exhibited only minor changes in $\Delta^{13}C_{ORG}$ (Fig. 2c, 5b), suggesting minimal changes in the isotopic fractionation of carbon into the organic matter. Moreover, the $\Delta^{13}C_{ORG}$ values for *G. huxleyi* are significantly more enriched (6 – 9 ‰) than those reported for *G. huxleyi* RuBisCO previously (11.1 ‰, Boller et al. 2011). These observations can be due to ample carbon supply that is meeting the cell's carbon demand owing to their small size (large SA:V ratio), and active carbon uptake under low $CO_2$ concentrations (Table S1). Moreover, no changes in Rayleigh fractionation are observed (through minimal changes in $\Delta^{13}C_{ORG}$) due to carbon supply being higher than demand under all pH/$CO_2$ conditions.

The lack of changes in $\Delta^{13}C_{ORG}$ values for *G. huxleyi* and *G. oceanica* in contrast to the observed changes in $\Delta^{13}C_{Coccolith}$ and $\Delta^{18}O_{Coccolith}$ values indicate a short carbon residence time for these species. A short residence time causes calcification and photosynthesis to "see" different carbon pools as if the processes were offset in time and/or space. The small cell size of *G. huxleyi* and *G. oceanica* (compared to other species in this study), corresponds to a small internal carbon pool in these species, and reduced internal pH buffering capacity. The higher SA:V ratio and fast calcification rates as reported previously (Balch *et al.*, 1993; Daniels *et al.*, 2014) lead to high $CO_2$ fluxes in and out of the cell, causing short residence times for carbon in the intracellular carbon pool. Alternatively, the lack of changes in $\Delta^{13}C_{ORG}$ values are possible if resource allocation favoured towards photosynthesis rather than calcification. This seems plausible since *G. huxleyi* exhibits evidence towards a decoupling between calcification photosynthesis as it

can still grow non-calcified in nature or when calcification is disrupted through calcium limitation in the laboratory (Paasche, 2001; Trimborn *et al.*, 2007).

$\Delta^{13}C_{Coccolith}$ and $\Delta^{18}O_{Coccolith}$ values for *G. huxleyi* and *G. oceanica* exhibit kinetic isotopic fractionation as both isotopic systems show depleting isotopic values with increasing diffusive $CO_2$ supply (Fig. 5c,d). This observation agrees with Hermoso (2015), where it was suggested that the source of carbon for the internal carbon pool in coccolithophores is mainly $CO_2$. Moreover, there is a pronounced change in the gradient of $\Delta^{13}C_{Coccolith}$ and $\Delta^{18}O_{Coccolith}$ values with increasing $\mu/CO_2$, illustrated by the line fits in Figure 5c, d. Under conditions of high $CO_2$/low pH and reduced growth rates, diffusive (isotopically light) $CO_2$ appears to imprint a small internal carbon pool, therefore, $\Delta^{13}C_{Coccolith}$ values become depleted in proportion to the excess $CO_2$ supply (Fig. 5c). As the $\mu/CO_2$ ratio increases, the demand for carbon escalates while the diffusive carbon supply diminishes, which results in enriched isotopic values in these species (Fig. 5c,d; Fig. 4 in McClelland et al., 2017).

Diffused $CO_2$ should experience a more pronounced depletion in $\delta^{18}O$ compared to $\delta^{13}C$ (Thiagarajan *et al.*, 2011). This is because the mass difference between $^{16}O$-$^{18}O$ is larger than that of $^{12}C$-$^{13}C$, leading to greater fractionation between O isotopes (Wanner & Hunkeler, 2019). In contrast, our study exhibits a larger depletion in the $\Delta^{13}C_{Coccolith}$ (depletion of up to ~ 6 ‰ from inorganic values at highest $CO_2$, Fig. 5c) compared to the $\Delta^{18}O_{Coccolith}$ (depletion of ~ 2 ‰ from inorganic values at highest $CO_2$, Fig. 5d). The smaller magnitude of change in $\delta^{18}O$ compared to $\delta^{13}C$ could be due to the small size of the internal carbon pool and rapid turnover time (fluxes in and out of the cell) for carbon which allows for larger isotopic shifts in $\delta^{13}C$ due to the addition of $CO_2$, but a greater abundance

of oxygen through $H_2O$ allows for partial equilibration of $\delta^{18}O$ in the intracellular carbon pool.

A departure from the steep gradient between $\Delta^{13}C_{Coccolith}$ and $\mu/CO_2$ emerges at high $\mu/CO_2$ (Fig. 5c, d), indicating an impact of the active $HCO_3^-$ uptake as is predicted for photosynthetic fixation (Laws *et al.*, 2002). This observation points to an active carbon supply mechanism within the cell, which could alleviate carbon limitation as suggested in previous studies (Kottmeier et al., 2016b; Zhang et al., 2021a). This is consistent with our growth rate optima for *G. huxleyi* and *G. oceanica,* which is at lower $CO_2$ concentrations compared to other species. Alternatively, a higher intracellular carbon concentration could enhance $CO_2$ leakage, driving the internal pool isotopically heavy. Distinguishing between active $HCO_3^-$ uptake and CA-facilitated inter-conversion of $HCO_3^-$ and $CO_2$, however, remains challenging due to the similarity in resultant isotopic compositions (Zeebe & Wolf-Gladrow, 2001; Uchikawa & Zeebe, 2012), despite evidence for the presence of external carbonic anhydrase in *G. huxleyi* (see for example, Rost et al. 2003; Stojkovic et al. 2013).

It is important to note that *G. oceanica* consistently exhibits more depleted $\Delta^{13}C_{Coccolith}$ and $\Delta^{18}O_{Coccolith}$ values but isotopically enriched $\Delta^{13}C_{ORG}$ values than *G. huxleyi*. Similar offsets between these two species have been previously observed (Hermoso *et al.*, 2016b). Such an effect could be causal, that is, removal of depleted carbon from the intracellular carbon pool into calcite leaves the pool isotopically enriched from which the organic matter draws its carbon. Alternatively, the smaller carbon isotopic fractionation into $\Delta^{13}C_{ORG}$ for *G. oceanica* compared to *G. huxleyi* could imply a smaller internal carbon pool in *G. oceanica*, which is then more susceptible to overprinting from the high diffusive supply rate of $CO_2$ at low pH and has less $CO_2$ to lose diffusively at low $CO_2$ (high pH) due to its larger cell

size. However, since the size of internal carbon pools are proportional to cell size, we suspect a comparatively larger internal pool in *G. oceanica*.

The $\Delta^{13}C_{Coccolith}$ and $\Delta^{18}O_{Coccolith}$ trends observed for *G. huxleyi* and *G. oceanica* in this study could also be a consequence of hydration/hydroxylation related kinetic isotope effects. However, the known presence of carbonic anhydrase negates this hypothesis (Rost *et al.*, 2003). Moreover, the trends in $\Delta^{13}C_{Coccolith}$ and $\Delta^{18}O_{Coccolith}$ show a significant shift in isotopic values at $CO_2$ of 17 μmol $kg^{-1}$ (pH 8.1), which cannot be explained by hydration/hydroxylation related kinetic isotope effects. Such a scenario is only possible if hydration/hydroxylation related kinetic isotope effects were taking place in addition to $CO_2$ leakage / $HCO_3^-$ uptake (as seen through the horizontal lines and enriched/heavy isotopic values in Fig. 3 and 5c,d). Moreover, photosynthetic carbon fixation and calcification would need to have distinct intracellular carbon pools such that carbonic anhydrase and Rayleigh fractionation due to RuBisCO do not affect the carbon pool allocated to calcification only. Such a mechanism could resolve the discrepancy between $\Delta^{13}C_{Coccolith}$ and $\Delta^{13}C_{ORG}$ values.

**Carbon vital effects in *C. carterae* are sensitive to changing carbon supply but long carbon residence times alleviate oxygen vital effects.**

$\Delta^{13}C_{Coccolith}$ values in *C. carterae* exhibit a linear trend despite varying growth rates across different $CO_2$ concentrations (Fig. 6a). This species lacks a covariation in $\Delta^{13}C_{Coccolith}$ and $\Delta^{18}O_{Coccolith}$ unlike any other species studied here (Fig 3, 6c,d). Moreover, depletion in the $\Delta^{13}C_{Coccolith}$ ($R^2$ = 0.86) and $\Delta^{13}C_{ORG}$ ($R^2$ = 0.88) linearly correlate with increasing [$CO_2$], suggesting that organic carbon fixation and calcification in *C. carterae* source their carbon from a shared intracellular carbon pool, with the same change in the carbon pool being reflected in both organic and inorganic carbon reservoirs (Fig. 6b). Such a shared intracellular carbon pool

appears to be integral, a concept previously observed (Liu *et al.*, 2018, 2021). The linear relationship also suggests high sensitivity to $CO_2$ concentrations across high growth conditions as well as $H^+$-inhibited growth rates, and that the carbon pool assimilates its carbon mainly from $CO_2$ (Hermoso, 2015). It is important to note, however, that the plateau between $\Delta^{13}C_{Coccolith}$ values and $\mu/CO_2$ (Fig. 6c) highlights either a notable contribution from $HCO_3^-$ uptake at lower [$CO_2$], or a diffusive loss of isotopically light $CO_2$ from the intracellular pool. A similar change is also evident in $\Delta^{13}C_{ORG}$ (Fig. S5), further suggesting a shared internal carbon pool.

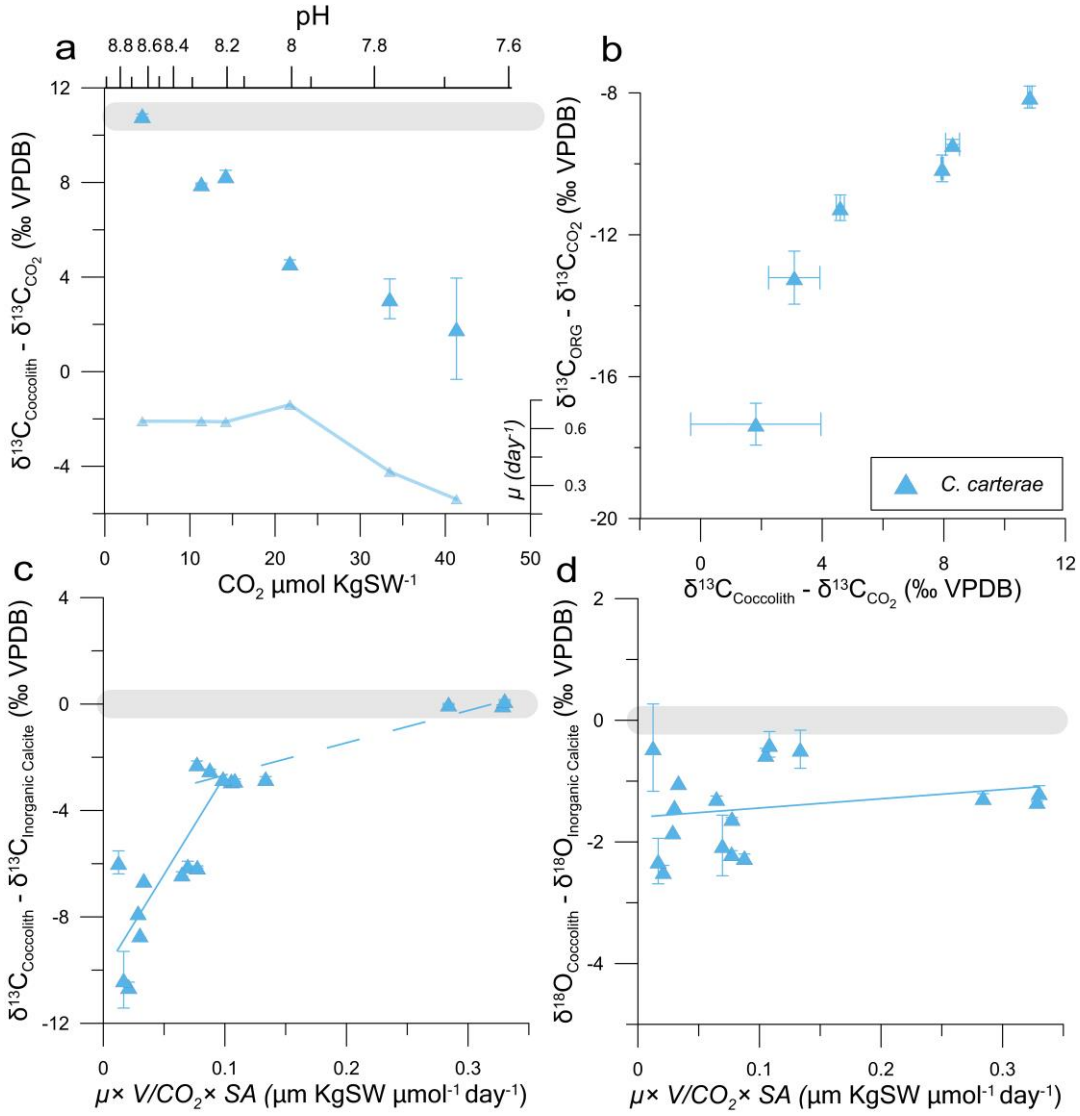


**Figure 6: (a)** $\delta^{13}C_{Coccolith} - \delta^{13}C_{CO2}$ for *C. carterae* (▲) with growth rate ($\mu$, day$^{-1}$) plotted as a subset. Grey line denotes inorganic calcite. **(b)** $\Delta^{13}C_{Coccolith}$ vs. $\Delta^{13}C_{ORG}$ **(c)** $\delta^{13}C_{Coccolith} - \delta^{13}C_{Inorganic\ Calcite}$ vs. $\mu \times V/CO_2 \times SA$ **(d)** $\delta^{18}O_{Coccolith} - \delta^{18}O_{Inorganic\ Calcite}$ vs. $\mu \times V/CO_2 \times SA$. The line

thickness at 0 ‰ accounts for the standard deviation in the isotopic composition of the inorganic calcite. Note that in (a) and (b), the replicates are averaged, while in (c) and (d), they are not averaged. $\delta^{13}C_{ORG}$ - $\delta^{13}C_{DIC}$ vs $\mu \times V/CO_2 \times SA$ can be found in the Supplementary Material (Fig. S5). $\delta^{13}C_{ORG}$ - $\delta^{13}C_{DIC}$ vs $\mu \times V/CO_2 \times SA$ can be found in the Supplementary Material (Fig. S5).

Regarding $\Delta^{18}O_{Coccolith}$ values, our observations align with the isotopic pattern of pH-corrected inorganic calcite, albeit influenced by a significant vital effect of ~2 ‰ (Fig. 2b, 3b, 6d). This finding suggests that the calcite precipitation occurs in oxygen isotopic equilibrium with the DIC, and the intracellular carbon pool comprises $CO_2$ fully isotopically equilibrated with $H_2O$. The observed isotopic offset towards depleted values is attributed to elevated intracellular pH during calcification across all treatments, a phenomenon comparable to observations in *C. leptoporus*. This highlights the physiological similarity between *C. carterae* and *C. leptoporus* where an offset towards depleted values in $\Delta^{18}O_{Coccolith}$ values and a $\mu_{opt}$ at relatively higher $CO_2$ concentrations could be caused by a higher intracellular pH and long residence times for carbon allowing sufficient time for isotopic equilibration.

*C. carterae* stands out from the other species in this study, with a distinctive cellular composition characterised by a low PIC content and a high POC content (Gafar et al., 2019; McClelland et al., 2017). In conjunction with the propensity of this species for rapid calcite production (yielding potentially more than 100 coccoliths per cell), and a large intracellular carbon pool that is likely due to a large cell size, the relatively modest extraction from this pool (due to the low PIC content) ensures ample time for intracellular carbon pool replenishment and equilibration with the DIC-$H_2O$ system. Moreover, a small SA:V ratio due to its large cell size reduces the area available for unequilibrated $CO_2$ diffusion/leakage to take place (Table S1). This can be observed in the unchanging $\Delta^{18}O_{Coccolith}$ values suggesting ample equilibration time for the oxygen isotopes across the different carbon species of the intracellular carbon pool, which is generally the rate limiting

equilibration within the calcification fluid-DIC-$H_2O$ system. Additionally, high carbonic anhydrase activity can cause rapid isotopic equilibration and therefore, alleviate kinetic isotope effects (Uchikawa and Zeebe, 2012; Thaler et al., 2017).

**Trends in carbon and oxygen isotopes as a measure of species-specific intracellular carbon residence times.**

Interrogation of the data indicated a relationship between the species-specific gradient of the $\Delta^{13}C_{Coccolith}$ vs. $\Delta^{18}O_{Coccolith}$ relationship, and the gradient of the $\Delta^{13}C_{ORG}$ vs. $\Delta^{13}C_{Coccolith}$ relationship (Fig. 7a). The residence time of carbon in an internal carbon pool may be the unifying factor driving this correlation. Carbon residence time is controlled by either the size of the internal pool and/or the rate of supply/demand (Hermoso *et al.*, 2016b). The steepness of the $\Delta^{13}C_{Coccolith}$ vs. $\Delta^{18}O_{Coccolith}$ gradient is likely driven in part by the time available for equilibration of oxygen isotopes amongst all the carbon ionic species and water, the longest equilibration time among the isotope systems (Zeebe & Wolf-Gladrow, 2001). Further, the degree to which carbon utilisation of an internal carbon pool drives Rayleigh fractionation within that internal carbon pool, and whether calcification and photosynthesis draw from an isotopically similar carbon pool also acts as measures of the residence time of carbon inside the cell (Sekino & Shiraiwa, 1996; Rickaby *et al.*, 2010; Bolton & Stoll, 2013; Holtz *et al.*, 2015; Hermoso, 2015; Hermoso *et al.*, 2016b).

The $\Delta^{13}C_{Coccolith}$ and $\Delta^{18}O_{Coccolith}$ values of coccolith calcite can be compared against theoretical maximums of pH-related and $CO_2$-diffusion-related change in $\Delta^{13}C_{Coccolith}$ and $\Delta^{18}O_{Coccolith}$ values (Fig. 7a; Chen et al., 2018). pH-related depletion in $\delta^{18}O$ values is a primary process that influences stable isotopes in coccolith calcite and is given by a horizontal slope (slope = 0; Zeebe, 1999). However, it is important to note that pH does not influence the $\delta^{13}C$ values of calcite, despite the distinct isotopic

compositions of various DIC species because, within an isotopically closed system, any alterations in $\delta^{13}C$ solely result from shifts in the $\delta^{13}C$ of the overall DIC (e.g., by adding or removing carbon of a certain $\delta^{13}C$ value; Zeebe and Wolf-Gladrow, 2001).

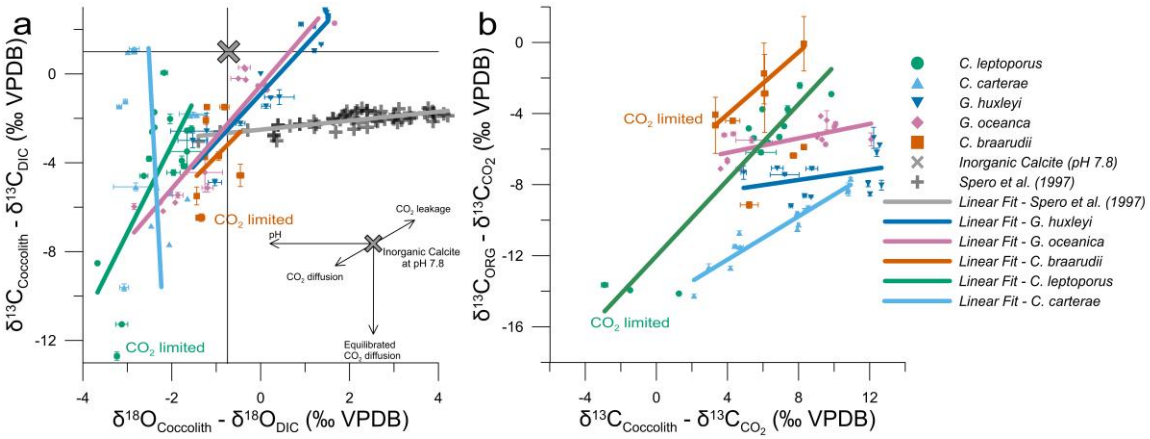


**Figure 7: (a)** $\Delta^{18}O_{Coccolith}$ vs. $\Delta^{13}C_{Coccolith}$ for *C. braarudii* (■), *C. leptoporus* (●), *C. carterae* (▲), *G. huxleyi* (▼), and *G. oceanica* (◆). Data from Spero et al. (1997) (+) and inorganic calcite (×) has been included for comparison. The vector diagram **(inset)** shows the isotopic effects of unequilibrated $CO_2$ diffusion (diffusion of 9 ‰ depleted $CO_2$ and diffusion related $CO_2$ fractionation), $CO_2$ leakage and photosynthetic uptake, and pH. **(b)** $\Delta^{13}C_{Coccolith}$ vs. $\Delta^{13}C_{ORG}$. Note that the $\Delta^{13}C_{ORG}$ gradients for *C. braarudii* and *C. leptoporus* are calculated using $\Delta^{13}C_{ORG}$ values at $CO_2$-limiting and values at the lowest non-limiting $CO_2$ concentrations.

Another theoretical maximum can be given by diffusive $CO_2$ that influences stable isotopes in coccolith calcite (Chen *et al.*, 2018). This process primarily results in a depletion of $\delta^{13}C$ values, provided that equilibration is established between diffusive $CO_2$ and the DIC-$H_2O$ system (Fig.7a-inset). This depletion occurs because the $\delta^{13}C$ of $CO_2$ is ~9 ‰ more depleted than $HCO_3^-$. The introduction of $CO_2$ to an isotopically closed system (e.g., intracellular carbon pool) results in an overall depletion of the $\delta^{13}C$ in the system in proportion to the amount of carbon therein. Furthermore, the equilibration of $H_2O$ and $CO_2$ causes isotopic equilibration in $\delta^{18}O$ values, but with slow (pH-dependent) kinetics, thus yielding a vertical slope (slope = infinity, Fig. 7a-inset; Zeebe and Wolf-Gladrow, 2001).

Under non-equilibrium conditions between diffusive $CO_2$ and $H_2O$, the $\delta^{18}O$ of $CO_2$ is heavier than that of $CO_3^{2-}$, $HCO_3^-$ and $H_2O$ (Zeebe & Wolf-Gladrow, 2001).

The emergence of a linear trend with a finite, non-zero slope in this dataset is a result of kinetic isotope effects impacting both $\delta^{18}O$ and $\delta^{13}C$ (McConnaughey, 1989b,a; Adkins *et al.*, 2003; Chen *et al.*, 2018). Two primary processes contributing to these kinetic isotope effects have been identified in this study: (unequilibrated) $CO_2$ diffusion, and $CO_2$ leakage related fractionation (Fig. 7a-inset). The unequilibrated diffusion of $CO_2$ across the cell membrane is driven by concentration gradients, which lead to depletions in both $\delta^{18}O$ and $\delta^{13}C$ compared to the residual reservoir (i.e., ambient seawater). Furthermore, isotopic fractionations in the diffusing $CO_2$ are a consequence of the isotopic composition of $CO_2$ (depleted in $\delta^{13}C$, enriched in $\delta^{18}O$ compared to DIC), which is coupled with the kinetic isotope effects of diffusion (depletion in both $\delta^{13}C$ and $\delta^{18}O$; O'Leary, 1984; Thiagarajan et al., 2011; Zeebe and Wolf-Gladrow, 2001). Moreover, $\delta^{18}O$ of the diffusing $CO_2$ can equilibrate with intracellular $H_2O$. The combination of these processes leads to a more substantial depletion in $\delta^{13}C$ than $\delta^{18}O$.

If complete equilibration of $\delta^{18}O$ of $CO_2$ in the intracellular carbon pool with the ambient seawater results in a vertical slope, the gradients observed here can be attributed to the extent of equilibration between the intracellular carbon pools and the DIC-$H_2O$ system. This in turn, serves as an indicator of the residence time of the intracellular carbon pool (Fig. 7a). The gradient between $\Delta^{13}C_{Coccolith}$ and $\Delta^{18}O_{Coccolith}$ values can be calculated as follows (Table S3):

$$Residence\ Time \propto \frac{\Delta^{13}C_{\mathrm{Coccolith}}}{\Delta^{18}O_{\mathrm{Coccolith}}} = \frac{Min(\Delta^{13}C_{\mathrm{Coccolith}}) - Max(\Delta^{13}C_{\mathrm{Coccolith}})}{Min(\Delta^{18}O_{\mathrm{Coccolith}}) - Max(\Delta^{18}O_{\mathrm{Coccolith}})}$$

As previously discussed, the pronounced correlation between $\Delta^{13}C_{Coccolith}$ and $\Delta^{18}O_{Coccolith}$ values for *G. oceanica* and *G. huxleyi* arise due to kinetic isotope effects

as a consequence of the short residence time for carbon within their intracellular carbon pool (Fig. 7a, 8; McConnaughey 1989a). Conversely, $\Delta^{13}C_{Coccolith}$ and $\Delta^{18}O_{Coccolith}$ values for *C. braarudii* are a consequence of long residence times for carbon, and intracellular pH buffered with the ambient pH. *C. leptoporus* exhibits long residence times for carbon in its relatively smaller internal carbon pool due to elevated intracellular pH compared to the ambient seawater. *C. braarudii* and *C. leptoporus* produce relatively steep gradients in their $\Delta^{13}C_{Coccolith}$ and $\Delta^{18}O_{Coccolith}$ values due to isotopic depletion caused by $CO_2$ diffusion under $CO_2$-limiting conditions (Fig 7a, 8). Finally, *C. carterae* exhibits a large and well-equilibrated internal carbon pool with long residence times for carbon (Fig. 8). Similar to *C. leptoporus*, *C. carterae* shows elevated intracellular pH, as evidenced by its consistently depleted $\Delta^{18}O_{Coccolith}$ values (Fig. 7a). Notably, *C. carterae* exhibits a near-vertical slope, i.e., minimal change in $\delta^{18}O$ with a trend closely resembling equilibrated diffusive $CO_2$, characterised by $\delta^{13}C$ depletion solely due to addition of (9 ‰ depleted) $CO_2$.

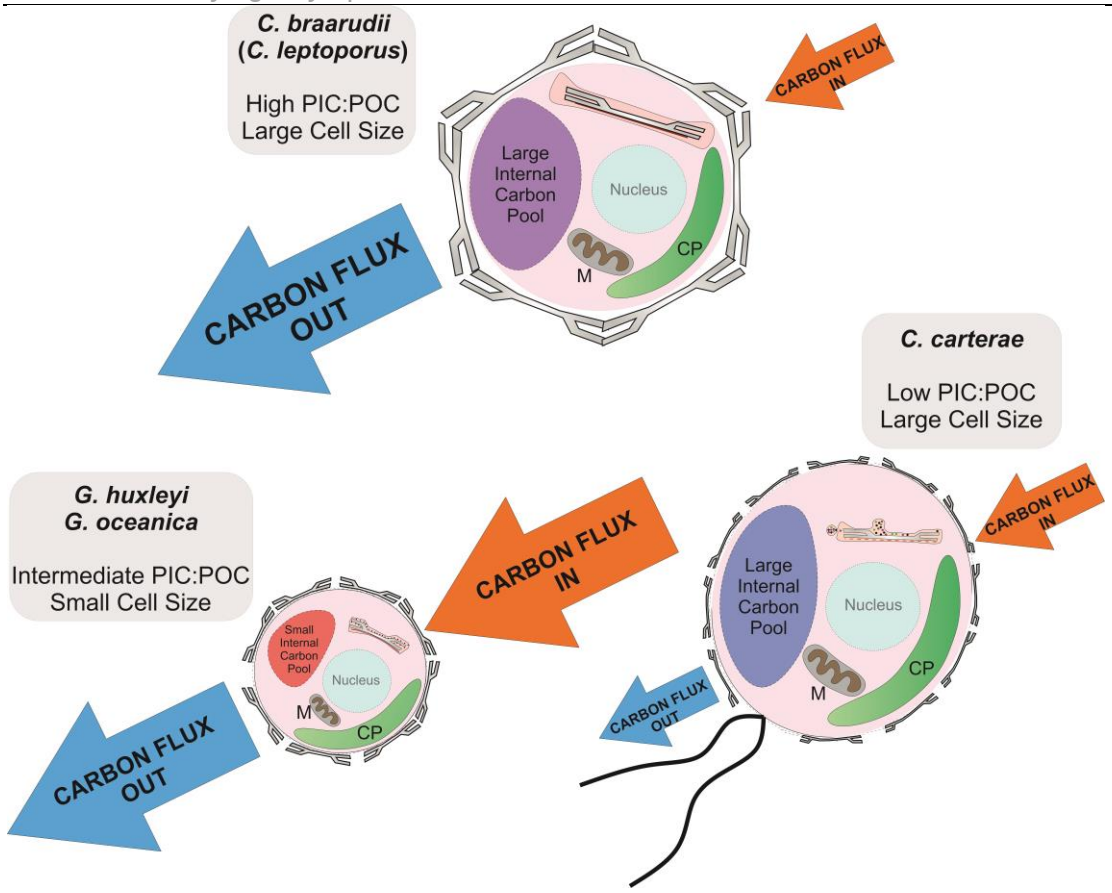


**Figure 8:** A diagram elucidating the three primary carbon regulation categories identified in this study. The magnitude of the blue and orange arrows signifies the extent of carbon fluxes, with inflows and outflows regulated by the SA:V ratio and PIC:POC ratio, respectively. The size of the internal carbon pool corresponds to cell size, and the colour of the internal carbon pool signifies its ability to raise intracellular pH (blue – higher pH; purple – pH similar to ambient; red – pH lowered by $CO_2$ fluxes). Although *C. leptoporus* is categorised alongside *C. braarudii* because of its high PIC:POC ratios and similarity in isotopic trends, it serves as an intermediary between *C. braarudii* and *C. carterae.* This positioning is attributed to its capacity to elevate intracellular pH akin to *C. carterae*. M: mitochondrion, CP: Chloroplast.

Gradients between $\Delta^{13}C_{ORG}$ and $\Delta^{13}C_{Coccolith}$ values for each species can also offer insights into the internal dynamics of the intracellular carbon pool (Fig. 7b). A steep gradient (e.g., *C. carterae*) implies a shared carbon pool between calcification and organic matter fixation such that each process draws from the same carbon pool, while a shallow gradient (e.g., *G. huxleyi*) suggests a decoupling of these processes due to a short residence time of carbon within the intracellular carbon pool. Therefore, the gradient between $\Delta^{13}C_{ORG}$ and $\Delta^{13}C_{Coccolith}$ is directly

proportional to the residence time of carbon within the intracellular carbon pool, and can be calculated as follows (Fig. 7b; Table S3):

$$Residence\ Time \propto \frac{\Delta^{13}C_{\mathrm{ORG}}}{\Delta^{13}C_{\mathrm{Coccolith}}} = \frac{Min(\Delta^{13}C_{\mathrm{ORG}}{}^{a}) - Max(\Delta^{13}C_{\mathrm{ORG}}{}^{a})}{Min(\Delta^{13}C_{\mathrm{Coccolith}}) - Max(\Delta^{13}C_{\mathrm{Coccolith}})}$$

[a]Note that the gradient is calculated using $\Delta^{13}C_{ORG}$ values at $CO_2$ concentrations of 2.83 μmol $kg^{-1}$ ($CO_2$-limiting) and 11.13 μmol $kg^{-1}$ (lowest non-limiting $CO_2$ concentration) for *C. braarudii.* This choice is made because $\Delta^{13}C_{ORG}$ values again show depletion with increasing $CO_2$ (Fig. 2c, 7b).

The relationship between the gradients of $\Delta^{13}C_{Coccolith}$ vs. $\Delta^{18}O_{Coccolith}$ and $\Delta^{13}C_{ORG}$ vs. $\Delta^{13}C_{Coccolith}$ can therefore be used as two independent measurements for characterising species-specific residence time of carbon within the intracellular carbon pool (Fig. 9). The carbon residence times obtained from this method agree with studies that have previously quantified the size of the internal carbon pool using stable isotopes. For instance, in agreement with Hermoso et al. (2016), this study suggested that high $CO_2$ diffusion into the cell leads to heavy $\delta^{18}O_{Coccolith}$ values and small cell size (high SA:V ratio, Table S1) results in short residence times for carbon in the cell. Additionally, this study shows that the $CO_2$ is the primary carbon substrate for the internal carbon pool; and that the degree of utilisation of the carbon pool (e.g., through PIC production) determines the extent of equilibration possible for its isotopes with the ambient DIC and $H_2O$, such that for species with large internal carbon pools, long carbon residence time allows re-equilibration of its isotopes, especially under non-$CO_2$ limiting conditions (Hermoso, 2014, 2015).

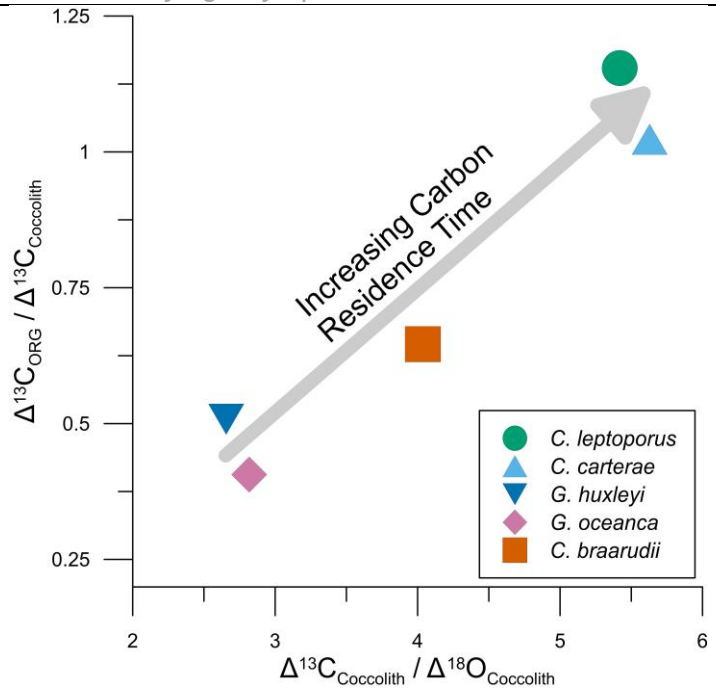


**Figure 9:** A plot between $\Delta^{13}C_{Coccolith}$ vs. $\Delta^{18}O_{Coccolith}$ and $\Delta^{13}C_{ORG}$ vs. $\Delta^{13}C_{Coccolith}$ values as two independent measurements of species-specific residence time for carbon in the intracellular carbon pool. Note that the $\Delta^{13}C_{ORG}$ gradients for *C. braarudii* and *C. leptoporus* are calculated using $\Delta^{13}C_{ORG}$ values at $CO_2$-limiting and values at the lowest non-limiting $CO_2$ concentrations.

The differential isotopic responses across various coccolithophore species presented in this study can offer a valuable tool to understand the dynamics of carbon regulation in coccolithophores that reveal susceptibility to environmental change and can be used to trace changing physiology in response to past environmental change. With recent insights into the mechanism of coccolith calcification in *G. huxleyi*, the diffusion-limited rates of calcification provide further insights into the turnover times for carbon in a small coccolithophore cell (Avrahami *et al.*, 2023). Furthermore, species-specific responses of coccolithophores to varying $CO_2$ concentrations have implications for understanding how these organisms might fare in the face of ocean acidification. This study contributes to a more comprehensive view of the geochemical dynamics that lead to vital effects and highlights the use of stable isotopes as a tool to understand the mechanisms of carbon regulation within coccolithophores

and broadly for phytoplankton. Organisms such as coccolithophores, with a calcification regime akin to a "closed system" due to their intracellular calcification mechanism provide significant differences to "open system" calcifying organisms such as foraminifers and corals. By harnessing clumped isotopes, numerical modelling and isotopic analyses on a finer scale, the implications of this work can be expanded to unravel carbon regulation in more complex organisms, thereby providing insights into the marine carbon cycle.

**Summary**

This study provides insights into the isotopic responses of coccolithophores to changing environmental conditions. The findings gleaned from this research, which employs carbon and oxygen isotopic approaches, show that isotopic gradients between $\Delta^{13}C_{Coccolith}$ –$\Delta^{18}O_{Coccolith}$ values and $\Delta^{13}C_{Coccolith}$ – $\Delta^{13}C_{ORG}$ values offer a quantitative indicator of the residence time of carbon within the intracellular carbon pool. This residence time plays a critical role in the physiological dynamics of coccolithophores, and the size of this internal carbon pool is proportional to the size of the coccolithophore cell. Moreover, certain species, such as *C. carterae* and *C. leptoporus* can elevate their intracellular pH to minimise $CO_2$ leakage. An exception to the cell size – internal carbon pool size relationship is *G. huxleyi*, which likely has a carbon pool larger than that of *G. oceanica* despite having a smaller cell size. This is evidenced by the isotopic offsets in the calcite and organic matter, which are heavier in the coccolith calcite for *G. huxleyi* compared to *G. oceanica.* Such an offset can be brought forward if *G. huxleyi* has a larger internal carbon pool, perhaps due to better $HCO_3^-$ transport that allows better equilibration at high $CO_2$, but the larger carbon pool causes more $CO_2$ loss under low $CO_2$ conditions due to its higher SA:V ratio (due to the small cell size) compared to *G. oceanica.*

The decoupling of carbon isotopes in calcite and organic matter for *G. huxleyi* and *G. oceanica* suggest a short residence time for carbon and a small size of the internal carbon pool. On the other extreme lies *C. carterae*, which exhibits extended residence times for carbon and the capacity for full equilibration. Such observations underscore species-specific nature of carbon residence times, reflecting a spectrum of physiologies in coccolithophores and possibly broadly in phytoplankton communities.

**Supplementary Material**

The supplementary material contains a detailed description of specific methodologies used in this study. We have also discussed our results with previous studies in the Results section (with corresponding plots). Additionally, plots (e.g., growth rates, $\Delta^{13}C_{Coccolith}$ and $\Delta^{18}O_{Coccolith,}$ and $\Delta^{13}C_{ORG}$) from the main document have been replotted to show every biological replicate, instead of their averages. The tables contain calculated stable isotope values of inorganic calcite based on Zeebe (1999), Kim & O'Neil (1997) and Watkins et al. (2013), and auxiliary data (e.g., cell dimensions, PIC:POC) for the coccolithophore species used in this study.

# Preliminary Investigations into the Intracellular Carbonate Chemistry of Coccolithophores: A step in the right direction?

## Introduction

It is clear that intracellular chemical conditions dictate many biochemical processes in coccolithophores. In chapter 1 of this thesis, it was shown that the stable isotopic composition of the organic matter and coccolith calcite is determined by the residence time of carbon in the internal carbon pool of coccolithophores. Distinct residence times were measured, where *G. huxleyi*, due to its small size exhibited no isotopic equilibration of its intracellular carbon pool due to high amounts of carbon flux going in and out of the cell, as a consequence of its high surface area to volume ratio, and a relatively fast calcification rate. On the other end, *C. carterae* exhibited an (isotopically) equilibrated internal carbon pool and long residence times due to a relatively low surface area to volume ratio and a relatively small PIC quota. These observations hint towards a mechanistic understanding of the intracellular carbonate chemistry of coccolithophores, where a species like *G. huxleyi* must have a small internal carbon pool and the pH of the internal pool should be well equilibrated with the pH of the external environment. Indeed, this has been shown, for instance, by (Suffrian *et al.*, 2011b), where they showed that pH changes in the external environment cause changes in the internal pH, which are observed very rapidly. Moreover, (Liu *et al.*, 2021) showed that the intracellular pH in *C. carterae,* does not change with changes in ambient pH, moreover, the intracellular pH is always offset by ~0.6 pH units to be more alkaline in the intracellular environment. These findings are in line with our

observations from chapter 1, however, a direct measurement of the internal carbon pool and the intracellular pH is needed to validate these arguments.

The presence of an internal carbon pool has been suggested to be an adaptation in algae (and other organisms) to the low $CO_2$ concentration in the present ocean-atmosphere system. Algae concentrate $CO_2$ intracellularly by a process called "carbon concentrating mechanism" (Badger *et al.*, 1980; Reinfelder, 2010). This higher concentration can then be used to provide $CO_2$ as a substrate for carbon fixation. Studies on *Chlamydomonas reinhardtii*, and *Anabaena variabilis* were amongst the first organisms to be studied with a higher concentration of inorganic carbon ($C_i$) inside the cell relative to the culture media. Subsequently, this "carbon pool" has been reported in many different taxa (Badger *et al.*, 1980; Raven, 1997; Kaplan & Reinhold, 2003). Although this has been relatively easy to measure in bacteria due to their large $C_i$ pool, the measurements are not accurate for algae, which have smaller pools relative to their size (Burns & Beardall, 1987). Studies that attempted to measure the $C_i$ pool in algae, found that a $C_i$ pool is present in green algae such as *Chlamydomonas, Dunaliella*, and *Chlorella*. However, other algae with non-green chlorophyll, such as *Phaeodactylum, Isochrysis, Porphyridium*, and *Chondrus crispus* had either small or no $C_i$ pools (Badger *et al.*, 1998). Previous reports have indicated the presence of significant $C_i$ pools in Diatoms (*Navicula pelliculosa,* and *Thalassiosira weissflogii*), dinoflagellates (*Peridinium gatunense*), coccolithophores (*Gephyrocapsa Huxleyi*), and rhodophytes (*Cyanidioschyzon merolae*) (Badger *et al.*, 1998; Isensee *et al.*, 2014).

Many studies have acknowledged the presence of an internal $C_i$ pool in coccolithophores (Sikes *et al.*, 1980; Nimer & Merrett, 1992; Herfort *et al.*, 2002; Rost *et al.*, 2006; Rickaby *et al.*, 2010, 2016; Krug *et al.*, 2011; Hermoso *et al.*, 2014; Lee *et al.*, 2016). One of the earliest reporting of a $C_i$ pool in *G. huxleyi* was from

Sikes et al. (1980), where the authors suggested that an acid-labile fraction of carbon persisted in the calcifying as well as non-calcifying cells of *G. huxleyi*. Studies have estimated different levels of $C_i$ accumulation in coccolithophores. These ranged from having no $C_i$ pool (Nimer & Merrett, 1992) to having a $C_i$ pool with carbon concentration more than 10-fold higher than ambient $C_i$ levels (Sekino & Shiraiwa, 1994) with others suggesting intermediate levels of $C_i$ concentration inside the cell (Sikes *et al.*, 1980). The motivation behind these studies has been to quantify the mechanisms of carbon acquisition and utilisation for calcification in coccolithophores. As discussed in the introduction, the carbonate species required for calcification has been thought to be $HCO_3^-$. However, quantifying the predominant carbon species in a given carbon pool is dependent on the intracellular pH.

Intracellular pH in coccolithophores has been a topic of interest for more than three decades, with one of the earliest reports of fluorescent dye-based measurements of intracellular pH of coccolithophores from (Dixon *et al.*, 1989). Several other studies have since attempted to constrain the pH of the coccolith vesicle (CV) in comparison to the cytosolic pH as well as the ambient seawater pH (Anning *et al.*, 1996). This has been done in an attempt to better understand the carbonate chemistry inside the CV, which is still not properly known. For instance, it is not yet known whether calcium influx into the CV occurs through the reticular body, the calcium-phosphate rich body, or via calcium channels (Gussone *et al.*, 2006; Mackinder *et al.*, 2010; Gal *et al.*, 2017). Moreover, there have been several studies supporting the hypothesis that calcification utilises the bicarbonate ion ($HCO_3^-$) for calcification, which may or may not be associated with the photosynthesis and chloroplast-related leakage (Nimer *et al.*, 1997; Herfort *et al.*, 2002; Rost *et al.*, 2003, 2006). (Suffrian *et al.*, 2011b) were able to show that high proton permeability in *G. huxleyi* causes rapid shifts in its intracellular pH in the

direction of ambient pH changes. More recently, (Kottmeier *et al.*, 2022) showed that the voltage gated proton channels in *C. braarudii* modulate its intracellular pH homeostasis, and a reduced activity in the proton channels reduces the cell's ability to buffer its intracellular pH from the ambient pH. Specifically, cultures acclimated to pH 7.55 exhibited a smaller change in the cytosolic pH with changes in ambient pH (measured as fluorescent changes through SNARF) compared to cultures acclimated to pH 8.15 and 8.75.

Despite significant progress, little is known about intracellular pH conditions and the size of the internal carbon pool in coccolithophores. Therefore, this study attempts to quantify the intracellular pH changes in coccolithophores using SNARF-AM, a fluorescent dye with an acetoxymethyl ester motif, that releases the pH sensitive fluorophore once it has passed through the cell membrane. We use this dye in a confocal microscope and flow cytometer. Moreover, we attempted to measure the size of the internal carbon pool in coccolithophores using a modified pulse-chase technique, where a stable isotope spike of $^{13}C$ was used instead of a radioactive $^{14}C$ spike.

**Previously reported methods of measuring an internal carbon pool**

Previous studies have used various methods to quantify the carbon pool. This includes (1) silicone oil centrifugation (SOC) method (Kaplan *et al.*, 1980), (2) Membrane inlet mass spectrometry (MIMS; (Badger *et al.*, 1994; Rost *et al.*, 2003)), and (3) $^{14}C$ pulse-chase technique (ter Kuile & Erez, 1988; Berman-Frank & Erez, 1996; Isensee *et al.*, 2014). In the Silicone-oil centrifugation technique, $NaH^{14}CO_3$ is added to the culture and centrifuged with a silicone-oil. $^{14}C$ activity is measured in the centrifuged pellet by a scintillation counter and the $C_i$ pool is calculated as the difference between the $^{14}C$ label taken up by the cell and the $^{14}C$ present as acid-stable carbon in the cell (Badger *et al.*, 1980). This technique assumes that

the $^{14}C$ which is acid-labile constitutes the $C_i$ pool. However, the technique is fraught with problems such as the inability to calculate the intracellular volume precisely, overestimation of the $C_i$ pool due to the $^{14}C$ label being present in acid-labile carbon on the cell surface, the method being applied in non-steady-state conditions (Badger *et al.*, 1994), and the technique requiring high cell densities, which are rarely found in real-world scenarios.

Membrane Inlet Mass Spectrometry (MIMS) uses the chemical disequilibrium between carbon species during steady-state photosynthesis and allows simultaneous measurement of $CO_2$ and $HCO_3^-$ fluxes by measuring the $HCO_3^-$ pool and determining the $CO_2$ concentration using kinetic constants for the rate of interconversion between the two carbon species (Badger et al., 1994). Therefore, this method relies on the quantification of the extent of disequilibrium between $CO_2$ and $HCO_3^-$ in the culturing media during photosynthesis. However, this method can only be applied to cells that lack CA activity.

The $^{14}C$ pulse-chase method measures the $C_i$ pool by recording the lag-time between the introduction of $^{14}C$ during the pulse period, and its incorporation into acid-stable carbon during the chase period. The concept suggests that the $^{14}C$, which is incorporated into the acid-stable carbon after the label has been removed from the medium, comes from the $C_i$ pool. The method uses natural cell densities and measures the $C_i$ pool in steady-state conditions (Berman-Frank and Erez, 1996). The technique assumes that there is a negligible amount of $^{14}C$ label present in the medium during the chase period, and an increase in the acid-stable $^{14}C$ must come from a $C_i$ pool. It also assumes that at the beginning of the chase period, the specific activity of $^{14}C$ in the $C_i$ pool is equal to that of the medium of the pulse period. The minimum size of the $C_i$ pool is estimated from the difference between the $^{14}C$ activity of the acid-stable carbon at the beginning of the chase period and

the maximum $^{14}C$ activity during the chase period. The size is considered as a minimum because some amount of the label could have been lost due to washing, or respiration, or DOC efflux (Isensee et al., 2014). The concentration of carbon in the cell is estimated from the size of the $C_i$ pool. However, this method assumes carbon enrichment in the entire volume of the cell because the cell membrane provides a much stricter constraint on the size than any localised $C_i$ pools which may be present surrounding the carbon fixation sites (Kaplan et al., 1980; Isensee et al., 2014).

The amount of time required for the isotopic equilibration of the $C_i$ pool and the time required for the assimilation of the pool into acid-stable carbon depends on the volume: surface area ratio of the cell (Berman-Frank and Erez, 1996). The $C_i$ pool kinetics and timescales are likely to vary within species due to the large difference in their relative sizes. This is because varying sizes would entail varying carbon and nutrient turnover rates, and variation in growth and calcification rates (Berman-Frank and Erez, 1996). In short, a larger cell will require a longer time to saturate their $C_i$ pool. There is also a considerable time lag noted by previous studies involved in the incorporation of the $^{14}C$ label during the pulse period (Berman-Frank and Erez, 1996). This has been attributed to the presence of the $C_i$ pool. Preincubation in the dark has been suggested to affect the lag times (Badger et al., 1994; Berman-Frank ad Erez, 1996; Kaplan et al., 1990; Rotatore and Colman, 1991; 1992).

Isensee et al. (2014) talked about the advantages of the pulse-chase method over SOC and MIMS. The use of significantly lower DIC concentrations for analysis using SOC and MIMS influences the intracellular pH. The pH has been reported to be reduced by 0.7 units, from 7 to 6.3 in less than 1 hour (Nimer *et al.*, 1994b) or even within seconds (Suffrian *et al.*, 2011b) causing a change in the carbonate

speciation within the cell. Such changes are therefore highly likely to alter the size and chemistry of the $C_i$ pool. This must be especially significant for small-sized unicellular algae such as coccolithophores due to their small equilibration times between the $C_i$ pool and surrounding medium (Berman-Frank and Erez, 1996). Moreover, SOC and MIMS require the cell densities to be significantly increased to get a measurable value (Nimer *et al.*, 1994b). The dense cultures are incubated for 10 seconds, and 10 minutes in a DIC-depleted medium for SOC and MIMS, respectively. The incubation times cannot be extended since that could affect the photosynthetic activity of the cells and thus, give erroneous values. However, the pulse-chase method measures the $C_i$ pool at ambient culturing conditions and cell densities.

There are some drawbacks to using the pulse-chase method as well. For instance, the method can be applied only to those organisms which have relatively longer pool turnover times (which is inversely proportional to the cell surface area: volume ratio), so that multiple measurements can be taken to quantify the size of the $C_i$ pool. Whereas for SOC and MIMS, changes in the $C_i$ pool can be analysed in less than a few minutes (Kaplan et al., 1980; Isensee et al., 2014). Subsequently, single-point measurement is insufficient for the quantification of the $C_i$ pool using the pulse-chase method, which is true for SOC and MIMS.

**Methods**

All cultures were grown in sterile filtered (0.22µm) Synthetic Ocean Water (SOW) buffered with Tris, based on the Aquil* media recipe (Morel *et al.*, 1979). Major nutrients, trace metals, and vitamins were added according to the modified K/2 media recipe used in chapter 1 (Keller & Guillard, 1985; Keller *et al.*, 1987). The cultures were maintained as dilute batch cultures in a 14:10 L:D cycle, with 150 µmol $m^{-2}$ $s^{-1}$ PPFD (measured with Fisher Scientific™ Traceable light meter), at 17°C

for all species. For both internal carbon pool experiment and the intracellular pH experiment, cell densities at the point of measurement were ~50,000 cells $mL^{-1}$ for *G. huxleyi*, 10,000 cells $mL^{-1}$ for *C. carterae,* and ~5000 cells $mL^{-1}$ for *C. braarudii*. DIC concentration was kept at ~2100 µmol $KgSW^{-1}$.

**Methodology for measuring the Internal C-pool**

Cultures were placed on a rotating shaker at 60 rpm and a 1m long cool white LED strip was taped around the culture bottle to allow photosynthetic carbon fixation to take place during the experiment. A background sample was taken, and the culture (~1L) was spiked (Pulse) with a 0.1% (99.9 %) $^{13}C$ spike. This was added as 1.78 mL of (0.0021 mol/L) $NaH^{13}CO_3$ in 1L medium to enrich the DIC from -2 ‰ $\delta^{13}C$ to ~85 ‰ $\delta^{13}C$ (VBDB). The rotator allowed proper mixing of the spike into the solution, and the LED light ensured the uptake of the spike into the organic matter. Two samples for the pulse phase were taken, each in 10-minute intervals. Immediately after taking the second pulse sample, the cultures were spiked with a (99.8%) $^{12}C$ spike. This was added as 1 mL of 0.21 mol/L in < 1L culture to start the chase phase of the experiment. This spike was depleted (high in 12C) enough to completely dilute the $^{13}C$ spike, and to bring back the DIC to < -2 ‰ $\delta^{13}C$. Immediately after adding the second spike, samples for the chase phase were taken every 30 seconds to 1 minute, with the time being noted for every sample. Since the samples were taken on a GF/F filter using a vacuum pump, the sampling wasn't instantaneous, and took ~ 15 seconds (see below for details), therefore, the precise time could not be noted. 10 samples during the chase phase were taken. Two replicates for each species were performed.

Sampling was done on pre-combusted (450˚C, overnight) GF/F filters using a vacuum pump. 100 mL of culture was decanted into the filter holder and vacuum was applied until all liquid passed through. 50 mL fresh media (without any

isotopic spike) was added to wash the samples and remove any extracellular isotope spike. Later, the filters were acidified with 230 µl of 0.1% HCl and dried at 60˚C overnight. Samples were run on an Elementar Vario Isotope Select Elemental Analyser linked to an Isoprime 100 continuous flow IRMS at the Stable Isotope Ratio Mass Spectrometry Laboratory, School of Ocean and Earth Science, University of Southampton, National Oceanography Centre in Southampton, UK.

**Methodology for measuring intracellular pH**

Cultures for each species were centrifuged at 700g for 3 minutes and the supernatant was carefully removed to leave the cells in ~0.5 mL seawater. The tube was gently shaken to dislodge the pellet and resuspend the cells into the seawater. Through optical microscopy, the viability of the concentrating procedure was analysed, and majority of cells were alive. The 0.5 mL culture was distributed evenly into 4 2mL-microcentrifuge tubes and topped up with 1.5 mL of fresh seawater of pH 7.6, 7.9, 8.2 or 8.8. Cultures were gently vortexed, centrifuged at 500g for 3 minutes, and resuspended in 1 mL (final volume) fresh seawater of their respective pH. 50 µL of 10% Pluronic F-127 and 10 µL of SNARF-AM (from 1mM stock) was added to each tube and vortexed. The cultures were covered with tin foil and incubated at 17˚C (typical growth conditions) for 30 minutes. The samples were then centrifuged at 500g for 3 minutes, the supernatant was discarded, and fresh media was added. This was repeated once more to remove the dye completely. Once resuspended in fresh media of the respective pH treatment, three replicated of 200 µL volume each were run for each species, each pH treatment on a BD Accuri Flow Cytometer with a 580 nm and 630 nm filter for absorption and the 488 nm laser for excitation. For the calibration curves, a similar methodology was used, however, instead of normal seawater, calcium-free seawater (of pH 7, 7.5, 8, 8.5, 9) were used to avoid calcium toxicity

during pH calibration using nigericin. Background fluorescence was corrected by subtracting the fluorescence obtained from non-dyed cells (control) that were treat the same way as the dyed cells but without the addition of SNARF-AM. Moreover, just before running the samples on the flow cytometer, 50 µL of 2M KCl and 1.5 µL of 6.7 mM Nigericin were added to each (1mL) sample. This perforated the cell membrane and allowed the intracellular pH to resemble the extracellular pH.

A similar approach was applied for confocal measurements, where the excitation wavelength was set as the 514 nm laser, with the emission spectra recorded at 585 nm and 630 nm (range of ± 10 nm for better quality). The cells were also decalcified using 0.1N HCl prior to imaging and allowed to recoverin normal seawater (pH 8.2) for 2 hours prior to imaging or staining. The Chlorophyll spectra should be from 650 nm to 700 nm with the peak at 683 nm. The settings were not changed between samples. A bit size of 16 was used with Z-stack of 512*512 frame size, pixel dwell time of ~1.5 µsec, mode = line, 1 Airy unit. The fluorescence emission measured at 585 nm (F1) and 630 nm (F2) from both instruments were used to measure the intracellular pH using the quotient R = F1/F2

**Results and Discussion**

**Internal Carbon Pool**

The stable isotope spike method showed preliminary changes as expected for normal carbon uptake. That is, the $\delta^{13}C$ value of the organic matter increased with time during the pulse period (blue region, Fig. 1), due to photosynthetic carbon uptake. If there were a detectable internal carbon pool present in the cells, we would see continued increase in $\delta^{13}C$ of organic matter with time in the chase period (beige region, Fig 1). This is because in the presence of an internal carbon pool, some amount of $^{13}C$ that would be taken up by the cell during the pulse

phase was stored inside the cell in the form of acid-labile carbon (internal carbon pool), to be fixed into organic, acid-stable carbon (Fig. 1).

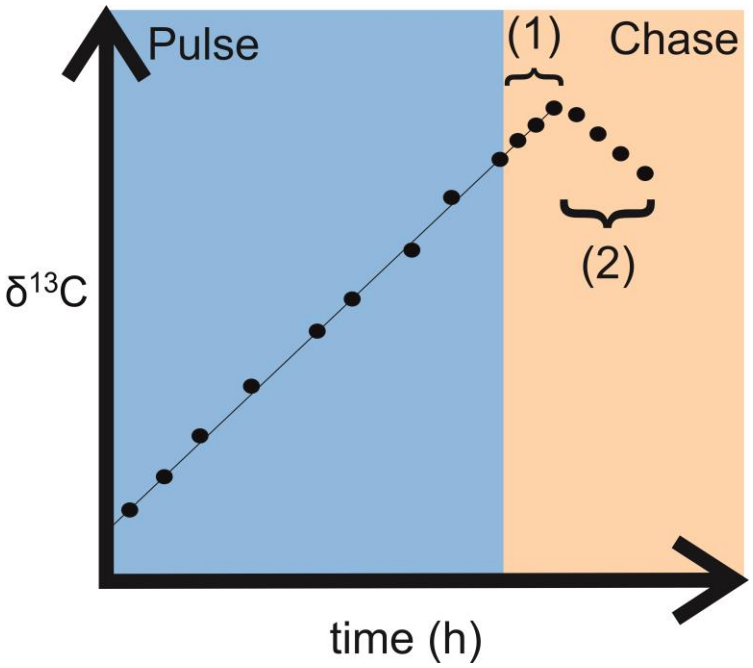


**Figure 1:** A theoretical schematic of a typical pulse chase experiment, where $^{13}C$ uptake leads to an increase in the $\delta^{13}C$ value of the organic matter during the pulse phase. If there is an internal carbon pool present (1), we would expect the $\delta^{13}C$ value of the organic matter to continue increasing in the chase phase, due to the presence of $^{13}C$ as acid-labile carbon in the carbon pool. Once this internal carbon pool is depleted of the $^{13}C$ taken during the pulse period and resupplied by fresh carbon from the DIC (during the chase phase, 2), the $\delta^{13}C$ value of the organic matter will start decreasing. In case there is no internal carbon pool present, we would see an immediate decrease in $\delta^{13}C$ value of the organic matter as soon as the chase phase begins.

Although a similar trend was observed in our experiment, we were not able to identify the presence of an internal carbon pool in any coccolithophore species (Fig. 2). This is because we did not observe an increase in the $\delta^{13}C$ value during the chase phase, which would signify the presence of an internal carbon pool. This is in contradiction to earlier studies, which have used other techniques to measure internal carbon pools in coccolithophores and have identified the presence of one (Isensee *et al.*, 2014).

In figure 2, we can see that the $\delta^{13}C$ value of the organic matter in the chase phase was not higher than those in the pulse phase in any case, which indicates that

there is no internal carbon pool present. However, in our previous chapter (Chapter 1), we showed that an internal carbon pool does exist in coccolithophores, as evaluated through stable isotope techniques. It is possible that there is indeed an internal carbon pool in coccolithophores, but the current technique was not able to measure it due to one or more of the following reasons:

1. Carbon in the internal carbon pool is present as acid-labile carbon, and only after passing through the Calvin cycle, this acid-labile carbon is converted to acid-stable carbon. Therefore, it is possible that the acidification step that was performed on all samples to remove coccolith calcite also removed the acid-labile carbon from the samples. To avoid such a scenario, acid-labile carbon can be extracted separately, so that calcite does not affect the isotopic values, and the acid-labile carbon can be measured, as done previously (Moutot *et al.*, 1986).
2. Alternatively, the time frame in which the samples were taken was too long to measure the internal carbon pool. That is, with a small spike (0.1% of standard DIC concentration), the amount of $^{13}C$ being taken up is small, as the $\delta^{13}C$ value of the DIC was ~ 85 ‰. This causes only small incremental increases in the $\delta^{13}C$ value of the internal carbon pool (compared to the fixed organic matter) and to resolve the change in $\delta^{13}C$ value due to the internal carbon pool, a larger spike, and more frequent sampling must be used.
3. The signal to noise ratio of the IRMS used to obtain $\delta^{13}C$ measurements was small, with the noise affecting the true value of the observed signal. The standard deviation on any $\delta^{13}C$ value obtained from the mass spectrometer is 0.1‰. Fig. 2 showed that the change in $\delta^{13}C$ value of the organic matter during the chase period is small, and it is possible that the signal for the internal carbon pool was muted due to a small signal to noise ratio.

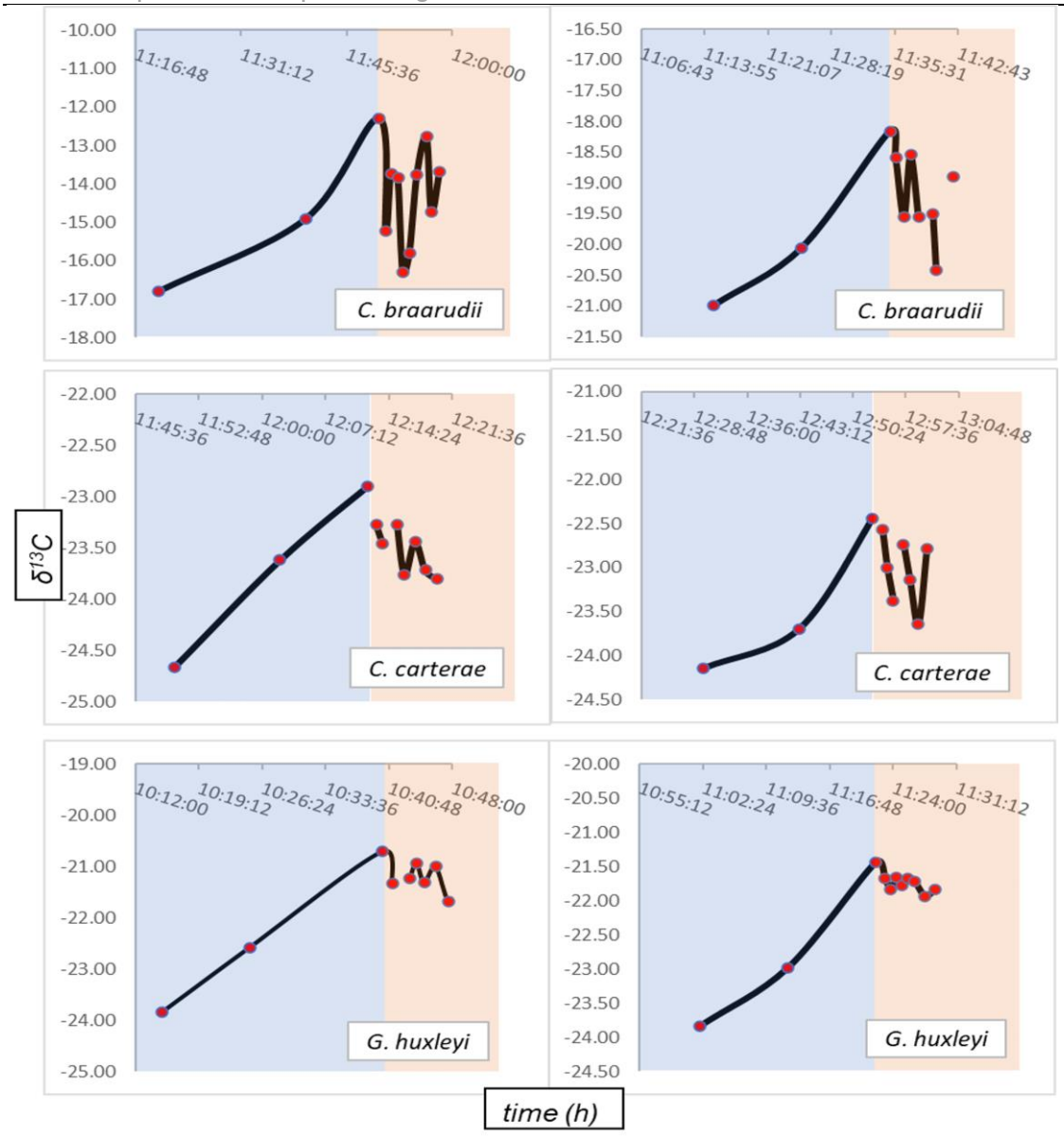


**Figure 2:** Pulse chase experiment using a $^{13}C$ spike, showing no increase in the $\delta^{13}C$ value during the chase phase of the experiment. Red dots represent the samples. The y axis in all plots represents $\delta^{13}C$ of organic matter, and the x axis denotes time in hours.

**Intracellular pH**

Confocal imaging showed that SNARF-AM was dispersed evenly in the cytoskeleton, where the CV and coccolith in formation can be pointed out from its shape and the absence of fluorescence in that region (Fig 3). However, use of confocal microscopy was found to be unfeasible, as only a few cells could be imaged in an hour, and the viability of the cells, and the fluorescence of the dye

were not constant during that time. This is because the fluorescence of SNARF-AM decays with time (Nakata *et al.*, 2011; Golda-VanEeckhoutte *et al.*, 2018). Moreover, due to the long time it takes to set up the imaging technique, nigericin-treated cells that were used for creating a calibration curve suffered from high mortality rates. Therefore, flow cytometry was considered a more feasible and faster option to measure intracellular pH.

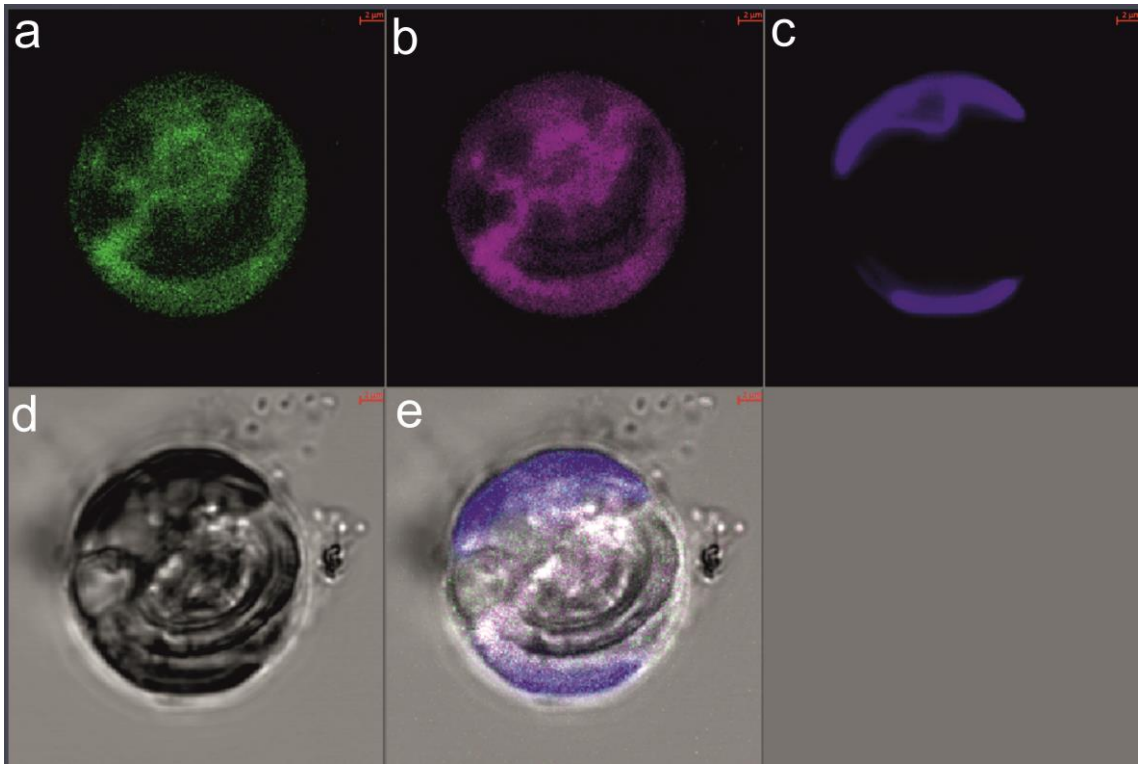


**Figure 3:** Confocal image of a decalcified *Coccolith braarudii* cell stained with SNARF-AM. (a) Fluorescence at 580 nm, (b) Fluorescence at 640 nm (c) Fluorescence at 680 nm (chlorophyll) (d) bright-field image (e) image stack containing all fluorescence and bright-field images. Red scale on the top right represents a 2 µm scale.

Flow cytometry allowed the measurement of thousands of cells at a time, with no need for background seawater correction as only an individual cell was imaged at a time. However, there were several problems with this experiment. First, the number of cells that showed any uptake of SNARF-AM (as measured through the number of cells showing a peak at 580 nm and 630 nm) varied significantly. For instance, ~ 52 % cells of *C. carterae* exhibited successful dye uptake. However,

only ~7 % cells of *G. huxleyi* and 9 % of *C. braarudii* showed successful uptake of the dye. Moreover, it was common to observe that the number of viable cells with positive fluorescence for SNARF-AM decreased with time. For instance, if well A01 had 70 % of cells were alive with positive dye uptake, cell D07, which comes after 20-25 wells had < 10 % cells that were alive or showed successful uptake of the dye.

Second, the calculation of calibration curves was unsuccessful as the cells treated with nigericin generally did not show an increase in their intracellular pH proportional to the extracellular pH. Consequently, calculation of absolute intracellular pH values was not possible for *G. huxleyi* and *C. braarudii*. However, using values from nigericin-treated *C. carterae*, a calibration curve was possible, and its slope and intercept were used to calculate ΔpH values in all three species. It must be emphasised that the change in pH between treatments of a single species only shows the relative change in fluorescence ratio for that species, and due to the absence of a calibration curve, the absolute pH values, or the absolute change could not be calculated. Even for *C. carterae*, the calibration curve was created based on one set of datapoints. Therefore, the intracellular pH values obtained from the calibration curve cannot be used in absolute terms.

The ΔpH values show a species-specific response (Fig. 4). We see that *G. huxleyi* had the largest variation in intracellular pH with changes in ambient pH, while the changes in *C. carterae* and *C. braarudii* were small. For reference, the intracellular pH values calculated in (Kottmeier *et al.*, 2022) were also added, and despite significant noise in the datapoints for *C. braarudii* in the present study, the slope of the pH change were similar.

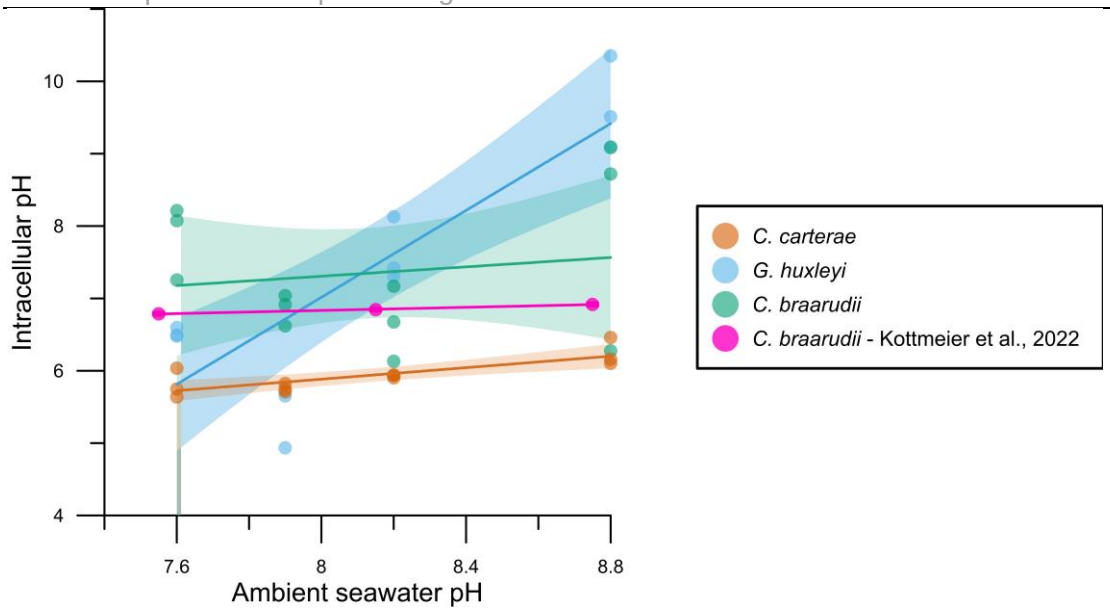


**Figure 4:** Intracellular pH changes in three coccolithophore species with changing ambient pH, as measured through changes in the fluorescence ratio for SNARF-AM. Note that the intracellular pH values are not absolute, as calculation of a calibration curve was not possible. Therefore, only relative changes in fluorescence ratios can be used to infer changes in intracellular pH with ambient pH. For reference, intracellular pH values as a consequence of changes in extracellular pH from Kottmeier et al. (2022) is given.

These observations are consistent with those from chapter 1, where *G. huxleyi* displays a small carbon pool and short residence time for carbon, which allows rapid equilibration of the intracellular pH with ambient conditions. On the other hand, large species such as *C. carterae* and *C. braarudii* do not show large changes in the intracellular pH despite large changes in the ambient conditions. These observations are consistent with the large internal carbon pool for the large sized coccolithophore species, that causes a slower equilibration of the intracellular pH conditions with ambient conditions. Alternatively, it may suggest that *G. huxleyi* is highly permeable to protons, which causes the calcite and organic matter isotopes to show a high degree of disequilibrium, whereas larger species such as *C. carterae* and *C. braarudii* are able to buffer their intracellular pH, which allows isotopic buffering as observed in the $\delta^{18}O$ values of the coccolith calcite in chapter 1.

**Future perspectives**

Although the experiments presented here were unsuccessful in unravelling the carbonate chemistry conditions inside a coccolithophore cell, they represent some of many avenues for future research. Through the confocal images in Fig. 3, and previous work by (Avrahami *et al.*, 2023), it is evident that the coccolith vesicle is tightly wrapped around the coccolith itself, with very little space for any fluorescent dye. Therefore, obtaining more information about the carbonate chemistry of the calcifying fluid through fluorescent dye techniques seems challenging. Boron isotopes in biogenic calcite are becoming more relevant, with some instances of use even for coccolithophores (Liu *et al.*, 2018, 2021). Using such isotopic systems, with a more systematic understanding of the biochemical processes that drive calcification (such as $Ca^{2+}/H^{+}$ exchangers, role of proteins and coccolith-associated polysaccharides) will enhance our understanding of the chemical nature of the calcifying fluid from which the coccolith is precipitated.

It is still important to note that intracellular pH measurements are crucial to validate isotopic data. For instance, our hypothesis in chapter 1 that *G. huxleyi* possessed a small carbon pool with short carbon residence times was based on the high degree of disequilibrium present in the stable isotopes of its coccolith calcite. Such an argument was validated through empirical evidence provided by (Suffrian *et al.*, 2011b), where they showed that the intracellular pH of *G. huxleyi* changes rapidly with changes in the ambient pH. It is important to extend these investigations to other coccolithophore species such as *C. braarudii* and *C. leptoporus*, which are key calcifiers in the polar oceans (Quinn *et al.*, 2004; Daniels *et al.*, 2016). Moreover, measuring the size of the internal carbon pool is equally important, as that determines the carbon concentrating capabilities of different

species, especially under low $CO_2$ conditions (Bolton *et al.*, 2012, 2016; Bolton & Stoll, 2013).

In chapter 1, we assumed that *C. leptoporus* had a small internal carbon pool compared to *C. braarudii* because the magnitude of vital effects observed in this *C. leptoporus* were larger under carbon limitation, suggesting more starved internal carbon pool. However, the high intracellular pH as evidenced through oxygen isotopes suggested long carbon residence times. Moreover, there were no signs of carbon limitation in the coccoliths at low $CO_2$ conditions in *C. leptoporus*, unlike *C. braarudii*. Therefore, it is possible that the carbon pool is indeed large, but the large vital effects were experienced as the calcification rate was higher in *C. leptoporus*. The $\mu_{opt}$ at comparatively lower $CO_2$ concentration for *C. leptoporus* also suggests that this species may not be as $CO_2$ limited as *C. braarudii.* Since calcification rates were not measured, it cannot be confirmed if calcification was indeed higher in *C. leptoporus* compared to *C. braarudii*. In such a scenario, measuring the size of the internal carbon pool is crucial for understanding species-specific tolerances to low $CO_2$ conditions. Similar to this scenario, *G. huxleyi* and *G. oceanica* exhibited a constant offset in their isotopic values from each other. Stable isotopes in coccolith calcite for *G. oceanica* were always lighter (depleted) than those of *G. huxleyi*, but the organic matter isotopes were always heavier (enriched). This characteristic was attributed to a smaller carbon pool in *G. oceanica*, despite being larger in size compared to *G. huxleyi*. However, higher calcification rates could have taken up the depleted carbon from the carbon pool, leaving the pool isotopically enriched. However, since calcification rates were not measured, and the size of the internal carbon pool is not known, the mechanism behind those observations remain unknown.

# Chapter 2: Contrasting Stress Response to Environmental pH Determines the Fate of Coccolithophores in Future Oceans

## Foreword

This chapter has been published in Marine Pollution Bulletin as a research article. However, some changes have been made to this chapter. Citations to Chauhan & Rickaby (2024) are referencing to the corresponding article to Chapter 1.

## Abstract

Molecular mechanisms underlying the contrasting sensitivity of different species to environmental pH remain elusive. Documenting these molecular mechanisms allows an understanding of the selection of diverse species by ecological niches and their ability to adapt to environmental change. To investigate the cellular processes governing physiological responses to seawater pH, we conducted physiological assessments (growth, photosynthesis, and respiration) and proteomic profiling across 3 coccolithophore species under 3 pH conditions. Our findings reveal that coccolithophores experience species-specific stress-induced responses to both acidic and alkaline pH conditions, potentially driven by cellular oxidative damage and alterations in membrane potential, as evident through upregulation in oxidative stress-management and membrane transport-related protein-groups. Proteomic analysis highlighted upregulation in antioxidant, DNA repair and cell cycle-related protein-groups, corresponding with reduced growth rates. Mitochondrial dysfunction inhibited respiration rates, while an upregulated TCA cycle generated essential metabolites for restoring cellular homeostasis. Photosynthetic activity correlated with $CO_2$ availability across the pH gradient but exhibited species-specific proteomic alterations. *Chrysotila carterae* displayed broad resilience to pH changes, attributed to its coastal habitat adaptation and

robust intracellular pH-buffering capacity. *Gephyrocapsa huxleyi* exhibited pronounced stress-related changes under alkaline conditions, but minimal changes under acidic conditions. Disruption of pH homeostasis triggered stress-related cellular responses in *Coccolithus braarudii* under both acidic and alkaline conditions as shaped potentially by its adaptive geologic history and habitat characteristics today. Notably, net carbon fixation at a cellular scale, approximated by the photosynthesis to respiration ratios, increased for all species in an acidic ocean, however, species-specific sensitivities and associated changes in growth rates impact carbon fixation under alkaline conditions. Furthermore, metabolic flexibility in the small lightly-calcified *G. huxleyi* and intracellular pH-buffering capacity of *C. carterae* will likely facilitate their adaptation to ocean acidification or artificial ocean alkalinisation. However, pH sensitivity of the larger and heavily-calcified *C. braarudii* will result in further shrinking of its ecological niche and reduced carbonate production rates.

## Introduction

Coccolithophores are ubiquitous marine algae that contribute to the global carbon cycle through photosynthetic carbon fixation and calcium carbonate precipitation in the form of coccolith calcite (Rost & Riebesell, 2004a). Coccolithophores, alongside foraminifera are the principal contributors to biogenic calcite burial in the open ocean (Hay, 2004). Within this group, calcite production rate may be controlled by the prevalence of the heavily calcifying but marginalised *Coccolithus braarudii* versus the ubiquitous but lightly calcifying *Gephyrocapsa huxleyi*. The ability of different coccolithophore species to occupy a wide variety of ecological niches plays a key role in their ecological success (Taylor *et al.*, 2017). In the present day, coccolithophores inhabit almost all oceans and marginal seas (Geisen *et al.*, 2002; Parente *et al.*, 2004; Kideys *et al.*, 2005; Houdan *et al.*, 2006; Henderiks

& Rickaby, 2007; Tyrrell *et al.*, 2008; Moore *et al.*, 2012; Winter *et al.*, 2014; Silkin *et al.*, 2014; De Vries *et al.*, 2021), where species-specific physiological and ecological characteristics dictate their distribution. Coccolithophore blooms occur in stratified oligotrophic waters due to the low nutrient and trace metal requirements for coccolithophores like *Gephyrocapsa huxleyi* compared to other phytoplankton (Rost & Riebesell, 2004a; Zhang et al., 2022). Previous studies have shown the ability of coccolithophores to utilise alkaline phosphatase and nitrogen-rich compounds such as amino acids, urea, and purines as alternative nutrient sources under phosphorous and nitrogen limitation, respectively (Palenik & Henson, 1997; Riegman et al., 2000b). The haplodiplontic life cycle in coccolithophores further allows the occupation of various light and nutritional regimes throughout the seasons (Houdan *et al.*, 2006; Cros & Estrada, 2013; De Vries *et al.*, 2021). Additionally, coccolithophores such as *G. huxleyi* lack photoinhibition even under very high light intensities (Nanninga & Tyrrell, 1996). These traits may give coccolithophores a competitive edge over other phytoplankton groups (Boyd *et al.*, 2010). However, despite low nutrient requirements and the ability of coccolithophores to occupy high-light and stratified oligotrophic waters, coccolithophores are limited by carbon in ambient $CO_2$ concentrations (Paasche, 1964; Nielsen, 1995; Rost *et al.*, 2003; Rickaby *et al.*, 2010).

Over the coming decades, climate change may have a complex influence on the carbon cycle due to altered community composition as a result of species-specific sensitivities to various environmental parameters (Balch, 2018). This is because climate change will bring about changes in pH (affecting calcification, ionic speciation, and cellular pH homeostasis), temperature (directly affecting growth rates), seawater stratification, and associated changes in light regime and nutrient supply (Rost & Riebesell, 2004a; Gerecht et al., 2014; Balch, 2018; Dedman et al.,

2023a). The emission of carbon dioxide from the burning of fossil fuels leads to increased uptake by the ocean, resulting in a decline in the ocean pH. Seawater pH has already decreased by 0.1 units compared to pre-industrial levels and decreases the calcium carbonate saturation state (Doney *et al.*, 2009). Calcifying organisms, including coccolithophores, face potential threats from anthropogenic ocean acidification (OA; Riebesell et al., 2000). By contrast, over the evolutionary history of the last tens of millions of years, the ocean has tended towards higher pH today (Hönisch *et al.*, 2012; Halevy & Bachan, 2017). Additionally, artificial ocean alkalinisation (AOA) has been proposed as a viable solution for $CO_2$ drawdown to counteract OA and climate change. This technology would enhance ocean alkalinity through accelerated rock weathering or addition of alkaline materials to the ocean (Bach *et al.*, 2019). Alongside increased oceanic carbon dioxide uptake, this technique can potentially raise ocean pH to levels higher than ever observed previously (Gore *et al.*, 2019).

Several studies have highlighted physiological changes in coccolithophores with decreasing seawater pH, marked by the inorganic carbon to organic carbon (PIC:POC) ratio. While such investigations significantly enhance our understanding of the effects of species-specific changes to carbon fixation, alterations in community composition and absolute abundances are more likely to influence carbon biogeochemistry than cellular PIC:POC alone (Bach *et al.*, 2015). Moreover, molecular mechanisms behind species- and strain-specific sensitivities to pH are still unknown (Riebesell *et al.*, 2000; Langer *et al.*, 2006, 2009; Rickaby *et al.*, 2010, 2016). Few studies (e.g., Richier et al., 2011; Rokitta et al., 2012; Jones et al., 2013; Dedman et al., 2023; Thangaraj et al., 2023) have examined cellular responses of coccolithophores to environmental changes, and most of these have focused solely on *Gephyrocapsa huxleyi* (formerly *Emiliania huxleyi;* (Bendif *et al.*, 2019;

Archontikis *et al.*, 2023), neglecting other ecologically significant coccolithophore species (Daniels *et al.*, 2016; Walker *et al.*, 2018).

Our current understanding of coccolithophore sensitivity to pH mostly stems from physiological studies (Gafar *et al.*, 2019b), with only some studies using techniques like transcriptome profiling, fluorescent dye, and patch-clamp electrodes to document the mechanisms underlying the physiological responses (Suffrian et al., 2011b; Rokitta et al., 2012a; Kottmeier et al., 2022). These studies revealed that pH sensitivities of the diploid life-cycle stage in coccolithophores were caused by elevated $H^+$ permeability through voltage-gated channels. Studies using isotopic techniques have further advanced our understanding of species-specific differences in intracellular pH buffering capacities and carbon residence times (Liu *et al.*, 2021; Chauhan & Rickaby, 2024). Physiological observations, with evidence from changes in PIC:POC ratios suggest that low pH is likely to have major implications for the selection of different species with contrasting calcite production rates and hence on global calcite production rates (Raven & Crawfurd, 2012; Krumhardt *et al.*, 2017; Brownlee *et al.*, 2021).

The impact of increase in ocean pH and/or alkalinization on coccolithophores has received less attention. Few studies have focused on the physiological changes or their molecular mechanisms under AOA. For example, (Gately *et al.*, 2023) showed no significant alterations in the elemental composition and growth rates of *G. huxleyi* under heightened alkalinity conditions. While *G. huxleyi* may not be heavily impacted by AOA according to the above study, species-specific responses observed in other contexts suggest that may not be true for other key coccolithophore species (Gafar *et al.*, 2019b). It is important to also recognise that the feasibility of AOA requires the addition of alkalinity-raising material in specific “hotspots,” primarily in coastal regions (Bach *et al.*, 2019). Therefore,

understanding the response of coastal species becomes paramount under these scenarios.

pH change (through either OA or AOA) triggers significant alterations in biocalcification regimes but may also potentially impact the cellular homeostasis of biological organisms. This is because cellular pH homeostasis depends on an electrochemical gradient and shifts in intracellular pH can alter the ionisation state of weak acids and bases, which includes numerous biomacromolecules such as proteins (Boron, 2004). An ability to maintain proper cellular pH homeostasis is crucial for biological processes and ultimately dictates the survival and proliferation of organisms (Casey *et al.*, 2009). Investigation of the molecular changes in coccolithophores in response to changes in ambient pH are key to understanding the species- and strain-specific differences in pH tolerances, and the downstream effects of these changes on physiology, and biogeochemistry.

This study aims to investigate the cellular response of three distinct coccolithophore species – *Gephyrocapsa huxleyi, Coccolithus braarudii*, and *Chrysotila carterae* – to variations in ambient seawater pH. These species were chosen based on their biogeochemical significance and previous findings that revealed species-specific sizes of internal carbon pools and carbon residence times suggestive of contrasting tolerances to changes in pH (Chauhan & Rickaby, 2024). The experimental setup involved acclimated exposure to acidic (pH 7.6) and alkaline (pH 8.8) conditions compared to a control (pH 8.2). Although such carbonate chemistry conditions are not true analogues of OA or AOA, as pH changes in both scenarios will accompany changes in DIC and/or alkalinity, this study will further our understanding of pH-related changes that can be extrapolated to real-world OA and AOA scenarios. Three key physiological parameters – growth rate, net photosynthetic rate, and dark respiration rate – were

additionally monitored to provide physiological context to the alterations in cellular function revealed by proteomic analysis and consider the respective performance of each species under future OA scenarios.

## Materials and Methods

### Algal Culturing

Monocultures of *Chrysotila carterae* (PLY 406) were obtained from the Marine Biological Association (MBA, UK), *Gephyrocapsa huxleyi* (RCC 1731) and *Coccolithus braarudii* (RCC 1198) were obtained from Roscoff Culture Collection (Roscoff, France). Cultures were grown in 1mM Tris buffered synthetic ocean water prepared according to the Aquil media recipe (Price *et al.*, 1989) The media was supplemented with 100 $\mu$M nitrate, 6.25 $\mu$M phosphate and 27 $\mu$M silicate with vitamins according to *f*/2 (Guillard & Ryther, 1962). Trace metals were added according to K/2 (Keller & Guillard, 1985; Keller *et al.*, 1987) with modifications according to (Rickaby *et al.*, 2010). pH was adjusted by adding calculated amounts of 1N NaCl and 1N HCl and measured using a 3-point calibrated benchtop pH meter (Mettler Toledo SevenEasy) to pH 7.6, 8.2 and 8.8. Carbonate chemistry was further analysed on a Metrohm 916 Ti-Touch titrator to determine the Total Alkalinity (TA) and pH (Table 2). The media was filtered through a sterile 0.22 µm Merck Steritop® bottle top filter into 250 mL sealed cap Falcon flasks and UV-C sterilised for one hour. Cultures were acclimatised for at least 10 generations before being grown in triplicate dilute batch cultures for the main characterisation and harvesting experiment. Cultures were kept in a PHCbi MLR-352 Climate Chamber at 17˚C with a 14:10 light:dark cycle and a light intensity of 60-80 $\mu$mol $m^{-2}$ $s^{-1}$.

**Table 1:** Carbonate chemistry parameters for the seawater used in this study. DIC (µmol $kgSW^{-1}$), $CO_2$ (µmol $kgSW^{-1}$) and Calcium carbonate saturation state (Ω) were calculated using average Total Alkalinity values through CO2SYS *(Lewis* et al.*, 1998)*.

The $K_1$ and $K_2$ constants were taken from *(Mehrbach* et al.*, 1973)*, refit by *(Dickson & Millero, 1987)*. Precision and drift were measured through a $CO_2$ in Seawater Dickson standard (Batch 197) over the course of analysing samples. No significant drift was detected.

| pH | Total Alkalinity (µmol $kgSW^{-1}$) | DIC (µmol $kgSW^{-1}$) | $CO_2$ (µmol $kgSW^{-1}$) | Ω |
|---|---|---|---|---|
| 7.62 ± 0.02 | 2126 ± 7 | 2094.7 | 52.17 | 1.21 |
| 8.23 ± 0.05 | 2540 ± 12 | 2244.5 | 12.99 | 5.01 |
| 8.81 ± 0.01 | 3253 ± 3 | 2355.2 | 2.85 | 15.89 |

Cultures were manually shaken at least once daily, and 600 $\mu$L of culture was pipetted into a 96 well plate to measure cell counts on a BD Accuri™ C6 Plus Flow Cytometer. Growth rates were calculated on log-transformed cell counts using $\ln(N_2/N_2)/\Delta t$ where $N_2$ and $N_1$ are cell counts on two days with $\Delta t$ days in between. Dark respiration and net photosynthetic rates were measured according to (Barton *et al.*, 2020) (See Supplementary Information for detailed methodology).

**Proteomic analysis**

In-solution protein extraction, dilution and digestion were carried out according to (Dedman *et al.*, 2023a). For detailed methodology, refer to the Supplementary Information. Peptides were stored at -80˚C before shipping on dry ice to the Metabolomics and Proteomics Laboratory, University of York. Peptides were loaded onto EvoTip Pure tips for introduction onto an EvoSep One nanoUPLC system. A pre-set 60 SPD gradient was used with an 8 cm EvoSep $C_{18}$ Performance column (8 cm x 150 □m x 3 □m).

The nanoUPLC system was interfaced to a timsTOF HT mass spectrometer (Bruker) with a CaptiveSpray ionisation source. Positive PASEF-DIA, nanoESI-MS and $MS^2$ spectra were acquired using Compass HyStar software (version 6.2, Bruker). Instrument source settings were: capillary voltage, 1,500 V; dry gas, 3 l/min; dry temperature; 180˚C. Spectra were acquired between *m/z* 100-1,700. DIA windows were set to 25 Th width between *m/z* 400-1201 and a TIMS range of 1/K0 0.6-1.60

V.s/cm$^2$. Collision energy was interpolated between 20 eV at 0.6 V.s/cm$^2$ to 59 eV at 1.6 V.s/cm$^2$.

Resulting DIA data in Bruker .d format were searched against the appropriate database using DIA-NN (1.8.2.27). *G. huxleyi* genome (strain CCMP1516; UP000013827) was downloaded on 10/10/2023 (UniProt). The *Chrysotila* and *Coccolithus* subset of NCBI proteins were downloaded on the 10/10/2023. An in-silico predicted spectral library was created with the DIA-NN software, which was then iterated against the DIA data generated for these samples. High precision robust LC option wan used for quantification (Kistner *et al.*, 2023). The search was run at 1% FDR. The DIA-NN .tsv output was compiled, filtered (≥ 2 peptides) and pivoted to a normalised protein group-centric output using custom KNIME pipelines. Sample minimum value imputation was applied. Available annotations, i.e., GO terms (Carbon *et al.*, 2019) and InterPro (Blum *et al.*, 2021) annotations were obtained for *C. carterae* and *C. braarudii* through the ID mapping tool in UniProt (www.uniprot.org; Bateman et al., 2015) and was used to infer protein function.

**Statistical analysis**

For proteomic data, statistical comparison of relative abundance between protein groups was undertaken using limma through FragPipe-Analyst, run as a local installation in R-Shiny. For multiple test correction the Benjamini and Hochberg approach was applied and thresholds for significance were set to 0.05 adjusted p-value. Statistical analysis for physiological measurements such as growth rates, net photosynthesis and dark respiration rates were undertaken in R. Normal distribution of the data could not be confirmed for some datasets due to limited number of samples per treatment per species ($n$ = 3 – 6), therefore, both parametric and non-parametric tests were performed depending on the sample

size and the type of distribution observed. The tests included Welch t-test, ANOVA, Wilcoxon Rank Sum test, and Kruskal Wallis rank sum test.

**Results and Discussion**

Proteomic analysis revealed systematic changes in protein abundance with changing pH (Table 2). The proportion of significantly upregulated or downregulated proteins, relative to the control, varied amongst species but seemed to correlate with the pH impact on growth rate (Fig. 1). The abundance of approximately 0.7 % of identified proteins in *G. huxleyi* exhibited significant changes at pH 7.6 (both up- and down-regulated), while 19 % showed alterations at pH 8.8. In *C. carterae*, 0.5 % of total identified proteins displayed significant changes at pH 7.6, compared to 0 % at pH 8.8. *C. braarudii* exhibited the largest changes, with 16 % proteins at pH 7.6 and 26 % at pH 8.8 displaying altered abundance. Previous studies reported similar observations for *G. huxleyi*, where exposure to acidic conditions did not bring about major changes in the proteome (Jones *et al.*, 2013). However, contrary to our findings for *C. carterae*, (Thangaraj *et al.*, 2023) observed major changes in photosynthesis, carbohydrate metabolism, and changes in metabolic pathways related to macromolecule synthesis and metabolism when exposed to lower pH and higher temperature conditions. This suggests that *C. carterae* may be resilient towards pH changes, but not to changes in temperature, or a combined effect of high temperature and low pH. This seems plausible, as previous studies have shown increased sensitivity of coccolithophores to combined effects of changing $CO_2$ levels and temperature, and other environmental parameters (Feng *et al.*, 2008; Sett *et al.*, 2014; Zhang & Gao, 2021).

An important caveat to mention is that only *G. huxleyi* had a complete (and available) reference genome at the time of undertaking this study, therefore, it is

possible that some pH sensitive proteins are missing from the available sequences for *C. carterae* and *C. braarudii* on the NCBI database. Consequently, the results of this study are not directly comparable between each species. However, given the >1000 protein-groups identified (Table 2), and the proportion of significant change in each species, the results strongly imply a varied pH sensitivity, which is supported by the physiological observations (Fig. 1, 2).

**Table 2:** Protein groups obtained from the proteomic analysis with those exhibiting significant up- or downregulation in abundance. We identified 286 uncharacterised proteins in *C. braarudii*, 6 in *C. carterae*, and 186 in *G. huxleyi,* which are included in the significantly expressed proteins in this table. However, these were not included in further analysis.

| Species | pH (vs. pH 8.2) | Total identified protein groups | Significant protein groups (treatment vs. control) | Up-regulated protein groups Total **(significant)** | Down-regulated protein groups Total **(significant)** |
|---|---|---|---|---|---|
| *G. huxleyi* | 7.6 | 4708 | 31 | 2435 **(20)** | 2245 **(11)** |
| | 8.8 | | 885 | 2017 **(253)** | 2664 **(632)** |
| *C. braarudii* | 7.6 | 2530 | 415 | 1462 **(335)** | 1053 **(80)** |
| | 8.8 | | 664 | 1452 **(501)** | 1064 **(163)** |
| *C. carterae* | 7.6 | 1678 | 9 | 777 **(2)** | 873 **(7)** |
| | 8.8 | | 0 | 746 **(0)** | 903 **(0)** |

**Changes in ambient pH cause species-specific alterations in coccolithophore growth.**

pH-induced stress disrupts cellular homeostasis, leading to the production of Reactive Oxygen Species (ROS; Rokitta et al., 2012). These ROS react rapidly with macromolecules, inhibiting their activity and consequently, impacting growth rates (Dawes, 2000). Overproduction of ROS can disrupt cell cycle regulation and damage DNA by targeting thymine and guanine residues, resulting in breaks in

DNA strands and interacting with nitrogenous bases and deoxyribose (Reichheld *et al.*, 1999). As a result, ROS can induce DNA fragmentation, hindering proper DNA coiling within chromatin, potentially leading to mutagenesis (Juan *et al.*, 2021). The cell cycle can be halted to repair any DNA damage to avoid mutagenesis and ensure proper DNA replication (Qi & Zhang, 2019). A delay in cell cycle progression causes growth arrest, evidenced by reduced growth rates and the upregulation in DNA repair and cell cycle-related proteins (Reichheld *et al.*, 1999).

Species-specific changes in growth rates were observed across varying seawater pH in this study (Fig. 1a). Growth rate reduced significantly for *G. huxleyi* at pH 8.8 compared to the control ($t_{10} = 5.71$, $p < 0.0002$), whereas growth rates increased at pH 7.6 (statistically insignificant). The increase in growth rates at pH 7.6, although statistically insignificant, may be caused by improved photosynthetic rates under high $CO_2$ availability, as previously reported (Iglesias-Rodriguez et al., 2008b). Reduced growth rates at pH 8.8 in *G. huxleyi* may be due to a combination of reduced $CO_2$ availability and heightened pH-induced stress, as previously suggested (Bach *et al.*, 2013). Notably, *G. huxleyi* exhibited significant downregulation in DNA synthesis and cell cycle related proteins at pH 8.8. For instance, ribonucleoside-diphosphate reductase small chain, which catalyses DNA biosynthesis and plays a role in DNA damage repair displayed a -6.5 Log2 Fold Change (LFC) downregulation, while DNA polymerase showed a -4.7 LFC downregulation indicating reduced DNA replication under stressed alkaline conditions. Furthermore, histones, the major protein components of chromatin were also significantly affected: histone deacetylase (-1.19 LFC), histone-binding protein RBBP4 (-3.60 LFC), and histone H2A (-3.90 LFC) were significantly downregulated at pH 8.8 in *G. huxleyi*.

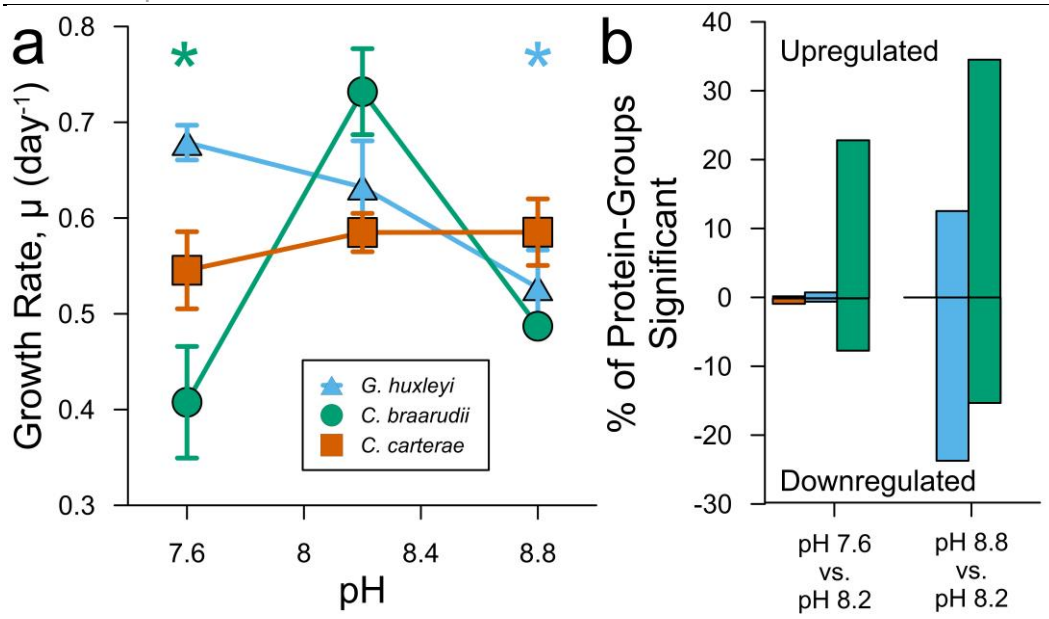


**Figure 1: (a)** Growth rates (day$^{-1}$) for *G. huxleyi* (●), *C. braarudii* (●), and *C. carterae* (●) grown at different seawater pH. $N = 2 - 10$. Only two measurements of growth rates were possible for *C. braarudii* at pH 8.8 due to cell clumping. Statistical tests were not performed for this particular treatment of *C. braarudii.* Statistically significant changes in growth rates were observed for *C. braarudii* at pH 7.6 (W = 0, *p*-value <0.05) and for *G. huxleyi* at pH 8.8 (W = 36, *p*-value < 0.01; $t_{10} = 5.71$, *p*-value < 0.0002). Colour coded asterisks (*) represent statistical significance (*p*-value < 0.05) for that treatment against the control (pH 8.2) within that species. **(b)** Percentage of significantly changed (upregulated and downregulated) protein-groups compared to the total identified protein-groups. Percent change of upregulated (or downregulated) proteins was calculated using the number of significantly upregulated (or downregulated) proteins for a given species and pH, versus the total number of significant proteins for that species at that pH. pH treatments were compared to the control (pH 8.2).

*C. carterae* displayed marginal increases in growth rates at pH 8.2 and 8.8 compared to pH 7.6, which were statistically insignificant. *C. carterae* exhibited only minor changes in DNA synthesis and cell-cycle-related proteins. For instance, ribonucleoside-diphosphate reductase showed a 0.58 LFC upregulation at pH 7.6 and a -2.24 LFC downregulation at pH 8.8. Moreover, Histone H2A, a structural constituent of chromatin was downregulated by -0.85 LFC at pH 7.6 and upregulated by 0.2 LFC at pH 8.8. However, these changes were not statistically significant when compared to the control (pH 8.2). The marginal changes in the whole-cell proteome of *C. carterae* supports the argument that this species is able to regulate its chemical environment through internal buffering, which allows

proper cellular functioning even under environmental change (Chauhan & Rickaby, 2024).

*C. braarudii* showed the highest growth rates at pH 8.2, with the most significant reduction in growth rates at pH 7.6 and pH 8.8 compared to the other species, indicating high sensitivity to pH-induced stress compared to the other two species. Significant alterations in cell-cycle-related protein-groups were observed at both pH 7.6 and pH 8.8 compared to the control. However, only two growth rate measurements were feasible at pH 8.8 for *C. braarudii* due to cell clumping, preventing statistical analyses of growth rates. Consequently, statistically significant changes were observed for *C. braarudii* only at pH 7.6 ($t_4$ = -5.01, $p$ < 0.01). Cell clumping in coccolithophores has been reported previously as a consequence of $CO_2$ and/or pH perturbations (Rickaby *et al.*, 2010; Langer & Bode, 2011; Walker *et al.*, 2018; Chauhan & Rickaby, 2024).

In *C. braarudii*, DNA replication licensing factor MCM7 was downregulated: -1.2 LFC at pH 7.6 and -1.5 LFC at pH 8.8, while cell cycle control protein 50A was upregulated: 1.52 LFC at pH 7.6 and 1.96 LFC at pH 8.8. Thymidylate synthase, involved in DNA biosynthesis was downregulated (-1.48 LFC) at pH 8.8 in *C. braarudii*. This species exhibited significant changes in multiple sugar phosphate transporter domain-containing proteins with up to 5.8 LFC at pH 7.6, and up to 7.7 LFC at pH 8.8. Such upregulation of sugar phosphate transporters has been directly linked to growth inhibition in *E. coli*, due to increased accumulation of organophosphates in the cell and/or depletion of inorganic phosphate pools due to the transportation process (Kadner *et al.*, 1992). Similar mechanisms of growth inhibition may be possible for *C. braarudii.*

Observations made in this study can be corroborated by evidence from previous studies. Jones et al. (2013) reported significant changes in histones in *G. huxleyi*

under ocean acidification, which they related to slower growth rates. Among the species studied here, *C. braarudii* appeared to display the highest sensitivity to pH, as evident by the percent change in protein-group abundance at different pH compared to the control. This aligns with its reported inability to maintain pH homeostasis due to reduced proton channel activity (Kottmeier *et al.*, 2022), and leading to substantial decreases in growth rates. *G. huxleyi* demonstrated proportional increases in growth rates with $CO_2$ availability, suggesting a preferential allocation of photosynthetically-derived resources towards growth under high $CO_2$ (low pH) conditions (Fig. 1a, 2a). The resilience of *G. huxleyi* to oxidative stress likely contributes to its higher growth rates compared to *C. braarudii*, as evidenced by the interspecific differences in the magnitude of change in protein-groups (Rokitta et al., 2012b; Barton et al., 2023). While *C. braarudii* exhibited the highest growth rates under control conditions (pH 8.2), these rates dropped under low pH conditions suggesting a high sensitivity to stress, despite increased $CO_2$ availability. *C. carterae* displayed insignificant changes in growth rates. Despite higher $CO_2$ availability at pH 7.6, growth rates did not change perhaps due to elevated stress-related energetic costs under acidic conditions. These physiological changes were evident through proteomic analyses, where higher stress at pH 7.6 corresponded to more significant alterations in protein expression compared to alkaline conditions (pH 8.8; Table 1).

Although changes in growth rates for *C. braarudii* and *C. carterae* were consistent with our previous observations, *G. huxleyi* showed a contrasting response (Chauhan & Rickaby, 2024; Kottmeier et al., 2022; White et al., 2018). *G. huxleyi* strain RCC 1731 used in this study exhibited an increase in growth rates with decreasing pH, while strain PLY 837 used in our previous work displayed the highest growth rates under alkaline conditions (Chauhan & Rickaby, 2024). Strain-

specific responses to changing environmental pH have been reported previously (Langer *et al.*, 2009; Rickaby *et al.*, 2016), which may be a consequence of different carbonate chemistries at the site of isolation of these strains (Blanco-Ameijeiras *et al.*, 2016). Notably, RCC 1731 was isolated near the coast of Ecuador (Lat: -2.67, Long: -82.72; Read et al., 2013) from $CO_2$-rich, low-pH waters (Chavez *et al.*, 2008). PLY 837 was isolated from the North Sea (original ID: D366 40-5; Lat: 56.5, Long: 3.65; Krueger-Hadfield et al., 2014) where seawater pH is comparatively more alkaline (Thomas *et al.*, 2007).

**Proteomic changes provide evidence towards the interplay between pH-induced stress and $CO_2$ availability during photosynthesis.**

Previous studies have emphasised the remarkable adaptability of the photosynthetic machinery in coccolithophores to variations in light intensity and $CO_2$ availability (Suggett *et al.*, 2007; Lefebvre *et al.*, 2010). All three coccolithophore species studied here exhibited a decrease in Net Photosynthetic (NP) rates under alkaline conditions (pH 8.8) compared to the control (pH 8.2; Fig. 2a). *G. huxleyi* and *C. carterae* exhibited an increase in NP rates under acidic conditions (pH 7.6) compared to the control, while *C. braarudii* exhibited marginal changes. Higher NP rates are consistent with higher $CO_2$ availability, as shown previously (Gao *et al.*, 1991; Zou, 2005; Mackey *et al.*, 2015).

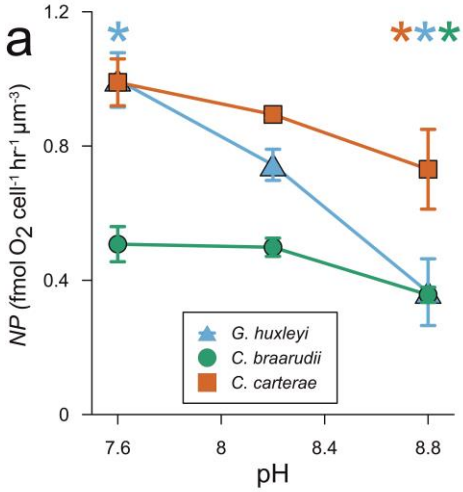


b

| Protein | *G. huxleyi* pH 7.6 | *G. huxleyi* pH 8.8 | *C. braarudii* pH 7.6 | *C. braarudii* pH 8.8 | *C. carterae* pH 7.6 | *C. carterae* pH 8.8 |
|---|---|---|---|---|---|---|
| Photosystem I P700 chlorophyll a apoprotein A1 | | | | | -1.91 | |
| Photosystem I iron-sulfur centre | | -2.78 | | | | |
| Photosystem I assembly protein Ycf4 | | -1.38 | | | | |
| Photosystem I subunit VII | | | | | -1.97 | |
| Photosystem II 47 kDa protein | | | | | -2.37 | |
| PSII assembly factor Ycf48/Hcf136 | | 0.66 | | 1.71 | | |
| Photosystem II reaction centre protein Y | | -2.74 | | | | |
| Photosystem II 11 kDa protein | | 0.93 | 1.33 | 1.84 | | |
| Photosystem II Psb27 protein | | | | | -1.55 | |
| Photosystem II CP43 reaction centre protein | | | 1.96 | 2.17 | | |
| Photosystem II protein D1 | | | | 2 | -2.12 | |
| PsbP C-terminal domain-containing protein | | 0.69 | 1.19 | 1.46 | | |
| Cytochrome c-553 | | | | -0.91 | | |
| Cytochrome b559 subunit alpha | | -1.79 | | | | |
| Cytochrome b6 | | | | | -1.5 | |
| Light harvesting proteins | -2 | -5.86 | 4.62 | 4.78 | | |
| Ferredoxin-sulfite reductase | -1.14 | | | 1.11 | | |
| Protochlorophyllide reductase | | 1.07 | | 1.09 | | |
| Plastocyanin | | 1.59 | | | | |
| Plastid lipid-associated protein/fibrillin | | | 0.72 | 2.35 | | |
| VDE lipocalin domain-containing protein | | | 0.88 | 0.77 | | |
| ATP synthase F1 complex delta/epsilon subunit | | 2 | 1.73 | | | |
| Fucoxanthin chlorophyll a/c binding protein | | | | | -2.08 | 0.51 |
| RuBisCO | | -0.51 | | | | |
| Fructose-bisphosphatase | | 0.56 | | | | |
| SBPase | | -0.89 | | | | |

**Figure 2: (a)** Net photosynthesis (NP) rates for *G. huxleyi* (●), *C. braarudii* (●), and *C. carterae* (●) grown at different seawater pH. Colour coded asterisks (*) represent statistical significance (*p*-value < 0.05) for that treatment against the control (pH 8.2) within that species. Absolute values for net photosynthetic rates and dark respiration rates were normalised based on average cell volumes for visual purposes. Cell diameter (decalcified) for calculating volumes for *G. huxleyi:* $\bar{x}$ = 4.23 µm (*n* = 465), *C. braarudii:* $\bar{x}$ = 15.54 µm (*n* = 1843), and *C. carterae:* $\bar{x}$ = 11.04 µm (*n* = 908) based on values obtained through a Beckman Z2 Coulter Counter (data not shown). Size-corrected net photosynthetic rates (fmol $O_2$ cell$^{-1}$ hr$^{-1}$ µm$^{-3}$). *n* = 4 – 5. Statistically significant changes in net photosynthetic rates were observed for C. braarudii at pH 8.8 ($t_4$ = 7.54, *p*-value <0.001; W = 9, *p*-value <0.05; $F_{1,4}$ = 56.91, *p*-value < 0.002; $H_1$ = 3.85, *p*-value <0.05), for G. huxleyi at pH 7.6 ($t_4$ = 3.85, *p*-value <0.02; $F_{1,4}$ = 14.85, *p*-value < 0.02; $H_1$ = 3.85, *p*-value <0.05), and pH 8.8 ($t_4$ = 6.89, *p*-value = 0.002; W = 9, *p*-value <0.05; $F_{1,4}$ = 47.59, *p*-value = 0.002; $H_1$ = 3.85, *p*-value <0.05), and for C. carterae at pH 8.8 (W = 9, *p*-value <0.05; $H_1$ = 3.85, *p*-value <0.05). **(b)** Heatmap displaying key photosynthetic proteins that were significantly altered in abundance at pH 7.6 and pH 8.8 compared to the control (pH 8.2). Relative protein abundances based on raw LFQ intensities are presented in a blue-to-red scale of increasing abundance. White spaces represent where a protein was not significantly altered relative to the control or was not identified by proteomic analysis for that particular species. Where more than one instances of the same protein were observed, only the maximal change has been reported in the table. Respective Log2 fold-changes for each protein at pH 7.6 and pH 8.8 are provided within the cell.

Volume corrected NP rates for *G. huxleyi* suggest that indeed, as previously reported, this species is carbon limited under control (pH 8.2) nutrient-replete conditions, as photosynthetic rates increased at higher $CO_2$ concentrations (pH 7.6; Paasche, 1964; Nielsen, 1995; Rost et al., 2003). NP rates for *G. huxleyi* further reduce at high pH (pH 8.8) due to reduced $CO_2$ availability, and its impact is observed through reduced growth rates (Fig. 1a). Indeed, RuBisCO was

downregulated in *G. huxleyi* at pH 8.8 (-0.51 LFC), which suggests reduced activity of the Calvin cycle. Reduced carbon fixation through the Calvin cycle is further evidenced by a downregulation of sedoheptulose-1,7-bisphosphatase (-0.89 LFC) at pH 8.8 in *G. huxleyi,* which is in line with reduced growth rates indicating redirection of energy away from carbon fixation and towards cellular maintenance (ATP used for ion transport, metabolite biosynthesis, and breakdown). It is also important to remember that changes in stromal pH can change the amount of $CO_2$ available for fixation (Werdan *et al.*, 1975). Moreover, changes in ambient pH have reportedly caused a shift in carbon fixation from 3-carbon compounds to 4-carbon compounds in green algae (Ouellet & Benson, 1952). Although it has been suggested that coccolithophores can utilise bicarbonate as a substrate for photosynthesis during low $CO_2$ availability via carbon concentrating mechanisms (CCMs), we observed a downregulation in 2 $HCO_3^-$ transporters (-2.72 and -1.94 LFC) in *G. huxleyi* at pH 8.8 (Nimer *et al.*, 1997). This observation seems contradictory to the suggested carbon limitation under alkaline conditions, but the downregulation of (chloroplastic) bicarbonate transporters under pH stress might be a way to regulate PSII activity and prevent the accumulation of ROS in the chloroplast (Xie *et al.*, 2021). However, the subcellular location of these bicarbonate transporters cannot be confirmed.

*C. carterae* shows the highest volume-corrected NP rates even under reduced $CO_2$ availability, perhaps due to the upregulation of carbonic anhydrase, as observed in this study (0.55 – 1.02 LFC between pH 8.2 and 8.8; statistically significant between pH 7.6 – 8.8; *p*-value = 0.04), or via active bicarbonate uptake (no significant differences found in this study). Out of the 9 significant proteins at pH 7.6 in *C. carterae*, 6 were photosynthesis-related, which were all downregulated (Fig. 2b). *G. huxleyi* showed significant downregulation of two Light Harvesting Proteins (LHPs) under acidic conditions, while 19 LHPs were downregulated under

alkaline conditions. LHPs are integral to the Light Harvesting Complex (LHC), transitioning from light harvesting to energy quenching to protect the photosynthetic machinery from damage under stress, known as Non-Photochemical Quenching (NPQ; (Trinh & Masuda, 2022). The LHC comprises LHP-chlorophyll pigment complexes. The upregulation of chlorophyll biosynthesis-related proteins in our study, combined with previous reports of increased chlorophyll pigment in response to lower pH suggests a multifaceted adaptation strategy of the photosynthetic machinery to environmental stress (Suggett *et al.*, 2007; Eberhard *et al.*, 2008; Gong *et al.*, 2020; Johnson *et al.*, 2022), where fine-tuning the amount of chlorophyll and accessory pigments, expression of LHPs, and the activity of light-dependent and -independent reactions determine the amount of light captured, NADPH and ATP produced, and how much of that energy is used for carbon fixation or cellular maintenance (Suggett et al., 2007; Muramatsu & Hihara, 2011; Rokitta et al., 2012a; Miyake, 2020). Such characteristics probably play a crucial role in implementing the lack of photoinhibition in *G. huxleyi*, even under very high light intensities (Nanninga & Tyrrell, 1996).

Alongside downregulated LHPs at pH 7.6, only Ferredoxin-Sulfite reductase is downregulated in *G. huxleyi,* whereas at pH 8.8, we observe widespread downregulation in PSII- and PSI-related proteins, although plastocyanin and ATP synthase were upregulated. This reduction in photosynthetic machinery may conserve energy when this machinery is not being used to its full potential under $CO_2$ limitation. This is consistent with the decline in growth rates and NP rates under alkaline conditions. The upregulation of plastocyanin and ATP synthase could be a response to increase/support cyclic electron flow in the photosystem, a process tightly linked to ROS production (Deng *et al.*, 2003; Miyake, 2020). Conversely, the downregulation of LHPs under acidic conditions could be a

strategy to allocate resources away from an efficient photosystem under high $CO_2$ availability, redirecting them towards growth (McCarthy et al., 2012; Rokitta et al., 2012a). This can also explain the responses observed at pH 7.6 in *C. carterae*, where an efficient photosynthetic machinery allowed downregulation of photosynthesis-related proteins so that additional resources (such as ATP, nitrogen) can be directed towards other cellular processes for stress management under reduced growth (Thangaraj *et al.*, 2023).

*C. braarudii* has the lowest volume-corrected NP rates (Fig. 2a). The marginal changes in NP rates even under higher $CO_2$ concentrations (pH 7.6) for *C. braarudii* in the present study may be related to higher energy requirements under low pH-related stress as well as increased non-photochemical quenching, as previously reported for other algae (Gao & Zheng, 2010). LHPs were significantly upregulated in *C. braarudii* at both pH 7.6 and pH 8.8. Although both treatments led to similar changes in the LHPs, they may have different drivers – the upregulation of LHPs under acidic conditions may be a response to capitalise on high $CO_2$ availability. However, its sensitivity to stress appears to hinder this upregulation from translating into improved photosynthetic performance, ultimately causing a reduction in growth rate in *C. braarudii*.

These changes provide further evidence towards species-specific responses to pH change, as both *C. carterae* and *G. huxleyi* exhibited downregulation in photosynthesis-related proteins at pH 7.6 (Fig. 2b). PSII and the LHP complex are upregulated under alkaline conditions due to PSII's higher susceptibility to stress requiring increased protein turnover (Xie *et al.*, 2021). LHPs may be upregulated to quench light energy that cannot be dissipated through photosynthesis due to reduced $CO_2$ availability. Another contrasting observation can be made between *C. braarudii* and *C. carterae*, where the former displays an upregulation of PSII

protein D1 at pH 8.8, while the latter exhibits a downregulation of the same protein at pH 7.6 (Fig. 2b). Protein D1 repairs photodamage to PSII and the production of D1 protein can be interrupted by limiting $CO_2$ fixation (Murata *et al.*, 2007). Disruption of pH homeostasis in the chloroplast can also degrade protein D1 in PSII reaction centres and inhibit the ability of the chloroplast to utilise light energy (Ma *et al.*, 2020).

Under low $CO_2$ availability at pH 8.8, *C. braarudii* may experience photoinhibition because the rate of consumption of light energy is slower than the rate of absorption under $CO_2$ limitation. Alternatively, *C. carterae* is possibly experiencing lower rates of photoinhibition under high $CO_2$ levels at pH 7.6, leading to the downregulation of protein D1 (Takahashi & Murata, 2008). In summary, higher $CO_2$ availability under acidic conditions generally enhances photosynthetic activity, as seen in *G. huxleyi*. However, increasing photosynthetic activity translates to higher growth rates only when photosynthesis outweighs stress-related energy requirements. This does not seem to be the case for *C. braarudii* at pH 7.6.

**Cellular requirement for metabolites and energy under stress dictate changes in energy metabolism.**

The mitochondrion is involved in almost every cellular process. Consequently, any shifts in cellular homeostasis impact respiration rates and mitochondrial activity (Spinelli & Haigis, 2018). Dark Respiration (DR) rates for *G. huxleyi* and *C. carterae* showed statistically insignificant changes with changing pH (Fig. 3a). However, DR rates for *C. braarudii* declined by ~86 % under alkaline conditions (pH 8.8) compared to the DR rates at pH 8.2 ($F_{1,4} = 376.7$, $p < 0.0001$). The reduced DR rates under changing pH may be due to reduced activity of the mitochondrial electron transport chain as a consequence of disrupted pH homeostasis (Vohwinkel *et al.*,

2011; Yu *et al.*, 2017; Zhang *et al.*, 2023). This is because the production of ATP via the consumption of oxygen (and metabolites) in the electron transport chain requires a stable proton gradient between the inner and outer mitochondrial membranes (Berg *et al.*, 2015). Several mitochondrial proteins were highly upregulated in *C. braarudii* under both pH 7.6 and pH 8.8 suggesting increased mitochondrial activity. These changes included an upregulation in mitochondrial carrier proteins, ADP/ATP translocases, and upregulation of SURF1-like protein and COX (cytochrome c oxidase) assembly protein. An upregulation in COX assembly proteins suggests increase cytochrome c oxidase biogenesis (Zhang *et al.*, 2023). Reduced DR rates under pH stress, coupled with the upregulation of Cytochrome oxidase and COX assembly proteins, seem contradictory. Yet, these findings are justified as stress-induced oxidative damage to mitochondrial DNA (mtDNA) leads to mitochondrial dysfunction, culminating in reduced respiration rates (Vohwinkel *et al.*, 2011; Brand & Nicholls, 2011). Individual enzymes within the respiratory chain could be upregulated as a compensatory mechanism to sustain normal mitochondrial function and respiratory activity (Yu *et al.*, 2017; Avram *et al.*, 2022).

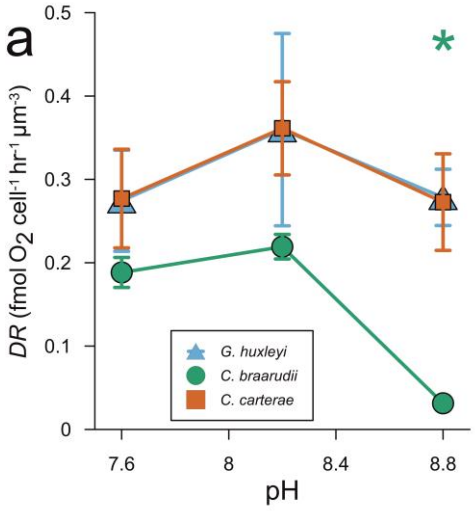


b

| Protein | *G. huxleyi* pH 7.6 | *G. huxleyi* pH 8.8 | *C. braarudii* pH 7.6 | *C. braarudii* pH 8.8 | *C. carterae* |
|---|---|---|---|---|---|
| **Glycolysis/Gluconeogenesis** | | | | | |
| Glycerol kinase | | 0.77 | | | |
| Glucokinase | | -1.09 | 1.18 | 1.51 | |
| Phosphofructokinase | | 0.88 | | -0.96 | |
| Aldolase | | -1.2 1.38 | 2.54 | -1.34 | |
| Glycerol-3-P dehydrogenase | | -4.15 | | | |
| Glyceraldehyde-3-P dehydrogenase | | -1.88 | | 0.65 | |
| Phosphoglycerate mutase | | 2.26 | -0.99 | 2.41 | |
| Pyruvate kinase | | 0.67 | | | No significant changes |
| Phosphotransferase | | -1.19 | | | |
| Triosephosphate isomerase | | -0.88 | | | |
| Glucose-6-P isomerase | | 0.54 | -0.84 | -0.67 | |
| Enolase | | | 2.09 | | |
| Phosphopyruvate hydratase | 2.09 | | | 0.87 | |
| Pyruvate carboxyltransferase | | | -1.1 | | |
| Fructose-bisphosphatase | | | 0.63 | 0.71 | |
| Phosphoglycerate kinase | | | | -1.2 | |
| **Pyruvate Dehydrogenase Complex** | | | | | |
| Lipoyl-binding protein | | | -1.14 | | |
| Dihydrolipoamide acetyltransferase | -0.93 | -1.1 1.1 | | | |
| PDH E1 component subunit α | | 0.6 | 0.81 | | |
| PDH E1 component subunit β | | | 0.66 | | |
| **TCA cycle** | | | | | |
| Fumarate hydratase | | 0.74 | | 0.62 | |
| Succinate CoA ligase | | 0.5 | | | |
| Isocitrate dehydrogenase | | 0.99 | | 0.82 | |
| Isocitrate lyase | | 1.15 | | | |
| Aconitate hydratase | | 0.89 | | | |
| Citrate synthase | | | 0.72 | 1.19 | |
| Malate dehydrogenase | | | 1.49 | 1.47 | |
| Succinate dehydrogenase | | | | 0.53 | |

**Figure 3: (a)** Size-corrected dark respiration rates (fmol $O_2$ $cell^{-1}$ $hr^{-1}$ $\mu m^{-3}$) for *G. huxleyi* (●), *C. braarudii* (●), and *C. carterae* (●) grown at different seawater pH ($n$ = 4 – 5). Colour coded asterisks (*) represent statistical significance ($p$-value < 0.05) for that treatment against the control (pH 8.2) within that species. Absolute values for net photosynthetic rates and dark respiration rates were normalised based on average cell volumes for visual purposes. Cell diameter (decalcified) for calculating volumes for *G. huxleyi:* $\bar{x}$ = 4.23 µm ($n$ = 465), *C. braarudii:* $\bar{x}$ = 15.54 µm ($n$ = 1843), and *C. carterae:* $\bar{x}$ = 11.04 µm ($n$ = 908) based on values obtained through a Beckman Z2 Coulter Counter (data not shown). Statistically significant changes in dark respiration rates were observed for *C. braarudii* at pH 8.8 ($t_4$ = -19.41, $p$-value <0.0001; W = 0, $p$-value <0.05; $F_{1,4}$ = 376.7, $p$-value < 0.0001; $H_1$ = 3.85, $p$-value <0.05). **(b)** Heatmap displaying key mitochondrial proteins that were significantly altered in abundance at pH 7.6 and pH 8.8 compared to the control (pH 8.2). Relative protein abundances based on raw LFQ intensities are presented in a blue-to-red scale of increasing abundance. White spaces represent where a protein was not significantly altered relative to the control or was not identified by proteomic analysis for that particular species. Where more than one instances of the same protein were observed, only the maximal change has been reported in the table. Respective Log2 fold-changes for each protein at pH 7.6 and pH 8.8 are provided within the cell. PDH: Pyruvate Dehydrogenase.

Several mitochondrial enzymes are pH-sensitive. For instance, the activity of phosphofructokinase, which is the rate limiting enzyme in glycolysis, increases with increasing pH within the physiological range (Ui, 1966; Fidelman *et al.*, 1982). For *G. huxleyi*, phosphofructokinase (0.88 LFC), and pyruvate kinase (0.67 LFC) exhibited an upregulation under alkaline conditions (Fig. 3b). This suggests an

increase in glycolytic activity; however, reduced respiration rates suggests that the intermediate products derived from glycolysis may be used in anabolic pathways for lipid and protein synthesis (Chandel, 2021). Under acidic conditions (pH 7.6), a notable change was only observed in enolase (2.09 LFC) suggesting increased production of phosphoenolpyruvate that can be used for biosynthesis of organic compounds or ATP production (Berg *et al.*, 2015). Insignificant changes were observed in the DR rates or glycolysis-related proteins in *C. carterae* under changing ambient pH. In the case of *C. braarudii*, glycolysis related proteins such as glucokinase (1.51 LFC) exhibited an upregulation, while glucose-6-phosphate isomerase (-0.67 LFC) and phosphofructokinase (-0.96 LFC) exhibited a downregulation under alkaline conditions (pH 8.8). This change in enzyme activity indicates that the metabolite glucose 6-phosphate derived from glucokinase may enter the pentose phosphate pathway, resulting in the generation of NADPH to maintain antioxidant capacity (Chen *et al.*, 2019).

The pyruvate dehydrogenase complex plays a key role in aerobic metabolism, and links glycolysis to the TCA cycle. Herein, *C. braarudii* exhibited changes in lipoyl-binding domain-containing protein (-1.14 LFC), pyruvate dehydrogenase E1 component subunit alpha (0.81 LFC) and subunit beta (0.66 LFC) at pH 7.6 while no such changes were observed at pH 8.8. *G. huxleyi* exhibited changes in dihydrolipoamide acetyltransferase (-1.12 – 1.09 LFC), Acetyl coenzyme A synthase (1 LFC) and pyruvate dehydrogenase E1, alpha subunit (0.60 LFC) at pH 8.8, while a change was only evident in dihydrolipoamide acetyltransferase (-0.93 LFC) at pH 7.6. Enzymes of the TCA cycle were also significantly changed in *G. huxleyi* and *C. braarudii*. The TCA cycle was generally upregulated in *G. huxleyi* under pH 8.8 whereas no changes were evident under pH 7.6 (Fig. 3b). Elevated expression of isocitrate dehydrogenase has been previously related to mitochondrial dysfunction and shown to cause inhibition in cell proliferation

(Vohwinkel *et al.*, 2011). Similarly, isocitrate dehydrogenase was upregulated in *G. huxleyi* (0.99 LFC) and *C. braarudii* (0.82 LFC) at pH 8.8. Increase in TCA cycle activity may be to support declining DR rates and indicates higher metabolite requirement for biosynthesis or increased recycling of internal metabolites under stress (Spinelli & Haigis, 2018).

Isocitrate lyase was shown to be significantly upregulated (1.15 LFC) at pH 8.8 in *G. huxleyi*. This enzyme skips several steps in the TCA cycle to produce succinate and glyoxylate (Dolan & Welch, 2018). This observation underscores a metabolic flexibility present, particularly in *G. huxleyi*, likely enhancing its respiratory performance under stress (O'Leary *et al.*, 2019). Similar observations under thermal stress suggest a generalised stress response for this species rather than a pH-unique one (Dedman *et al.*, 2023a). Such metabolic plasticity may contribute to its greater physiological resilience to environmental changes, and its ecological success in the present-day oceans.

*C. braarudii* also exhibited an upregulation in TCA cycle-related enzymes. For example, malate dehydrogenase, which catalyses the oxidation of malate to oxaloacetate, was upregulated by 1.5 LFC under both pH 7.6 and 8.8. However, while only 3 enzymes of the TCA cycle were upregulated at pH 7.6 in *C. braarudii*, 6 enzymes were upregulated at pH 8.8. Despite mitochondrial dysfunction, its activity remains vital for providing metabolites necessary for macromolecular synthesis. Although *C. carterae* did not exhibit significant changes in most metabolic proteins, some unique observations can be made: F-type ATPase was significantly downregulated at pH 7.6, and Pyrophosphate-fructose 6-phosphate 1-phosphotransferase exhibited significant upregulation when pH 7.6 was compared to pH 8.8. The downregulation in ATPase activity may be due to

sufficient energy being available through photosynthesis under high $CO_2$ availability.

In summary, changes in mitochondrion-related proteins did not translate to higher/lower DR rates, as reductions in DR rates were mostly statistically insignificant (Fig. 3a), which is consistent with the lack of changes observed in enzymes related to oxidative phosphorylation. ATP production through oxidative phosphorylation may not be upregulated due to disruptions in pH homeostasis under pH stress, however, glycolysis, TCA cycle, and other mitochondrial processes remained active, or were even upregulated to provide energy and metabolites for cellular maintenance under pH stress and to counteract mitochondrial dysfunction. Isocitrate lyase activity in *G. huxleyi* highlighted metabolic plasticity in this species, which potentially contributes to its physiological resilience to environmental stress. Additionally, the lack of changes in *C. carterae* provide further evidence that the internal buffering capacity of this species to chemical changes in the environment allows it to thrive under changing conditions.

**Changes in Net Photosynthesis and Respiration determine the fate of cellular carbon fixation in acidic and alkaline oceans.**

The proportional change in NP rates with $CO_2$ availability and reduced DR rates under pH stress observed in this study are likely to alter the ratio of carbon fixed versus respired under ocean acidification (OA) and artificial ocean alkalinisation (AOA) scenarios (Fig. 4). This net photosynthesis to dark respiration (NP:DR) ratio has been extensively studied in response to nutrient limitation and global warming (Steinacher *et al.*, 2010; Barton *et al.*, 2020), and is crucial in determining the balance of carbon flux towards the biological carbon pump, at least at the scale of a single cell (Field *et al.*, 1998). All three coccolithophores species in the

present study have nearly identical NP:DR ratios at control conditions (pH 8.2, 2.1 ≤ NP:DR ≥ 2.5) suggesting that the contribution of these species to biological carbon fixation is almost the same at an individual scale (Fig. 4). However, the NP:DR ratios change significantly under changing pH in coccolithophores. NP:DR ratios increase for all three coccolithophore species under acidic conditions (statistically insignificant increase for *C. braarudii*), suggesting that carbon fixation at an individual scale would be higher in an OA scenario. In comparison, a variable response is observed under alkaline conditions. Extreme reduction in respiration rates observed in *C. braarudii* at pH 8.8 leads to a very high NP:DR ratio. While a short-term increase in the NP:DR ratio for *C. braarudii* at pH 8.8 indicates increased primary productivity, this does not translate into higher growth rates due to the increase cost of repair associated with its sensitivity to stress. It is important to note that although carbon fixation through primary productivity in an OA scenario may increase for coccolithophores, changes in inorganic carbon to organic carbon (PIC:POC) ratios will also have an impact on the amount of carbon fixed (Riebesell et al., 2000; Iglesias-Rodriguez et al., 2008b; Krumhardt et al., 2017). Moreover, the contribution of coccolithophores to the global biological carbon pump will depend on the population sizes for each species, which may vary significantly, for instance, due to the bloom-forming capabilities of *G. huxleyi* (Tyrrell & Merico, 2004).

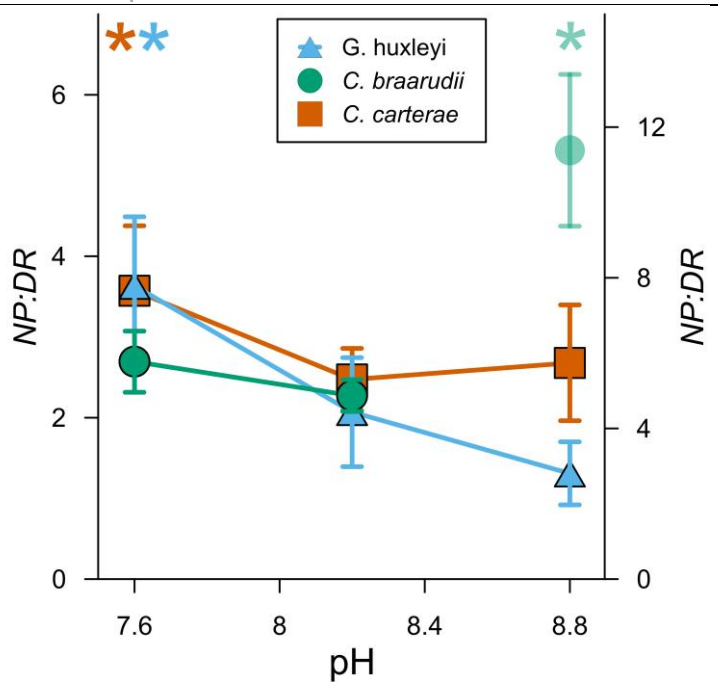


**Figure 4:** NP:DR ratios for *G. huxleyi* (●), *C. braarudii* (●), and *C. carterae* (●) grown at different seawater pH ($n$ = 4 – 5). Colour coded asterisks (*) represent statistical significance ($p$-value < 0.05) for that treatment against the control (pH 8.2) within that species. Note that the datapoint for *C. braarudii* at pH 8.8 has been plotted on a secondary Y-axis for better representation of the data. Significant changes in the NP:DR ratios were observed for *G. huxleyi* at pH 7.6 (W = 9, $p$-value <0.05; $H_1$ = 3.85, $p$-value <0.05), *C. carterae* at pH 7.6 (W = 9, $p$-value <0.05; $H_1$ = 3.85, $p$-value <0.05), and *C. braarudii* at pH 8.8 ($t_4$ = -8.78, $p$-value <0.001; W = 0, $p$-value <0.05; $F_{1,4}$ = 77.17, $p$-value < 0.001; $H_1$ = 3.85, $p$-value <0.05).

**Oxidative stress triggers the cellular stress response.**

A sizable proportion of the significantly changed protein-groups in *C. braarudii* (at pH 7.6 and pH 8.8) and *G. huxleyi* (at pH 8.8) were related to the Cellular Stress Response (CSR) and redox-scavenging pathways (Fig. 5; Kültz, 2004). The CSR encompasses a diverse array of proteins involved in various biological pathways due to the role ROS plays in cellular signalling. For example, NADPH oxidases in mitochondria typically generate ROS during oxidative metabolism. Under normal circumstances, production of ROS signals antioxidant enzymes such as superoxide dismutase to neutralise this ROS to avoid oxidative damage to the cell (Loschen *et al.*, 1974). However, alterations in mitochondrial membrane potential

(via pH) can lead to oxidative stress through excessive ROS production (Inzé & Montagu, 1995; Sena & Chandel, 2012).

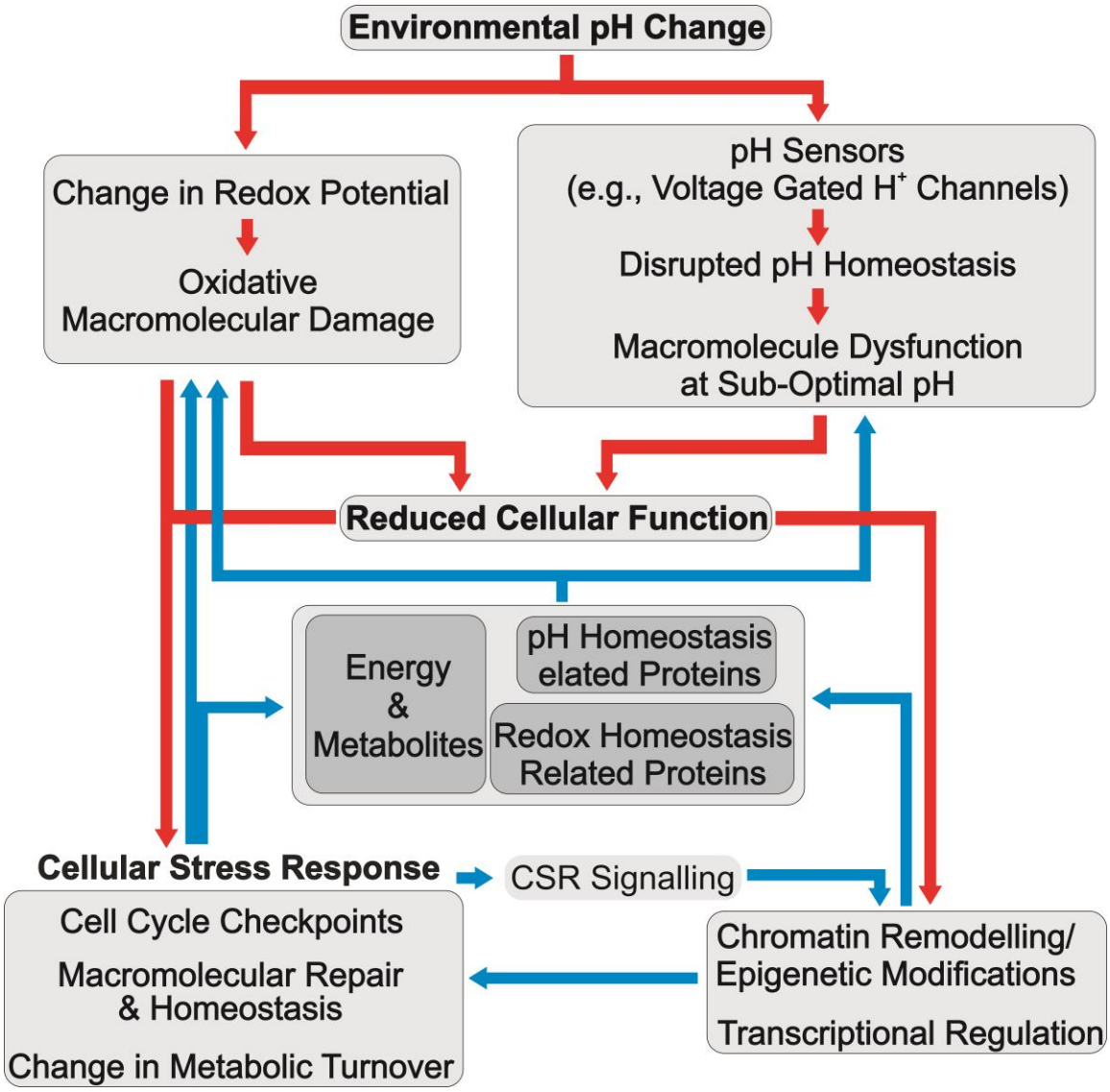


**Figure 5:** Schematic representation of the broad functions related to the Cellular Stress Response (CSR). Environmental pH stress triggers changes in cellular redox potential and pH-regulated voltage potential. Disruption in pH homeostasis leads to macromolecular dysfunction, which necessitates activation of specific proteins to restore pH homeostasis. Moreover, generation of ROS causes damage to macromolecules such as proteins, lipids, and DNA. Enzymes regulating the cell cycle, energy metabolism, protein repair, stabilisation, and degradation are notably expressed under stress conditions (Kültz, 2004). Additionally, macromolecular damage impedes normal cellular function, necessitating the involvement of proteins in redox regulation, DNA repair, protein degradation, molecular chaperones, fatty acid metabolism, and energy metabolism (Dawes, 2000).

Proteins related to redox homeostasis were evident in the coccolithophore species *C. braarudii* and *G. huxleyi* under stressed conditions. Several oxidoreductases, such as NADP-dependant oxidoreductase, were upregulated. ROS scavenging proteins such as glutathione synthase, glutaredoxin and thioredoxin were significantly upregulated at pH 8.8 in *G. huxleyi*, and at both pH 7.6 and 8.8 in *C. braarudii*. For instance, *C. braarudii* exhibited an upregulation in 6 thioredoxins with 0.58 – 1.95 LFC at pH 7.6 and upregulation in 9 thioredoxins (0.71 – 3.23 LFC) at pH 8.8. Thioredoxin acts as the primary antioxidant system in eukaryotes (Lu & Holmgren, 2014). Accumulation of ROS and significant changes in redox-related proteins under high $CO_2$ (low pH) conditions has been shown previously in *G. huxleyi* (Rokitta et al., 2012a; Vázquez et al., 2023). Although oxidative protein-groups did not show significant changes in *G. huxleyi* under acidic conditions (pH 7.6) in this study. However, it is likely that other *G. huxleyi* strains with ecological niches in seawater at comparatively higher pH (such as strain PLY 837) may experience oxidative stress under low pH (Chauhan & Rickaby, 2024). Higher temperature is also known to cause higher levels of ROS in *G. huxleyi*, and in plants (Rikhvanov *et al.*, 2014; Dedman *et al.*, 2023a). Moreover, higher ROS levels have been associated with the onset of viral infections in *G. huxleyi* (Sheyn *et al.*, 2016).

Notably for *C. carterae*, Thangaraj et al. (2023) did not report any changes in redox-related proteins under a combined ocean warming and acidification scenario. This is consistent with the findings of this study, where no changes in oxidative-stress-related proteins were observed for *C. carterae* with changing pH (Fig. 1b, Table 1). These observations suggest that the resilience to environmental changes in *C. carterae* is associated with its intracellular physicochemical properties, where a low surface area to volume ratio (as a consequence of large cell size) may provide a greater barrier for ions (such as $H^+$), and a large internal carbon pool and high intracellular pH which allows greater buffering of the

internal environment against chemical changes in the extracellular environment (Chauhan & Rickaby, 2024).

Oxidative stress also impacts various cellular components such as lipids, nucleic acids, and proteins. This damage disrupts the structure and function of cellular membranes, cytoskeletal proteins, and proteins of diverse functions (See Supplementary Information for detailed description of these results). Previous studies have reported upregulation of genes related to redox activity, fatty acid biosynthesis and protein signalling in coccolithophores under ocean acidification (Rokitta et al., 2012a; Thangaraj et al., 2023). Our observations agree, with upregulation noted in fatty acid biosynthesis to restore damaged lipids and aldehyde dehydrogenases to neutralise aldehydes formed during lipid peroxidation (Singh *et al.*, 2013). Additionally, a decrease in ribosomal activity coupled with increased proteolytic activity suggests inhibition of ribosomal translation and enhanced degradation of damaged proteins (Chondrogianni *et al.*, 2014). Notably, *G. huxleyi* and *C. braarudii* exhibited significant upregulation of proteases and PPIases, indicating increased activity in protein folding and degradation. A contrasting regulation of Derlin, an endoplasmic reticulum (ER)-associated degradation protein was observed between *G. huxleyi* and *C. braarudii,* where Derlin was downregulated at both pH 7.6 (-6.66 LFC) and pH 8.8 (-7.16 LFC) in *G. huxleyi*, but highly upregulated in *C. braarudii* (4.57 LFC at pH 7.6, 4.77 LFC at pH 8.8). This suggests species-specific stress responses, possibly impacting ER protein quality control mechanisms (Sugiyama *et al.*, 2021). Moreover, downregulation of HSPs in *G. huxleyi*, which are also ER-associated, further supports this species-specific stress response (Wang *et al.*, 2008).

Changes in ambient pH affects the electrochemical gradient between the ambient seawater and the cytoplasm. The pH of the cytoplasm must be maintained within

a narrow range as most proteins have a pH optimum. Consequently, a cell attempts to restore pH/electrochemical homeostasis via voltage-gated proton channels (Taylor *et al.*, 2011) and co-transporters via a "biophysical pH stat" mechanism (Smith & Reid, 1991). The activity of symporters or antiporters, which expel protons out into the seawater often bring about activity in other ion transporters, since ion homeostasis is disrupted during such cellular activity. In this study, several ion transporters changed significantly within the different coccolithophore species. *C. braarudii* exhibited notable changes in ABC transporters (-2.93 – 1.79, -1.65 – 1.67 LFC), V-type $H^+$ ATPase (1.33, 1.59 LFC), cation/ $H^+$ exchanger (1.17, 1.46 LFC), $Cl^-/HCO_3^-$ exchanger (1.46, 1.68 LFC), proton translocating transhydrogenase (1.51, 2.37 – 2.97 LFC), Cation-transporting P-type ATPase (1.62, 1.89 LFC), and Na/Ca exchanger (4.96, 2.55 – 4.77 LFC) at pH 7.6 and pH 8.8, respectively. Additionally, *C. braarudii* displayed upregulation of anion transporting ATPase (0.88 LFC), proton transporting diphosphatase (3.62 LFC), voltage gated anion channel (3.25 LFC), Ca/cation antiporter (2.19 LFC), major facilitator superfamily (MFS) profile domain-containing protein (4.06 – 4.41 LFC) at pH 8.8. *G. huxleyi* showed upregulation in five V-type $H^+$ ATPases (0.50 – 1.2 LFC), and downregulation in five ABC transporters (-5.46 – -0.6 LFC) at pH 8.8, but no significant changes at pH 7.6. Oxidative inhibition of V-type ATPases has been shown previously in mammals, plants and yeast, and the upregulation of these ATPases indicates the occurrence of a similar mechanism in *C. braarudii* and *G. huxleyi* under pH-induced oxidative stress in this study (Seidel *et al.*, 2012). *C. carterae* exhibited no significant changes in membrane transport activity under changing pH conditions, further corroborating the argument that its intracellular buffering capacity makes *C. carterae* resistant to chemical changes in the ambient environment (Chauhan & Rickaby, 2024).

**How does carbonate chemistry dictate coccolithophore ecology?**

If the findings of this study are broadly indicative of physiological and cellular changes in coccolithophores in an acidic or alkaline ocean, they suggest that highly species-specific responses may have a significant impact on the carbon fixing capabilities and ecological niches of coccolithophores in the future. The overarching question regarding species-specific tolerances to pH changes can be attributed to two phenomena: genetic adaptation of a given species to changing environment, and acclimation to ambient environmental changes (Moreno & Martiny, 2018). Physiological resilience in *G. huxleyi* may stem from its exceptional ability to withstand significant environmental stress. Despite a low surface area to volume ratio that makes it vulnerable to rapid intracellular pH fluctuations (Suffrian et al., 2011), this species might be "accustomed" to such changes. Consequently, it likely has effective stress-management mechanisms already in place (van der Wal *et al.*, 1985; Paasche, 2001; Barton *et al.*, 2023). Such a resilience to extracellular ROS has been observed for *G. huxleyi* previously but not in other coccolithophore species, suggesting a physiological characteristic unique to the *Gephyrocapsa* lineage (Barton *et al.*, 2023). Although its high surface area to volume ratio (as a consequence of small cell size) makes *G. huxleyi* vulnerable to greater ionic fluxes (Suffrian *et al.*, 2011b), the resilience of *G. huxleyi* can be attributed to its high cellular plasticity. For instance, through the expression of isocitrate lyase to bypass several steps of the TCA cycle and its ability to reallocate resources away from certain cellular processes (e.g., photosynthesis) during high efficiency (pH 7.6) or low activity (pH 8.8). This species also has the ability to switch its mode of carbon uptake from $CO_2$ diffusion under high $CO_2$ to utilise active $HCO_3^-$ uptake under low $CO_2$ concentrations (Kottmeier *et al.*, 2014, 2016c). Furthermore, the downregulation of HSPs, Derlin, and 26S proteasome under changing pH conditions further suggests unique mechanisms of metabolite

recycling. However, without additional studies on metabolomics, it is difficult to elaborate specific metabolic pathways involved in such processes. The physiological resilience, along with the genetic diversity of *G. huxleyi* may have facilitated the occupation of almost every ecological niche of the present-day ocean and will probably facilitate its adaptation to future ocean conditions (Rickaby *et al.*, 2016; Blanco-Ameijeiras *et al.*, 2016; Wheeler *et al.*, 2023).

A good example for high tolerance to environmental changes is *C. carterae*, which potentially experiences high magnitudes of change in ambient pH, salinity, light, and temperature in its coastal environment (Jordan, 2009). It is possible that the presence of specific osmotic solutes in the metabolome of *C. carterae* may assist this species in managing environment-related stress (Zhou *et al.*, 2016). However, the lack of proteomic changes under acidic or alkaline conditions in this study suggest that due to the coastal nature of *C. carterae*, this species may be preadapted to a wide range of environmental changes. Furthermore, the lack of changes in ion transport-related proteins further support the argument that the remarkable buffering capacity of *C. carterae* allows it to regulate its chemical environment, which translates into marginal changes in its physiology across a broad range of pH changes (1.2 pH units in this study). Genetic shifts have been reported to be responsible for the adaptation of other algae to highly acidic environments (e.g., Hirooka et al., 2017), and probably explain the ability of *C. carterae* to occupy a highly dynamic coastal niche and explains the ease of cultivating this species in a broad spectrum of seawater chemistries and chemical conditions (Probert & Houdan, 2004).

The high sensitivity of *C. braarudii* to pH changes as observed through reduced growth rates and changes in the proteome may be due to its dependence on voltage-gated proton channels for pH homeostasis (Taylor *et al.*, 2011; Kottmeier

*et al.*, 2022), which also explains its narrow ecological niche in present-day oceans (Daniels *et al.*, 2014, 2016). Although *G. huxleyi* also reportedly has high proton permeability (Suffrian *et al.*, 2011b), its ecological success may be related to its metabolic plasticity and genetic diversity as discussed above (Rickaby *et al.*, 2016). The large size of *C. braarudii* may allow some internal buffering to chemical changes in the environment (similar to *C. carterae*), the high calcification rate for this species results in substantial $H^+$ in the cell (Kottmeier *et al.*, 2022). Moreover, the lack of metabolic plasticity, such as the use of isocitrate lyase, active bicarbonate uptake (as seen in *G. huxleyi*), or carbonic anhydrase (as seen in *C. carterae*) makes it more reliant on "traditional" metabolic pathways. For instance, protein degradation, ion transport activity, photosynthetic machinery, and redox-scavenging proteins, which were all upregulated at both acidic and alkaline pH, in order to restore homeostasis and cellular productivity in *C. braarudii*. This is in contrast to observations made for *G. huxleyi*, which shows evidence of reduced activity of cellular processes to avoid redox-related damage and conserve energy.

Moreover, the requirement for calcification in *C. braarudii* is closely tied to its cell cycle, something which is not observed in the other two species studied here (Paasche, 2001; Frada *et al.*, 2018; Walker *et al.*, 2018). Therefore, impacts on calcification through changes in the calcium carbonate saturation state may have additional implications on calcification-related sensitivity of *C. braarudii* to changing ambient pH. The geologic past of *C. braarudii* may provide some reasoning for our observations. In the Eocene, *C. braarudii* proliferated under high $CO_2$ and lower pH conditions compared to the present-day oceans (Ridgwell, 2005; Agnini *et al.*, 2014). Today, this species occupies mostly upwelling and polar regions of the ocean, where dissolved $CO_2$ concentrations are higher, and pH is lower (Henderiks & Rickaby, 2007; Daniels *et al.*, 2016). Thus, the constraints imposed by the inability of *C. braarudii* to adjust cellular processes to prioritise

essential functions, its incapacity to suspend cellular activities during stress and limited substrate availability, and its reliance on high $CO_2$ levels elucidate the narrow ecological range of this species in contemporary oceans. While rising $CO_2$ levels under ocean acidification scenarios might offer some expansion opportunities for this species, its inability to adapt to shifting conditions could pose a significant hindrance.

The contrasting pH-related sensitivities of the coccolithophore species studied here suggest that lower-pH (OA) scenarios may select for low-pH adapted *G. huxleyi* strains such as the strain used in this study (RCC 1731). On the other hand, a higher-pH (AOA) scenario may also select for a high-pH adapted *G. huxleyi* strain such as the one used in our previous study (PLY 837; Chauhan & Rickaby, 2024). Population sizes for *C. braarudii* may decline drastically, although a growth optimum at slightly lower pH than present has been seen before (Chauhan & Rickaby, 2024). The changes (or lack thereof) in *C. carterae* suggest no major ecological changes for this species.

It is important to recognise that this experiment was conducted under constant temperature, light, and nutrient replete conditions, whereas future climate scenarios will entail higher temperatures and drastic shifts to light and nutrient regimes due to increased seawater stratification. The combined effect of these parameters will potentially have a greater or compounding impact on coccolithophore physiology and cellular processes (De Bodt *et al.*, 2010; Benner *et al.*, 2013; Sett *et al.*, 2014; Barton & Yvon-Durocher, 2019; Zhang & Gao, 2021; Johnson *et al.*, 2022). Additionally, the lack of reference genomes for all except one coccolithophore species drastically inhibits the quality of molecular studies on coccolithophore species (Skeffington *et al.*, 2023). Clearly, further work will be required to understand the interplay between environmental parameters and their

combined impact on the cellular biology of different species. Nevertheless, our results contribute to understanding the molecular mechanisms behind species-specific sensitivities to pH changes and their ecology in the modern ocean. These findings can be used to for better representation of different species in OA or AOA experiments, and to consider adaptive diversity in coccolithophore species in response to the impacts that humans exert on their environment.

**Supporting Information**

**The Supplementary text file** contains detailed descriptions of the methodology used in measuring the Net Photosynthetic and Dark Respiration rates, as well as the methodology for in-solution digestion of cellular biomass for proteomic analysis. Supplementary results, that are not directly related to, but complement the findings of the main text are also discussed. These include proteomic changes related to various cellular processes that displayed significant alterations in the present study.

# Statement of Authorship for joint/multi-authored papers for PGR thesis

To appear at the end of each thesis chapter submitted as an article/paper

The statement shall describe the candidate's and co-authors' independent research contributions in the thesis publications. For each publication there should exist a complete statement that is to be filled out and signed by the candidate and supervisor **(only required where there isn't already a statement of contribution within the paper itself).**

| | |
|---|---|
| Title of Paper | Contrasting Stress Response to Environmental pH Determines the Fate of Coccolithophores in Future Oceans |
| Publication Status | ☑ Published ☐ Accepted for Publication<br>☐ Submitted for Publication ☐ Unpublished and unsubmitted work written in a manuscript style |
| Publication Details | Nishant Chauhan, Craig J. Dedman, Chloë Baldreki, Adam A. Dowle, Tony R. Larson, Rosalind E.M. Rickaby, Contrasting species-specific stress response to environmental pH determines the fate of coccolithophores in future oceans, Marine Pollution Bulletin, Volume 209, Part A, 2024, 117136, ISSN 0025-326X, https://doi.org/10.1016/j.marpolbul.2024.117136. |

## Student Confirmation

| | | | |
|---|---|---|---|
| Student Name: | Nishant Chauhan | | |
| Contribution to the Paper | Performed culturing of algae, sample collection, processing, and analysis, interpreted data with help of co-authors, wrote first draft, revised the manuscript with the help of co-authors. | | |
| Signature | 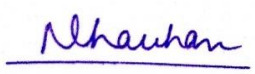 | Date | 15 April 2024 |

## Supervisor Confirmation

By signing the Statement of Authorship, you are certifying that the candidate made a substantial contribution to the publication, and that the description described above is accurate.

| | | |
|---|---|---|
| Supervisor name and title: Prof Rosalind Rickaby | | |
| Supervisor comments: I helped devise the analysis and then helped with editing of the draft. Nick was instrumental in leading the analysis and write up with the guidance of Craig and myself. | | |
| Signature 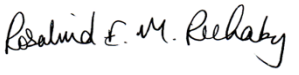 | Date | 16 April 2024 |

# Chapter 3: Species-specific Variability in Coccolithophore Physiology under Changing Seawater pH and Its Impact on Marine Biogeochemical Cycles

## Foreword

This chapter has been accepted for publication as a research article in the journal Oceanography and Limnology. Chapter 1 has been referenced as Chauhan & Rickaby (2024) and Chapter 2 has been referenced as "Chapter 2".

## Abstract

Coccolithophores are pivotal players in ocean biogeochemistry, yet the impact of changing carbonate chemistry on different species remains unclear as *G. huxleyi* has been emphasised and meta-analyses remain challenging due to differences in culture conditions. This study investigated the response of three species – *Gephyrocapsa huxleyi*, *Coccolithus braarudii* and *Chrysotila carterae* – under varying $CO_2$ conditions (via pH). All species showed reduced growth rates under the highest $CO_2$/lowest pH treatment due to $H^+$-related inhibition. *C. carterae* exhibited increased coccosphere size with rising $CO_2$, with corresponding changes in elemental ratios. *C. braarudii* sizes were proportional to growth rates, with the highest growth and size observed at ~11 µmol $CO_2$ $KgSW^{-1}$, resulting in high carbon production rates and inorganic to organic carbon (PIC:POC) ratios. *G. huxleyi* showed minor changes in coccosphere size or elemental quotas, but its PIC:POC ratios declined with increasing $CO_2$/decreasing pH. Literature synthesis showed that growth rates and PIC:POC generally declined with increasing $CO_2$, but strain-specific $CO_2$ optima contributed to variability within the responses of a single species, likely due to adaptation to carbonate chemistry conditions at the site of isolation. Overall, species-specific changes in elemental stoichiometry will impact nutrient and carbon export locally. Unlike coastal species, open ocean species are

likely to experience reduced carbon and nutrient export under higher $CO_2$ levels causing reduced food quality. Species-specific sensitivities to pH will allow species like *G. huxleyi* to outperform others like *C. braarudii*. Moreover, strains with a growth optimum at higher $CO_2$ levels may outcompete those with a growth optimum at lower $CO_2$ levels.

**Introduction**

Climate change has diverse impacts, affecting various aspects of our environment. For instance, global warming alters the very nature of our oceans, influencing factors like circulation, stratification, and gas solubility (Bindoff *et al.*, 2007). Additionally, the rising absorption of $CO_2$ by oceans triggers chemical transformations in seawater, such as altering carbon concentrations, pH levels, and metal speciation (Doney *et al.*, 2009). These changes ripple through marine ecosystems, impacting phytoplankton diversity, species distribution, cellular processes, and elemental composition, thereby affecting higher trophic levels (Sterner & Elser, 2003; Steinacher *et al.*, 2010; Moreno & Martiny, 2018).

Investigating the carbon-nitrogen-phosphorus, or Redfield ratio in phytoplankton is crucial to understanding the implications of climate change on food chains and carbon cycles (Geider & La Roche, 2002; Sterner & Elser, 2003). Nitrogen is a key component of biological macromolecules such as nucleic acid, proteins, and chlorophyll (Gruber, 2008). Phosphorous is essential for a multitude of cellular processes, such as energy storage and transfer, signal transduction, and formation of cellular components such as nucleic acids and cell membranes (Elser, 2012). Phytoplankton growth is heavily dictated by the amount of nitrogen and phosphorous present in the seawater, and nutrient availability has a strong control over primary productivity. Any available nutrients, whether transported to the surface ocean through terrestrial sources, or through nitrogen-fixing

organisms, is readily taken up by phytoplankton. Consequently, nitrogen and phosphorous cycles of the ocean are heavily dictated by primary productivity in the surface ocean.

The response of phytoplankton under environmental changes apart from nutrient limitations is primarily caused by cellular changes, for instance, by size, change in chlorophyll concentrations, or synthesis of amino acids and DNA. Changes in the Redfield ratio of phytoplankton-derived organic matter as a consequence of environmental changes will likely influence the food quality of higher tropic levels and alter nutrient cycles even in those regions where nutrients are not limited (e.g., estuarine, and coastal areas).

Coccolithophores contribute to global biogeochemical cycles through long term carbon sequestration as coccolith calcite, short term $CO_2$ release and alkalinity drawdown during the calcification process, and fixing carbon as organic matter through photosynthesis (Rost & Riebesell, 2004b). Specifically, coccolithophores contribute about 10 % to primary production in the surface ocean (Poulton *et al.*, 2007) and about 50 % to open ocean calcite export (Broecker & Clark, 2009). Coccolithophore species such as *Coccolithus braarudii* export the largest amounts of calcite in polar and coastal waters (Daniels *et al.*, 2014, 2016), while species such as *Gephyrocapsa huxleyi* form large-scale blooms and are ubiquitously present in the modern oceans (Tyrrell & Merico, 2004; Wheeler *et al.*, 2023).

*C. braarudii* has a long geologic history and was a key calcifier in the Eocene (Agnini *et al.*, 2014), despite declining $CO_2$ levels (Claxton *et al.*, 2022). *G. huxleyi* is a more recent species, only originating ~200 kiloyears ago (Thierstein *et al.*, 1977). *C. carterae*, frequently blooms in coastal waters (White *et al.*, 2018). This species diversity makes coccolithophores one of the key phytoplankton groups of the modern ocean (Eikrem *et al.*, 2016). Many coccolithophore species exhibit

distinct physiological traits. For instance, *C. carterae* utilises coccolithosomes and three coccolith-associated polysaccharides (CAPs) during calcification, unlike any other known coccolithophore species (van der Wal *et al.*, 1983; Marsh *et al.*, 1992). Calcification in *C. braarudii* has been linked to its cell cycle, where a disruption in calcification severely impacted growth (Walker *et al.*, 2018). *G. huxleyi* is the smallest among the three coccolithophore species described above, and also possesses some unique qualities. For instance, *G. huxleyi* is the only coccolithophore species reported so far that does not experience photoinhibition even under very high light levels (Nanninga & Tyrrell, 1996). Despite their differences in environmental sensitivity, the fate of these species in response to climate change remains uncertain. While *G. huxleyi* has been extensively studied, there's a notable gap in understanding the responses of other species.

Prior research has revealed varying levels of carbon limitation across different coccolithophore species when exposed to low $CO_2$ conditions. In our previous investigation, we demonstrated that *C. braarudii* experienced more pronounced carbon limitation under low $CO_2$ compared to *C. carterae* or *G. huxleyi* (Chauhan & Rickaby, 2024). Certain species, like *G. huxleyi*, possess the ability to actively uptake bicarbonate, whereas others, such as *C. carterae*, utilise carbonic anhydrase (Chapter 2). Although the notion of carbon concentrating mechanisms in coccolithophores has been discussed previously, little is known about the diversity in CCM strategies that exist in coccolithophores, and how they vary among species (Reinfelder, 2010; Stoll *et al.*, 2019). These findings underscore a complex and multifaceted response among coccolithophores to changes in carbonate chemistry.

Short-term “acclimation” studies have attempted to disentangle the effects of seawater pH and $CO_2$ availability, as contradictory responses to changes in

carbonate chemistry have been reported (Riebesell et al., 2000; Iglesias-Rodriguez et al., 2008b; Bach et al., 2011a; Fiorini et al., 2011; Kottmeier et al., 2016a; Liu et al., 2018; Vázquez et al., 2023). The contradictions amongst studies have partly originated due to the differences in methodologies used to manipulate carbonate chemistry in laboratories. Some studies have reported similar coccolithophore responses to elevated $pCO_2$ concentrations regardless of whether carbonate chemistry was manipulated through the addition of acid/base or through $CO_2$ bubbling (Shi *et al.*, 2009; Hoppe *et al.*, 2011), while others have shown distinct responses to $CO_2$ and pH changes (e.g., Fukuda *et al.*, 2014; Vázquez *et al.*, 2023). A meta-analysis by Meyer & Riebesell (2015) proposed that while the method of ocean acidification simulation may not affect calcification or PIC:POC ratio, it does influence photosynthesis. Moreover, (Bach *et al.*, 2015) suggested that the varying responses of coccolithophore to changing carbonate chemistry may be related to the different culture conditions applied in various studies, such as temperature, light level, day-light period length and nutrients.

This has provoked debate regarding best practices for laboratory-based experiments and discrepancies between studies (see for example, Iglesias-Rodriguez et al., 2008b,a; Riebesell et al., 2008). Variables such as number of generations subjected to experimental conditions for acclimation, methodologies used to manipulate carbonate chemistry, and use of specific nutrient concentrations in laboratory-based experiments have been questioned (LaRoche *et al.*, 2010).

Conflicting findings have also emerged regarding coccolithophore responses to seawater pH alterations in long-term “adaptation” studies, where some studies suggested that calcification rates in coccolithophores can rebound to higher levels compared to short-term studies (Lohbeck *et al.*, 2012, 2014). Conversely, other

research indicated detrimental effects of pH changes, even over extended periods (Tong *et al.*, 2018). Additionally, experiments have shown initial recovery in calcification rates followed by decline, suggesting that long-term laboratory simulations of adaptive evolution may not accurately represent species behaviour under stress (Schlüter *et al.*, 2014, 2016).

The large variation in culturing techniques, and the lack of representation of coccolithophore diversity in most studies suggests that there is still a need to understand the mechanism behind physiological responses for biogeochemically relevant species across a broad pH range. Although nutrients and light are thought to drive population dynamics amongst phytoplankton taxa, the significance of pH on the of niche partitioning of various coccolithophore species is still unclear (Field *et al.*, 1998). By utilising our previous findings, this study aims to elucidate the mechanistic reasons behind physiological responses of three distinct coccolithophore species under changing seawater pH. We aim to deconvolve contrasting physiologies of coccolithophore species to highlight species-specific responses to changes in seawater pH.

## Methods

### Culturing and Media Preparation

*Coccolithus braarudii* (RCC 1198), *Gephyrocapsa huxleyi* (PLY 837), and *Chrysotila carterae* (PLY 406) cultures were cultivated in sterile artificial seawater prepared using the Aquil recipe (Price *et al.*, 1989). These species were selected based on their interspecific diversities in cell sizes, ecological niches, and calcification requirements. The seawater was supplemented with 100 $\mu$M nitrate, 6.25 $\mu$M phosphate and 27 $\mu$M silicate with vitamins according to *f*/2 (Guillard & Ryther, 1962) and trace metals according to K/2 (Keller & Guillard, 1985; Keller *et al.*, 1987), with modifications as per (Rickaby *et al.*, 2010). pH adjustments were made

using calculated amounts of 1N HCl or 1N NaOH, and pH monitored using a 3-point calibrated benchtop pH meter.

Cultures were maintained at 17˚C under a 14:10 light:dark cycle with alight intensity of 80 $\mu$mol $m^{-2}$ $s^{-1}$. Prior to the main experiment, cultures were acclimated to different pH conditions for 7-14 generations and then inoculated in triplicate during the mid-exponential growth phase. To minimise carbonate chemistry drift and substrate limitation, a dilute batch culture method was employed. Initial cell densities were maintained at ~ 400 cells $mL^{-1}$ for *C. braarudii*, ~ 120 cells $mL^{-1}$ for *C. carterae*, and ~ 65 cells $mL^{-1}$ for *G. huxleyi. F*inal cell densities did not exceed ~ 5000 cells $mL^{-1}$ for *C. braarudii*, ~ 10,000 cells $mL^{-1}$ for *C. carterae*, and ~ 50,000 cells $mL^{-1}$ for *G. huxleyi* based on recommendations by (Langer *et al.*, 2006; LaRoche *et al.*, 2010). Cultures were grown in a 2.4L polycarbonate bottles without headspace. All samples were taken 6 hours into the light phase and the sampling took less than 1 hour.

**Growth Rates**

Cell growth was assessed via cell counts and chlorophyll fluorescence using a Z2 Coulter Counter and a TECAN Spark® Multimode Microplate Reader, respectively. Growth rates were calculated from chlorophyll fluorescence values using linear regression on log-transformed data from multiple days ($n \geq 5$) during exponential growth. Cell count-based growth rates were determined using the equation: $\ln(N_2/N_1)/\Delta t$, where $N_2$ and $N_1$ represent cell counts and $\Delta t$ indicated the time difference between measurements. Preliminary analyses of chlorophyll fluorescence values in *G. huxleyi* suggested that these values did not change within an acclimated culture during exponential growth phase, and therefore, can be reliably used.

**Photosynthetic Parameters**

Photosynthetic performance was evaluated through the quantum efficiency of Photosystem II ($F_v/F_m$), measured using a Satlantic FIRe fluorometer. Biological replicates (cultures) were acclimatized to darkness for 1 hour before analysis. Chlorophyll *a* and *c* pigment concentrations were determined by pelleting 50 mL of culture in light-safe centrifuge tubes at 4000g for 15 minutes at 4˚C. Chlorophyll was extracted in 3 mL 100% Ethanol at 4˚C overnight and measured at 667 nm for chlorophyll *a,* and 626 nm for chlorophyll *c* on a TECAN Spark® Multimode Microplate Reader. Equations for chlorophyll *a* and *c* were taken from (Ritchie, 2006) and plate-reader path length corrections were made according to (Warren, 2008)

**C:N:P and PIC:POC**

Samples for elemental analyses were collected on pre-combusted GF/F filters (12h, 450˚C). Filters for POC analyses were acidified using 230 $\mu$L of 0.1N HCl. All filters were dried at 40˚C overnight and stored at -20˚C until further analysis. Particulate Organic Carbon (POC; pg $cell^{-1}$) and Particulate Organic Nitrogen (PON; pg $cell^{-1}$) were measured on an Elementar Vario Isotope Select Elemental Analyser linked to an Isoprime 100 continuous flow IRMS at the Stable Isotope Ratio Mass Spectrometry Laboratory, National Oceanography Centre in Southampton, UK. Relative masses (in mg) of C and N were calculated using %N and %C by assuming a constant overall mass of 1 mg for each filter. Therefore, the PIC, POC and PON values presented in this study are relative to the arbitrarily assumed 1 mg mass of the filter and are not absolute per cell values. Standard deviations were measured using internal standards (Spirulina and acetanilide) and were always better than 0.21% for %N and 0.32% for %C.

Particulate Organic Phosphate (POP; pg $cell^{-1}$) was measured spectrophotometrically after oxidation, following adapted wet chemistry methods from (Raimbault *et al.*, 1999) and (Murphy & Riley, 1962). Briefly, cells collected on a pre-combusted GF/F filter were oxidised using a $Na_2B_4O_7$ and $K_2S_2O_8$ reagent and a phosphate reagent and measured spectrophotometrically on a TECAN Spark® Multimode Microplate Reader at 882 nm. Due to the high volume of culture required for accurate Particulate Organic Phosphate (POP; pg $cell^{-1}$) analyses, only one sample per biological replicate was taken. Particulate Inorganic to Organic carbon (PIC:POC) ratios were determined in-house using a Thermo EA Isolink CN analyser. PIC values were obtained by subtracting POC values from Total Particulate Carbon (TPC) values. Only relative masses were obtained by assuming an initial mass of 444 mg for all samples. %C accuracy on actual organic carbon (Urea) and inorganic carbon (Calcite) was always better than 3%. POC, PIC, PON, and POP production rates were obtained by multiplying the respective value with growth rates.

**Morphological measurements**

Cell diameter measurements were obtained from the Coulter Counter, while coccosphere diameter was derived from Scanning Electron images taken on a Zeiss Sigma FIG-SEM. Due to potential errors in cell size estimation from Coulter Counter measurements caused by coccosphere dissolution in the isotonic solution, coccosphere diameters were used for further analyses. 1 mL cultures were filtered onto 0.8-µm pore size polycarbonate filters (Millipore) for scanning electron microscopy. Subsequently, the filters were washed twice with 70% Ethanol and air-dried overnight. Morphological measurements on coccoliths were performed on SEM images of *Coccolithus braarudii*, focusing on the longest dimensions of the coccolith and the central area (see Supplementary Information for reference). A total of 70 images were analysed for each treatment, with

measurements exclusively conducted for treatments at pH 8.8, 8.2, and 7.6. All analyses were performed in ImageJ.

**Carbonate Chemistry**

12 ml aliquots of Seawater samples were taken on the day of inoculation and harvest day by filtering media through a 0.22 $\mu$m pore size syringe filter into an exetainer vial with no headspace. The samples were stored at 4°C in the dark until further analysis. Samples were titrated with 0.01N HCl standardised solution on a Metrohm 916 Ti-Touch titrator to determine Total alkalinity (TA) and pH. The pH probe was calibrated once daily using NIST reference standards and certified Dickson $CO_2$ seawater reference were measured the same way as samples to measure analytical drift and accuracy. Other carbonate chemistry parameters were calculated using CO2SYS (Pierrot *et al.*, 2006). $K_1$ and $K_2$ constants were taken from (Mehrbach *et al.*, 1973), refit by (Dickson & Millero, 1987).

**Literature review**

A literature review was conducted to obtain growth rates, PIC:POC ratios, POC, PON, and POP cellular quotas for *G. huxleyi*, *C. braarudii*, and *C. carterae*. All studies manipulating carbonate chemistry were considered, where carbonate chemistry was changed by addition of acid/base (e.g., Langer et al., 2006), $CO_2$ bubbling (e.g., Langer et al., 2009), addition of DIC to increase $CO_2$ with (e.g., Rickaby et al., 2010) or without (e.g., Claxton, 2022) keeping the pH constant. Any study where light, temperature, or nutrients were also changed was removed. Several datapoints for *G. huxleyi* were obtained from the literature review done by (Sheward *et al.*, 2023). In total, 82 unique datasets were used where either the species, strain or experiment differed. Out of these, 66 datasets were attributed to *G. huxleyi,* 7 to *C. carterae*, and 9 to *C. braarudii*. For comparison of existing data with this study, the cutoff value for x axis was set as 60 µmol $CO_2$ $KgSW^{-1}$.

Studies where relevant data was used, but not publicly available could not be incorporated.

**Results**

An accompanying study was published previously to show species-specific isotopic vital effects in coccolithophores, which were dependant on cell sizes and corresponding internal carbon pools (Chauhan & Rickaby, 2024). We were able to show that out of the five species studied, carbon and oxygen isotopes in the coccolith calcite of *G. huxleyi* and *G. oceanica* behaved similarly due to short carbon residence times in their internal carbon pools. A similarity in the isotopic chemistry was also evident for *C. braarudii* and *C. leptoporus*, where both species were susceptible to large vital effects during $CO_2$ limitation and high carbon demand but maintained constant isotopic values under non-limiting $CO_2$ conditions. Finally, carbon and oxygen isotopes in *C. carterae* exhibited isotopic equilibration of its large internal carbon pool, suggesting long carbon residence times (Chauhan & Rickaby, 2024). To maintain clarity, only *C. carterae*, *C. braarudii*, and *G. huxleyi*, each representing the three categories were presented in this study. An average drift of 4.7% in the DIC, and a pH drift of 0.04 units were observed from the start to the end of the dilute batch-culture experiments. Therefore, the initial carbonate chemistry parameters were used to present the data in this study.

A following study was conducted on these three coccolithophore species to investigate changes in cellular processes through proteomics and physiological measurements of net photosynthesis and respiration (Chapter 2). It was reported that *C. braarudii* exhibited high sensitivity to pH stress, with significant changes in cellular processes at pH 8.8 and pH 7.6 compared to standard culturing conditions (pH 8.2). Protein-groups related to oxidative stress management, ion

transport, fatty acid biosynthesis and metabolism, mitochondrial and chloroplastic proteins and many other processes showed significant changes in *C. braarudii*. *C. carterae* showed the least sensitivity to pH stress with marginal changes in growth, photosynthesis, or respiration. Furthermore, little change was observed through proteomic analysis, with a few chloroplastic proteins being downregulated under acidic conditions. *G. huxleyi* demonstrated significant adaptability in cellular processes, with the upregulation of isocitrate lyase under stress, and distinct changes in protein activity related to chaperoning (HSPs, EF hand containing), and protein folding and degradation (Derlin, PPIases). Moreover, Rubisco and light-harvesting proteins were downregulated under alkaline conditions, possibly due to the reduced photosynthetic rates under $CO_2$ limitation, which were evident through physiological measurements. It is therefore clear that these coccolithophore species show distinct responses to pH in stable isotopes and cellular proteome. The aim of this study is to utilise prior knowledge to understand physiological changes from a biogeochemical point of view.

**Growth Rate and Cell Size**

Following the earlier report, growth rates were further analysed using linear regression on log-transformed chlorophyll fluorescence as well as cell counts from two points on the exponential growth curve. This allowed for more robust comparisons between species, and a validation of the results obtained previously (Chauhan & Rickaby, 2024). All three species exhibited a growth optimum with variable $CO_2$ and pH (Fig. 1a). Growth rates were generally consistent but declined sharply for all three species at the lowest pH/highest $CO_2$. *C. braarudii* exhibited a reduction of up to 52% in growth rates at the lowest pH compared to highest observed growth rates. *G. huxleyi* displayed an 87% reduction and *C. carterae* showed a 79% reduction in their growth rates at the lowest pH. The decrease in growth rates at the highest pH/lowest $CO_2$ conditions were also evident, although

these changes were of smaller magnitude. Notably, *C. braarudii* exhibited a 12% decrease in growth rates at high pH compared to highest observed growth rates, *C. carterae* exhibited an 18% reduction, while *G. huxleyi* showed a 10% decline in its growth rates. The highest growth rates, or growth optima for pH and/or $CO_2$, differed for different species, with *C. carterae* exhibiting highest growth at ~pH 8 (~22 µmol $CO_2$ $KgSW^{-1}$), while *G. huxleyi* showing highest growth at ~pH 8.2 (~16 µmol $CO_2$ $KgSW^{-1}$). Growth rate optima for *C. braarudii* seems at ~pH 8.3 (~11 µmol $CO_2$ $KgSW^{-1}$), however, this cannot be confirmed without more datapoints. The absolute growth rate values for *C. braarudii* were consistently lower than those for *G. huxleyi* and *C. carterae,* as reported in previous studies (Rickaby et al., 2010; Hermoso, 2015; Hermoso et al., 2016a).

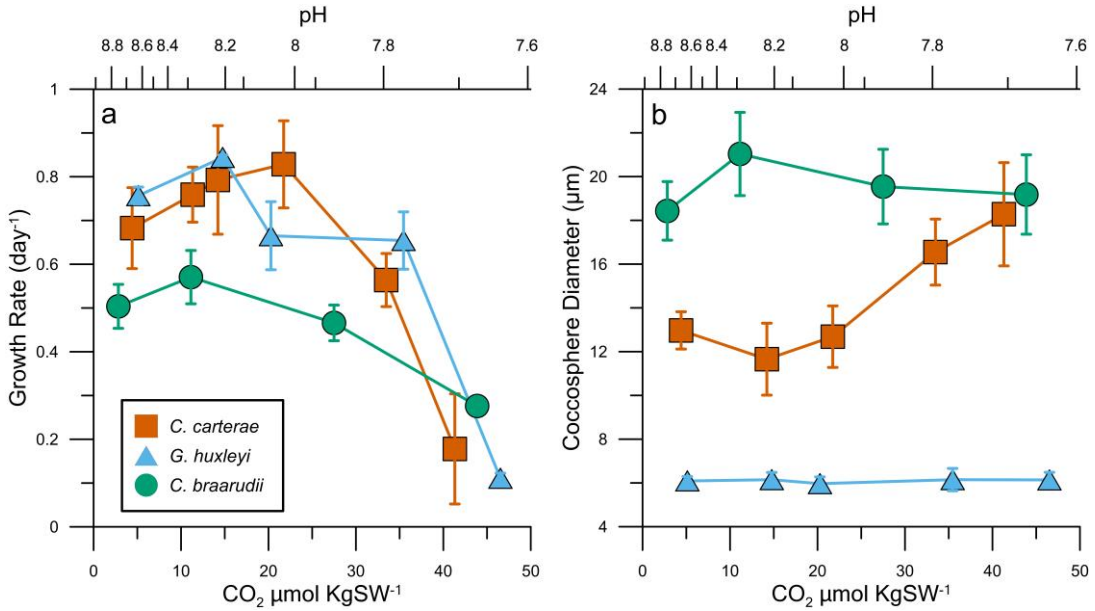


**Figure 1: (a)** Growth rates ($day^{-1}$) for *G. huxleyi* (●), *C. braarudii* (●), and *C. carterae* (●) grown at different seawater pH. Growth rates were determined by the slope of log-transformed chlorophyll fluorescence over multiple datapoints in the exponential phase. Growth rates obtained via cell counts are presented in the Supplementary Information (Fig. S1). **(b)** Coccosphere diameter (µm) based on measurements on SEM images ($n \geq 30$).

Chlorophyll fluorescence was used to calculate growth rates as cell counts for *C. braarudii* were prone to error. This may be because *C. braarudii* has the highest settling velocity amongst coccolithophores and were inaccurately counted on the

coulter counter (Zhang *et al.*, 2018). Therefore, cell counts for *C. braarudii* report a lower growth rate when compared to growth rates measured via log-transformed chlorophyll fluorescence (Fig. 1a, Fig. S1: Supplementary Information). Importantly, the trends between the two methods of growth rate measurements are the same for *C. braarudii*.

When compared to growth rates obtained from previous studies, it is evident that *C. braarudii* has a broad $CO_2$ and/or pH optimum (Fig. 2). Contrary to the growth rates observed in this study, the polynomial fit indicated that growth rates for *C. braarudii* did not change until between 10 – 30 µmol $CO_2$ $KgSW^{-1}$. The $CO_2$ optimum for *G. huxleyi* was even broader, with minimal changes observed between 0 – 40 µmol $CO_2$ $KgSW^{-1}$. It is important to note that strain-specific optima may partly be responsible for the broad $CO_2$ optima for *C. braarudii* and *G. huxleyi* (See discussion). Although *C. carterae* exhibited a drop in growth rates at the highest $CO_2$ levels, these might be biased by the sharp decline in growth rates observed in the current study, and due to the lack of datapoints from other studies (as shown by the standard error). Growth rates from this study were generally close to the polynomial fit, except values at the lowest pH/highest $CO_2$.

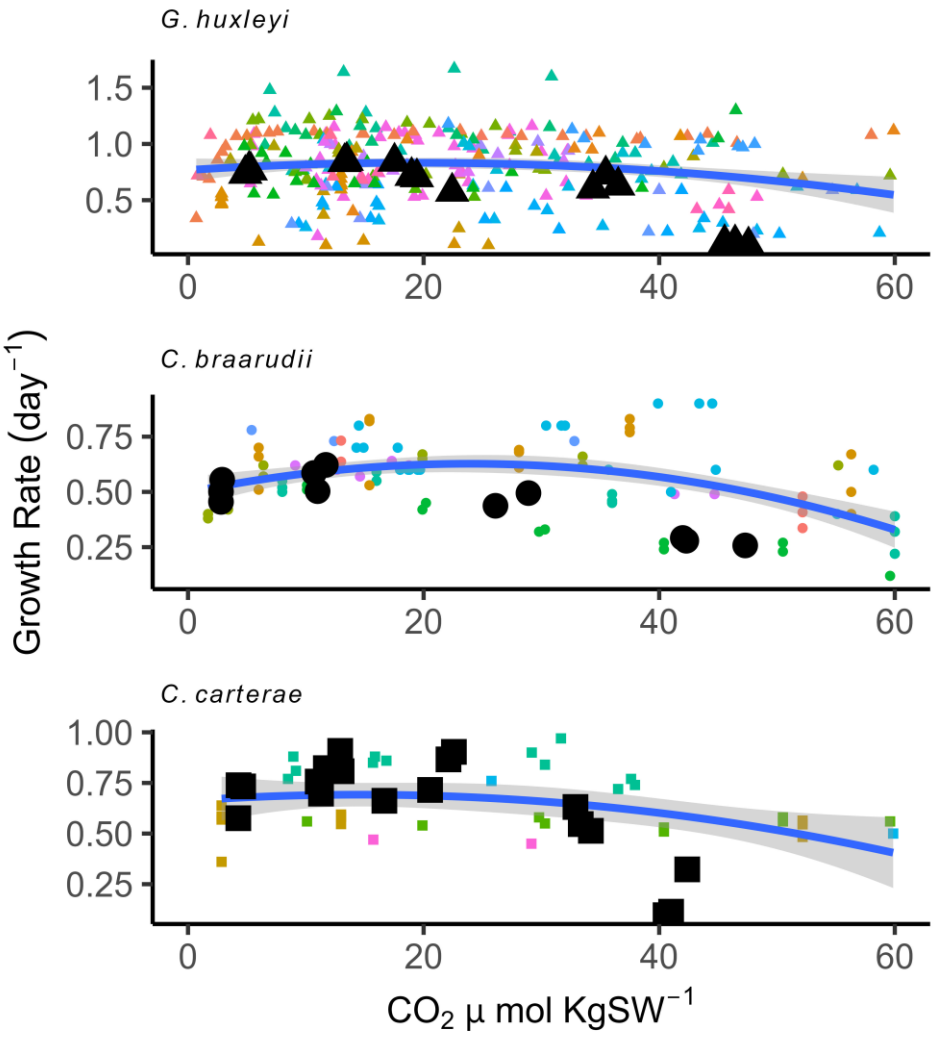


**Figure 2:** A compilation of growth rates from previous studies where pH and/or $CO_2$ were manipulated. Due to a large number of studies used, the plot legend has been provided in the Supplementary Information to maintain clarity (Fig. S2). **Black symbols** in each plot represent datapoints from the present study. A polynomial fit (degree = 2) is indicated by a solid blue line with the standard error represented by the shaded grey area. Adding a secondary x axis denoting pH values (similar to other figures in this study) was not possible as the literature review also consisted of studies were pH was not changed (e.g., Rickaby et al., 2010). A figure containing the slopes (coefficients) from linear fits of growth rates versus $CO_2$ obtained from the literature review is presented in the Supplementary Information (Fig. S3), which shows that if slopes from studies are considered and strain-specific effects are disregarded then the general response of coccolithophores is towards declining growth under high $CO_2$ conditions.

Coccosphere diameter exhibited minute changes in *G. huxleyi* and correlated with growth rates for *C. braarudii* (Fig. 1b). However, coccosphere size increased drastically with decreasing pH in case of *C. carterae*. Coccolith malformations

were observed under acidic conditions (low pH) for *G. huxleyi* and *C. braarudii* (Fig. 3). Malformations in *C. braarudii* were also apparent at the highest pH (lowest $CO_2$). *C. carterae* exhibited no apparent malformations in its coccoliths.

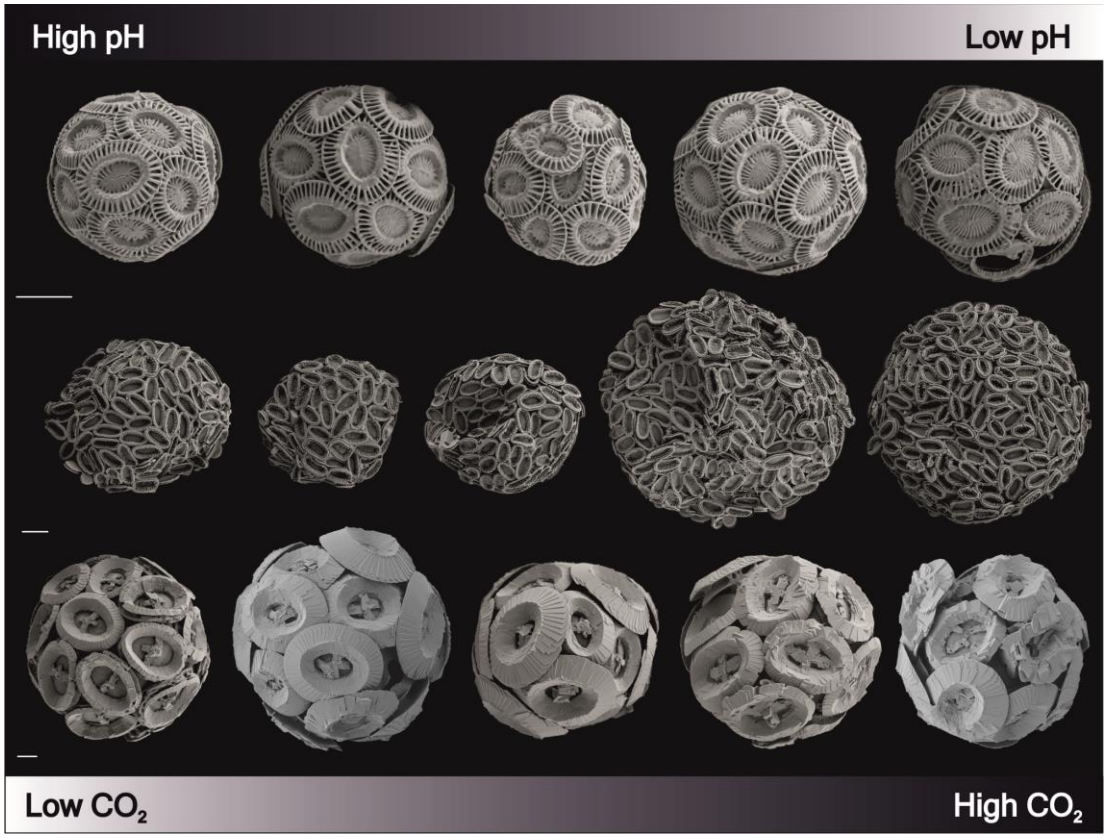


**Figure 3:** Scanning Electron Microscope images for *G. huxleyi*, *C. carterae*, and *C. braarudii* (from top to bottom, respectively). Images are ordered from low $CO_2$ (high pH) to high $CO_2$ (low pH) from left to right. Adapted from Chauhan & Rickaby (2024). Scale bars at the bottom left of each species represent 2 µm. Coccolith malformations are evident at low and high $CO_2$ for *C. braarudii*, and at high $CO_2$ for *G. huxleyi*. Change in cell sizes are evident for *C. carterae* with changing pH. Note that 4 pH/$CO_2$ treatments for *C. braarudii* were investigated in this study, while the SEM images display 5 treatments. The treatment at pH 8.19 (bottom row, third image) was not used elsewhere due to insufficient data.

**Photosynthesis**

Chlorophyll pigment (*a* and *c*) concentration increased for *C. carterae* with increasing $CO_2$/decreasing pH (Fig. 4a,b). However, increased pigment concentrations were mostly due to changes in cell sizes (Fig. 1b). Volume-corrected chlorophyll *a* suggests marginal changes in chlorophyll *a* with changing $CO_2$/pH (Fig. 4c). Maximum quantum yield of PSII, which is calculated as the

difference between maximum fluorescence ($F_m$) and variable fluorescence ($F_v = F_m - F_o$), or $F_v/F_m$, decreased with increasing $CO_2$/decreasing pH for *C. carterae* and *G. huxleyi*, while marginal changes were observed for *C. braarudii* (Fig. 4d). Notably, *C. carterae* exhibited a 14% decrease in $F_v/F_m$ values at the lowest pH, compared to its highest $F_v/F_m$ value observed at pH 8.65. *G. huxleyi* displayed a maximum change of only 6.4% in $F_v/F_m$ values, while *C. braarudii* showed a 4 % change.

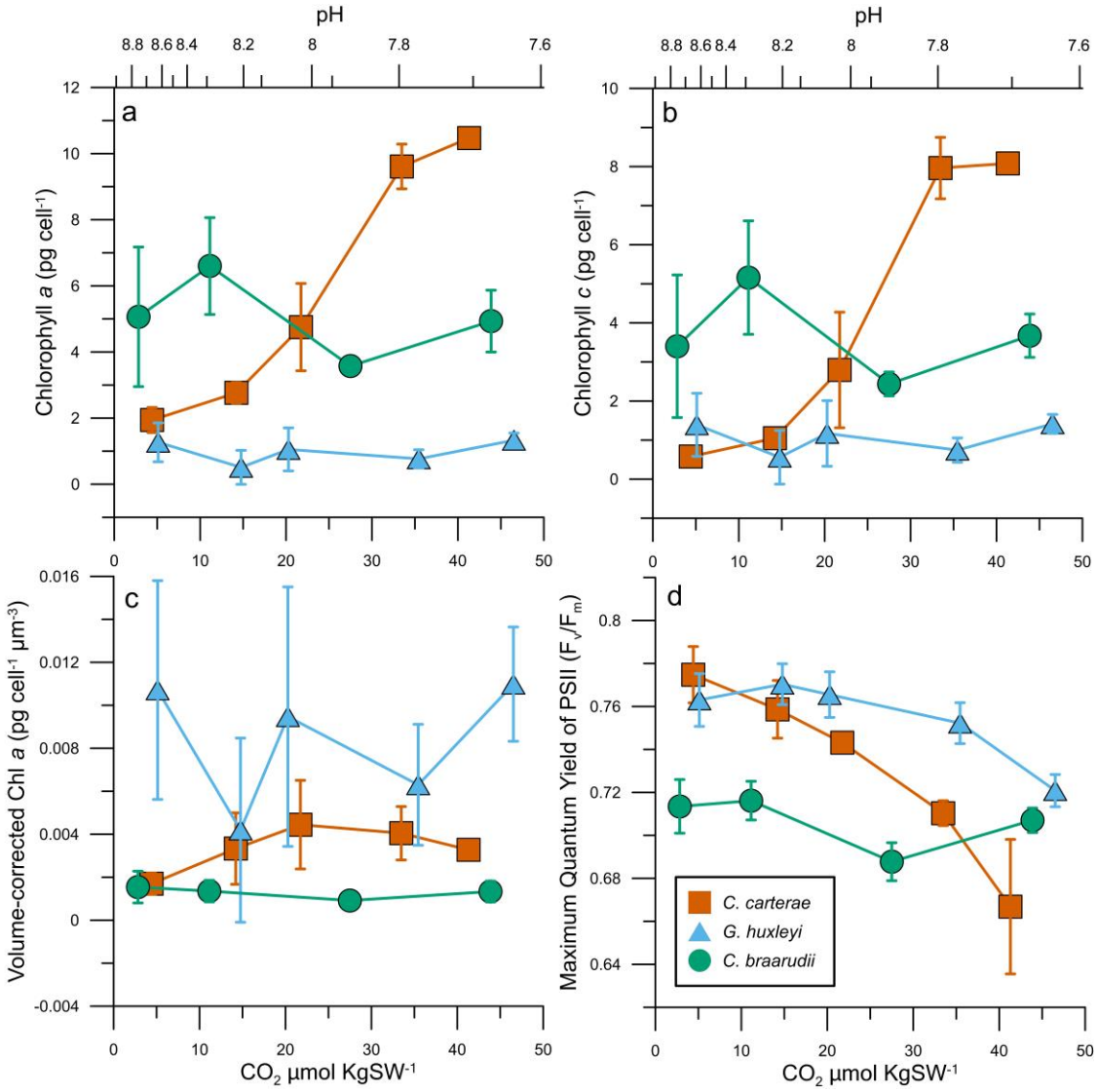


**Figure 4: (a)** Chlorophyll *a* (pg cell$^{-1}$) for *G. huxleyi* (●), *C. braarudii* (●), and *C. carterae* (●) grown at different seawater pH. **(b)** Chlorophyll *c* (pg cell$^{-1}$). Changes in Chlorophyll pigment concentrations were consistent with changes in cell size (Fig. 1b). **(c)** Volume-corrected chlorophyll *a* (pg cell$^{-1}$ µm$^{-3}$). Note that the large variations and error bars for *G. huxleyi* are due to error propagated values. Volumes were calculated based on coccosphere diameters. **(d)** Maximum quantum yield of PSII, or $F_v/F_m$ exhibited decreasing values with increasing $CO_2$/decreasing

pH for *C. carterae* and *G. huxleyi*, while no apparent trend was observed for *C. braarudii*. Note that changes in $F_v/F_m$ values have been exaggerated for better visualisation by scaling the y axis between 0.62 – 0.82.

**Carbon Allocation**

Absolute values for PIC:POC ratios (under standard culture conditions: pH 8.1 – 8.3) were consistent with previous reports, with *C. braarudii* having the highest value and *C. carterae* having the lowest value (Gafar et al., 2019c). PIC:POC ratios displayed species-specific responses with changing seawater pH (Fig. 5). PIC:POC values for *C. carterae* were highly variable and exhibited marginal changes with changing pH/$CO_2$. *G. huxleyi* showed a ~55 % decline in PIC:POC ratios with increasing $CO_2$/decreasing pH. PIC:POC ratio for *C. braarudii*, the highest values (~ 0.6) were observed at 10 – 30 µmol $CO_2$ $KgSW^{-1}$ while the PIC:POC ratio decreased by ~ 57 % at lower (~3 µmol $KgSW^{-1}$) and higher (~44 µmol $KgSW^{-1}$) $CO_2$ values.

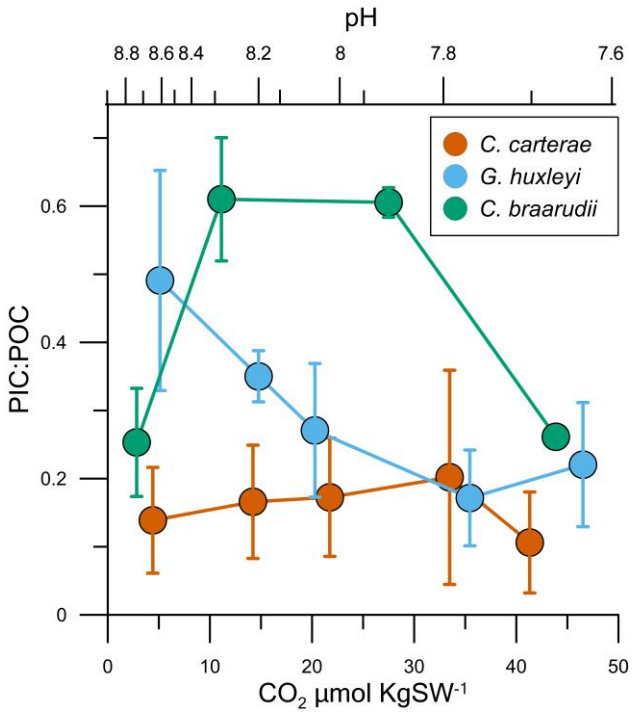


**Figure 5:** PIC:POC ratios for *G. huxleyi* (●), *C. braarudii* (●), and *C. carterae* (●) grown at different seawater pH. *C. braarudii* showed highest values between 10 – 30 µmol $CO_2$ $KgSW^{-1}$ and values declined at higher and lower $CO_2$ conditions. Changes in the PIC:POC ratio for *C. carterae* were indistinguishable due to large errors associated with measurements. *G. huxleyi* showed a consistent decline in PIC:POC ratios with increasing $CO_2$/decreasing pH.

Comparing the results presented in this study with previous studies revealed that PIC:POC ratios for *G. huxleyi* and *C. braarudii* declined with increasing $CO_2$/decreasing pH (Fig. 6). PIC:POC ratios for *G. huxleyi* and *C. braarudii* from the present study were consistently lower than the average. Only three datasets were available for *C. carterae* (including the present study), where PIC:POC ratios generally remained unchanged.

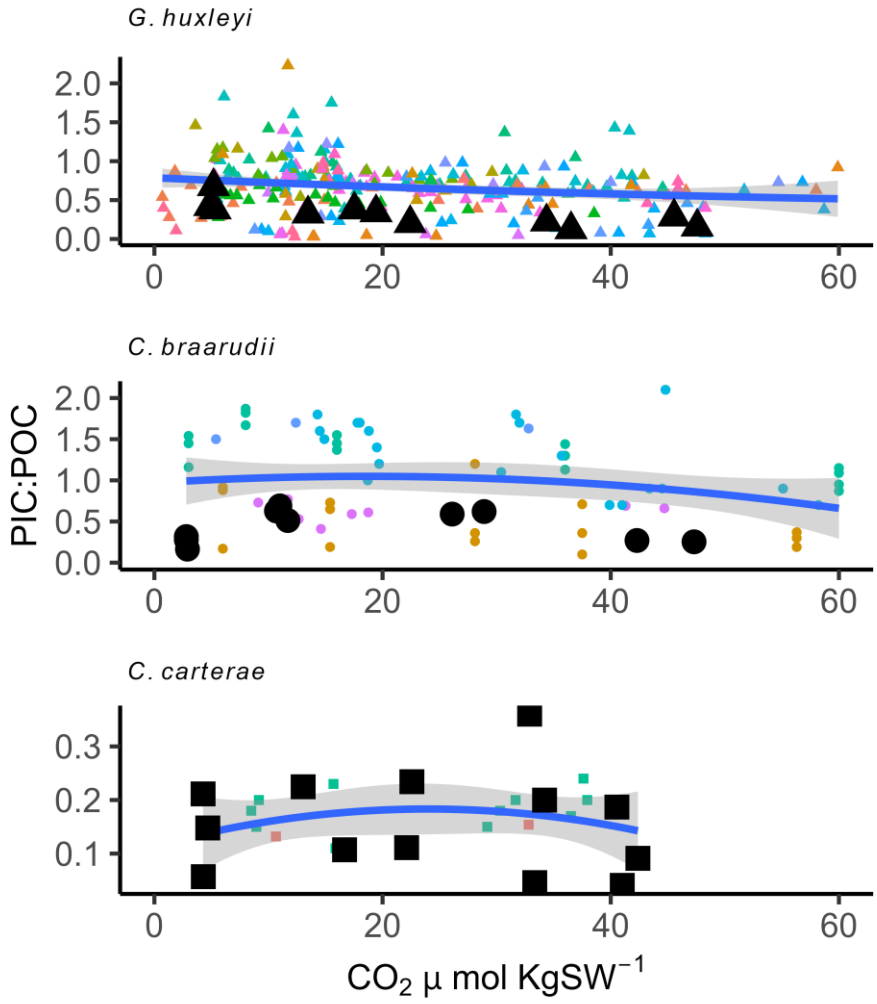


**Figure 6:** A compilation of PIC:POC ratios from previous studies where pH and/or $CO_2$ were manipulated. Due to a large number of studies used, the plot legend has been provided in the Supplementary Information to maintain clarity (Fig. S2). **Black symbols** in each plot represent datapoints from the present study. A polynomial fit (degree = 2) is indicated by a solid blue line with the standard error represented by the shaded grey area. Note that only three studies (including the present study) were available, to our knowledge, for *C. carterae* where pH and/or $CO_2$ were manipulated in nutrient-replete conditions.

**Elemental Stoichiometry**

Particulate organic carbon (POC), Particulate organic nitrogen (PON), and particulate organic phosphorous (POP) exhibited notable changes with changing seawater pH (Fig. 7). Although absolute POC and PON values were not possible (see methods), their ratios and relative changes within and between species can be used to infer changes in the elemental stoichiometry in coccolithophores with changing seawater pH. A consistent increase in POC:N values was observed for *G. huxleyi* and *C. carterae* with decreasing pH (increasing $CO_2$). POC:N values for *C. braarudii* exhibited a variable response, with the highest POC:N values at ~11 µmol $CO_2$ $kgSW^{-1}$. This trend was similar to the trend observed in its growth rates and coccosphere size (Fig. 3). POC:P ratio increased in *C. carterae* with decreasing pH (increasing $CO_2$), similar to the changes observed in its cell size (Fig. 1b). Conversely, *C. braarudii* and *G. huxleyi* showed no specific trend in POC:P changes with changing seawater pH. The absolute POC:P values were the highest for *C. braarudii* at ~11 µmol $CO_2$ $kgSW^{-1}$, due to its high POC quota under those conditions. N:P ratios in *C. carterae* also exhibited increasing values with decreasing pH, corresponding to changes in cell size. *C. braarudii* and *G. huxleyi* displayed a contrasting decreasing trend in N:P values with decreasing pH (increasing $CO_2$). The highest N:P values for *C. braarudii* were observed at ~ 11 µmol $CO_2$ $KgSW^{-1}$, which is also evident through growth rates (Fig. 1a) and coccosphere size (Fig. 1b). Moreover, trends in *C. carterae* were generally correlated with its change in cell size (Fig. 1b). POC:Chlorophyll *a* ratio decreased for *C. carterae*, while they remained consistent for *C. braarudii* and *G. huxleyi*.

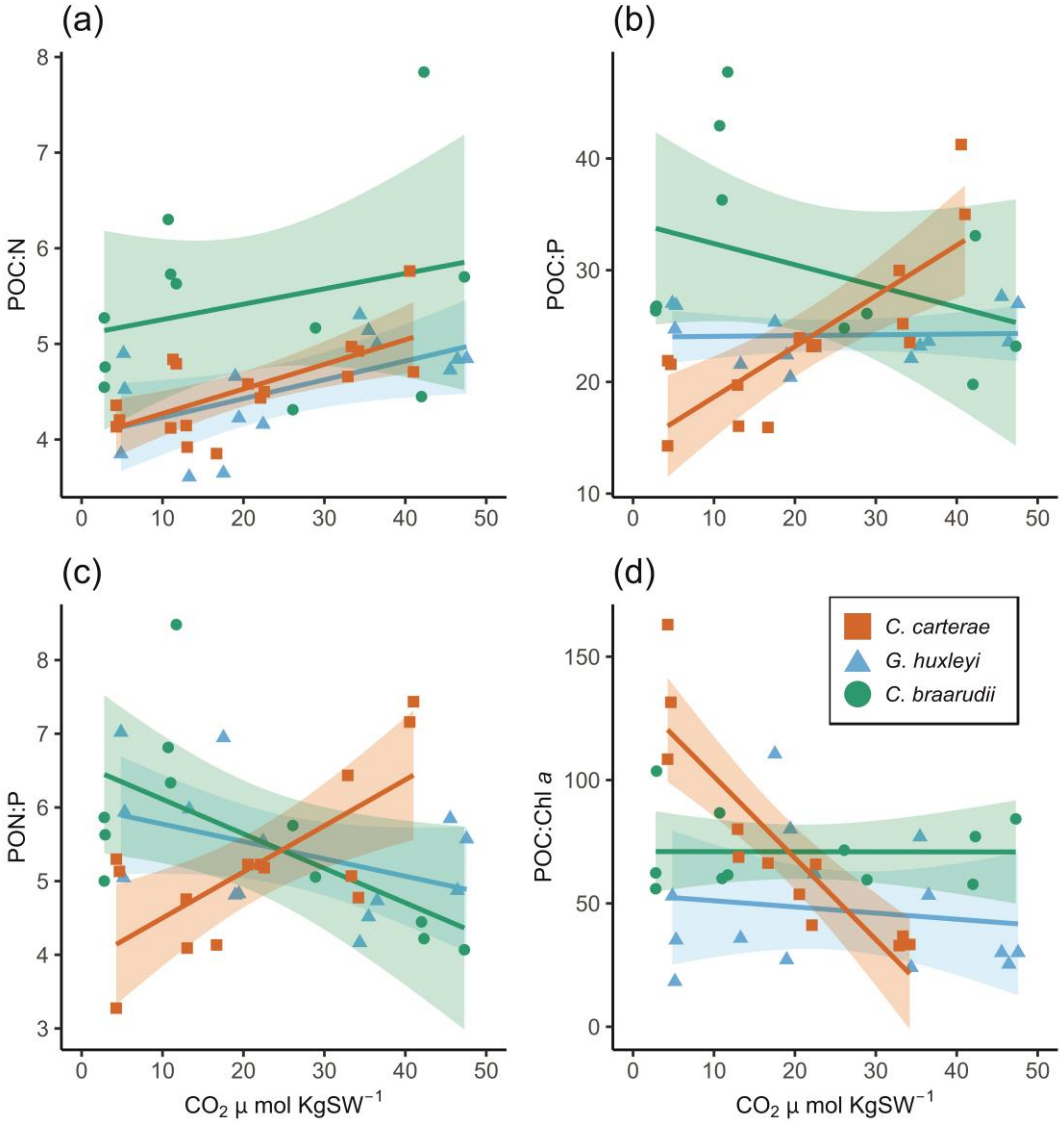


**Figure 7:** Elemental ratios for *G. huxleyi* (●), *C. braarudii* (●), and *C. carterae* (●) grown at different seawater pH. All elemental ratios (e.g., POC:N) were calculated using elemental quotas in pg cell$^{-1}$ (e.g., pg POC cell$^{-1}$). **(a)** All three species show an increasing trend for POC:N ratios with decreasing pH/increasing $CO_2$. Both POC and PON are not absolute values as initial mass of the sample was assumed to be 1 mg (see methods). The shaded area represents 95% confidence intervals (5000 iterations) for the linear trend of each species. for clarity. **(b)** POC:P values exhibit an increasing trend for *C. carterae* but no changes in *G. huxleyi* or *C. braarudii*. **(c)** N:P ratios show an increasing trend for *C. carterae* corresponding to the changes in cell size but a decreasing trend for *C. braarudii* and *G. huxleyi*. **(d)** POC:Chlorophyll *a* ratios show a decreasing trend for *C. carterae* with increasing $CO_2$ but no change for *C. braarudii* or *G. huxleyi*.

POC:N ratios from this study generally agreed with previous literature (Fig. 8). POC:N ratios for *G. huxleyi* increased with increasing $CO_2$. However, due to the lack of available datasets for *C. braarudii* and *C. carterae,* robust observations could

not be made. Datasets measuring N:P ratios were significantly lower, even for *G. huxleyi*, where only three data sets (including the present study) were available. Therefore, plots comparing N:P ratios and C:P ratios are provided in the Supplementary Information (Fig. S6, 7).

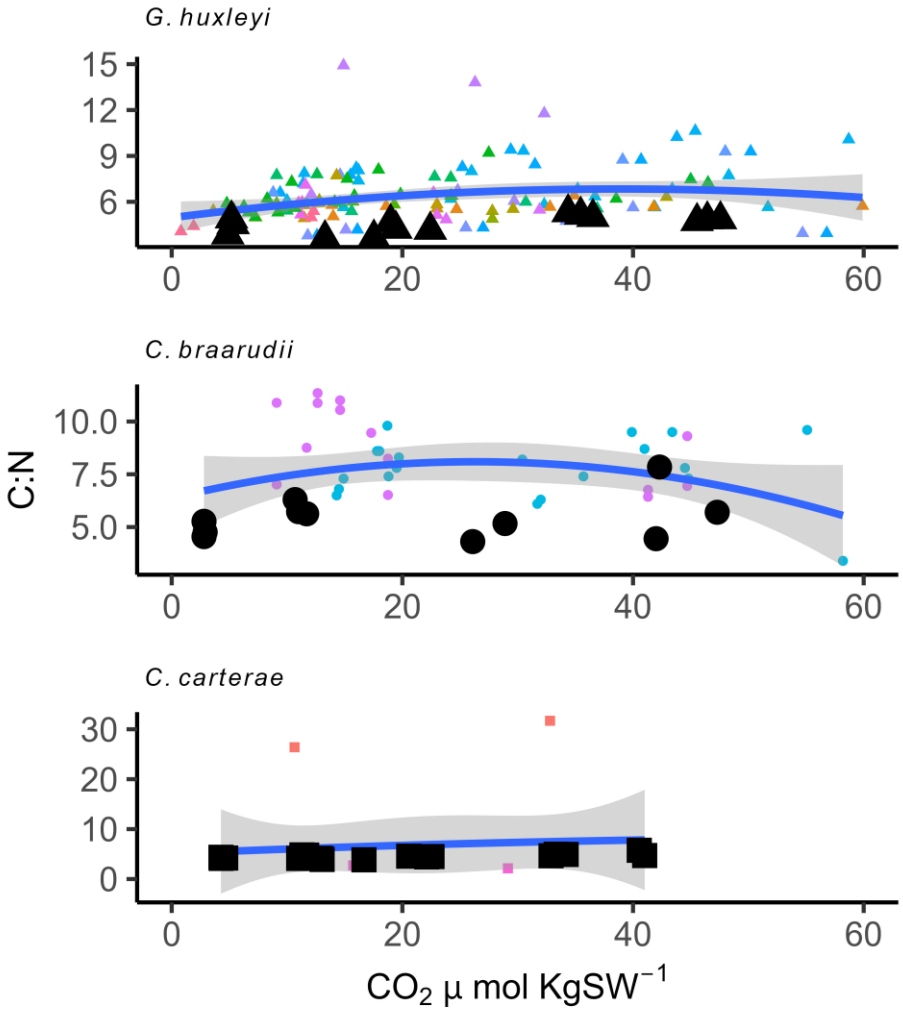


**Figure 8:** A compilation of POC:N ratios from previous studies where pH and/or $CO_2$ were manipulated. Due to a large number of studies used, the plot legend has been provided in the Supplementary Information to maintain clarity (Fig. S2). **Black symbols** in each plot represent datapoints from the present study. A polynomial fit (degree = 2) is indicated by a solid blue line with the standard error represented by the shaded grey area. Note that only three studies (including the present study) were available, to our knowledge, for *C. carterae* and *C. braarudii* where pH and/or $CO_2$ were manipulated in nutrient-replete conditions.

**Production Rates**

POC, PIC, N, and P export from the surface ocean are effected by their production rates, which are determined by their per cell quotas and growth rates (Fig. 9). Absolute production rates vary drastically between species. Under standard culturing conditions (pH 8.2), *C. braarudii* has the highest PIC and POC production rates due to its large cell size and high PIC per cell quotas. *G. huxleyi* has the lowest PIC and POC production rates, due to its small size and small PIC quota (Fig. 6a,b). The high POC production rates for *C. carterae* are correlated with its large cell size and the low PIC production rates are due to its low PIC quota (Fig. 5, 6a,b). Both POC and PIC production rates in *C. braarudii* exhibited highest production rates at ~11 µmol $CO_2$ $KgSW^{-1}$. POC and PIC production rates for *C. carterae* remained largely unchanged, except at the lowest pH when the values dropped considerably. On the other hand, *G. huxleyi* exhibited a gradual decline in POC (max. 87 % decline) and PIC (max. 92 % decline) production rates with decreasing pH.

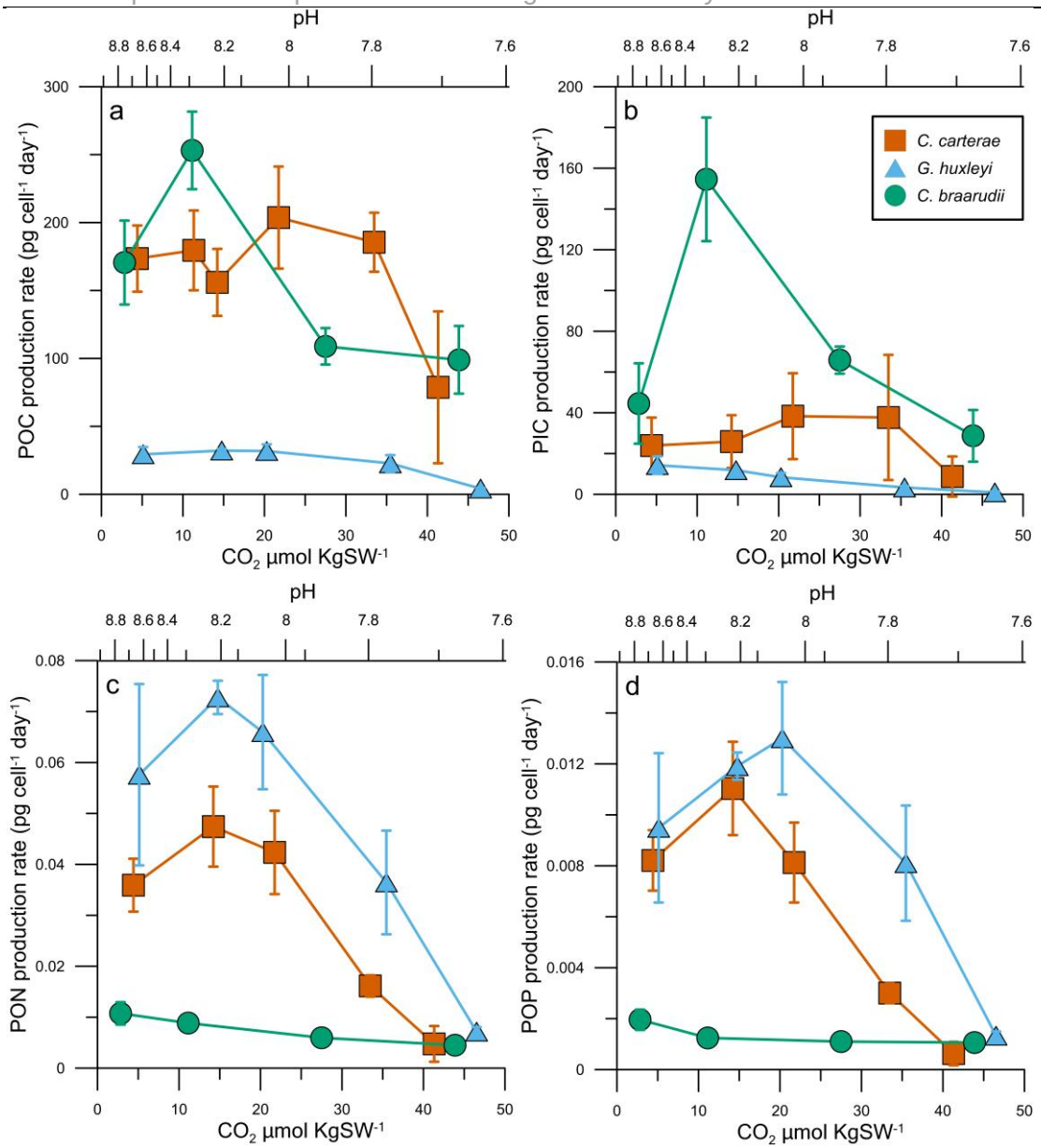


**Figure 9:** POC, PIC, PON and POP production rates for *G. huxleyi* (●), *C. braarudii* (●), and *C. carterae* (●) grown at different seawater pH. Please note that the POC, PIC and PON values are not absolute as the initial mass of the sample was assumed to be 1 mg (see methods). Production rates were obtained by multiplying per cell elemental values with growth rate. **(a)** POC production rates are generally related to cell size and growth rates, with *G. huxleyi* exhibiting the lowest POC production due to its small size, while *C. carterae* and *C. braarudii* show high POC production due to their large sizes. **(b)** PIC production in *C. braarudii* showed a sharp decline under increasing and decreasing $CO_2$, while changes in PIC production for *C. carterae* were marginal. **(c)** *G. huxleyi* and *C. carterae* exhibit reduced PON and **(d)** POP production with increasing and decreasing $CO_2$ levels, while *C. braarudii* displays a consistent decline with increasing $CO_2$.

Absolute PON and POP production rates are the highest for *G. huxleyi* and the lowest for *C. braarudii*, perhaps due to a relatively small difference in per cell

quotas but large differences in growth rates. PON and POP production exhibited a $CO_2$ and/or pH optima for *G. huxleyi* and *C. carterae*, while values for *C. braarudii* displayed a gradual decline with decreasing pH/ increasing $CO_2$. *G. huxleyi* showed a ~ 90 % decline in PON production rates and an 89 % decline in POP production rate at the lowest pH compared to its optimum. *C. carterae* exhibited a 90 % decline in PON production rates and a 94 % decline in POP production rate at the lowest pH compared to its optimum.

**Discussion**

This study investigated physiological responses of three coccolithophore species, each with distinct ecological niches (Paasche, 2001; Houdan *et al.*, 2004, 2006; Daniels *et al.*, 2016), PIC:POC ratios (Fig. 5; Gafar et al., 2019b), and cell sizes (Fig. 1b; Gafar et al., 2019b) to understand interspecific responses to pH changes. The findings presented in this study regarding growth rates (Fig. 1a, 2) and elemental ratios (Fig. 7, 8) of *G. huxleyi* align with previous research. Specifically, growth rates exhibited minor changes with increasing $CO_2$ except at the highest $CO_2$ levels, where growth rates declined sharply. Similar trends were also observed for *C. carterae*, where growth rates were generally consistent, but declined drastically at the lowest pH. Low growth rates at low pH may be related to $H^+$-driven inhibition, while the observed decrease in growth rates at the highest pH may be due to $CO_2$ limitation (Bach *et al.*, 2015). As shown earlier, growth optima for pH and/or $CO_2$ differed for different species, with *C. carterae* exhibiting highest growth at ~pH 8 (~22 μmol $CO_2$ $KgSW^{-1}$), while *G. huxleyi* showing highest growth at ~pH 8.2 (~16 μmol $CO_2$ $KgSW^{-1}$). Species and strain-specific growth optima are likely influenced by the carbonate chemistry conditions at the site of strain/species isolation and species-specific carbon demand (Rickaby *et al.*, 2016; Chauhan & Rickaby, 2024).

Strain-specific sensitivity to pH (and $CO_2$) has been reported previously (e.g., Langer et al., 2009; Bach et al., 2011).

Changes in carbon uptake mechanisms, nutrient acquisition and metabolic pathways have been attributed as some viable pathways for coccolithophores to adapt to climate change (Riegman et al., 2000a; Lohbeck & Riebesell, 2012; Jin et al., 2013; Kottmeier et al., 2016c; Heidenreich et al., 2019; Dedman et al., 2023). However, these changes also bring about changes in the elemental stoichiometry of a coccolithophore cell, which consequently affects marine biogeochemical cycles (Falkowski, 2000). Understanding changes in elemental stoichiometry of phytoplankton is important since the carbon cycle in the ocean is complexly linked to cycles of limiting nutrients, such as phosphate (Geider *et al.*, 2009).

This study did not observe an increase in POC quotas with $CO_2$ for *G. huxleyi* (Fig. S5). Although a lack of change in POC quotas in *G. huxleyi* has been reported in some studies (Langer *et al.*, 2009; Heidenreich *et al.*, 2019), others have reported an increase in POC quotas with higher $CO_2$ availability (Iglesias-Rodriguez et al., 2008b; Rokitta & Rost, 2012b). (Rokitta et al., 2012b) suggested that an increase in POC quota for *G. huxleyi* with increasing $CO_2$ can be a consequence of increased lipid accumulation in *G. huxleyi* caused by changes in calcium and proton signalling. Riebesell et al. (2000) suggested that an increase in POC quota may be due to improved carbon fixation under higher $CO_2$ availability. The lack of change in POC quotas despite increasing $CO_2$ availability may stem from prioritising the allocation of photosynthetically-derived ATP into establishing pH homeostasis under acidic conditions (Chapter 2; Behrenfeld et al., 2008). Under low pH/high $CO_2$ conditions, the cell may divert resources (e.g., ATP, NADPH) towards management of oxidative stress, repairing macromolecular damage and restoring chemical homeostasis rather than carbon fixation or cell proliferation, which is

evident through reduced growth rates (Chapter 2; Rokitta et al., 2012). Although POC:N ratio for *G. huxleyi* increased with increasing CO2 (Fig. 4a), the lack of significant changes in both POC and PON quotas suggest that marginal changes in POC and PON quotas may have resulted in the increase in POC:N ratios for *G. huxleyi*, which is consistent with previous studies (Fig. 8).

Disruption of cellular pH homeostasis can impair photosynthetic performance by damaging the photosynthetic machinery, as evident through declining $F_v/F_m$ ratios (Lichtenthaler *et al.*, 2005). Although this study shows a decline in photosynthetic performance with decreasing pH in *G. huxleyi*, contrasting results have been reported; Fukuda et al. (2014) did not observe any significant damage to photosystem II through $F_v/F_m$ with acidification through acid addition but reported decreased $F_v/F_m$ values when acidification was done through $CO_2$ bubbling. Jones et al. (2013) reported no change in $F_v/F_m$ values with increasing $CO_2$, while Feng et al. (2008) saw an increase in photosystem II efficiency with increasing $CO_2$. The decreasing photosynthetic performance with declining pH in this study agrees with the findings of Heinze & Dau (1996), who also reported reduced photosynthetic performance due to photosystem II damage at low pH in a green alga. This was suggested to have been caused by acidification inside the thylakoid membrane, which causes increased photoinhibition and affects protein synthesis and degradation in PSII (Heinze & Dau, 1996; Gómez *et al.*, 2004; Ma *et al.*, 2020). Our previous work has shown that light-harvesting proteins were downregulated at high $CO_2$ (low pH) in *G. huxleyi* (Chapter 2). Photosynthetic rates may increase in *G. huxleyi* with increasing $CO_2$, as shown previously (Chapter 2). However, photosynthetic performance of coccolithophores may be impacted due to the disruption of pH gradient within the chloroplast, causing reduced $F_v/F_m$ ratios. This reduction in photosynthetic performance may also be related to the observed downregulation in light-harvesting proteins to avoid photoinhibition (Trinh &

Masuda, 2022; Pedraza-González *et al.*, 2023). Moreover, such changes may take place without noticeable changes in chlorophyll pigment concentrations (Suggett et al., 2007; Rokitta & Rost, 2012b; McCarthy et al., 2012; Vázquez et al., 2023).

A small-sized species such as *G. huxleyi* is highly susceptible to changes in its ambient environment due to its high surface area to volume (SA:V) ratio (Burkhardt et al., 1999b; Suffrian et al., 2011b). Our previous study corroborates this argument by the lack of isotopic equilibration in its coccolith isotopes (Chauhan & Rickaby, 2024). Under acidic conditions, proton accumulation disrupts the ionic homeostasis between the intracellular and extracellular environments, prompting the cell to utilize ATP-dependent ion transporters to return to steady-state conditions (Chapter 2). Disrupted pH gradients in organelles like the chloroplast and mitochondria may lead to the formation of reactive oxygen species (ROS), further damaging cellular components and necessitating additional energy for repair (Chapter 2). These changes may be related to the decrease in growth rates under low pH conditions (Fig. 1a).

Previous studies have proposed that increased RNA production during high growth rates causes lower N:P ratios in *G. huxleyi*, particularly under P-limited conditions (Zhang et al., 2021b). However, in P-replete conditions such as this study, this relationship may not hold (Elser *et al.*, 2003; Moreno & Martiny, 2018). Accordingly, neither PON nor POP quotas for *G. huxleyi* exhibited substantial changes with increasing $CO_2$ levels, in agreement with previous studies (Engel *et al.*, 2014; Johnson *et al.*, 2022; Sheward *et al.*, 2023). Minor changes in both PON and POP quotas influenced N:P ratios. However, this is in contrast to other studies that have reported changes in C:N:P ratios in *G. huxleyi* under changing pH/$CO_2$ (Feng et al., 2018; Zhang et al., 2021b), which might be a strain-specific response as both studies used different strains (NIWA1108, RCC 1266, respectively) to the

one used here (PLY 837; Fig. S3). Overall, N:P ratios for *G. huxleyi* seem to decline with increasing $CO_2$, which may have implications on the contribution of *G. huxleyi* to biogeochemical cycles of major nutrients and food quality of higher trophic levels (Johnson *et al.*, 2022).

The decline in PIC:POC ratios with decreasing pH aligns with previous findings (Fig. 6) and is attributed to disruptions in intracellular calcium carbonate saturation states ($\Omega_{Calcite}$) and calcification. Specifically, the small size and high SA:V ratio for *G. huxleyi* makes it more susceptible to disruptions in pH homeostasis (Burkhardt et al., 1999b; Suffrian et al., 2011b; Chauhan & Rickaby, 2024). A decrease in the PIC:POC ratio with increasing $CO_2$ suggests a potential decline in short-term calcification-related $CO_2$ release, however, reduced calcite export from the surface ocean may influence particle sinking rates, as coccolith calcite coagulates with other organic material and enhance carbon export to the deeper ocean (Klaas & Archer, 2002; Engel *et al.*, 2009).

PIC:POC ratios for *C. braarudii* also decreased with increasing $CO_2$, in line with previous findings (Fig. 6). Specifically, PIC:POC ratios for *C. braarudii* from the present study were in line with (Rickaby *et al.*, 2010; Claxton, 2022), however, they were lower than PIC:POC ratios from other studies (Langer *et al.*, 2006; Kottmeier *et al.*, 2022). These are possibly related to strain-specific characteristics as Claxton (2022) used the same *C. braarudii* strain (RCC 1198) as this study, while Kottmeier et al., (2022) used a different strain (PLY 182g; see below). PIC:POC ratios decreased at the highest $CO_2$ concentrations but remained constant within 10–30 µmol $CO_2$ $kgSW^{-1}$ (Fig. 3). This finding contrasts with previous studies such as (Langer *et al.*, 2006), which reported no pH-related changes in PIC:POC ratios. However, a pH/$CO_2$ optimum for PIC:POC as in this study has been observed previously (Krug *et al.*, 2011; Kottmeier *et al.*, 2022).

Notably, a decrease in PIC:POC ratio was also observed for *C. braarudii* under low $CO_2$/ high pH conditions (Fig. 6), which might be related to $CO_2$ limitation. Our previous work has shown high reliance of *C. braarudii* on diffusive $CO_2$ (Chauhan & Rickaby, 2024). Decreasing PIC:POC ratios and increasing coccolith malformations are evidence for this phenomenon (Fig. 3, see below). Carbon limitation at the lowest $CO_2$ (highest pH) is also evident through reduced growth rates (Fig. 1a) and smaller POC quotas (Fig. S5). The diminished growth rates observed at high $CO_2$ levels and low pH may be attributed to the inability of this species to regulate pH homeostasis effectively, potentially stemming from disruptions in voltage-gated proton channels under acidic conditions (Taylor *et al.*, 2011; Kottmeier *et al.*, 2022).

Elemental stoichiometry of *C. braarudii*, especially POC and PON quotas were tightly coupled to growth rates and coccosphere size. Similar dependence of cellular elemental stoichiometry on growth rates and cell sizes have been documented previously in phytoplankton (Garcia *et al.*, 2016). It is possible that the correlation between size, growth and elemental quotas is a consequence of disruption in the cell cycle, caused by a delay in the onset of mitosis. Under pH-related stress, lower growth rates are accompanied with changes in the amount of ATP and NADPH available for cellular N and P uptake. For instance, N assimilation requires a substantial proportion of reducing power generated through photosynthesis, while P assimilation does not (Turpin 1991). This might have caused the decreased PON quotas under low pH when the reducing power is utilised for the management of oxidative stress, while POP quotas did not change, as no reducing power is required for its assimilation. Disruption in cellular pH homeostasis has previously been reported to induce production of ROS and upregulation of ROS scavenging mechanisms in *C. braarudii* (Chapter 2). Since cell division is tightly regulated by redox signalling, the presence of ROS can impede

cell division (Wang *et al.*, 2017). The disruption to calcification may have also affected the cell cycle, as previously shown (Walker et al., 2018).

Growth rates of < 1 $day^{-1}$ meant that cell doublings per day for *C. braarudii* were ~0.4 ($day^{-1}$) at the highest $CO_2$ levels and ~0.83 ($day^{-1}$) at ~ 11 µmol $CO_2$ $KgSW^{-1}$. Scanning electron microscopy showed notable variability in cell sizes under changing $CO_2$/pH conditions, with evidence of newly-divided paired cells. All samples were taken at the same time during the light phase (see methods); therefore, delayed mitosis in stressed treatments (high $CO_2$/low pH) may lead to cell division at a later hour compared to non-stressed treatments (e.g., at ~ 11 µmol $CO_2$ $KgSW^{-1}$), leading to smaller sizes at the time of sampling. Since the dilute batch cultures for *C. braarudii* typically had < 5,000 cells $mL^{-1}$, and due to the large size of *C. braarudii* cells, artefacts related to size and growth can show large changes in elemental stoichiometry.

POP quota per cell was inversely proportional to growth rates (Fig. S5). High phosphorous uptake under low growth may be a way to maximise the possibility of cellular growth by "luxury" uptake of phosphorous in P-replete conditions, whereas phosphorous uptake rates may be on par with high growth rates at ~ 11 µmol $CO_2$ $KgSW^{-1}$ (Azad & Borchardt, 1970). Although *G. huxleyi* may not consume surplus P (Rost & Riebesell, 2004b), the high POP quotas in *C. braarudii* suggest species-specific characteristics in P uptake. Phosphate-rich cellular compartments have previously been reported in coccolithophores, which may be related to cellular POP quotas (Sviben *et al.*, 2016). Consequently, POC:N ratios, POC:P ratios and N:P ratios exhibited highest values at ~ 11 µmol $CO_2$ $KgSW^{-1}$. These trends were mostly due to changes in POC and PON quotas, which correlated to changes in growth rate (Burkhardt et al., 1999c).

While previous studies have indicated heightened sensitivity of *Chrysotila dentata* (similar to *C. carterae* of this study) to combined temperature and pH changes (Thangaraj *et al.*, 2023), our study primarily focused on pH variations. Growth rates exhibited a broad $CO_2$ optimum that only declined substantially at the lowest pH due to $H^+$-mediated inhibition (Fig 1; Bach et al., 2011). This observation aligns with our previous findings of minimal proteomic changes in *C. carterae* in response to pH changes (Chapter 2).

In *C. carterae*, a notable characteristic is the variation in cell size (Fig. 1b). Cell sizes are generally considered to be an interplay between optimising diffusive resource acquisition and managing ballasting capabilities under sufficient light for photosynthesis (Chisholm, 1992). It is possible that the enlargement of cell size in *C. carterae* could stem from reduced doubling rates during slower growth rates at low pH. However, the optimum $CO_2$/pH conditions for growth do not align with the smallest cell size observed. Moreover, cell sizes increased despite minor changes in growth rates (Fig 1a). This suggests a possibility that the cell actively increased its size under low pH (high $CO_2$) conditions, potentially to reduce its SA:V ratio (Fig. 1). Being of coastal nature, size plasticity may allow *C. carterae* to respond to shifts in the environment (Morabito *et al.*, 2007; Olson *et al.*, 2017). Such a strategy could enhance the cell's internal buffering capacity against higher ambient proton levels during low pH, as demonstrated by our previous study using oxygen isotopes of the coccolith calcite (Chauhan & Rickaby, 2024). Moreover, increased SA:V ratio due to a smaller cell size may be related to the cell's attempt at increasing $CO_2$ diffusion under low $CO_2$ and high pH conditions. Similar observations have been previously observed for *G. huxleyi* (Olson *et al.*, 2017). Although this study did not observe any substantial changes in the size of *G. huxleyi*, the plasticity in cell size for coccolithophores points towards a dynamic capability in this phytoplankton group to changing environmental conditions.

POC and PON quotas for *C. carterae* proportionally increased with increasing $CO_2$, which may be related to shifts in cell size (Marañón, 2008; Lim *et al.*, 2022). POP quotas did not correlate with cell size, potentially due to the lack of significant changes in P-rich macromolecules under phosphorous-replete conditions (Chapter 2) (Moreno & Martiny, 2018).

While the C:N ratio for *C. carterae* generally increased with increasing $CO_2$ levels, aligning with trends observed in *G. huxleyi* and *C. braarudii*, the N:P ratio presented a contrasting pattern. The N:P ratio declined with increasing $CO_2$ in *C. braarudii* and *G. huxleyi*, while it increased in *C. carterae*, attributed to shifts in its cell size (Fig. 1b, 4c). Chlorophyll *a* concentration for *C. carterae* increased slightly at higher $CO_2$ levels, even after adjusting for changes in cell size (Fig. 4c), while our earlier study revealed a downregulation in photosynthesis-related proteins in *C. carterae* under high $CO_2$ conditions (Chapter 2). These changes were associated with a decreased photosynthetic performance (Fig. 4) and marginal increase in net photosynthetic rates under high $CO_2$ conditions (Chapter 2). These observations suggest that coccolithophores may be capable of adapting their photosynthetic machinery in response to alterations in ambient pH (Suggett *et al.*, 2007; McCarthy *et al.*, 2012). Notably, carbon fixation by rubisco may increase under high $CO_2$ levels, but photosensitivity, and the ability to utilise (and dissipate) captured light may be influenced by cellular stress and disruption of ion homeostasis under low pH (Heinze & Dau, 1996; Asada, 2003; Trinh & Masuda, 2022). These changes may serve as a mechanism for reallocating resources toward cellular repair, mitigating oxidative stress, and maintaining ion homeostasis amidst heightened ambient proton concentrations by optimising the photosynthetic apparatus (Chapter 2).

**Variability in coccolithophore responses due to strain specific characteristics**

Through the synthesis of data from existing studies with the observations made in the present study, it is evident that overall, the three species exhibited a broad $CO_2$ optimum (Fig. 2, S3). Although the median growth rates declined for all three species with increasing $CO_2$ levels, measuring the gradient of change for individual datasets revealed that growth rates exhibited high variability (Fig S3), which may be due to strain-specific adaptation to different carbonate chemistry conditions, as highlighted previously (Rickaby *et al.*, 2016). Indeed, when the growth rates from this study are compared with those from previous studies, notable differences in pH/$CO_2$ optima are observed (Fig. 10). For instance, the four different strains of *C. braarudii* used in Figure 10 exhibited unique $CO_2$ optima, which were related to the carbonate chemistry at their respective isolation sites. Strain RCC 1200 used by (Krug *et al.*, 2011) was isolated close to the Namibian coast, which is an active upwelling area that brings up low-pH $CO_2$-rich waters (Emeis *et al.*, 2018). Similarly, RCC 1202 used by (Hermoso, 2015) was isolated near the western Iberian coast, which is also an upwelling region (Relvas *et al.*, 2007). Notably, both these strains exhibited a $CO_2$ optimum at high $CO_2$ levels than the strains isolated from the English Channel (RCC 1198, PLY 182g, this study, Kottmeier et al., 2022) where the pH levels can be considerably higher (Kitidis *et al.*, 2012).

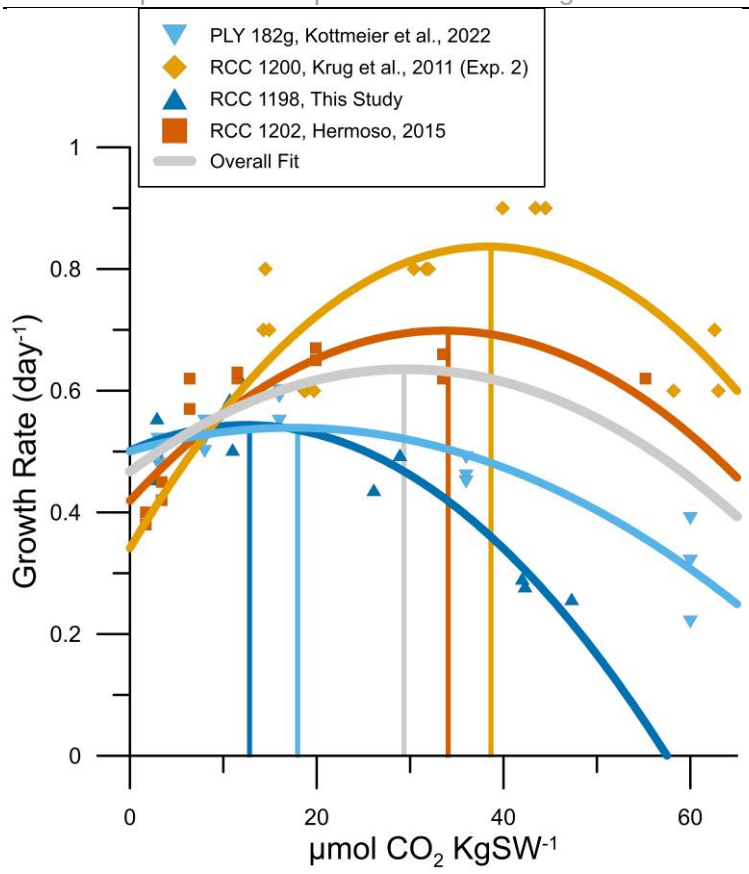


**Figure 10:** Growth rates versus $CO_2$ from four studies (including the present study) that show strain-specific variability in $CO_2$ optima. Note that RCC 1200 and 1202 were isolated from coastal upwelling zones, while RCC 1198 and PLY 182g were isolated from the English Channel. Vertical bars indicate the modelled $CO_2$ optima for each strain based on the polynomial fit (degree = 2). All four studies simulated carbonate chemistry manipulations through addition of acid/base. The method of carbonate chemistry manipulation can also have an impact on the responses of coccolithophores to increasing $CO_2$ (See Supplementary Figure S4). A blanket polynomial fit (degree = 2, grey curve) mutes any strain-specific responses and gives a false idea of pH/$CO_2$ optimum for a given species.

Utilising a general polynomial fit (Fig. 10, grey curve) disregards strain-specific behaviours and can give a false impression on the sensitivity of a given species to pH and/or $CO_2$ changes, as also shown by the polynomial fit in Figure 2 (blue curve). Note that a comparison of growth optima between different studies is only possible for studies that have used the same method for carbonate chemistry manipulation (Bach et al., 2011a). This is because a given strain can show a different response if carbonate chemistry was manipulated in another way (Fig. S4). Moreover, despite accounting for the carbonate chemistry conditions at the

sight of isolation and the method of carbonate chemistry manipulation, there can still be strain-specific physiological characteristics, such as the PIC:POC ratio (Fig. S4).

Based on the observations above, it's evident that short-term acclimation studies can't suppress the adaptation-related physiological responses of a particular algae. Despite being cultured for over 25 years, strain RCC 1198 of *C. braarudii* (this study) exhibited a strain-specific response to varying $CO_2$ levels (Fig. 10, roscoff-culture-collection.org). The variations in responses does not imply that significant conclusions cannot be drawn regarding the fate of coccolithophores during climate change. Nonetheless, extrapolating from a single strain should be approached cautiously. The response of a specific strain should be evaluated in relation to the environmental conditions at its isolation site.

**A note on coccolith malformations**

The impact of pH can be observed through malformations in the coccolith calcite (Fig. 11). Malformations may arise due to a reduced $\Omega_{Calcite}$ within the coccolith vesicle when intracellular pH is lowered (Zeebe & Wolf-Gladrow, 2001), or due to a pH-induced reduction in the activity of coccolith associated polysaccharides (CAPs) (Henriksen & Stipp, 2009; BeMiller, 2019). Reduced $H^+$ homeostasis due to disruption of voltage gated channel activity in *C. braarudii*, and high proton permeability in *G. huxleyi* due to its high SA:V ratio may cause changes in the intracellular $\Omega_{Calcite}$ (Suffrian et al., 2011b; Kottmeier et al., 2022). Consequently, malformations are evident in *C. braarudii* and *G. huxleyi* under the lowest pH conditions (Fig. 11).

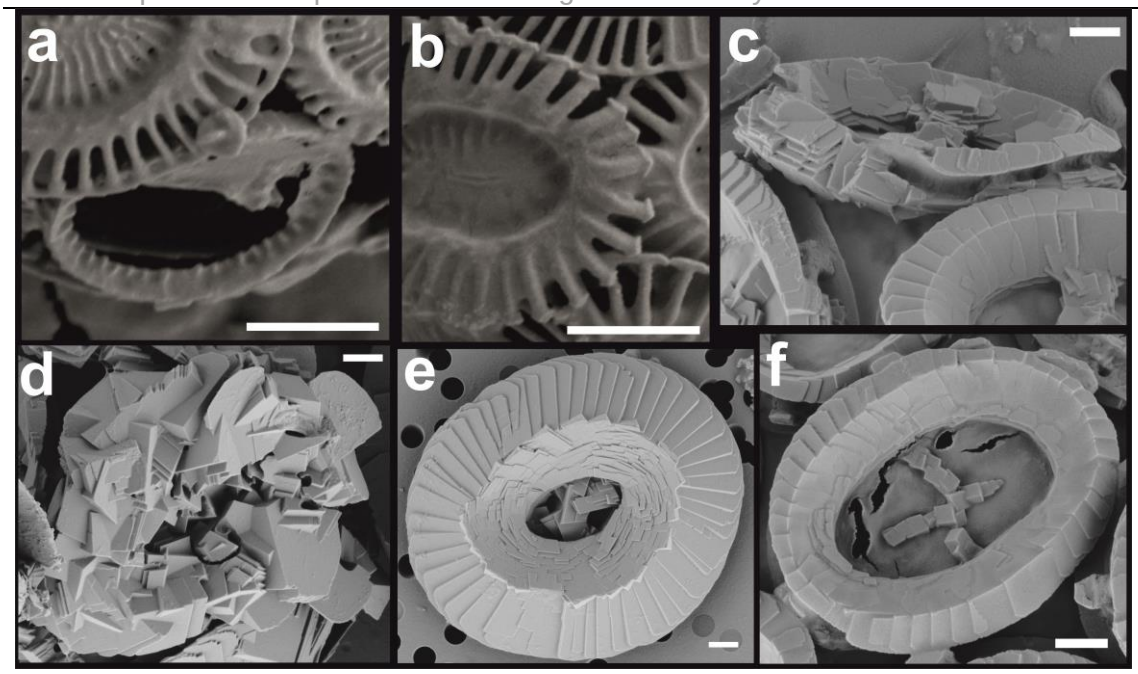


**Figure 11:** Scanning Electron Microscope images of coccoliths of *G. huxleyi* (a, b) and *C. braarudii* (c – f). **(a)** A protococcolith ring and **(b)** incomplete T elements of a coccolith from *G. huxleyi* (pH 7.6). Malformations in *G. huxleyi* were rare, but typically occurred as these two types in acidic conditions. **(c)** An "incomplete" coccolith typically representative of the malformations in *C. braarudii* at pH 8.8. **(d)** A "blocky" coccolith typically representative of the type of malformations in *C. braarudii* under acidic conditions (pH 7.6). **(e)** A typical example of a "normal" coccolith, from a *C. braarudii* grown at pH 8.2. **(f)** Top view of an "incomplete" coccolith from *C. braarudii* grown under high pH conditions. White scale bar represents 1 µm. Note that scale changes between images for adequate visualisation. (c) and (f) show that *C. braarudii* coccoliths are not prone to "blocky" malformations under high pH, but "incompleteness" due to $CO_2$ limitation. Similar observations have been previously made by Kottmeier et al. (2022). Notably, (d) is an extreme example of "blocky" malformations, used here to make the comparison between the type of malformations clearer. Although malformations ranged from minor to extreme for *C. braarudii* under low pH, typical "blocky" malformations can be seen in Fig. 3.

In *C. braarudii*, malformations are particularly pronounced, manifesting as "blocky" coccoliths under low pH conditions (Fig. 11). On the other hand, malformations in *G. huxleyi* appear as incomplete coccoliths, or protococcolith rings. Lower uronic acid content in the CAPs of *C. braarudii* may possibly make them more susceptible to reduced activity under high $H^+$ concentrations under low pH (Henriksen & Stipp, 2009; Lee *et al.*, 2016). Conversely, coccolith production in *G. huxleyi* may be more energy-intensive under low pH, requiring greater energy for the active removal of protons from the coccolith vesicle (CV).

Therefore, *G. huxleyi* may extrude incomplete coccoliths in order to avoid spending excess energy on maintaining high (and stable) $\Omega_{Calcite}$ within the CV. At higher pH levels, *C. braarudii* exhibits a distinct form of malformation characterised by incomplete coccolith formation. Such malformations brought significant changes in coccolith dimensions for *C. braarudii* under low $CO_2$ conditions (Fig. 12). However, these types of malformations were absent from any other coccolithophore species, suggesting *C. braarudii* has the highest carbon requirements amongst the species studied here. These anomalies may stem from carbon limitation, a factor previously identified to induce significant changes in the stable isotopic composition of coccolith calcite (Chauhan & Rickaby, 2024).

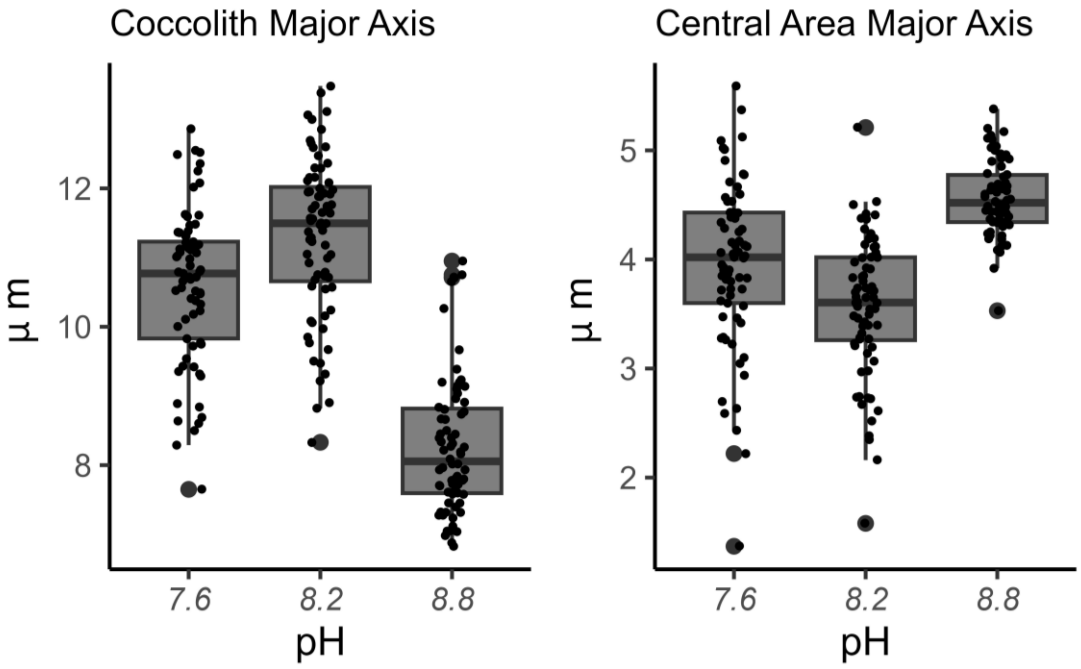


**Figure 12:** Coccolith length and Central Area major axes from the coccoliths of *C. braarudii* grown under varying pH conditions. Dimensions from the coccoliths of highest pH (pH 8.8) and lowest pH (pH 7.6) and intermediate pH (pH 8.2) are displayed. At least 60 coccoliths were measured for each treatment, and only the longest axes (the major axis) of the coccoliths, and their central areas were measured (see Supplementary Information for a schematic). It is evident that coccoliths are the largest in size at pH 8.2, with the smallest central area, while coccoliths are the smallest at pH 8.8 with the largest central area. These generally look "incomplete" (see Fig. 11). Coccoliths at pH 7.6 are slightly smaller than those at pH 8.2 and have slightly larger central areas. These generally look "blocky" (see

Fig. 11). Similar measurements were made for *G. huxleyi* and *C. carterae*, but no variations between treatments were found.

Coccolith malformations have been reported many times previously (Kleijne, 1990; Trimborn *et al.*, 2007; Ziveri *et al.*, 2014; Kottmeier *et al.*, 2022), however, the mechanisms that dictate the possibility and severity of malformations have not been discussed (Shetye *et al.*, 2023). This is perhaps because the causal mechanisms that drive malformations in coccoliths can be deeply engrained in other biological processes. For instance, both nitrogen and phosphorous limitations have been associated with malformations in coccoliths, despite any obvious relationship to the calcification process (Yang *et al.*, 2004; Langer *et al.*, 2023a). Similarly, absence of silicon, presence of germanium, or cytoskeletal inhibition have been associated with malformations in coccoliths, even though calcification only requires calcium and carbonate ions, and the process is confined to the coccolith vesicle (Durak *et al.*, 2017; Langer *et al.*, 2021, 2023b). In the present study, changes in pH may disrupt $\Omega_{Calcite}$ and cause coccolith malformations, in agreement with previous (Langer *et al.*, 2006; Rickaby *et al.*, 2010; Kottmeier *et al.*, 2022; Shetye *et al.*, 2023). Notably, incomplete coccoliths in *C. braarudii* were observed due to carbon limitation at low $CO_2$ levels.

**Implications for marine biogeochemistry**

Cellular elemental ratios of carbon, nitrogen and phosphorous (C:N:P, or the Redfield ratio) can vary at different levels: cellular (macromolecular), species (individual), and ecological (ecosystem) (Moreno & Martiny, 2018). However, they are fundamentally important to understanding the link between cellular biochemistry and marine biogeochemical cycles (Daines *et al.*, 2014). While extensive research has been conducted on Redfield ratios of *G. huxleyi* (for a recent review, refer to Sheward et al., 2023), few studies have focused on other

coccolithophore species, particularly under varying pH/$CO_2$ conditions (Rickaby *et al.*, 2010; Krug *et al.*, 2011; Thangaraj *et al.*, 2023; Wu *et al.*, 2023).

In this study, we observed an increase in the POC:N ratios across all three species with increasing $CO_2$, suggesting a potential change in the ratio of organic carbon to nitrogen export to the ocean, at least at an individual level (Fig. 7a; Rost & Riebesell, 2004). Although these observations are likely to differ based on strain-specific tolerances to higher $CO_2$ conditions, general inferences can be made. N:P ratios decreased for *C. braarudii* and *G. huxleyi* but increased for *C. carterae,* indicating species-specific effects on elemental stoichiometry that could influence the food quality of higher trophic levels and the biogeochemical cycles of N and P (Auguères & Loreau, 2015). Although changes in N:P ratios varied between species, both N and P production rates decreased across all species at high $CO_2$ levels, possibly due to declining growth rates at low pH (Fig. 9c,d). Both *C. carterae* and *G. huxleyi* exhibited a $CO_2$ and/or pH optimum, aligning with their respective growth rate optima. However, such an optimum in N and P production rates was not observed for *C. braarudii*. Additionally, N and P production rates in *C. braarudii* were low, suggesting that the contribution of this species to N and P biogeochemical cycles is significantly lower than that of *C. carterae* and *G. huxleyi*. Given the importance of *C. braarudii* in polar oceans and of *G. huxleyi* worldwide, changes in N and P quotas and production rates in these open ocean species will seriously impact biogeochemical cycling of N and P (Westbroek *et al.*, 1993; Daniels *et al.*, 2014). It is worth noting that N and P production rates for *G. huxleyi* and *C. carterae* also decreased at the highest pH (lowest $CO_2$) levels, indicating a potential decline in their contribution to N and P cycling under artificially enhanced ocean alkalinity scenarios (Bach *et al.*, 2019).

Carbon to chlorophyll *a* ratios are an important variable for global biogeochemical models as this ratio can be used for normalising light-limited and light-saturated

photosynthetic rates from chlorophyll a, and carbon, respectively (Geider, 1987). Satellite-based estimates for primary productivity and growth rates are often estimated through Chlorophyll *a* measurement (Westberry *et al.*, 2008). Although changes in C:Chla ratios due to temperature and light have been documented previously, changes due to pH and $CO_2$, especially for coccolithophores have not received much attention (Geider, 1987; Westberry *et al.*, 2008; Geider *et al.*, 2009). This study showed that C:Chla ratios stayed consistent for *C. braarudii* and *G. huxleyi*, suggesting that this ratio may only change in relation to temperature and light-related effects on carbon fixation and light capture. However, *C. carterae* exhibited a decrease in C:Chla ratios with increasing $CO_2$, suggesting that the assessment of primary production in coastal areas, especially during *C. carterae* blooms may be compromised.

Despite *C. braarudii* displaying lower growth rates than other coccolithophore species under all $CO_2$/pH conditions, its POC production rates were the highest amongst all species (due to its large cell size), peaking at ~11 µmol $CO_2$ $KgSW^{-1}$. Conversely, POC production rates for *C. carterae* remained relatively stable with changing $CO_2$ up to 35 µmol $KgSW^{-1}$, potentially due to the compensatory effects of increasing cell size and decreasing growth rates. However, at the highest $CO_2$ concentrations, POC production rates for *C. carterae* dropped sharply due to the decline in growth rates outweighing any increase in cell size. *G. huxleyi* displayed the lowest POC production rates, owing to its small cell size (Fig. 6a). This species exhibited relatively stable POC production rates under most $CO_2$ concentrations, except at the highest levels, when POC production rate dropped. PIC:POC ratios and PIC production rates have received much attention in coccolithophore-related physiological studies, as they release carbon dioxide in the short term and contribute to long-term carbon burial through vertical calcite flux (Rost & Riebesell, 2004b). Although species-specific PIC:POC ratios have been described

as a predictor of sensitivity to low pH and ocean acidification (Gafar et al., 2019c), our study revealed species-specific changes in PIC:POC ratios and PIC production rates as a consequence of pH changes (Fig. 5, 6b). While PIC:POC ratios show a broad $CO_2$/pH optimum for *C. braarudii*, they show a consistent decline with increasing $CO_2$ in *G. huxleyi*. Due to the low PIC:POC ratio of *C. carterae,* any changes in this ratio with increasing $CO_2$ were indistinguishable in this study. PIC production rates were highest for *C. braarudii*, corresponding to its high PIC quotas, with maximum rates at ~11 µmol $CO_2$ $KgSW^{-1}$, corresponding to changes in growth rates and POC quotas. However, PIC production rates for *C. carterae* and *G. huxleyi* were low due to the low PIC quotas for both species.

Given the relative importance of *G. huxleyi* and *C. braarudii* in calcite export (Tyrrell & Merico, 2004; Daniels *et al.*, 2014, 2016), it is evident through this and many previous studies that PIC production will decrease with increasing $CO_2$ (Krumhardt *et al.*, 2017). These changes are likely to come into place with reduced N and P export, as shown in this study. Smaller species are generally numerically more abundant than larger species, however, their contribution to biogeochemical cycles is smaller. Moreover, it was evident through the findings of this study that cell size plays a major role in determining per cell quotas of C, N and P.

Changes in the community size structure are likely to play a role in shifts within coccolithophore-related nutrient export. Moreover, changes in seawater carbonate chemistry will affect ecological niches occupied by different species and affect coccolithophore biodiversity in future oceans (Käse & Geuer, 2018). However, as mentioned earlier, strain-specific $CO_2$ optimum likely mean that certain strains may perform better under higher $CO_2$ scenarios (Rickaby *et al.*, 2016), that is, for strains with a $CO_2$ optimum at higher $CO_2$ levels than present-day oceans, we may witness an expansion in their biogeographical niche in higher $CO_2$/lower pH future oceans.

Previous assumptions based on studies dominated by *G. huxleyi* must be reconsidered to incorporate the diversity in coccolithophores (Geisen *et al.*, 2004; Wheeler *et al.*, 2023). Studies investigating coccolithophore responses to changing carbonate chemistry conditions must emphasise the carbonate chemistry conditions of the isolation site. Furthermore, this diversity must be incorporated into earth system models using coccolithophore abundance data to understand global niche partitioning between species, consequential changes in nutritional regimes for higher trophic levels and calcite production rates (Terrats *et al.*, 2023).

**Supplementary Information**

This supplementary section provides information on methodology of coccolith measurements and detailed description of the results obtained in this study has been provided separate to the main text to maintain clarity.

# Conclusion

The objective of this thesis was to improve our understanding of coccolithophore biology and its implications on physiology and chemistry, while emphasising species-specific responses to environmental changes. To gain a holistic understanding of coccolithophore biology, I used a multidisciplinary approach, utilising stable isotopes, proteomics, and physiological measurements of growth, photosynthesis, calcification, and elemental stoichiometry. The results highlighted innate differences in coccolithophore species, where size-dependent dynamics, biological requirement for calcification and environmental habitat drive species-specific responses to changes in seawater pH and $CO_2$ concentrations.

### Summary of Key Findings

### Chapter 1: Size-Dependent Dynamics of the Internal Carbon Pool Drive Isotopic Vital Effects in Calcifying Phytoplankton

In the first chapter, I showed that the stable isotopic composition of coccolith calcite and organic matter changes with varying carbonate chemistry (pH and $CO_2$). In agreement with previous studies, I showed that large and heavily calcifying species such as *C. braarudii* and *C. leptoporus* are carbon limited under low $CO_2$ concentrations. This carbon limitation drives large kinetic isotope effects in $\Delta^{13}C_{Coccolith}$ and $\Delta^{13}C_{ORG}$. On the other hand, under non-$CO_2$-limiting conditions, both species show a consistent isotopic value, despite changing $CO_2$ levels, suggesting long carbon residence times in the internal carbon pool, allowing for isotopic equilibration of the intracellular carbon. This may be a consequence of the large size, allowing for a larger internal carbon pool, along with high carbon demand for calcification and organic matter fixation.

Conversely, *G. huxleyi* and *G. oceanica,* being comparatively lightly calcifying and smaller in size, show a high degree of kinetic fractionation in both $\Delta^{13}C_{Coccolith}$ and $\Delta^{18}O_{Coccolith}$. This is due to the high surface area to volume ratio, which permits large fluxes of $CO_2$ to diminish any isotopic equilibration of the internal carbon pool. On the other hand, $\Delta^{13}C_{ORG}$ values for both species showed consistent values despite changing carbonate chemistry, possibly due to negligible Rayleigh fractionation in the organic matter, due to the aforementioned high carbon fluxes and constant replenishment of the internal carbon pool. These observations suggested that small species, with a lower carbon demand due to their smaller size and calcification requirements, and due to the small size of the internal carbon pool due to their small size, the flux of carbon going into and out of the cell is high, and the residence time of carbon in the internal carbon pool is short.

Finally, *C. carterae* displayed a high degree of isotopic equilibration in its internal carbon pool through $\Delta^{13}C_{Coccolith}$ and $\Delta^{13}C_{ORG}$ values that were proportional to the changes in $CO_2$ concentration and through consistent $\Delta^{18}O_{Coccolith}$ values representing lack of kinetic isotope effects. This may be due to the large internal carbon pool size as a consequence of a large cell size, but also low carbon demand due to low calcification requirements. I demonstrated that isotopic gradients between $\Delta^{13}C_{Coccolith}$ – $\Delta^{18}O_{Coccolith}$ values and $\Delta^{13}C_{Coccolith}$ – $\Delta^{13}C_{ORG}$ values serve as quantitative indicators of carbon residence time within the intracellular carbon pool. This residence time significantly influences the physiological dynamics of carbon regulation in coccolithophores, with the size of the internal carbon pool directly proportional to the size of the coccolithophore cell. Furthermore, certain species, such as *C. carterae* and *C. leptoporus* showed evidence of elevated intracellular pH that directly or indirectly assisted to minimise $CO_2$ leakage.

**Preliminary Investigations into the Intracellular Carbonate Chemistry of Coccolithophores: A step in the right direction?**

I attempted to quantify the size of the internal carbon pool by measuring the time it takes to isotopically equilibrate the internal carbon pool during a pulse chase experiment. For this, I utilised a novel $^{13}C$ spike pulse chase technique that would allow the quantification of internal carbon pools using standard isotopic ratio mass spectrometers (IRMSs). I attempted this technique on the three key species identified in Chapter 1, that is, *C. braarudii*, *C. carterae* and *G. huxleyi*. However, this technique failed to detect the presence of a carbon pool. This could have been due to many reasons: the small concentration of spike used (~80 ‰); possibly inadequate sampling requiring higher frequency of sampling; the acid-labile carbon pool may have been washed during the acidification step that was necessary to remove coccolith calcite to be able to accurately measure the isotopic composition of the organic matter.

I also attempted to quantify the intracellular pH conditions and the pH buffering capacity of those three coccolithophore species using a fluorescent dye SNARF-AM. Although intracellular pH changes showed a linear relationship with changes in extracellular pH conditions for *G. huxleyi* and *C. carterae*, the trend was less apparent in *C. braarudii*. Moreover, absolute intracellular pH values were not possible as dye loading was not uniform between species and replicates. Moreover, a drift in the fluorescence ratio was observed with time, suggesting the need for experiments of a shorter duration. This work highlighted that quantifying intracellular pH conditions in coccolithophores is essential as coccolith calcification is believed to produce $H^+$ ions, which must be expelled out of the cell in order to avoid excessive intracellular acidification. The ability to maintain a consistent intracellular pH may differ between species, as some species (e.g., *C.*

*braarudii*) are more susceptible to coccolith malformations under low pH, possibly due to the changes in $\Omega_{calcite}$. Moreover, quantification of the intracellular pH conditions is necessary to understand the mechanisms of isotopic fractionation that lead to different species having their unique isotopic compositions. Investigating such mechanisms will improve the accuracy and reliability of coccolith calcite for the use of paleoenvironmental reconstruction.

**Chapter 2: Contrasting Stress Response to Environmental pH Determines the Fate of Coccolithophores in Future Oceans**

This chapter utilised proteomics and physiological measurements to quantify differences in pH sensitivity between coccolithophore species. Proteomic analysis revealed that the number of significantly changed proteins roughly correlated with the decrease in growth rates under pH stress. Through the changes in cellular proteome, it was apparent that pH changes in the environment had caused oxidative stress in the cell, possibly due to changes in membrane potential in the chloroplasts and mitochondria. Consequently, reactive oxygen species (ROS)-scavenging proteins, and proteins related to oxidative stress management and cellular repair were upregulated. Broadly, heightened activity was evident in ion transport, oxidative stress management, DNA repair and cell cycle control proteins, signalling proteins, protein folding, degradation and repair proteins in *C. braarudii* and *G. huxleyi* under changing pH conditions. *C. braarudii* was highly sensitive to pH stress, showing significant changes in several mitochondrial, photosynthetic, biosynthetic proteins in addition to those mentioned above. This suggested that cellular activity in general was upregulated in *C. braarudii*, possibly in an attempt to restore cellular homeostasis. However, upregulation of these cellular pathways came at additional substrate and energetic costs, which was reflected in the decline in growth rates, as energy was probably being diverted to

cellular damage repair instead of cell division and DNA replication to obtain cellular homeostasis.

The upregulation of "standard" metabolic pathways in *C. braarudii* suggested heightened stress under non-optimal pH conditions and an inability to dynamically regulate metabolic processes during stress. The high pH sensitivity of *C. braarudii* might stem from its poor ability to establish pH homeostasis, triggering further cellular changes. Consequently, ion channels, oxidative stress-related proteins, and macromolecular damage repair mechanisms were upregulated. These molecular alterations were reflected in physiological changes such as growth and respiration rates. This correlation highlighted the importance of growth dynamics in *C. braarudii* and its response to environmental stress, aligning with Raven's cost-benefit analysis (Raven, 1984). That is, under "typical" growth conditions (pH ~ 8.0 – 8.2), *C. braarudii* maximises spending its energetic and nutritional resources into cell growth and division., whereas under stress conditions, such as those stimulated in this thesis, the organism prioritises its survival, and may conduct molecular changes to acclimate to the new conditions (such as higher ion channel activity). Such changes, however, have an impact on the cellular elemental quotas, which are likely to affect biogeochemical cycles in the open ocean under future climate scenarios (Chapter 3).

In contrast to *C. braarudii*, *C. carterae* exhibited very low sensitivity to changes in pH possibly due to the high variability observed between replicates for this species in all pH conditions, and due to its resilience to environmental changes. Under alkaline conditions (pH 8.8), this species did not show any significant changes in proteomics, while only 9 proteins were significantly changed under acidic conditions (pH 7.6). Most of the significant changes were downregulations in the photosynthetic machinery, possibly as a consequence of higher $CO_2$ availability,

allowing the cell to redirect its resources to cell growth. Indeed, small increases in growth rates were observed, although these were statistically insignificant. An upregulation of carbonic anhydrase was also observed under high pH conditions, possibly as a response to low $CO_2$ levels. The lack of changes in the proteome of *C. carterae* is likely evidence of its high resilience to environmental change. Given the coastal nature of this species, it likely experiences large fluctuations in temperature, salinity, and carbonate chemistry, which potentially aided in its adaptation.

Growth rates for *G. huxleyi* where the highest at pH 7.6, and lowest at pH 8.8, possibly due to pH stress and $CO_2$ availability. This observation was in contrast to the growth rates observed for the *G. huxleyi* strain used in Chapter 1, where growth rates increased with increasing pH. Such disparity might be a consequence of strain-specific pH optima, which depends on the carbonate chemistry at the site of isolation of a specific strain. Proteomic changes in *G. huxleyi* were intermediate, with larger changes observed under alkaline conditions (pH 8.8) compared to acidic conditions (pH 7.6). Although proteomic changes in *G. huxleyi* aligned with those observed in *C. braarudii,* unique observations were also made. An upregulation in ion transport, protein folding and repair, and oxidative stress management was observed, in alignment with changes in *C. braarudii*. However, an upregulation of isocitrate lyase was also observed at pH 8.8, which was unique to this species. Isocitrate lyase bypasses several steps in the TCA cycle and can be utilised for carbon conservation. The upregulation of this enzyme suggests an increased effort from *G. huxleyi* to mitigate carbon limitation under alkaline conditions. Moreover, proteolytic enzymes such as 26S proteasome, Derlin, heat-shock proteins, and protein synthesis-related ribosomal proteins exhibited downregulation but several PPIases and peptidases were upregulated, suggesting unique ER mechanisms for recycling damaged proteins. These cellular

adjustments in *G. huxleyi* likely facilitate resource allocation based on necessity, enhancing its ecological success in modern oceans.

These observations underscore the multifaceted impact of environmental perturbations on organisms. This is especially true for pH, which influences $CO_2$ concentrations, changes in trace metal speciation and ion homeostasis within cells. The biochemistry of a cell depends highly on pH homeostasis, as both the mitochondrion and the chloroplast rely on proton gradients for ATP production. Moreover, the activity of biomolecules such as proteins depends heavily on intracellular pH.

**Chapter 3: Species-specific Variability in Coccolithophore Physiology under Changing Seawater pH and Its Impact on Marine Biogeochemical Cycles**

Environmental changes, particularly pH stress, trigger biochemical adjustments crucial for organismal adaptation. As seen in Chapter 2, these alterations impact various cellular processes, including nucleic acid synthesis, protein metabolism, lipid peroxidation, and carbohydrate metabolism, particularly in the case of *C. braarudii*. These cellular modifications lead to shifts in elemental stoichiometry, as reflected by changes in C:N and N:P quotas and affect nutrient export from the surface oceans to higher trophic levels and the broader nutrient biogeochemical cycles. In chapter 3, we observed a tight coupling between growth rates and cell sizes in *C. braarudii,* where alterations in these parameters resulted in corresponding shifts in cellular elemental stoichiometry, i.e., changes in POC, PIC and PON quotas were correlated with growth rates and cell sizes. Correspondingly, elemental ratios changing with changing pH, with increasing C:N ratios with increasing $CO_2$, decreasing N:P and C:P ratios with increasing $CO_2$, suggesting higher carbon export under ocean acidification conditions, but lower N and P contributions from *C. braarudii*. However, despite evident stoichiometric changes

in *C. braarudii* and fluctuations in its PIC:POC ratio, stable isotopes in Chapter 1 remained unchanged with varying pH. This indicateed that while the quantity of carbon fixed as organic or inorganic carbon may fluctuate, its isotopic composition remains equilibrated due to prolonged residence time in the internal carbon pool.

*C. braarudii* displayed a heightened susceptibility to coccolith calcite malformations, a phenomenon well-documented in prior studies. For example, Kottmeier et al. (2022) demonstrated that inhibiting proton channels in *C. braarudii* led to malformations by impairing its ability to expel protons from the intracellular space, potentially altering the calcium carbonate saturation state of the coccolith vesicle. While coccolith malformations at low pH in Chapter 3 of this thesis can arise from similar mechanisms, those observed at high pH cannot be attributed to protons alone. Rickaby et al. (2010) reported coccolith malformations in high DIC conditions despite pH being constant, indicating that carbonate chemistry plays a significant role. It is conceivable that alterations in carbonate chemistry impact CAP (coccolith-associated polysaccharide) chemistry, thereby influencing CAP-calcite interactions. Considering the low uronic acid content in the CAP of *C. braarudii*, changes in internal calcium carbonate saturation state may modulate the carboxyl group's calcium binding capacity.

*G. huxleyi* demonstrated a distinct response compared to *C. braarudii*. Two different strains of *G. huxleyi* used in this thesis exhibited varying growth rate preferences in relation to pH and/or $CO_2$ levels. This variability may stem from differing carbonate chemistry conditions at their respective isolation sites, as suggested in Chapter 2. While substantial changes in cellular processes were observed in *G. huxleyi* with pH fluctuations via proteomics (Chapter 2), elemental quotas remained relatively stable. This aligns with prior studies where elemental

quotas or the Redfield ratio for *G. huxleyi* changed by less than 30% due to varying $CO_2$ levels (Sheward et al., 2023). However, elemental production rates decreased significantly with increasing $CO_2$, reflecting declining growth rates. This implies potential changes in carbon, nitrogen, and phosphorus export from *G. huxleyi* under lower ocean pH scenarios. The main driver of changes in elemental production rates were changes in growth rates, as elemental quotas for POC, PIC, PON and POP did not change significantly with pH. From a biogeochemical perspective, alterations in carbon export rates are pivotal in the carbon cycle, and this thesis elucidates species-specific differences in PIC and POC production rates and their responses to increasing $CO_2$ levels. While these findings generally align with previous research, it is essential to acknowledge species-specific and strain-specific differences. For example, while the *G. huxleyi* strain PLY 837 used in chapter 3 exhibited continually decreasing PIC:POC ratios with increasing $CO_2$, in line with its decreasing growth rates, the same may not hold true for the other strain RCC 1731 used in chapter 2. Previous studies by Langer et al. (2009) and Rickaby et al. (2016) demonstrated how different strains of *G. huxleyi* exhibited diverse responses to changing pH and $CO_2$ levels.

*C. carterae* exhibited unique responses across all three chapters of this thesis. Stable isotopes of *C. carterae* in Chapter 1 indicated a high degree of isotopic equilibration within the internal carbon pool. In Chapter 3, *C. carterae* displayed notable fluctuations in cell sizes, driving changes in elemental quotas and, consequently, C:P and N:P ratios. Furthermore, the strong correlation in elemental stoichiometry with cell sizes challenges the growth rate hypothesis (Elser et al., 2003), where elemental ratios, especially POP, are suggested to be proportional to growth rates. This is because higher growth rates go hand in hand with the amount of RNA. PIC:POC ratios remained largely unchanged with increasing $CO_2$ in *C. carterae*. Moreover, growth rates exhibited minimal variations over a wide pH

range, with reduced rates observed only under the lowest pH conditions. These observations support the hypothesis proposed in the Chapter 1, suggesting that the internal chemical buffering capacity of *C. carterae*, allowing for equilibrated oxygen isotopes and minimal changes in cellular proteome, may be attributed to its habitat characteristics. Specifically, its coastal habitat, subject to diverse environmental conditions, likely drove genetic adaptations enabling it to cope with environmental changes more effectively.

**Concluding remarks**

The findings of this thesis provide valuable insights into the varying sensitivity of coccolithophore species to changes in seawater pH. *G. huxleyi* demonstrates remarkable adaptability to a wide range of environmental pH conditions, owing to its physiological plasticity and genetic diversity. Despite fluctuations in cellular processes, as evidenced through proteomic changes, *G. huxleyi* maintained stable N and P stoichiometry. Moreover, the susceptibility to external pH changes in this species was evident through the large kinetic isotope effects in its coccolith calcite, and through changes in intracellular pH. The effect of these changes was also evident through its consistently declining PIC:POC ratios. However, despite these changes, *G. huxleyi* showed marginal changes in its elemental stoichiometry, suggesting the likelihood of its dominance and consistent biogeochemical contributions in the future oceans.

In contrast, *C. braarudii* exhibited high sensitivity to pH changes, leading to significant alterations in cellular processes, growth rates, coccolith morphology and elemental stoichiometry. Stable isotopes suggested long carbon residence times, but proteomic analysis showed the detrimental effect of pH on the cellular homeostasis of *C. braarudii*. Changes in ambient pH clearly resulted in altered membrane potential, causing the upregulation of various ion transporters.

Changes in membrane potential of the mitochondria and chloroplasts also resulted in overproduction of ROS, which caused downstream effects on a host of cellular processes. These processes potentially led to changes in elemental stoichiometry, however, these were mostly correlated with growth rates and cell size. On the other hand, *C. carterae* displayed the highest resilience among the studied species, likely attributed to its coastal habitat characteristics.

These findings have significant implications for global biogeochemical processes. Species such as *C. braarudii*, which are large and heavily calcifying, may face marginalisation under lower pH conditions, potentially restricting their ecological niche. In contrast, the physiological plasticity and genetic diversity of *G. huxleyi* may enable it to adapt to future ocean scenarios. Despite potential biogeographical changes, the pre-existing high resilience of *C. carterae* suggests its ecological niche is unlikely to contract. However, adjustments in habitat preferences may still occur as *C. carterae*, like any species, would inhabit conditions closer to its optimum. Overall, these findings emphasise the importance of understanding species-specific responses to environmental changes, particularly in the context of ocean acidification, for predicting the future dynamics of marine ecosystems.

**Future directions**

While the internal carbon pool measurements and intracellular pH experiments faced setbacks, this thesis underscores the critical importance of understanding the carbonate chemistry conditions within the coccolith vesicle for comprehending biocalcification in coccolithophores. Although isotopic evidence from chapter one allows for indirect analyses of the conditions inside the coccolith vesicle, there is room for further exploration. Understanding isotopic fractionation in coccolith calcite and organic matter as a function of light:dark

cycles, which dictate the onset and cessation of calcification and cellular growth may have profound impacts on our understanding of the regulation of carbon within a coccolithophore cell. Furthermore, for a complete understanding of intracellular carbonate chemistry conditions within coccolithophores, much work is needed to understand the processes that dictate calcium import into the cell, how this sis managed to avoid cell toxicity, and measuring the magnitude of calcium flux into the cell before, during and after calcification (dawn, G1 phase and dusk) will be highly important to further our understanding of carbonate chemistry dynamics within the cell.

Moreover, utilising knowledge of internal biological and chemical processes is essential for predicting physiological and, consequently, biogeochemical changes, which can be validated through empirical evidence. Understanding species succession in response to climate and ecological changes require further work. As chapter 3 elucidated, strain-specific responses are not only evident in *G. huxleyi*, but also in other species such as *C. braarudii*. These findings highlight the possibility of an expansion of biogeographical niches of those strains that are pre-adapted to higher $CO_2$ lower pH waters, such as those found in upwelling areas. These changes will come into effect, on top of species-specific tolerances to environmental changes. Chapter 2 demonstrated the differences in sensitivities of three coccolithophore species to changing pH. Such differences are likely to exacerbate the shrinking diversity that may plague future oceans, as more resilient species may outcompete less resilient species, even in their own ecological niche. This knowledge could inform the development of numerical cell models to elucidate the dynamics of various intracellular processes in coccolithophores. Additionally, these models could address longstanding inquiries regarding the applicability of stable isotopes for paleoclimatic purposes, understanding the biochemical mechanisms underlying changes in alkenones and elemental

stoichiometry, and pinpointing the processes involved in coccolith calcification. The inferences drawn in this thesis regarding changes in CAP chemistry and activity due to external carbonate chemistry require validation.

# Supplementary Information: Chapter 1

## Introduction

The supplementary material includes detailed methodology, results, eight figures (S1(a-f), S2, S3) and three tables. The methodology contains details about seawater preparation, dilute batch culturing, measurement of growth rate, use of Dickson standards for the measurement of carbonate chemistry parameters, and coccolith calcite cleaning for stable isotope analysis. The results and Fig. S1(a-f) explain and display the data obtained in this study with previously published studies for $\Delta^{13}C_{Coccolith,}$ $\Delta^{18}O_{Coccolith}$ and $\Delta^{13}C_{Org.}$ Fig. S2 displays the change in coccosphere diameter with changing $CO_2$/pH and Fig. S3 displays individual data points for growth rates used in this study. Fig. S4 shows individual data points for $\Delta^{13}C_{Coccolith}$ , $\Delta^{18}O_{Coccolith}$, and $\Delta^{13}C_{ORG}$ values used in this study (Fig. 2, main text). Fig. S5 shows $\delta^{13}C_{ORG}$ - $\delta^{13}C_{DIC}$ vs $\mu \times V/CO_2 \times SA$. Fig. S6 displays the Scanning Electron Micrographs for the five species studied here with changing $CO_2$/pH. Table S1 contains the $\mu_{opt}$, PIC, POC, coccosphere diameter and surface area to volume ratio under pre-industrial conditions obtained from published literature. Table S2 contains $\delta^{13}C$ and $\delta^{18}O$ for inorganic calcite used for quantifying vital effects in coccolith calcite compared to the inorganic calcite values. Table S3 contains gradients for $\Delta^{13}C_{Coccolith}$ vs. $\Delta^{18}O_{Coccolith}$ and $\Delta^{13}C_{ORG}$ vs. $\Delta^{13}C_{Coccolith}$ that are used in the discussion.

## Methods:

**Seawater:** TRIS buffer, and ammonium chloride were omitted from the major nutrient stock. Cu was omitted from the trace metal stock to avoid toxicity as the reagent-grade chemicals that were used to prepare the SOW contained trace amounts of Cu. Additionally, $6.25 \times 10^{-9}$ M Ni and $1 \times 10^{-8}$ M Se were added and $1/10^{th}$ of the original EDTA concentration was used.

**Dilute batch cultures:** Initial cell densities for the main experiment being approximately 400 cells $mL^{-1}$ for *C. braarudii*, 120 cells $mL^{-1}$ for *C. leptoporus*, 80 cells $mL^{-1}$ for *G. oceanica*, 120 cells $mL^{-1}$ for *C. carterae*, and 65 cells $mL^{-1}$ for *G. huxleyi.* The cell densities at the time of harvest did not exceed ~5000 cells $mL^{-1}$ for *C. braarudii*, 6000 cells $mL^{-1}$ for *C. leptoporus*, 20,000 cells $mL^{-1}$ for *G. oceanica*, 10,000 cells $mL^{-1}$ for *C. carterae*, and 50,000 cells $mL^{-1}$ for *G. huxleyi.* These cell densities were adopted based on recommendations by previous literature to avoid

substrate limitation (e.g., major nutrients), and to constrain a drift in the DIC concentration to not more than 5% (Langer *et al.*, 2006; LaRoche *et al.*, 2010; Rickaby *et al.*, 2010; Paleoceanography & 2015, 2015).

**Growth rate:** The standard practice for measuring specific growth rate in coccolithophores is through cell counts at two points during exponential growth (e.g., Dedman et al., 2023; Langer et al., 2006). However, in the case of *C. leptoporus,* we encountered severe cell clumping in the experiments conducted at high [$CO_2$] (>30 μmol $kg^{-1}$), which made accurate cell counts challenging. Furthermore, due to the dilute nature of our experiments, the coulter counter produced large errors in cell counts at dilute cell concentrations.

Therefore, we used *in vivo* log change in chlorophyll fluorescence per unit time to measure growth (See Chapter 18, Andersen, 2005). Previously, absorbance at specific wavelengths (750 nm), referred to as "optical density" or "turbidity," has been used to measure growth in bacterial and algal cultures (Toennies & Gallant, 1949; Shuler, 1992). However, turbidity measurements can overestimate growth due to the presence of loose coccoliths. Consequently, we determined chlorophyll fluorescence to be the optimal parameter for measuring growth.

Although concerns have been raised about the reliability of fluorescence parameters for estimating growth, specifically regarding the potential for pigment concentration changes with culture age and environmental conditions (Nicholls *et al.*, 1978; Healey, 1978; Griffiths *et al.*, 2011); these factors were effectively eliminated in our study. Our experimental cultures were acclimatised for 14 or more generations, and growth measurements were performed in very dilute cultures. Therefore, the influences of nutrient limitation, environmental changes (e.g., pH), and culture age on chlorophyll fluorescence were negligible. Additionally, separate experiments demonstrated a linear relationship between chlorophyll fluorescence and cell counts in *G. huxleyi*, particularly at low cell concentrations (data not shown).

**Dickson standards:** The alkalinity measurements of the Dickson standards yielded a precision of 17.28 μmol $kg^{-1}$ and an accuracy of 16.72 μmol $kg^{-1}$ for Batch 197 (n = 13). The precision for pH was 0.03. For Batch 126, the precision for alkalinity was 14.75 μmol $kg^{-1}$, with an accuracy of 131.02 μmol $kg^{-1}$ and an average alkalinity of 2191.527 μmol $kg^{-1}$ (n = 30). The precision for pH was 0.04. It should be noted that the deviation from the absolute value of the Dickson standard Batch

126 (TA = 2322.55 ± 0.38 μmol $kg^{-1}$) may be due to its bottling over 10 years ago. Its use was necessitated by supply-chain issues caused by COVID-19. However, the precision of the standard is high, enabling relative comparisons to be made between species and experiments.

**Calcite cleaning for isotopic analysis:** the harvested cell pellet was centrifuged, resuspended in a solution of 4.5% NaOCl and 0.625 % v/v Triton X-100 buffered with 0.03 M $NaHCO_3$ (same reagent as the one used for DIC in the seawater, therefore, same isotopic composition as that of DIC) for 30 minutes to remove the organic matter. After this, the sample was centrifuged and washed three times to remove any traces of NaOCl and/or organic matter and oven dried at 40˚C.

**Data Availability:** All data are available through Zenodo at:

https://zenodo.org/doi/10.5281/zenodo.8265649

**Results:**

The $\Delta^{13}C_{Coccolith}$ and $\Delta^{18}O_{Coccolith}$ values for all species at pre-industrial conditions (i.e., [$CO_2$] between 10–20 μmol $kg^{-1}$) aligned with the findings of Ziveri et al. (2003), where $\Delta^{18}O_{Coccolith}$ became more depleted for species having progressively larger cell sizes. Moreover, in agreement with Ziveri et al. (2003), $\Delta^{18}O_{Coccolith}$ for species *C. carterae,* and *C. leptoporus* were lighter than that of inorganic calcite ($\Delta^{18}O_{Inorganic\ calcite}$, calcite in equilibrium with $H_2O$ and DIC), whereas $\Delta^{18}O_{Coccolith}$ for smaller sized species (*G. huxleyi* and *G. oceanica*) were heavier than $\Delta^{18}O_{Inorganic\ calcite}$. *C. braarudii* exhibited near-inorganic $\Delta^{18}O_{Coccolith}$ values. These observations agree with all previous findings (Dudley *et al.*, 1986; Ziveri *et al.*, 2003, 2012; Rickaby *et al.*, 2010; Hermoso *et al.*, 2014, 2015, 2016b,a; Hermoso, 2015; McClelland *et al.*, 2017). The isotopic compositions also agreed with the observations of McClelland et al. (2017), where vital effects at pre-industrial conditions became more depleted as the PIC:POC ratio increased between species. However, an exception to both McClelland's and Ziveri's observations was *C. carterae*, which exhibited more depleted $\Delta^{18}O_{Coccolith}$ than *C. braarudii* and *C. leptoporus* under pre-industrial conditions despite having a smaller coccosphere size. Additionally, *C. carterae* showed depleted isotopic composition despite having the smallest PIC:POC ratio.

When comparing the results of the study with previously published work, a high degree of agreement in the general trend was observed for *C. braarudii* and

*C. leptoporus* in $\Delta^{13}C_{Coccolith}$ and $\Delta^{18}O_{Coccolith}$ values (Fig. S1, Supplementary Material; Rickaby et al. 2010; Ziveri et al. 2012; Hermoso 2015; Hermoso et al. 2016).

The data for *G. huxleyi* and *G. oceanica* were generally consistent at $CO_2$ below 20 µmol $kg^{-1}$ with (Rost *et al.*, 2002; Rickaby *et al.*, 2010; Hermoso *et al.*, 2016a; McClelland *et al.*, 2017). However, differences in $\Delta^{13}C_{Coccolith}$ and $\Delta^{18}O_{Coccolith}$ trends were observed, especially above $CO_2$ of 20 µmol $kg^{-1}$ for *G. huxleyi* and *G. oceanica*. The magnitude of change in isotopic values with changing $CO_2$ reported in this study is significantly higher than most previous studies. Moreover, $\Delta^{13}C_{Coccolith}$ for *G. oceanica* did not change with increasing $CO_2$ for Rickaby et al. (2010).

## Tables

Table S1: $\mu_{opt}$, PIC, POC and Coccosphere diameter under pre-industrial conditions.

| Species | $\mu_{opt}$ [a] | PIC: POC [b] | PIC (pg C $cell^{-1}$) [c] | POC (pg C $cell^{-1}$) [a,d] | Coccosphere diameter (µm ) [a,e] | Surface Area to Volume Ratio [a,f] |
|---|---|---|---|---|---|---|
| *C. carterae* | 13.5 | 0.17 | 21.5 | 202±17.8 | 11.98±1.63 | 0.5±0.28 |
| *G. huxleyi* | - | 0.5 | 7.2 | 35.6±2.4 | 6.13±0.32 | 0.98±0.19 |
| *G. oceanica* | 3.5 | 1.10 | 24.5 | 85.2±1.5 | 8.53±0.6 | 0.70±0.19 |
| *C. braarudii* | 21.05 | 1.2 | 347 | 445±13.2 | 21.03±1.9 | 0.29±0.1 |
| *C. leptoporus* | 16.3 | 2.2 | 157.6 [*] | 372±5.7 | 13.42±1.3 | 0.45±0.17 |

[a]This study.
[b]Taken from McClelland et al. (2017).
[c]Taken from Gafar et al. (2019b).
[d]Note that the POC values reported here are relative only. These are not absolute values.
[e]Please note that coccosphere diameter was used for volume and surface area estimation in this study as we were not able to obtain true cell sizes (i.e., naked cells) through the coulter counter. This is because upon acidification of the sample, the coulter counter produced large errors in the cell count and cell volume (possibly due to increased decalcified coccolith debris, and possible cell shrinkage upon acidification).
[*]Large discrepancy in published values.
[f]SA:V ratios have been calculated using coccosphere diameter as a proxy for cell size.

**Table S2**: $\delta^{13}C$ and $\delta^{18}O$ for inorganic calcite.

| $CO_2$ (µmol $KgSW^{-1}$) | $CO_3^{2-}$ (µmol $KgSW^{-1}$) | pH | $\delta^{13}C_{INORG}$ (‰ VPDB)[b] | $\delta^{18}O_{SOW}$ (‰ SMOW)[c] | $\delta^{18O}_{INORG}$ (‰ VPDB)[d] | $\delta^{18O}_{Equilibrium\ Calcite}$ (‰ VPDB)[d] | $\delta^{18O}_{INORG\ (pH)}$ (‰ VPDB)[d,e] |
|---|---|---|---|---|---|---|---|
| 52.98 | 47.16 | 7.6 | 1 | 0 | -0.72 | 0.995 | -0.55 |
| 42.06 | 59.33 | 7.7 | 1 | 0 | -0.72 | 0.995 | -0.58 |
| 33.3 | 74.45 | 7.8 | 1 | 0 | -0.72 | 0.995 | -0.62 |
| 26.29 | 93.15 | 7.9 | 1 | 0 | -0.72 | 0.995 | -0.66 |
| 16.23 | 144.45 | 8.1 | 1 | 0 | -0.72 | 0.995 | -0.78 |
| 12.68 | 178.85 | 8.2 | 1 | 0 | -0.72 | 0.995 | -0.87 |
| 9.86 | 220.42 | 8.3 | 1 | 0 | -0.72 | 0.995 | -0.97 |
| 7.62 | 270.18 | 8.4 | 1 | 0 | -0.72 | 0.995 | -1.09 |
| 5.86 | 329.06 | 8.5 | 1 | 0 | -0.72 | 0.995 | -1.23 |
| 4.47 | 397.82 | 8.6 | 1 | 0 | -0.72 | 0.995 | -1.39 |
| 3.38 | 476.87 | 8.7 | 1 | 0 | -0.72 | 0.995 | -1.58 |
| 2.53 | 566.13 | 8.8 | 1 | 0 | -0.72 | 0.995 | -1.80 |
| 1.87 | 664.92 | 8.9 | 1 | 0 | -0.72 | 0.995 | -2.03 |
| 1.37 | 771.84 | 9 | 1 | 0 | -0.72 | 0.995 | -2.29 |

[a]This study.
[b]Calculated according to Romanek et al. (1992).
[c]$\delta^{18}O_{SOW}$ (‰ SMOW) is taken as 0 ‰ as all isotopic values are corrected for changes in $\delta^{18}O$.
[d]Calculated according to Kim & O'Neil (1997).
[e]Calculated according to Zeebe (1999).

**Table S3:** Gradients for $\Delta^{13}C_{Coccolith}$ vs. $\Delta^{18}O_{Coccolith}$ and $\Delta^{13}C_{ORG}$ vs. $\Delta^{13}C_{Coccolith}$ values as calculated using the formulas provided in the discussion:

| Species | $\Delta^{13}C_{Coccolith}$ vs. $\Delta^{18}O_{Coccolith}$ | $\Delta^{13}C_{ORG}$ vs. $\Delta^{13}C_{Coccolith}$ |
|---|---|---|
| *C. carterae* | 5.63 | 1.02 |
| *G. huxleyi* | 2.66 | 0.51 |
| *C. leptoporus* | 5.42 | 1.15 |
| *G. oceanica* | 2.82 | 0.41 |
| *C. braarudii* | 4.04 | 0.65 |

## Figures

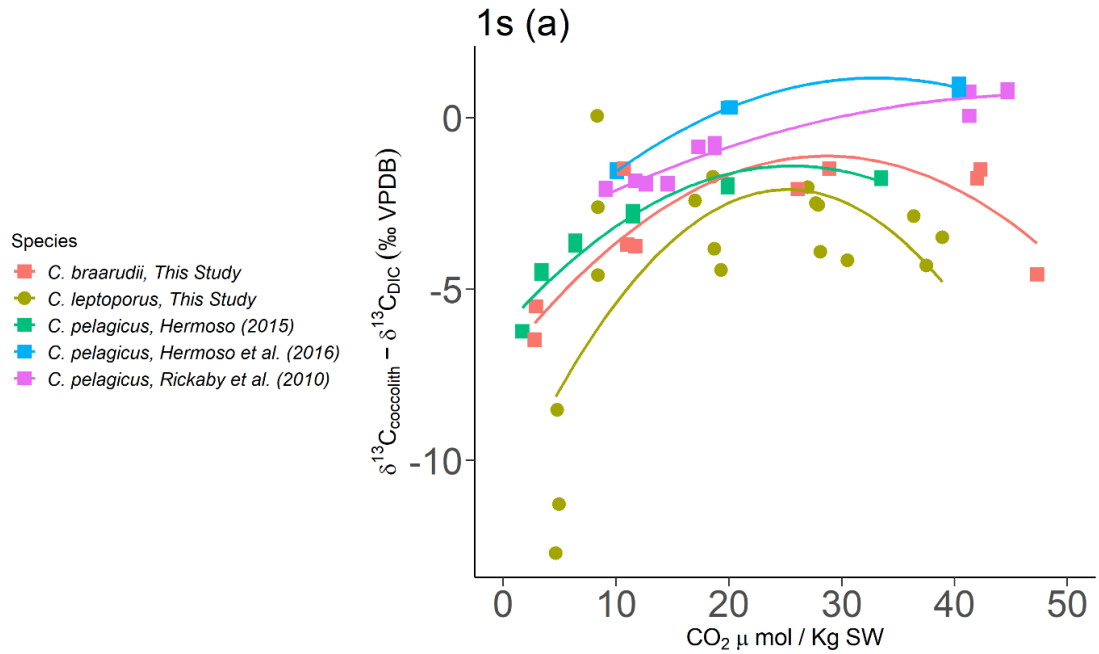
1s (a)
Species
C. braarudii, This Study
C. leptoporus, This Study
C. pelagicus, Hermoso (2015)
C. pelagicus, Hermoso et al. (2016)
C. pelagicus, Rickaby et al. (2010)
δ13Ccoccolith – δ13CDIC (‰ VPDB)
0
-5
-10
0
10
20
30
40
50
CO2 µ mol / Kg SW

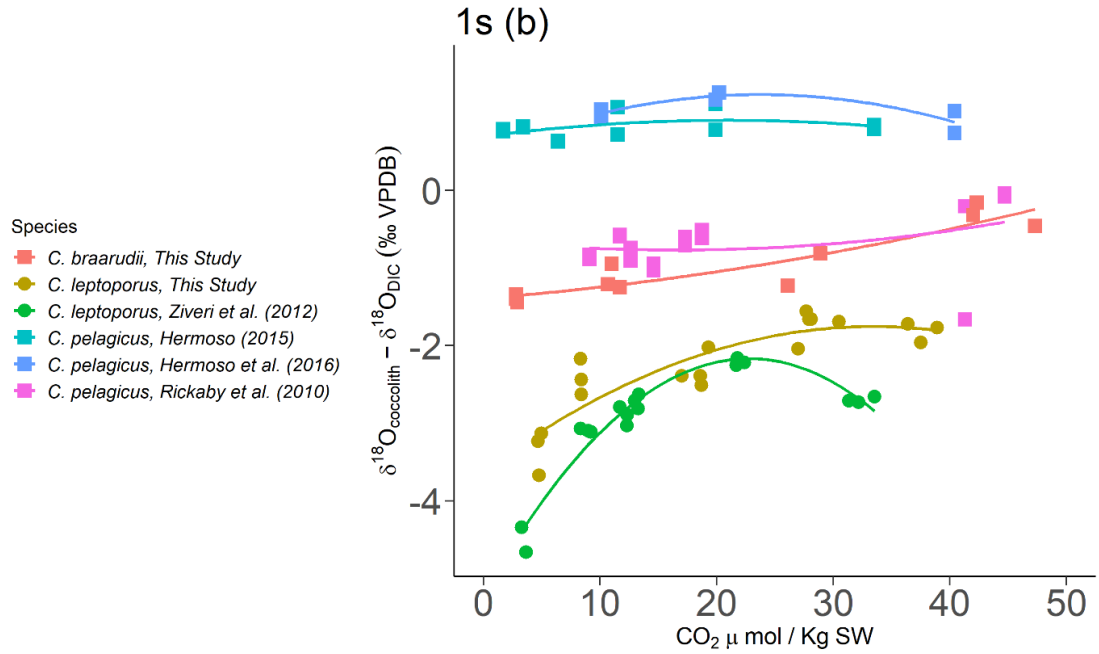
1s (b)
Species
C. braarudii, This Study
C. leptoporus, This Study
C. leptoporus, Ziveri et al. (2012)
C. pelagicus, Hermoso (2015)
C. pelagicus, Hermoso et al. (2016)
C. pelagicus, Rickaby et al. (2010)
δ18Ococcolith – δ18ODIC (‰ VPDB)
0
-2
-4
0
10
20
30
40
50
CO2 µ mol / Kg SW

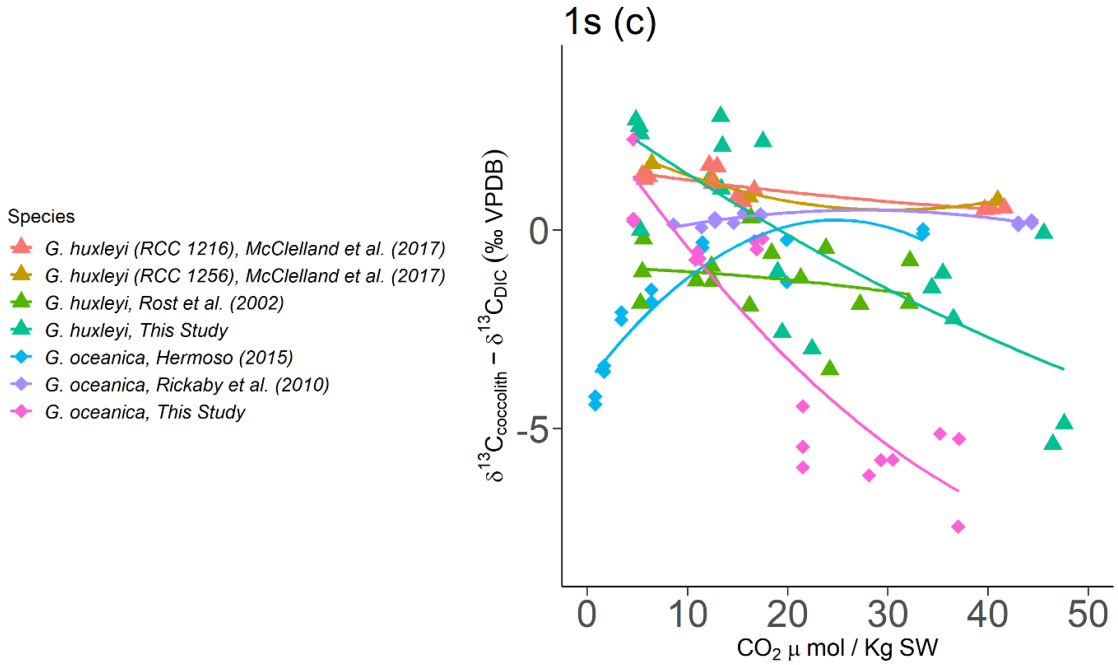
1s (c)
Species
G. huxleyi (RCC 1216), McClelland et al. (2017)
G. huxleyi (RCC 1256), McClelland et al. (2017)
G. huxleyi, Rost et al. (2002)
G. huxleyi, This Study
G. oceanica, Hermoso (2015)
G. oceanica, Rickaby et al. (2010)
G. oceanica, This Study
δ13Ccoccolith − δ13CDIC (‰ VPDB)
0
-5
0
10
20
30
40
50
CO2 μ mol / Kg SW

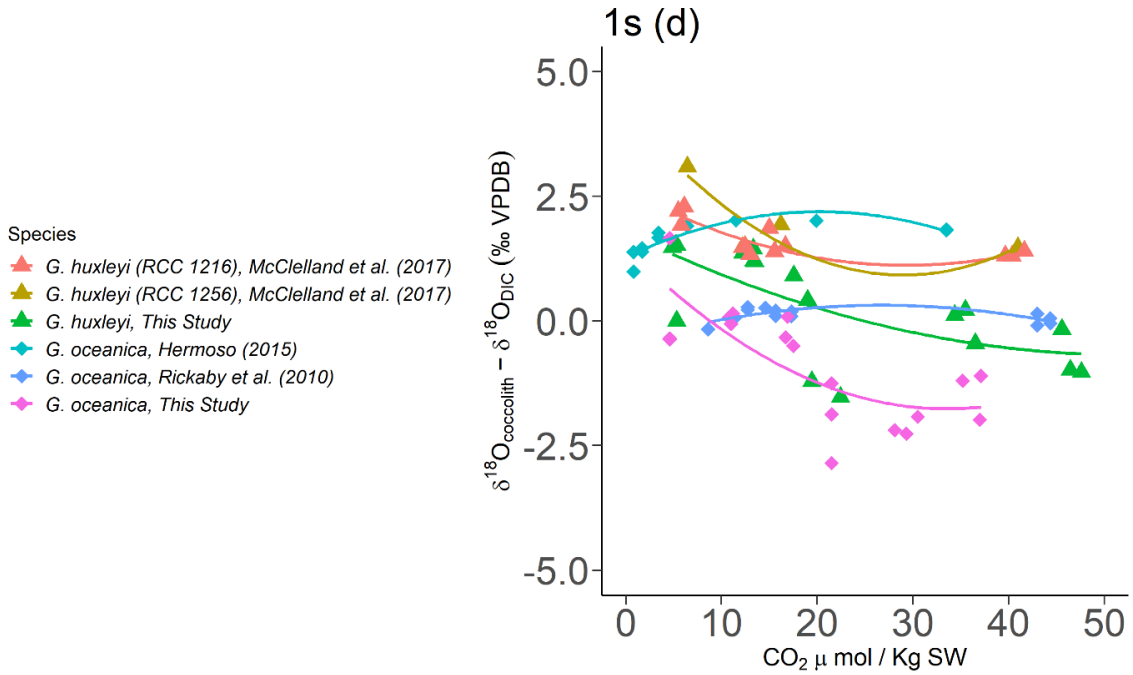
1s (d)
Species
G. huxleyi (RCC 1216), McClelland et al. (2017)
G. huxleyi (RCC 1256), McClelland et al. (2017)
G. huxleyi, This Study
G. oceanica, Hermoso (2015)
G. oceanica, Rickaby et al. (2010)
G. oceanica, This Study
δ18Ococcolith − δ18ODIC (‰ VPDB)
5.0
2.5
0.0
-2.5
-5.0
0
10
20
30
40
50
CO2 μ mol / Kg SW

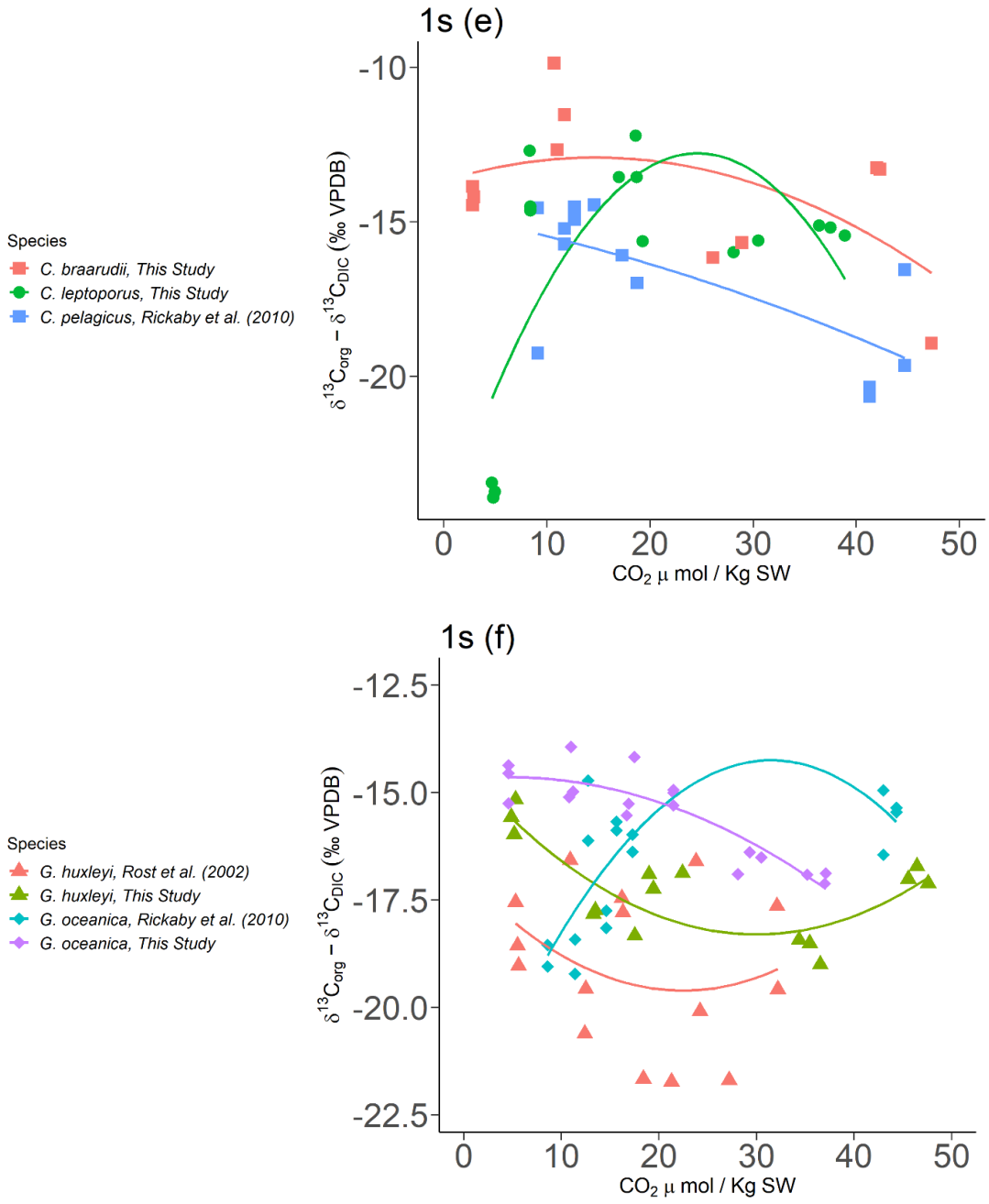


***Figure S1:*** Comparing stable isotopes for *C. braarudii, C. leptoporus, C. carterae, G. huxleyi, and G. oceanica* with data from previously published studies: *(Rost* et al., *2002; Rickaby* et al., *2010; Ziveri* et al., *2012; Hermoso, 2015; Hermoso* et al., *2016a; McClelland* et al., *2017)*

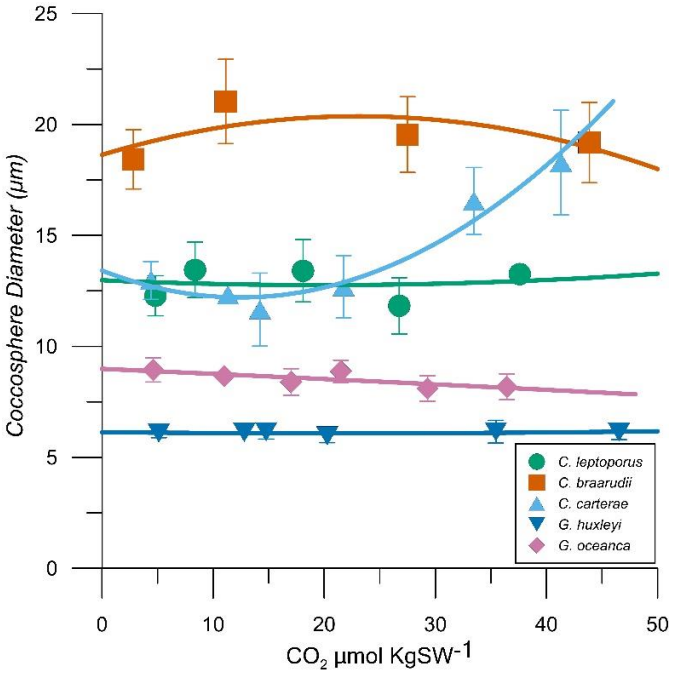


***Figure S2:*** *Coccosphere diameter (µm) for C. braarudii (■), C. leptoporus (●), C. carterae (▲), G. huxleyi (▼), and G. oceanica (◆).*

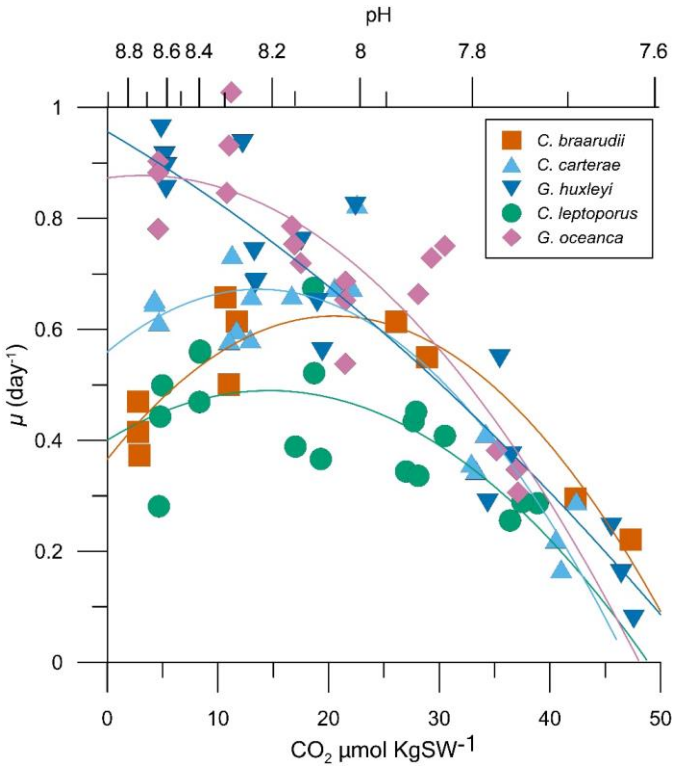


**Figure S3:** Growth rates (day$^{-1}$) for *C. braarudii (■), C. leptoporus (●), C. carterae (▲), G. huxleyi (▼),* and *G. oceanica* (◆). Datapoints obtained from all biological replicates have been plotted. The curved lines represent 2$^{nd}$–degree polynomial fits.

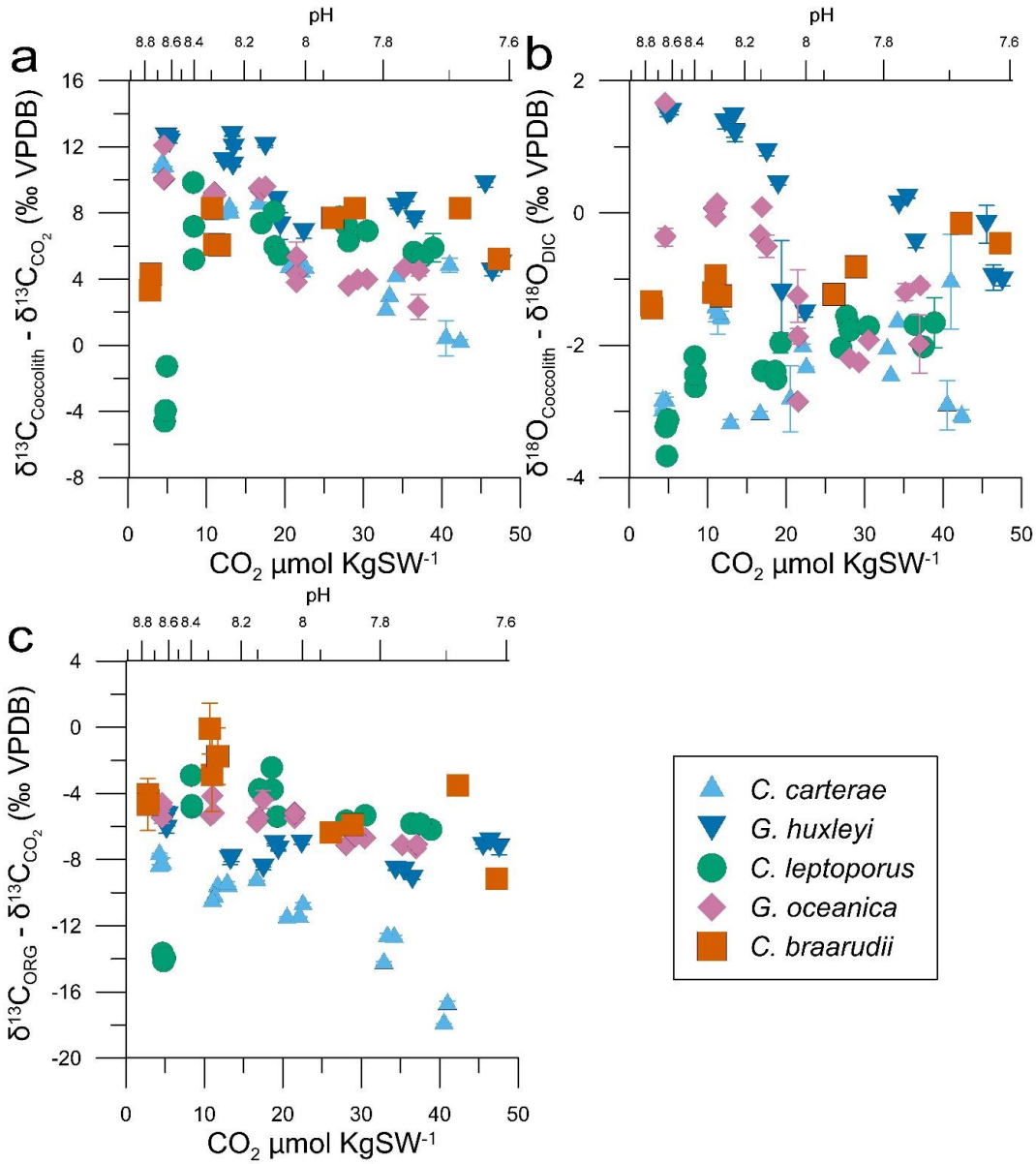


**Figure S4:** (a) $\Delta^{13}C_{Coccolith}$, (b) $\Delta^{18}O_{Coccolith}$, (c) $\Delta^{13}C_{ORG}$ values for *C. braarudii* (■), *C. leptoporus* (●), *C. carterae* (▲), *G. huxleyi* (▼), and *G. oceanica* (◆). Note the change in y-axes. Each data point signifies one biological replicate, each with at least 3 replicate measurements. Error bars represent one standard deviation.

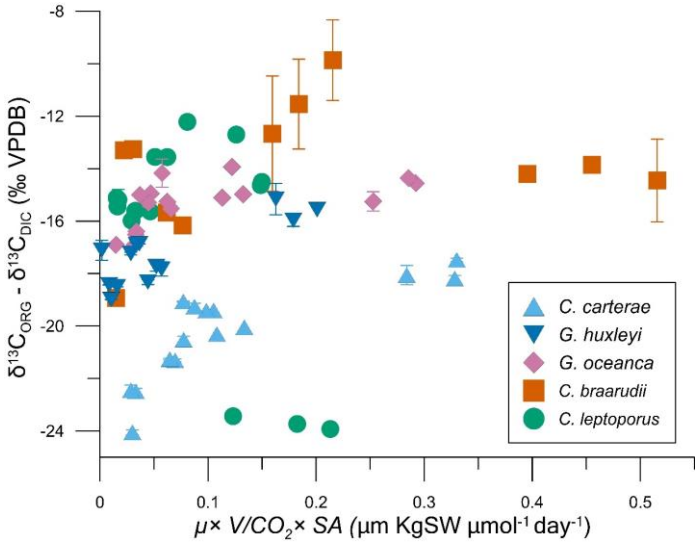


**Figure S5:** $\delta^{13}C_{ORG}$ - $\delta^{13}C_{DIC}$ *vs* μ×V/$CO_2$×SA *for* C. braarudii *(■),* C. leptoporus *(●),* C. carterae *(▲),* G. huxleyi *(▼),* and G. oceanica *(◆).* Each data point signifies *one* biological replicate, each *with at least* 3 replicate measurements. Error bars represent one standard deviation.

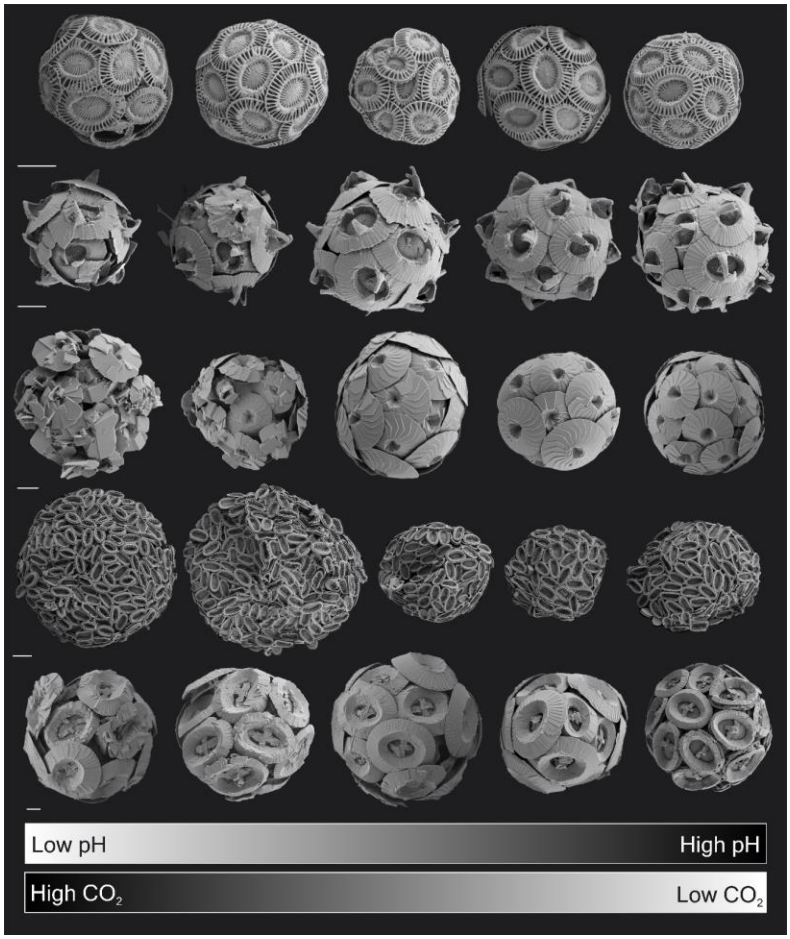


***Figure S6:*** *Scanning Electron Micrographs of G. huxleyi, G. oceanica, C. leptoporus, C. carterae, and C. braarudii (top to bottom), with decreasing $CO_2$ and increasing pH (left to right). Horizontal bars on the bottom left of each species represent scale bars equivalent to 2 μm.*

# Supplementary Information: Chapter 2

## Introduction:

This supplementary section provides detailed information on the methodology used for measurement of Net photosynthesis and Dark respiration rates, in-solution protein digestion of samples for proteomic analysis. Furthermore, detailed description of the results obtained in this study has been provided separate to the main text to maintain clarity.

## Methodology:

### Measurement of Dark Respiration and Net Photosynthesis (Barton et al., 2019)

Measurement of dark respiration and gross photosynthetic rates were taken on a minimum of 3 biological replicates per species for each treatment. A Clark-type oxygen electrode was used as part of a Hansatech Oxytrace+ system (Hansatech Ltd, King's Lynn, UK) to measure net oxygen evolution rate in the light (net photosynthesis) and oxygen consumption in the dark (dark respiration). Measurements were made at 17˚C with a light intensity of 80 $\mu$mol $m^{-2}$ $s^{-1}$ to simulate regular growth conditions. To obtain a good signal to noise ratio, cultures were concentrated by gentle centrifugation at 500g for 5 minutes at 17˚C and transferred into fresh media (of the respective pH treatments) and cultures were acclimated in the dark at 17˚C for 15 minutes prior to the measurements based on previous recommendations (Barton et al 2020). Stock cultures from early exponential phase were used to ensure minimal deviation from the target carbonate chemistry conditions and to avoid substrate limitation. The drift in the oxygen signal caused by oxygen consumption by the electrode was corrected for by subtracting the blank rate measured on sterile media after every 3 runs under the same conditions (temperature, pH, duration). The final unit for net photosynthesis and dark respiration were mol $O_2$ $cell^{-1}$ $hr^{-1}$.

### In-solution protein digestion (adapted from Dedman et al., 2023)

Cultures were harvested during early exponential phase to avoid significant deviations from the targeted carbonate chemistry conditions and to avoid nutrient limitations. Cells were harvested by centrifugation at 4000g for 15 minutes at 4˚C and the supernatant was discarded. Pellets were flash frozen and stored at -80˚C

until further processing. To extract proteins for shotgun proteomic analysis, pellets were thawed at room temperature and resuspended in 1mL of 20mM Tris HCl (pH 7.5) and lysed by alternating between sonication on ice (30 seconds) and vortexing (2000 rpm, 15 seconds) 5-6 times. The concentrations of proteins within the lysate were measured on a NanoDrop before being stored at -80˚C until further processing. In-solution trypsin digestion was carried out according to (Dedman et al., 2022). In brief, proteins were denatured in a 4 M urea and 100 mM ammonium bicarbonate solution at room temperature with shaking at 650 rpm for 10 minutes. Subsequently, cysteines were reduced with 10 mM tris(2-carboxyethyl)phosphine (TCEP) for 30 minutes at room temperature and then alkylated with 50 mM iodoacetamide in the dark for an additional 30 minutes. Proteins were pre-digested using LysC at a ratio of 1 µg per 100 µg protein, incubated for 2 hours at 37˚C with shaking at 800 rpm. Urea concentrations were then reduced to 2 M, and 2 mM $CaCl_2$ was added. Trypsin was added at a ratio of 2.5 µg per 100 µg of protein. The trypsin reaction occurred for 20 hours at 37˚C with shaking at 800 rpm and the reaction was halted by adding 5% formic acid. Following this, the samples were desalted using a C18 column, dried overnight with a speed-vacuum, and stored at -20˚C until analysis.

**Results:**

**Table S1:** Absolute Growth rates, net photosynthetic rates, and dark respiration rates. Note that the NP rates and DR rates are absolute values that have not been divided by cell volume.

| Species | pH | Growth Rate ($day^{-1}$) | Dark Respiration Rate (fmol $O_2$ $cell^{-1}$ $hour^{-1}$) | Net Photosynthesis Rate (fmol $O_2$ $cell^{-1}$ $hour^{-1}$) | Photosynthesis to Respiration Ratio |
|---|---|---|---|---|---|
| *C. carterae* | 7.6 | 0.546±0.040 | 195.08±41.69 | 696.92±49.20 | 3.57±0.80 |
| *C. carterae* | 8.2 | 0.585±0.020 | 254.44±39.37 | 629.48±6.64 | 2.47±0.38 |
| *C. carterae* | 8.8 | 0.585±0.035 | 192.05±40.79 | 514.65±83.61 | 2.68±0.72 |
| *C. braarudii* | 7.6 | 0.408±0.058 | 369.89±35.37 | 996.66±102.87 | 2.69±0.38 |
| *C. braarudii* | 8.2 | 0.732±0.045 | 430.52±29.02 | 978.76±53.40 | 2.27±0.20 |
| *C. braarudii* | 8.8 | 0.487±0.000 | 61.52±10.16 | 700.36±44.52 | 11.38±2.01 |
| *G. huxleyi* | 7.6 | 0.679±0.018 | 14.22±3.15 | 51.68±4.21 | 3.63±0.86 |
| *G. huxleyi* | 8.2 | 0.632±0.048 | 18.64±5.98 | 38.57±2.41 | 2.07±0.68 |
| *G. huxleyi* | 8.8 | 0.527±0.039 | 14.43±1.75 | 18.90±5.16 | 1.31±0.39 |

**Cellular Stress Response.**

Glutathione synthase exhibited a 1.04 LFC in *C. braarudii* at pH 7.6 and a 1.14 LFC at pH 8.8. In *G. huxleyi*, Glutathione S-transferase displayed a 1.01 LFC

upregulation at pH 8.8, directly involved in detoxifying ROS within the cytosol (Nebert & Vasiliou, 2004). Additionally, enzymes of the ascorbate-glutathione cycle, such as ascorbate peroxidase showed significant upregulation at pH 8.8 in *G. huxleyi,* and at both pH 7.6 and pH 8.8 in *C. braarudii*. *G. huxleyi* exhibited an upregulation in thioredoxin (0.74 LFC) and downregulation in 6 thioredoxin-domain containing proteins (-1.43 – -0.56 LFC) at pH 8.8. *C. braarudii* exhibited upregulation of 6 thioredoxins (0.58 – 1.95 LFC) at pH 7.6 and upregulation of 9 thioredoxins (0.71 – 3.23 LFC) at pH 8.8. Moreover, peroxidase proteins were significantly upregulated at pH 8.8, with up to a 1.79 LFC in *C. braarudii* and a 1.22 LFC increase in *G. huxleyi*.

**Oxidative stress impeded DNA synthesis and hampered cell cycle progression.**

*G. huxleyi* exhibited downregulation of a SMC (Structural Maintenance of Chromosomes) hinge domain-containing protein (-3.88 LFC at pH 8.8) while in *C. braarudii,* it was upregulated (1.24 LFC at pH 7.6). These proteins ensure proper segregation of chromosomes under cell division (Cobbe & Heck, 2000). *G. huxleyi* also exhibited a downregulation of exportin 1 (-2.56 – -0.92 LFC) and importin (-0.74 LFC) at pH 8.8. Importin is a nuclear localisation signal receptor that regulates nucleocytoplasmic transport and accumulates in the nucleus under oxidative stress (Ray *et al.*, 2012). Both *C. braarudii* and *G. huxleyi* exhibited downregulation in RuvB like helicases and CTP synthase at pH 8.8. Specifically, CTP synthase was downregulated by -7.8 LFC for *G. huxleyi* and two instances of -0.79 LFC in *C. braarudii*. This protein is related to pyrimidine nucleotide biosynthesis and participates in establishing genome integrity (Daumann *et al.*, 2018). Protein arginine N-methyltransferase was downregulated by -2.09 LFC at pH 7.6 and -1.21 LFC at pH 8.8 in *C. braarudii*, and by -1.23 LFC in *G. huxleyi* at pH 8.8. A downregulation in arginine N-methyltransferases can directly impact the G1/S cell cycle progression (Amici *et al.*, 2021).

**Ribosomal activity and protein processing were significantly impacted by pH-induced oxidative stress.**

RNA has a high susceptibility to chemical damage from ROS (Yan & Zaher, 2019). Moreover, proteins are severely inhibited by changes in pH since their ionisation state changes with pH (Whitten *et al.*, 2005). Minor changes in RNA can seriously impact normal cellular function (Wurtmann & Wolin, 2009). A considerable proportion of protein groups that showed significant changes under pH stress in

the species studied here were related to RNA translation, protein degradation, molecular chaperoning activity and protein transport. For instance, at least 70 proteins related to RNA translation, methylation, acetylation, or splicing were downregulated (-4.51 – -0.48 LFC) in *G. huxleyi* at pH 8.8 with the largest changes observed for KRR1 small subunit (-4.51 LFC), Sde2 N-terminal ubiquitin domain-containing protein (-2.63 LFC), PCIF1 WW domain-containing protein (-2.35 LFC), and WD40 repeat-containing protein SMU1 (-2.27 LFC). 6 RNA helicases were also downregulated (-3.31 – -0.59 LFC). RNA damage has been considered trivial due to the rapid turnover of mRNA. However, tRNA have much longer half-lives, and therefore, damage to their function or structure can have lasting effects on the cell (Deutscher, 2006). In the present study, 9 tRNA ligases were significantly changed in *G. huxleyi* at pH 8.8. Out of these, two tRNA ligases, cysteine tRNA ligase (0.74 LFC) and methionine tRNA ligase (0.6 LFC) were upregulated, while the rest were downregulated. *C. braarudii* also exhibited downregulation of ribosomal proteins, such as SAP domain-containing protein (-0.93 LFC) at pH 7.6 and small ribosomal subunit protein eS1 (-1.52 LFC), ribosome biogenesis protein NOP53 (-1.05 LFC), and RNA helicase (-1.02 – 0.80 LFC) at pH 8.8. Over 15 RNA-binding proteins exhibited downregulation at pH 8.8, and 6 proteins at pH 7.6 in *C. braarudii*. KOW domain-containing protein was downregulated at both pH 7.6 (-1.02 LFC) and 8.8 (-1.23 LFC). RRM domain containing RNA binding protein was upregulated at pH 7.6 (0.93 LFC), and 5 RRM domain proteins were downregulated at pH 8.8 (down to -1.47 LFC). RNA Recognition Motif-containing proteins are involved in most post-transcriptional gene expression processes (SenGupta, 2013). *G. huxleyi* exhibited significant downregulation in DNA (cytosine-5) methyltransferase (-2.92 LFC) at pH 8.8. This enzyme plays a key role in gene expression, catalysing the methylation of cytosine (Adams, 1995). *C. braarudii* exhibited downregulation of a CCHC-type zinc finger nucleic acid binging protein (-1.08 LFC), transcription elongation factor S-II (-3.45 LFC), and a helicase C-terminal domain-containing protein (-3.01 LFC) at pH 8.8.

Changes to proteins caused by oxidative stress causes misfolding and improper function. Misfolded or proteins damaged by ROS often form oligomeric complexes and accumulate together as aggregates. Moreover, the cell may not be able to degrade these atypical proteins (Chondrogianni *et al.*, 2014). 11 proteins related to proteolysis were significantly changed, with 6 proteins downregulated and 5 proteins upregulated (-1.41 to 1.28 LFC) in *G. huxleyi* at pH 8.8. For instance,

proteasome alpha-type subunit was downregulated (-2.48 LFC), while proteasome activator PA28 C-terminal domain-containing protein was upregulated (1.13 LFC). Others included aminopeptidases, carboxypeptidases, oligopeptidases, and peptidases with 1, A2, M1, M14, M41, S9, S49, S53 domains. 2 Cullins were observed to be downregulated (-0.87 LFC) and 14 proteins related to protein transport (-4.01 to -0.67 LFC) and 8 protein kinases (-0.71 to -1.97 LFC) were downregulated in *G. huxleyi* at pH 8.8. DnaJ/HSP40 (-5.11 LFC) and DnaK/HSP70 (-1.49 LFC) were significantly downregulated in *G. huxleyi*. HSP 40 and HSP 70 coordinate with 26S Proteasome for protein degradation, and their concurrent downregulation suggests lower necessity for degradation of ubiquitinated proteins. Downregulation in proteasome activity has been previously suggested under oxidative stress. This is because oxidised proteins are not considered as proper substrates for degradation, and in turn, inhibit the proteasome (Chondrogianni *et al.*, 2014). *C. braarudii* also exhibited significant changes in peptidases. For instance, prolyl endopeptidase was significantly upregulated at pH 8.8 (up to 1.54 LFC), and pH 7.6 (up to 1.12 LFC). Overall, 12 proteolysis-related proteins such as peptidase S49 (1.93 LFC), and Peptidase S8/S53 (1.86 LFC) were upregulated at pH 7.6 in *C. braarudii*. Additionally, 23 proteolysis-related proteins, such as serine-type exopeptidase (3.02 LFC), and Peptidase S49 (2.14 LFC) were significantly upregulated at pH 8.8. However, this species showed the largest downregulation in Cystatin domain-containing protein (-6.04 LFC), a family of cysteine protease inhibitor at pH 8.8. Protein transport related proteins such as GPI inositol-deacylase (2.29 LFC) and small COPII coat GTPase SAR1 (1.47 LFC) were generally upregulated at pH 8.8 in *C. braarudii.*

J-domain containing proteins, which bind to HSP70 and are involved in protein folding also exhibited significant changes under pH-induced stress conditions. Four J-domain proteins were downregulated at pH 8.8 (down to -2.74 LFC) in *G. huxleyi* and exhibited changes at pH 8.8 (-1.03 – 1.59 LFC) and pH 7.6 (-1.03 – 1.69 LFC) in *C. braarudii*. Other heat shock proteins such as HSP 90, HSP90 activating protein and small HSPs were significantly downregulated in *C. braarudii* at pH 8.8. Downregulation of these proteins suggests a reduced requirement for chaperone activity under pH-induced stress conditions. Prefoldin, that is related to protein folding, exhibited significant changes. 4 prefoldin subunits (1,3,4 and 6) were downregulated (down to -1.22 LFC) at pH 8.8 in *C. braarudii*, whereas only prefoldin subunit 6 (-1.41 LFC) was downregulated at pH 8.8 in *G. huxleyi*. T-

complex proteins involved in protein folding were significantly changed in *G. huxleyi* under alkaline conditions (pH 8.8). Interestingly, Derlin, which is found on the endoplasmic reticulum membrane, and involved in degradation of misfolded proteins was highly downregulated at both pH 7.6 (-6.66 LFC) and pH 8.8 (-7.16 LFC) in *G. huxleyi*, although it was highly upregulated under those pH conditions in *C. braarudii* (4.57 LFC at pH 7.6, 4.77 LFC at pH 8.8), suggesting species-specific responses to pH stress. *C. carterae* only exhibited an insignificant change in PUB domain-containing protein, which links to ubiquitin-proteasome for protein degradation and protein-tyrosine-phosphatase.

Ubiquitous proteins that are involved in several functions were significantly changed in *G. huxleyi* and *C. braarudii*. For instance, 7 peptidyl prolyl cis-trans isomerases (up to 2.3 LFC) were upregulated in *C. braarudii* at pH 7.6 and 10 (up to 2.71 LFC) were upregulated at pH 8.8. *G. huxleyi* exhibited a downregulated in 7 PPIase (down to -1.91 LFC) and an upregulation in 12 PPIases (up to 1.28 LFC) at pH 8.8. No such changes were observed in *G. huxleyi* at pH 7.6. Calcium binding proteins such as calmodulin (-0.59 LFC) and calnexin (-1.92 LFC) were downregulated at pH 8.8 in *G. huxleyi*. In *C. braarudii*, calmodulin was significantly changed at pH 7.6 (-0.66 – 1.39 LFC) and pH 8.8 (-1.10 – 1.34 LFC). Moreover, a 0.77 LFC was observed for calreticulin at pH 8.8 in *C. braarudii*. Several EF-hand domains-containing proteins were also significantly changed in *C. braarudii*. For instance, at pH 7.6, 4 EF-hand domain containing proteins were upregulated (0.85 – 1.4 LFC), whereas at pH 8.8, 5 of these proteins were upregulated (0.58 – 2.19 LFC). Conversely, in *G. huxleyi*, out of the 6 EF-hand domain containing proteins at pH 8.8, 5 were downregulated (down to -4.9 LFC). However, 2 EF hand domain containing proteins were upregulated at pH 7.6 (up to 2.35 LFC). 14-3-3 proteins that are regulatory players in the cell cycle and regulate the activity of various enzymes, exhibited a downregulation at pH 8.8 in *G. huxleyi* (-2 LFC) and *C. braarudii* (-2.17 LFC).

Several proteins related to amino acid and nucleotide biosynthesis were also significantly changed. For instance, at pH 8.8, *G. huxleyi* exhibited an upregulation in dihydroorotase (3.04 LFC) associated with the pyrimidine nucleobase biosynthetic process. Homoserine kinase (0.67 LFC), tryptophan synthase beta chain-like PALP domain-containing protein (0.89 LFC), and formamidase (4.81 LFC) were also upregulated while others were downregulated. No such changes were observed at pH 7.6 for *G. huxleyi*. On the other hand, *C. braarudii* exhibited

significant changes in amino acid biosynthesis at both pH 7.6 and pH 8.8. The largest downregulation at pH 7.6 were observed for indole-3-glycerol-phosphate synthase (down to -4.3 LFC) related to the tryptophan biosynthetic process, while the largest upregulation was observed for Phosphoribosyl-AMP cyclohydrolase domain-containing protein (1.65 LFC) related to histidine biosynthesis, and serine hydroxymethyltransferase (1.13 LFC). At pH 8.8, *C. braarudii* exhibited changes in proteins such as 5-proFAR isomerase (-2.17 LFC), Phosphoribosyl-AMP cyclohydrolase domain-containing protein (2.08 LFC) related to histidine biosynthesis, and serine hydroxymethyltransferase (1.59 LFC). Upregulation of arginine biosynthesis was evident under stressed conditions in *C. braarudii*. L-Arginine supresses oxidative stress by promoting glutathione synthesis and therefore, minimises ROS-induced oxidative damage in the cell (Liang *et al.*, 2018). Consequently, arginine biosynthesis bifunctional protein ArgJ was upregulated at pH 7.6 (0.67 LFC) and pH 8.8 (0.62 LFC). Several ubiquitous proteins involved in signalling and general cellular activity were also significantly upregulated. For instance, 7 peptidyl prolyl cis-trans isomerases (up to 2.3 LFC) were upregulated in *C. braarudii* at pH 7.6 and 10 (up to 2.71 LFC) were upregulated at pH 8.8. *G. huxleyi* exhibited a downregulated in 7 PPIase (down to -1.91 LFC) and an upregulation in 12 PPIases (up to 1.28 LFC) at pH 8.8. Calcium binding proteins involved in cellular signalling such as calmodulin, calnexin, EF hand domain, and calreticulin also displayed significant changes.

**pH-mediated ROS production enhances fatty acid biosynthesis, while pH change promotes membrane transport.**

ROS generated under altered pH conditions oxidise lipids with carbon-carbon double bonds, such as unsaturated chains of fatty acids, leading to lipid peroxidation and the formation of cytotoxins like aldehyde and malondialdehyde (Fritz & Petersen, 2013). These cytotoxins can then disrupt protein structure and impede proper cellular function (Catalá, 2009). Aldehyde dehydrogenases were notably upregulated at both pH 7.6 (1.05 – 3.04 LFC) and pH 8.8 (1.12 – 3.08 LFC) for *C. braarudii*. Additionally, four-carbon acid sugar kinase nucleotide binding domain-containing protein with aldehyde-lyase activity was upregulated (0.91 LFC) at pH 8.8. These enzymes metabolise aldehydes, and therefore mitigate intracellular oxidative stress (Singh *et al.*, 2013). Fatty acids are essential components of membrane lipids and various proteins involved in fatty acid biosynthesis showed significant changes. For example, enoyl-CoA hydratase (0.54

LFC), 3-oxoacyl reductase (0.77 LFC), and glycerol kinase (0.64 LFC) were amongst many significantly upregulated in *C. braarudii* at pH 8.8. However, a downregulation in 4-hydroxy-3-methylbut-2-en-1-yl diphosphate synthase (-1.87 LFC) related to the terpenoid biosynthetic process was observed at pH 8.8 in *C. braarudii*.

*G. huxleyi* also displayed significant upregulation in eight fatty acid biosynthesis-related proteins at pH 8.8, including 3-oxoacyl reductase (2.08 LFC), Acetyl-CoA carboxylase (0.6 – 1.5 LFC), and glycerol kinase (0.77 LFC). However, squalene synthase (-2.4 LFC) and terpene cyclase/mutase family member (-1.86 LFC) related to the triterpenoid biosynthetic process, and methyltransferase (-1.82 LFC) related to steroid biosynthesis were downregulated. Four fatty acid desaturases were downregulated (-1.91 – -6.51 LFC) in *G. huxleyi* at pH 8.8. Additionally, enzymes related to fatty acid metabolism pathway were also significantly changed. These included proteins such as Acetyl-CoA acyltransferase (0.76 LFC) and long chain acyl CoA dehydrogenase (0.78 – 3.37 LFC) for *C. braarudii* at pH 8.8, and 3-hydroxyacyl-CoA dehydrogenase (0.53 LFC) for *G. huxleyi* at pH 8.8. *G. huxleyi* also exhibited significant upregulation of the GP-PDE domain containing protein related to lipid metabolism at pH 7.6 (2.41 LFC) and pH 8.8 (1.22 LFC). Contrasting changes between *C. braarudii* and *G. huxleyi* were also observed. For instance, lipase-like domain containing proteins were downregulated (-5.14 LFC) at pH 8.8 in *G. huxleyi*, while such proteins were upregulated (1.28 LFC) in *C. braarudii*. No significant changes were observed in the case of *C. carterae*. The downregulation of Choline/carnitine acyltransferase (-0.94 LFC) and the upregulation of Acetyl-CoA carboxylase (1.5 LFC) at pH 8.8 in *G. huxleyi* further indicates reduced fatty acid oxidation in the mitochondria, and elevated fatty acid synthesis using Malonyl CoA (Spinelli & Haigis, 2018).

**pH-induced oxidative stress leads to cytoskeletal damage.**

Microtubules and actin filaments are the key constituents of the cytoskeleton and provide mechanical properties to the cell. These mechanical properties facilitate intracellular signalling and control cellular shape (Salbreux *et al.*, 2012). However, actin and microtubules contain cysteine and methionine residues that are susceptible to oxidative stress, and their oxidation reduces the ability of microtubules to polymerise (Dalle-Donne *et al.*, 2001; Nakao *et al.*, 2023). Consequently, the degree of polymerisation severely affects the mechanical properties of actin microfilaments (Wakatsuki *et al.*, 2001). Significant

downregulation of cytoskeletal proteins was evident in *C. braarudii*; actin (-1.67, -1.42 LFC), F-actin capping protein subunit beta (-0.81, -0.62 LFC), TOG domain-containing (-0.72, -0.66 LFC), and profilin (-0.98, -0.89 LFC) were notably downregulated at pH 7.6 and 8.8, respectively. Conversely, dynactin subunit 6 exhibited an upregulation at pH 7.6 (1.19 LFC) and pH 8.8 (2.13 LFC). Dynactin interacts with dynein that are responsible for the transportation of intracellular cargo, and their upregulation indicates increased intracellular movement of macromolecules (Schroer, 2004). KIF-binding proteins that facilitate microtubule movements were also downregulated (-1.05 LFC) at pH 7.6 in *C. braarudii*. *G. huxleyi* exhibited significant changes, albeit only under alkaline (pH 8.8) conditions. For instance, actin (-1.01 LFC) and actin-related protein 5 (-2.04 LFC) were downregulated, along with cofilin (-0.73 LFC), TOG domain containing protein (-0.97 LFC), tubulin (-1.32 LFC), centrin (-0.72 LFC), and calponin-homology domain containing protein (-1.17 LFC). Calponin bind to actin and are involved in cytoskeletal movement and signal transduction (Korenbaum & Rivero, 2002). TOG domain containing proteins bind to tubulin to regulate microtubule polymerisation and mitotic spindle formation, and their downregulation under varying pH suggests compromised cell division (Al-Bassam & Chang, 2011; Byrnes & Slep, 2017). *G. huxleyi* also exhibited downregulation in ankyrin repeat domain containing protein (-1.53 LFC) and 5 PDZ domain containing proteins (-1.27 – 0.7 LFC) under pH 8.8. Ankyrins are involved in the attachment of membrane proteins to the cytoskeleton and anchor to specific ion channels in the plasma membrane (Cunha & Mohler, 2009). Although not statistically significant, *C. carterae* exhibited a 0.7 LFC and a -1.6 LFC in CLASP N-terminal domain containing protein under pH 7.6 and 8.8, respectively. This domain regulates stability of microtubules in the cytoskeleton and aids in cell division (Ambrose *et al.*, 2007).

**Photosynthesis.**

Given the importance of pH regulation within the chloroplast, several pH sensors have been reported in different types of photosynthesising organisms. Coincidentally, many of these were significantly expressed by the three coccolithophore species studied here (Fig. 3). ATP synthase (Hahn *et al.*, 2018) exhibited up to 2 LFC at pH 8.8 in *G. huxleyi*, and 1.73 and 0.77 LFC in *C. braarudii* at pH 7.6 and 8.8, respectively. While an upregulation in ATPases was noted, their subcellular location cannot be confirmed, and it is possible that the ATPases detected were from the chloroplast, mitochondria, or both. Violaxanthin de-

epoxidase activity (Arnoux *et al.*, 2009) was significantly upregulated in *C. braarudii* at pH 7.6 (0.88 LFC), and pH 8.8 (0.77 LFC). Plastocyanin (Sas *et al.*, 2006) exhibited significant upregulation (1.59 LFC) under alkaline conditions (pH 8.8) in *G. huxleyi*. Finally, photosystem I (PSI)-fucoxanthin-chlorophyll a/c protein complex (Nagao *et al.*, 2019) exhibited significant changes in *C. carterae* when pH 7.6 was compared to pH 8.8 (-2.58 LFC). Under acidic conditions (pH 7.6), *G. huxleyi* exhibited a downregulation of light harvesting proteins and Ferredoxin-sulfite reductase, which are important electron carriers for photosynthesis. At pH 8.8, *G. huxleyi* exhibited downregulation in several photosynthetic proteins including 19 light harvesting proteins (up to -5.86 LFC). An upregulation in protochlorophyllide reductase (1.07 LFC), PsbP C-terminal domain (0.69 LFC), and Photosynthesis system II assembly factor Ycf48/Hcf136 (0.66 LFC) was observed at pH 8.8 in *G. huxleyi,* suggesting enhanced chlorophyll biosynthesis and stabilisation of PSII photosynthetic machinery under stress (Bricker *et al.*, 2013; Kang *et al.*, 2017). Contrary to *G. huxleyi* and *C. carterae*, *C. braarudii* exhibited an upregulation in 20 light harvesting proteins (up to 4.62 LFC) at pH 7.6 and an upregulation in 29 light harvesting proteins (up to 4.78 LFC) at pH 8.8. Other photosynthetic proteins were generally upregulated at pH 8.8, except cytochrome c-553 (-0.91 LFC). Similar to *G. huxleyi*, PsbP C-terminal domain-containing protein was upregulated at pH 7.6 (0.76 – 1.19 LFC), and pH 8.8 (0.66 – 1.46 LFC). At pH 8.8, *C. braarudii* saw a further upregulation of protochlorophyllide reductase (up to 1.09 LFC), Glutamate-1-semialdehyde 2,1-aminomutase (2.13 LFC) and photosynthesis system II assembly factor Ycf48/Hcf136 (1.71 LFC). Fructose-bisphosphatase was upregulated at pH 7.6 (0.63 LFC) and pH 8.8 (0.71 LFC) in *C. braarudii,* and by 0.56 LFC in *G. huxleyi* at pH 8.8. However, localisation of fructose bisphosphatase in the chloroplast cannot be confirmed as it is involved in both the Calvin cycle and gluconeogenesis in the mitochondria, where it interconverts fructose-1,6-bisphosphate and fructose 6-phosphate and plays a key role in metabolism by directing photosynthetically derived metabolites for carbohydrate storage (Marcus *et al.*, 1986).

**Metabolism.**

In the case of *C. braarudii*, glycolysis related proteins such as glucokinase (1.51 LFC) exhibited an upregulation, while glucose-6-phosphate isomerase (-0.67 LFC) and phosphofructokinase (-0.96 LFC) exhibited a downregulation under alkaline conditions. This change in enzyme activity indicates that the metabolite glucose

6-phosphate derived from glucokinase may enter the pentose phosphate pathway, resulting in the generation of NADPH to maintain antioxidant capacity (Chen *et al.*, 2019). A similar change was also observed in glucokinase (1.18 LFC) and glucose-6-phosphate isomerase (-0.84 LFC) at pH 7.6.

One-carbon metabolic pathway that plays a key role in nucleotide synthesis and redox management exhibited significant changes in *G. huxleyi* and *C. braarudii.* These included Serine hydroxymethyltransferase, Methylenetetrahydrofolate reductase, and Methylenetetrahydrofolate dehydrogenase. Additionally, Letm1 RBD domain-containing protein was upregulated in *C. braarudii* under pH 7.6 (1.29 LFC) and pH 8.8 (1.65 LFC). Letm1 partakes in mitochondrial homeostasis, and its upregulation suggests a higher requirement for cellular homeostasis-related proteins under stress (Li *et al.*, 2019). Proteins related to polysaccharide metabolism, biosynthesis, and interconversion also exhibited significant upregulation under stressed conditions. For example, *C. braarudii* exhibited a high change in Glycoside hydrolase family 19 catalytic domain-containing protein, with a 5.52 LFC at pH 7.6 and a 5.96 LFC at pH 8.8. These proteins are ubiquitous and take part in the catalytic machinery of a cell, breaking glycosidic bonds with chitin. Glycoside hydrolase GH18 domain was significantly upregulated (1.33 LFC) at pH 7.6 in *G. huxleyi*. Moreover, *G. huxleyi* exhibited an upregulation in phytase like domain containing protein (2.29 LFC at pH 7.6, 1.4 LFC at pH 8.8). Ammonia is a byproduct of many mitochondrial metabolic pathways, which is utilised by the urea cycle. An increase in urease activity was evident in *G. huxleyi* and *C. carterae*. Urease can also play a role in pH homeostasis by converting urea into $CO_2$ and $NH_4$ (Krajewska, 2009).

# Supplementary Information: Chapter 3

**Introduction:**

This supplementary section provides information on the methodology used for measurement of coccolith length and central area major axis. Furthermore, detailed description of the results obtained in this study has been provided separate to the main text to maintain clarity.

**Methods**

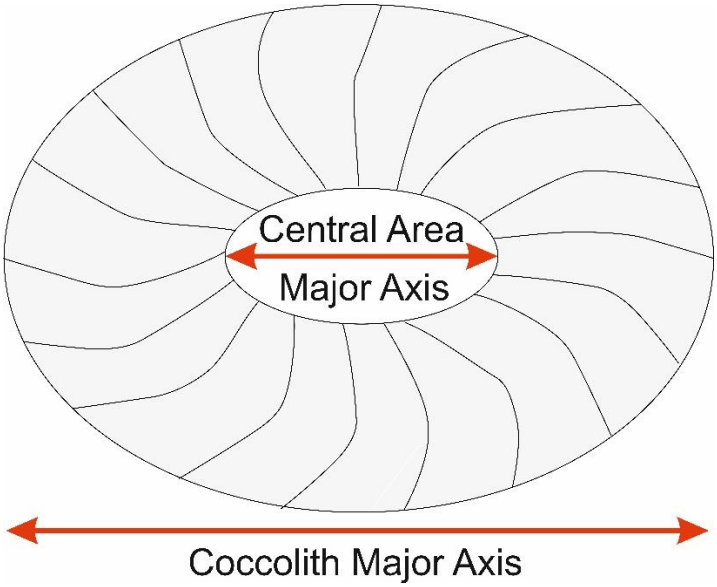


Schematic for measuring coccolith length and central area major axis. Only flat-lying coccoliths were measured. If a coccolith was upside down, only the coccolith length (coccolith major axis) was measured for that coccolith.

## Results

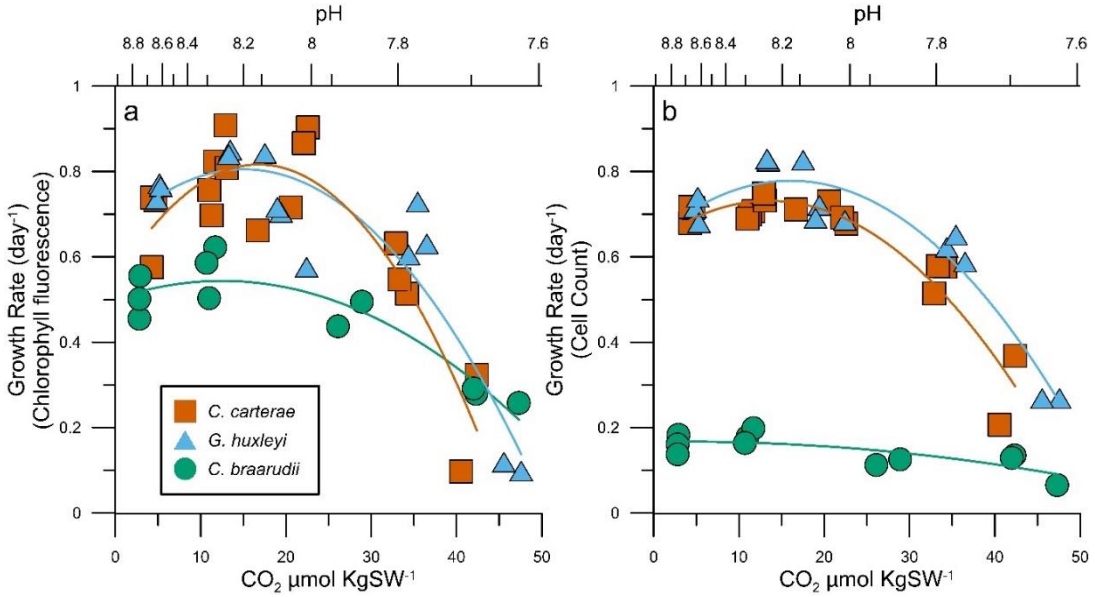


***Figure S9:*** *Growth rates for G. huxleyi, C. braarudii and C. carterae obtained from (a) linear regression of log-transformed chlorophyll fluorescence data, and (b) cell counts.*

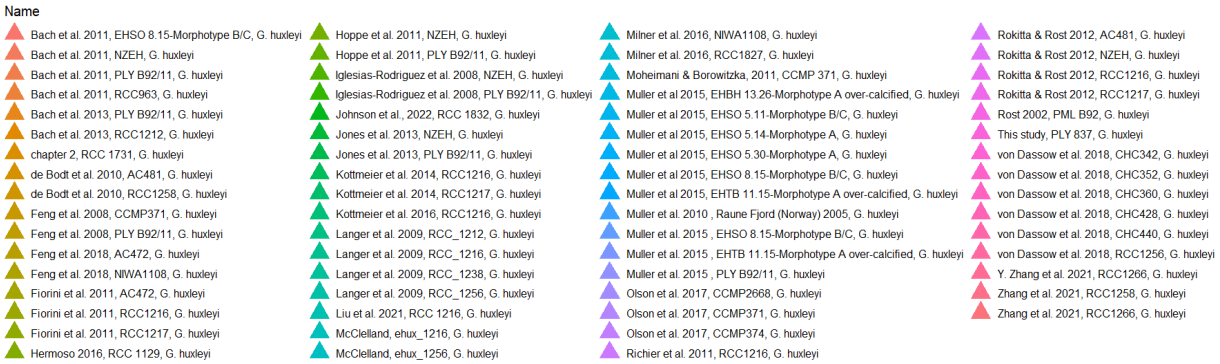


**Figure S10a:** Legend for G. huxleyi in Figures 2, 6 and 8.

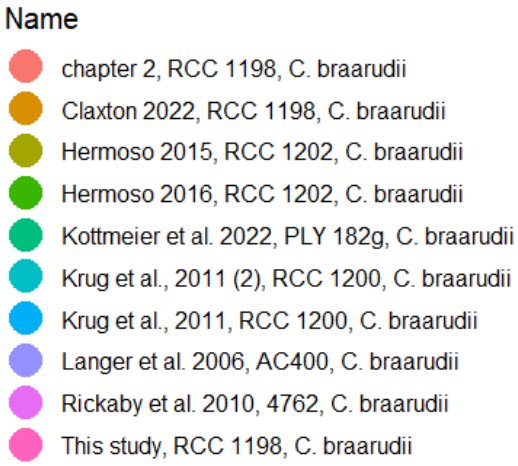


***Figure S2b****: Legend for C. braarudii in Figures 2, 6 and 8.*

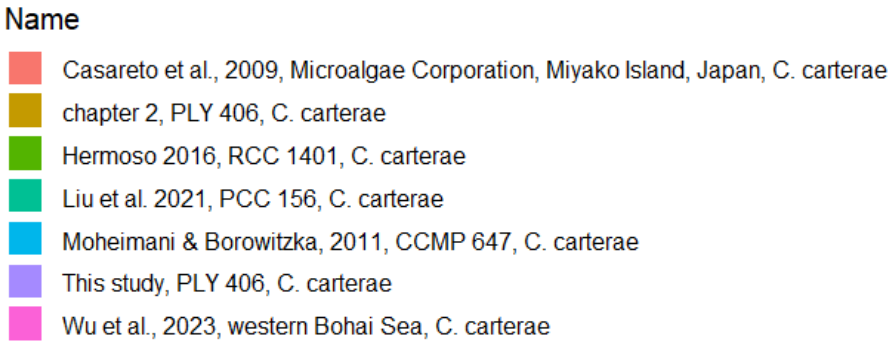


***Figure S2c:*** *Legend for C. carterae in Figure 2, 6 and 8.*

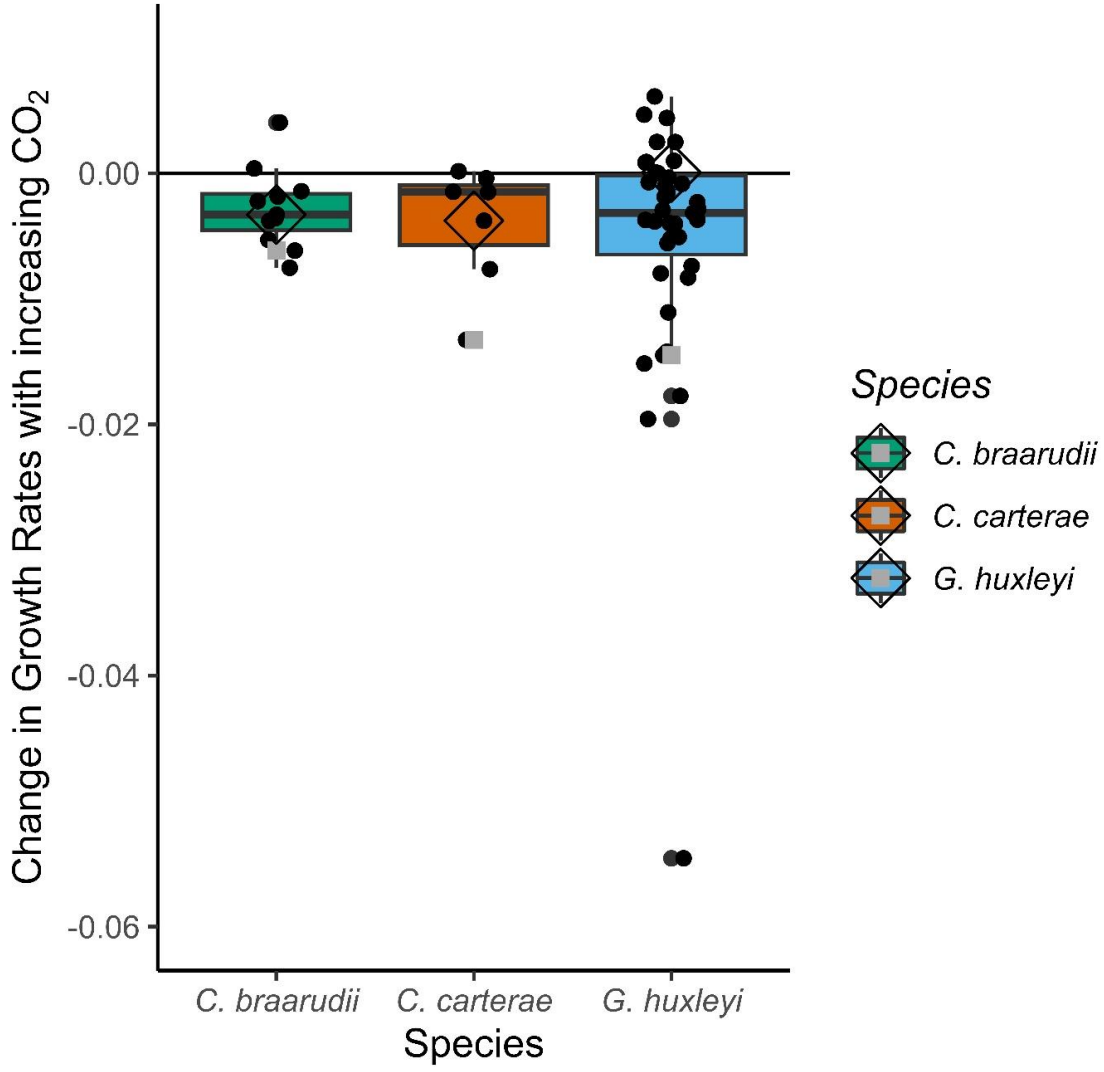


***Figure S3:*** A boxplot showing the slopes (coefficients) from linear fits of growth rates versus $CO_2$ for *G. huxleyi*, *C. braarudii*, and *C. carterae* obtained from the literature review. A negative value (y-axis) suggests that growth rates will decline at higher $CO_2$ levels, while a positive value suggests they will increase. Grey squares indicate coefficients generated from growth rates measured in this study. Open diamonds represent mean coefficient for each species based on combined growth rate data from the literature review. It must be noted that the confidence

in growth rate changes for *C. braarudii* and *C. carterae* are limited by the small number of studies conducted. The median values (horizontal bars in each box) suggest that all three species will show poorer growth under high $CO_2$ scenarios.

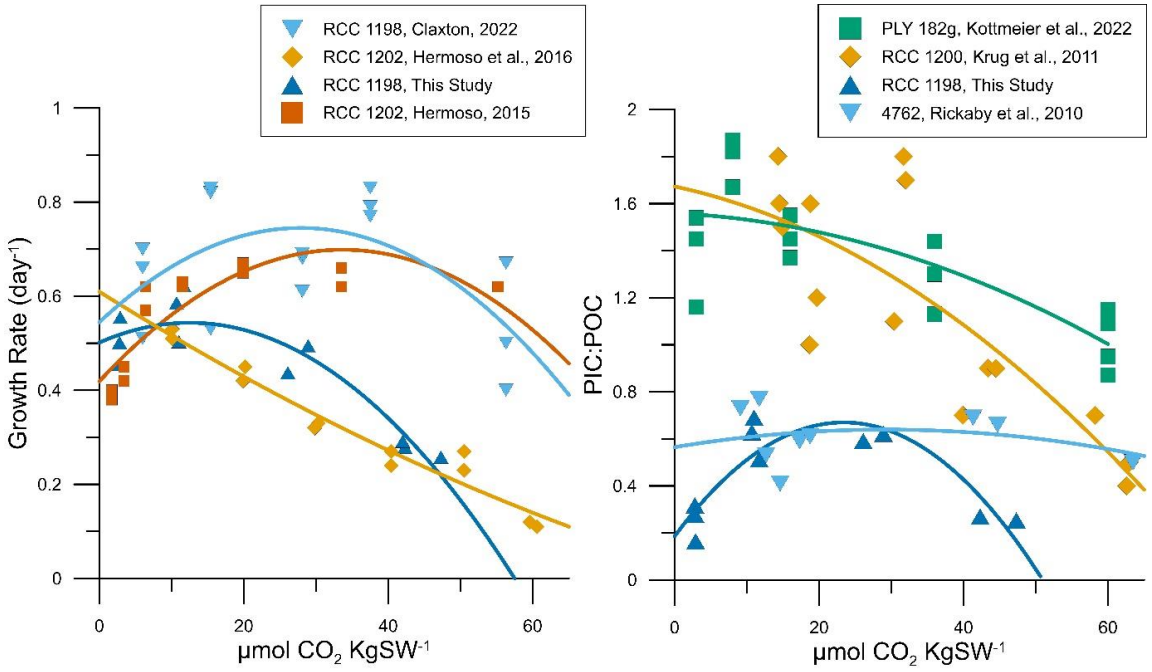


**Figure S4:** (a) Variation in growth rates of the same strain depending on the method of carbonate chemistry manipulation. Hermoso (2015) and this study used acid/base addition to change pH and $CO_2$ under constant DIC, whereas Hermoso et al. (2016) and Claxton (2022) changed carbonate chemistry through DIC addition. (b) PIC:POC ratios for PLY 182g (Kottmeier et al., 2022) and RCC 1198 (This study) are different, despite being isolated from the English Channel. Similarly, strain 4762 (Rickaby et al., 2010) is a different strain to RCC 1198, but shows similar PIC:POC ratios, especially under typical culturing conditions (DIC = 2 – 2.5 mmol $KgSW^{-1}$, pH 8.2). RCC 1200 and PLY 182g, although isolated from different locations (Namibian coast and English Channel, respectively) show similar PIC:POC ratios. These observations highlight the need to account for the method of carbonate chemistry manipulation, site of strain isolation, and other strain-specific differences when comparing coccolithophore responses to changing carbonate chemistry.

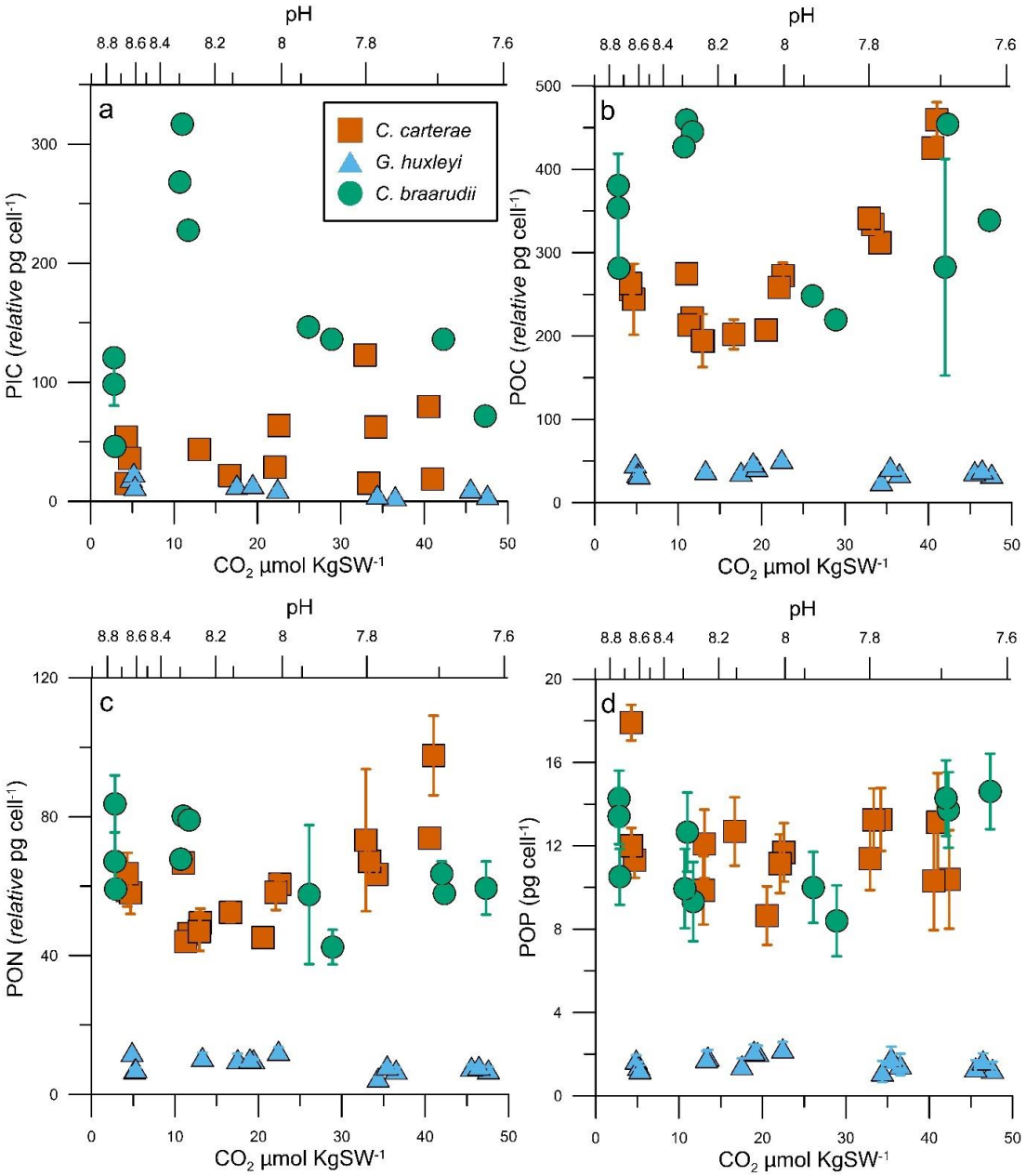


***Figure S5:*** *(a) PIC (b) POC (c) PON and (d) POP quotas for G. huxleyi, C. braarudii and C. carterae measured in this study. Note that (a), (b), and (c) are relative values.*

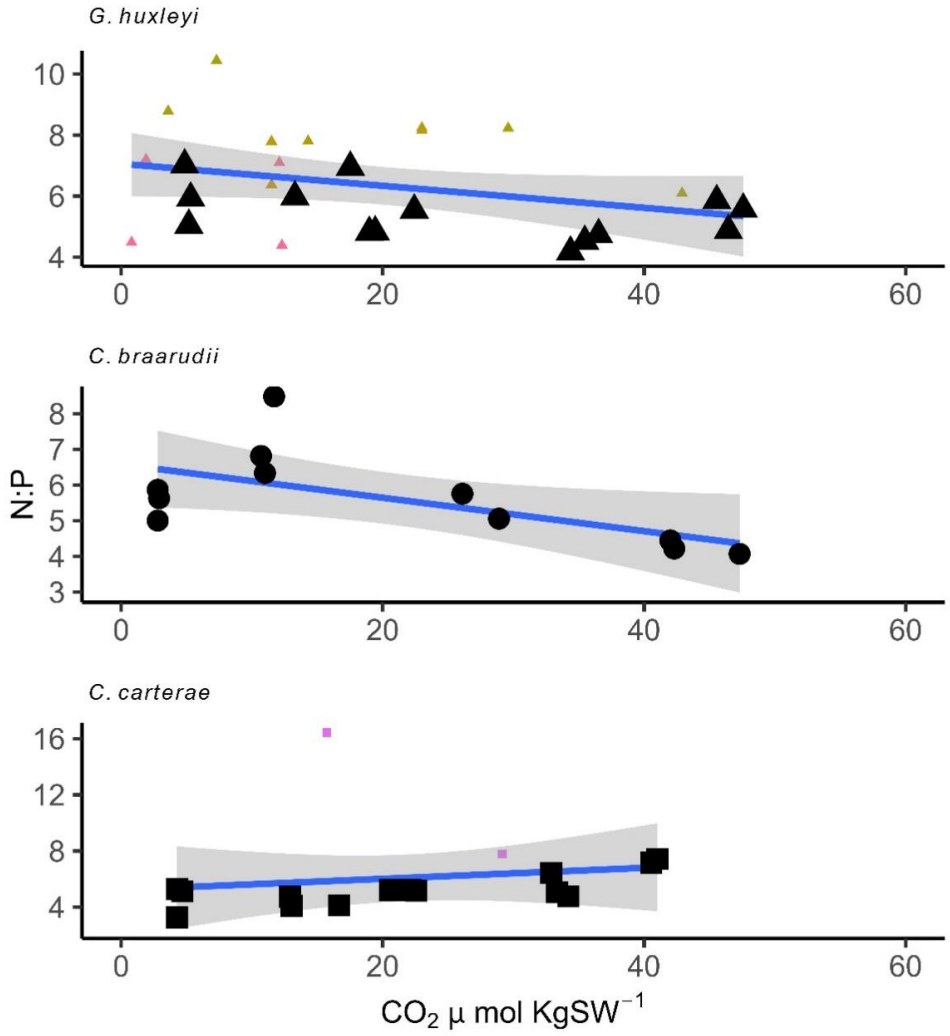


***Figure S6:*** *N:P ratios for G. huxleyi, C. braarudii and C. carterae from multiple studies. Only two studies for G. huxleyi and one study for C. carterae reported N and P quotas under changing $CO_2$ levels. Therefore, only these could be implemented. Note that PON values obtained from this study are not absolute, as an initial sample mass of 1mg was assumed for all samples (see methods). Therefore, only the trends can be compared but not absolute values.*

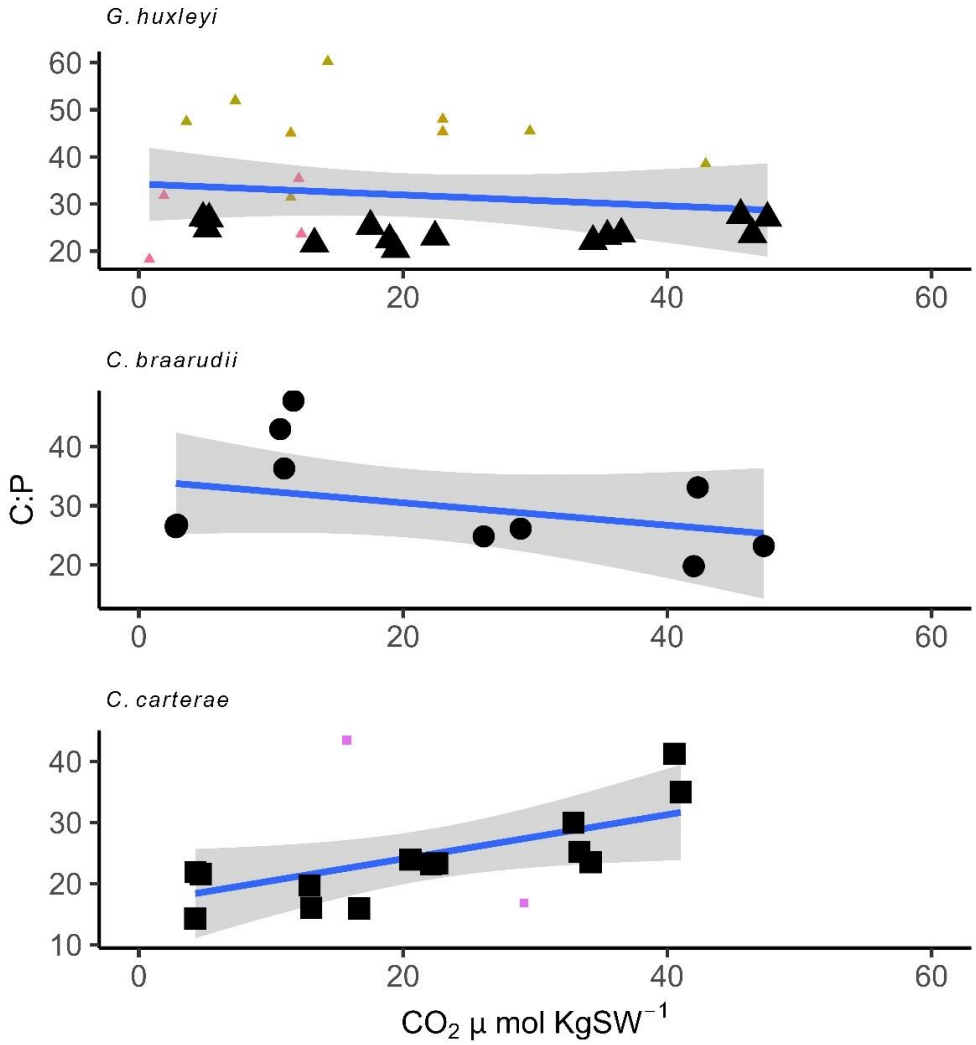


***Figure S7:*** *POC:P ratios for G. huxleyi, C. braarudii and C. carterae from multiple studies. Only two studies for G. huxleyi and one study for C. carterae reported P quotas under changing $CO_2$ levels. Therefore, only these could be implemented. Note that POC values obtained from this study are not absolute, as an initial sample mass of 1mg was assumed for all samples (see methods). Therefore, only the trends can be compared but not absolute values.*

The data used in this study is provided on the next page.

| Strain | Species | chlorophyll_fluorescence_Growth_rate | cell_count_Gr owth_rate | initial_cell_count | final_cell_count | fv_fm | sd_fv_fm | av_chla_pg_cell | av_chlc_value_pg_cell | sd_chlc_value_pg_cell | sd_chla_value_pg_cell | POP_pg_cell | av_POC_value_pg_cell | sd_POC_value_pg_cell | av_PON_value_pg_cell | sd_PON_value_pg_cell | sd_initial_alk_umol_per_kgSW | av_initial_alk_umol_per_kgSW | sd_initial_pH_value | av_initial_pH_value | DIC_initial_umol_per_kgSW | pCO2_initial_uatm | HCO3_initial_umol_per_kgSW | CO3_initial_umol_per_kgSW | CO2_initial_umol_per_kgSW | omega_calcite_initial | coccos phere_size | coccos phere_sd | PIC_PO C | PIC_pg_cell_(pg_cell_(relative_values)) | std_PIC pg_cell_(relative_values) | std_volume_corrected_chla | std_volume_corrected_chlc | av_C_N | sd_C_N | av_C_P | sd_C_P | av_N_P | sd_N_P | POC.Chla | sd_POC.Chla |
|---|---|---|---|---|---|---|---|---|---|---|---|---|---|---|---|---|---|---|---|---|---|---|---|---|---|---|---|---|---|---|---|---|---|---|---|---|---|---|---|---|---|
| PLY406 C. carterae | C. carterae | 0.58 | 0.68 | 128 | 7533 | 0.761 | 0.00 | 2.36 | 0.61 | 0.13 | 0.10 | 17.91 | 255.66 | 10.88 | 58.67 | 4.51 | 3009.50 | 1.7 | 8.66 | 0.01 | 2312.50 | 121.40 | 1800.20 | 508.03 | 4.27 | 12.10 | 12.97 | 0.85 | 0.21 | 54.06 | 2.30 | 0.00054 | 0.00005 | 0.00054 | 0.00010 | 4.36 | 0.38 | 14.28 | 0.61 | 3.28 | 0.25 | 108.46 | 7.43 |
| PLY406 C. carterae | C. carterae | 0.73 | 0.71 | 128 | 9300 | 0.776 | 0.00 | 1.86 | 0.56 | 0.23 | 0.17 | 11.31 | 244.09 | 42.58 | 58.06 | 6.08 | 2957.80 | 13.3 | 8.63 | 0.01 | 2302.50 | 132.90 | 1822.30 | 475.55 | 4.68 | 11.33 | 12.97 | 0.85 | 0.15 | 36.08 | 6.29 | 0.00049 | 0.00007 | 0.00049 | 0.00015 | 4.20 | 0.86 | 21.57 | 3.76 | 5.13 | 0.54 | 131.55 | 28.31 |
| PLY406 C. carterae | C. carterae | 0.74 | 0.72 | 128 | 9433 | 0.788 | 0.00 | 1.61 | 0.56 | 0.20 | 0.18 | 12.00 | 282.90 | 22.49 | 63.60 | 6.00 | 3011.80 | 5.9 | 8.66 | 0.01 | 2315.30 | 121.90 | 1803.30 | 507.74 | 4.29 | 12.09 | 12.97 | 0.85 | 0.06 | 14.97 | 1.28 | 0.00049 | 0.00007 | 0.00049 | 0.00016 | 4.13 | 0.53 | 21.90 | 1.87 | 5.30 | 0.50 | 163.01 | 24.52 |
| PLY406 C. carterae | C. carterae | 0.71 | 0.71 | 101 | 14250 | NA | NA | NA | NA | NA | NA | NA | 221.85 | NA | 46.30 | NA | 2660.30 | 12.0 | 8.29 | 0.01 | 2320.20 | 332.50 | 2064.50 | 244.00 | 11.70 | 5.81 | NA | NA | NA | NA | NA | NA | NA | NA | NA | 4.79 | NA | NA | NA | NA | NA | NA | NA | NA |
| PLY406 C. carterae | C. carterae | 0.70 | 0.70 | 101 | 13500 | NA | NA | NA | NA | NA | NA | NA | 213.10 | NA | 44.05 | NA | 2678.45 | 11.4 | 8.30 | 0.00 | 2326.80 | 321.00 | 2063.10 | 252.40 | 11.29 | 6.01 | NA | NA | NA | NA | NA | NA | NA | NA | NA | 4.84 | NA | NA | NA | NA | NA | NA | NA | NA |
| PLY406 C. carterae | C. carterae | 0.76 | 0.69 | 101 | 12600 | NA | NA | NA | NA | NA | NA | NA | 274.73 | NA | 66.67 | NA | 2650.55 | 27.1 | 8.31 | 0.01 | 2298.20 | 313.10 | 2035.30 | 251.89 | 11.01 | NA | NA | NA | NA | NA | NA | NA | NA | NA | NA | 4.12 | NA | NA | NA | NA | NA | NA | NA | NA |
| PLY406 C. carterae | C. carterae | 0.81 | 0.73 | 115 | 9300 | 0.749 | 0.00 | 2.82 | 1.02 | 0.24 | 0.24 | 12.09 | 193.91 | 2.53 | 49.46 | 4.06 | 2465.25 | 5.3 | 8.22 | 0.02 | 2183.00 | 370.80 | 1970.60 | 199.37 | 13.04 | 4.75 | 11.66 | 1.65 | 0.22 | 43.58 | 0.57 | 0.00123 | 0.00020 | 0.00123 | 0.00034 | 3.92 | 0.33 | 16.04 | 0.21 | 4.09 | 0.34 | 68.77 | 5.87 |
| PLY406 C. carterae | C. carterae | 0.66 | 0.71 | 115 | 8200 | 0.753 | 0.00 | 3.05 | 1.14 | 0.25 | 0.35 | 12.69 | 202.03 | 17.82 | 52.44 | 2.67 | 2499.10 | 7.4 | 8.13 | 0.02 | 2260.80 | 474.10 | 2071.80 | 172.35 | 16.67 | 4.11 | 11.66 | 1.65 | 0.11 | 21.64 | 1.91 | 0.00138 | 0.00022 | 0.00138 | 0.00046 | 3.85 | 0.40 | 15.93 | 1.40 | 4.13 | 0.23 | 66.33 | 8.05 |
| PLY406 C. carterae | C. carterae | 0.91 | 0.75 | 115 | 10233 | 0.774 | NA | 2.43 | 0.98 | 0.25 | 0.19 | 9.86 | 194.46 | 31.79 | 46.91 | 5.53 | 2493.25 | 8.8 | 8.23 | 0.00 | 2204.40 | 367.50 | 1987.00 | 204.54 | 12.92 | 4.87 | 11.66 | 1.65 | NA | NA | 0.00119 | 0.00021 | 0.00119 | 0.00029 | 4.15 | 0.84 | 19.72 | 3.22 | 4.76 | 0.56 | 80.10 | 15.46 |
| PLY406 C. carterae | C. carterae | 0.72 | 0.73 | 130 | 10400 | 0.741 | 0.00 | 3.86 | 2.06 | 1.27 | 1.30 | 8.65 | 207.05 | 9.97 | 45.19 | 1.36 | 2338.25 | 4.5 | 8.03 | 0.00 | 2159.10 | 584.30 | 2007.30 | 131.28 | 20.55 | 3.13 | 12.69 | 1.41 | NA | NA | 0.00193 | 0.00067 | 0.00193 | 0.00124 | 4.58 | 0.26 | 23.94 | 1.15 | 5.23 | 0.16 | 53.68 | 17.83 |
| PLY406 C. carterae | C. carterae | 0.90 | 0.68 | 130 | 7600 | 0.743 | 0.00 | 4.13 | 1.82 | 0.23 | 0.22 | 11.68 | 272.37 | 15.51 | 60.53 | 1.24 | 2331.40 | 5.4 | 7.99 | 0.01 | 2168.40 | 641.60 | 2024.30 | 121.58 | 22.57 | 2.90 | 12.69 | 1.41 | 0.23 | 63.78 | 3.63 | 0.00170 | 0.00021 | 0.00170 | 0.00028 | 4.50 | 0.27 | 23.31 | 1.33 | 5.18 | 0.11 | 65.87 | 5.19 |
| PLY406 C. carterae | C. carterae | 0.87 | 0.69 | 130 | 8300 | 0.747 | 0.00 | 6.27 | 4.50 | 2.27 | 2.64 | 11.14 | 258.23 | 0.57 | 58.23 | 5.11 | 2352.60 | 13.6 | 8.00 | 0.00 | 2183.80 | 628.50 | 2036.10 | 125.57 | 22.11 | 2.99 | 12.69 | 1.41 | 0.11 | 28.71 | 0.06 | 0.00421 | 0.00159 | 0.00421 | 0.00251 | 4.43 | 0.39 | 23.17 | 0.05 | 5.23 | 0.46 | 41.18 | 14.92 |
| PLY406 C. carterae | C. carterae | 0.51 | 0.58 | 124 | 7050 | 0.705 | 0.00 | 9.36 | 7.70 | 0.42 | 0.45 | 13.27 | 312.06 | 9.36 | 63.36 | 2.67 | 2192.85 | 5.4 | 7.80 | 0.02 | 2104.00 | 972.40 | 1992.10 | 77.69 | 34.20 | 1.85 | 16.55 | 1.51 | 0.20 | 62.35 | 1.87 | 0.00324 | 0.00033 | 0.00324 | 0.00035 | 4.93 | 0.26 | 23.52 | 0.71 | 4.78 | 0.20 | 33.34 | 1.80 |
| PLY406 C. carterae | C. carterae | 0.55 | 0.58 | 124 | 7100 | 0.710 | 0.00 | 9.10 | 7.34 | 0.69 | 0.67 | 13.25 | 333.80 | 9.96 | 67.14 | 5.98 | 2205.60 | 2.5 | 7.82 | 0.01 | 2112.30 | 947.90 | 1998.70 | 80.23 | 33.34 | 1.91 | 16.55 | 1.51 | 0.05 | 15.30 | 0.46 | 0.00309 | 0.00037 | 0.00309 | 0.00040 | 4.97 | 0.47 | 25.20 | 0.75 | 5.07 | 0.45 | 36.70 | 3.00 |
| PLY406 C. carterae | C. carterae | 0.63 | 0.51 | 124 | 7600 | 0.717 | 0.00 | 10.38 | 8.85 | 0.47 | 0.39 | 11.38 | 341.23 | 8.68 | 73.25 | 20.47 | 2206.35 | 16.9 | 7.82 | 0.00 | 2111.20 | 935.20 | 1997.10 | 81.18 | 32.89 | 1.93 | 16.55 | 1.51 | 0.36 | 122.93 | 3.13 | 0.00373 | 0.00038 | 0.00373 | 0.00038 | 4.66 | 1.31 | 29.98 | 0.76 | 6.44 | 1.80 | 32.89 | 1.70 |
| PLY406 C. carterae | C. carterae | 0.32 | 0.37 | 102 | 8450 | 0.703 | 0.00 | 10.47 | 8.08 | 0.70 | 0.45 | 10.39 | NA | NA | NA | NA | 2148.65 | 2.3 | 7.71 | 0.00 | 2090.50 | 1205.00 | 1985.80 | 62.30 | 42.38 | 1.48 | 18.28 | 2.36 | 0.09 | NA | NA | 0.00253 | 0.00037 | 0.00253 | 0.00038 | NA | NA | NA | NA | NA | NA | NA | NA |
| PLY406 C. carterae | C. carterae | 0.10 | 0.21 | 102 | 7767 | 0.654 | 0.00 | NA | NA | NA | NA | 10.31 | 425.32 | 3.03 | 73.82 | 1.21 | 2164.95 | 5.2 | 7.73 | 0.00 | 2100.20 | 1152.80 | 1994.00 | 65.66 | 40.54 | 1.56 | 18.28 | 2.36 | 0.19 | 79.46 | 0.57 | NA | NA | NA | NA | 5.76 | 0.10 | 41.25 | 0.29 | 7.16 | 0.12 | NA | NA |
| PLY406 C. carterae | C. carterae | 0.11 | 0.20 | 102 | 7000 | 0.644 | 0.01 | NA | NA | NA | NA | 13.13 | 459.52 | 20.88 | 97.62 | 11.45 | 2157.75 | 5.0 | 7.72 | 0.01 | 2094.90 | 1166.10 | 1989.30 | 64.61 | 41.01 | 1.54 | 18.28 | 2.36 | 0.04 | 18.70 | 0.85 | NA | NA | NA | NA | 4.71 | 0.59 | 35.00 | 1.59 | 7.43 | 0.87 | NA | NA |
| PLY837 G. huxleyi | G. huxleyi | 0.73 | 0.71 | 71 | 43700 | 0.749 | NA | 0.89 | 0.89 | 0.39 | 0.42 | 1.74 | 46.99 | NA | 12.20 | NA | 3016.75 | 19.3 | 8.62 | 0.01 | 2356.80 | 138.20 | 1870.00 | 481.87 | 4.86 | 11.48 | 6.09 | 0.20 | 0.42 | 19.69 | NA | 0.00757 | 0.00332 | 0.00757 | 0.00359 | 3.85 | NA | 27.03 | NA | 7.02 | NA | 52.96 | NA |
| PLY837 G. huxleyi | G. huxleyi | 0.77 | 0.74 | 71 | 55000 | 0.768 | NA | 1.94 | 2.32 | 1.97 | 2.82 | 1.44 | 35.64 | 2.42 | 7.27 | 0.21 | 3024.90 | 7.6 | 8.60 | 0.00 | 2381.80 | 147.10 | 1906.40 | 470.20 | 5.18 | 11.20 | 6.09 | 0.20 | 0.68 | 24.08 | 1.64 | 0.01963 | 0.01988 | 0.01963 | 0.02385 | 4.90 | 0.36 | 24.72 | 1.68 | 5.05 | 0.15 | 18.32 | 18.60 |
| PLY837 G. huxleyi | G. huxleyi | 0.76 | 0.68 | 71 | 63200 | 0.772 | 0.00 | 0.97 | 0.96 | 0.50 | 0.56 | 1.27 | 34.12 | 5.74 | 7.54 | 0.22 | 2976.70 | 12.9 | 8.59 | 0.01 | 2354.50 | 151.20 | 1898.30 | 452.89 | 5.32 | 10.79 | 6.09 | 0.20 | 0.38 | 12.88 | 2.17 | 0.00808 | 0.00414 | 0.00808 | 0.00471 | 4.52 | 0.77 | 26.85 | 4.52 | 5.93 | 0.18 | 35.16 | 18.94 |
| PLY837 G. huxleyi | G. huxleyi | 0.84 | 0.83 | 62 | 46000 | 0.780 | NA | 0.34 | 0.27 | 0.24 | 0.26 | 1.47 | 37.13 | 0.00 | 10.18 | 1.60 | 2457.70 | 18.0 | 8.11 | 0.01 | 2234.80 | 498.30 | 2055.80 | 161.46 | 17.53 | 3.85 | 6.15 | 0.33 | 0.38 | 13.99 | 0.00 | 0.00221 | 0.00160 | 0.00221 | 0.00215 | 3.65 | 0.57 | 25.34 | 0.00 | 6.95 | 1.09 | 110.58 | 79.68 |
| PLY837 G. huxleyi | G. huxleyi | 0.85 | 0.82 | 62 | 45100 | 0.770 | 0.00 | 0.11 | 0.07 | 0.02 | 0.02 | 1.88 | NA | NA | NA | NA | 2448.00 | 4.5 | 8.20 | 0.01 | 2175.20 | 383.10 | 1969.10 | 192.68 | 13.47 | 4.59 | 6.15 | 0.33 | 0.32 | NA | NA | 0.00054 | 0.00012 | 0.00054 | 0.00017 | NA | NA | NA | NA | NA | NA | NA | NA |
| PLY837 G. huxleyi | G. huxleyi | 0.84 | 0.83 | 62 | 47050 | 0.761 | 0.01 | 1.09 | 1.35 | 1.04 | 1.54 | 1.81 | 39.11 | 0.60 | 10.84 | 1.20 | 2439.20 | 23.6 | 8.21 | 0.00 | 2165.20 | 378.00 | 1958.70 | 193.21 | 13.29 | 4.60 | 6.15 | 0.33 | NA | NA | 0.01104 | 0.01056 | 0.01104 | 0.01262 | 3.61 | 0.40 | 21.57 | 0.33 | 5.98 | 0.66 | 35.87 | 34.24 |
| PLY837 G. huxleyi | G. huxleyi | 0.58 | 0.69 | 65 | 31125 | NA | NA | 0.85 | 0.87 | 0.46 | 0.54 | 2.28 | 52.45 | 0.57 | 12.61 | 1.02 | 2293.65 | 3.7 | 7.99 | 0.01 | 2134.00 | 637.60 | 1993.00 | 118.60 | 22.42 | 2.83 | 5.97 | 0.31 | 0.20 | 10.57 | 0.11 | 0.00782 | 0.00427 | 0.00782 | 0.00484 | 4.16 | 0.34 | 23.05 | 0.25 | 5.54 | 0.45 | 62.01 | 33.75 |
| PLY837 G. huxleyi | G. huxleyi | 0.70 | 0.72 | 65 | 42650 | 0.773 | 0.00 | 0.53 | 0.52 | 0.38 | 0.41 | 2.10 | 42.85 | 0.08 | 10.14 | 0.08 | 2312.85 | 7.4 | 8.05 | 0.01 | 2127.50 | 552.50 | 1973.80 | 134.24 | 19.43 | 3.20 | 5.97 | 0.31 | 0.34 | 14.58 | 0.03 | 0.00471 | 0.00331 | 0.00471 | 0.00370 | 4.23 | 0.04 | 20.40 | 0.04 | 4.83 | 0.04 | 80.10 | 56.17 |
| PLY837 G. huxleyi | G. huxleyi | 0.72 | 0.69 | 65 | 32500 | 0.758 | 0.00 | 1.78 | 2.12 | 1.64 | 2.44 | 2.16 | 48.38 | 1.20 | 10.38 | 0.33 | 2325.50 | 5.1 | 8.06 | 0.00 | 2134.50 | 539.70 | 1977.60 | 137.95 | 18.98 | 3.29 | 5.97 | 0.31 | NA | NA | 0.01903 | 0.01749 | 0.01903 | 0.02194 | 4.66 | 0.19 | 22.42 | 0.55 | 4.81 | 0.15 | 27.13 | 24.91 |
| PLY837 G. huxleyi | G. huxleyi | 0.63 | 0.59 | 70 | 45225 | 0.744 | 0.00 | 0.67 | 0.63 | 0.25 | 0.27 | 1.51 | 35.60 | 0.47 | 7.13 | 0.70 | 2232.15 | 7.3 | 7.78 | 0.00 | 2148.80 | 1038.40 | 2036.30 | 76.02 | 36.52 | 1.81 | 6.15 | 0.51 | 0.12 | 4.34 | 0.06 | 0.00514 | 0.00195 | 0.00514 | 0.00222 | 4.99 | 0.50 | 23.63 | 0.31 | 4.73 | 0.47 | 53.29 | 19.71 |
| PLY837 G. huxleyi | G. huxleyi | 0.60 | 0.62 | 70 | 65650 | 0.750 | 0.00 | 1.08 | 1.10 | 1.01 | 1.10 | 1.17 | 25.86 | 1.24 | 4.87 | 0.11 | 2247.20 | 3.5 | 7.81 | 0.01 | 2154.50 | 977.20 | 2039.10 | 81.01 | 34.37 | 1.93 | 6.15 | 0.51 | 0.22 | 5.72 | 0.27 | 0.00901 | 0.00852 | 0.00901 | 0.00909 | 5.30 | 0.28 | 22.10 | 1.06 | 4.17 | 0.09 | 24.01 | 22.64 |
| PLY837 G. huxleyi | G. huxleyi | 0.73 | 0.65 | 70 | 46933 | 0.763 | 0.01 | 0.56 | 0.51 | 0.30 | 0.33 | 1.85 | 42.99 | 0.68 | 8.36 | 0.23 | 2238.50 | 1.4 | 7.80 | 0.00 | 2150.70 | 1008.10 | 2036.90 | 78.35 | 35.46 | 1.87 | 6.15 | 0.51 | NA | NA | 0.00416 | 0.00224 | 0.00416 | 0.00270 | 5.14 | 0.16 | 23.21 | 0.37 | 4.52 | 0.12 | 76.96 | 40.88 |
| PLY837 G. huxleyi | G. huxleyi | 0.10 | 0.27 | 61 | 49650 | 0.722 | 0.00 | 1.16 | 1.23 | 0.23 | 0.25 | 1.29 | 34.89 | 0.07 | 7.20 | 0.78 | 2115.10 | 1.6 | 7.66 | 0.00 | 2073.30 | 1352.80 | 1971.10 | 54.67 | 47.58 | 1.30 | 6.14 | 0.34 | 0.16 | 5.45 | 0.01 | 0.01017 | 0.00208 | 0.01017 | 0.00212 | 4.85 | 0.53 | 27.00 | 0.06 | 5.57 | 0.61 | 30.06 | 5.93 |
| PLY837 G. huxleyi | G. huxleyi | 0.12 | 0.27 | 61 | 49200 | 0.713 | 0.01 | 1.25 | 1.32 | 0.14 | 0.14 | 1.36 | 37.70 | 0.57 | 7.98 | 0.65 | 2131.70 | 1.8 | 7.68 | 0.01 | 2083.60 | 1285.00 | 1980.40 | 57.65 | 45.55 | 1.37 | 6.14 | 0.34 | 0.29 | 10.75 | 0.16 | 0.01093 | 0.00138 | 0.01093 | 0.00133 | 4.73 | 0.39 | 27.64 | 0.42 | 5.85 | 0.47 | 30.06 | 3.46 |
| PLY837 G. huxleyi | G. huxleyi | 0.12 | 0.26 | 61 | 45050 | 0.728 | 0.00 | 1.58 | 1.69 | 0.19 | 0.21 | 1.70 | 40.01 | 0.55 | 8.27 | 0.08 | 2126.00 | 8.1 | 7.67 | 0.00 | 2080.60 | 1320.40 | 1977.80 | 56.40 | 46.44 | 1.34 | 6.14 | 0.34 | NA | NA | 0.01396 | 0.00183 | 0.01396 | 0.00190 | 4.84 | 0.08 | 23.57 | 0.32 | 4.87 | 0.05 | 25.36 | 3.02 |
| RCC111C. braarudii | C. braarudii | 0.56 | 0.18 | 428 | 6633 | 0.700 | 0.01 | 2.72 | 1.41 | 0.34 | 0.43 | 10.51 | 281.53 | 5.86 | 59.17 | 2.66 | 3282.90 | 16.4 | 8.81 | 0.01 | 2378.00 | 81.70 | 1700.90 | 674.20 | 2.90 | 16.06 | 18.43 | 1.34 | 0.16 | 46.24 | 0.96 | 0.00043 | 0.00006 | 0.00043 | 0.00013 | 4.76 | 0.24 | 26.78 | 0.56 | 5.63 | 0.25 | 103.63 | 13.10 |
| RCC111C. braarudii | C. braarudii | 0.45 | 0.16 | 428 | 4750 | 0.718 | 0.00 | 6.80 | 4.99 | 2.45 | 2.41 | 14.27 | 380.53 | 0.74 | 83.68 | 8.19 | 3253.45 | 2.9 | 8.81 | 0.01 | 2352.80 | 80.40 | 1680.80 | 669.20 | 2.80 | 15.94 | 18.43 | 1.34 | 0.32 | 120.61 | 0.24 | 0.00152 | 0.00056 | 0.00152 | 0.00074 | 4.55 | 0.44 | 26.67 | 0.05 | 5.86 | 0.57 | 55.95 | 20.14 |
| RCC111C. braarudii | C. braarudii | 0.50 | 0.14 | 428 | 5067 | 0.724 | 0.00 | 5.67 | 3.81 | 2.08 | 2.10 | 13.42 | 353.78 | 64.90 | 67.11 | 8.37 | 3263.40 | NA | 8.81 | NA | 2360.00 | 80.50 | 1685.40 | 671.80 | 2.80 | 16.00 | 18.43 | 1.34 | 0.28 | 98.40 | 18.05 | 0.00116 | 0.00043 | 0.00116 | 0.00065 | 5.27 | 1.17 | 26.37 | 4.84 | 5.00 | 0.62 | 62.35 | 25.60 |
| RCC111C. braarudii | C. braarudii | 0.50 | 0.18 | 402 | 4067 | 0.707 | 0.00 | 7.64 | 6.19 | 1.49 | 1.73 | 12.66 | 459.22 | NA | 80.16 | NA | 2602.70 | 15.8 | 8.30 | 0.01 | 2259.10 | 312.90 | 2003.80 | 244.30 | 11.00 | 5.82 | 21.03 | 1.90 | 0.89 | 316.84 | NA | 0.00127 | 0.00027 | 0.00127 | 0.00037 | 5.73 | NA | 36.29 | NA | 6.33 | NA | 60.09 | NA |
| RCC111C. braarudii | C. braarudii | 0.62 | 0.20 | 402 | 5300 | 0.717 | 0.00 | 7.23 | 5.78 | 1.83 | 2.15 | 9.32 | 445.00 | NA | 79.06 | NA | 2922.35 | 20.6 | 8.32 | 0.00 | 2534.80 | 334.10 | 2237.70 | 285.40 | 11.70 | 6.80 | 21.03 | 1.90 | 0.51 | 227.76 | NA | 0.00119 | 0.00032 | 0.00119 | 0.00045 | 5.63 | NA | 47.74 | NA | 8.48 | NA | 61.53 | NA |
| RCC111C. braarudii | C. braarudii | 0.59 | 0.16 | 402 | 5533 | 0.725 | 0.00 | 4.92 | 3.50 | 1.32 | 1.54 | 9.94 | 426.87 | NA | 67.75 | NA | 2593.30 | 5.7 | 8.31 | 0.01 | 2245.40 | 304.70 | 1987.80 | 246.90 | 10.70 | 5.88 | 21.03 | 1.90 | 0.83 | 268.19 | NA | 0.00072 | 0.00020 | 0.00072 | 0.00032 | 6.30 | NA | 42.93 | NA | 6.81 | NA | 86.67 | NA |
| RCC111C. braarudii | C. braarudii | 0.44 | 0.11 | 448 | 5300 | 0.694 | NA | 3.47 | 2.22 | 0.48 | 0.42 | 10.00 | 248.11 | 5.34 | 57.55 | 20.01 | 2276.50 | 35.1 | 7.93 | 0.01 | 2141.90 | 741.50 | 2011.90 | 103.90 | 26.10 | 2.48 | 19.54 | 1.70 | 0.59 | 146.41 | 3.15 | 0.00057 | 0.00009 | 0.00057 | 0.00012 | 4.31 | 1.50 | 24.81 | 0.53 | 5.75 | 2.00 | 71.59 | 9.96 |
| RCC111C. braarudii | C. braarudii | 0.49 | 0.13 | 448 | 7067 | 0.682 | 0.00 | 3.68 | 2.65 | 1.87 | 1.55 | 8.40 | 219.34 | 9.01 | 42.45 | 5.00 | 2402.50 | NA | 7.91 | 0.00 | 2270.80 | 821.60 | 2136.20 | 105.70 | 28.90 | 2.52 | 19.54 | 1.70 | 0.62 | 136.17 | 5.59 | 0.00068 | 0.00035 | 0.00068 | 0.00040 | 5.17 | 0.64 | 26.12 | 1.07 | 5.06 | 0.60 | 59.56 | 30.40 |
| RCC111C. braarudii | C. braarudii | 0.26 | 0.07 | 205 | 5090 | 0.703 | 0.00 | 4.02 | 3.51 | 2.66 | 3.15 | 14.61 | 338.79 | 1.39 | 59.43 | 7.64 | 2085.15 | 18.9 | 7.65 | 0.00 | 2044.50 | 1344.80 | 1943.70 | 53.50 | 47.30 | 1.27 | 19.18 | 1.81 | 0.25 | 71.66 | 0.35 | 0.00095 | 0.00063 | 0.00095 | 0.00086 | 5.70 | 0.73 | 23.19 | 0.10 | 4.07 | 0.52 | 84.26 | 55.65 |
| RCC111C. braarudii | C. braarudii | 0.28 | 0.13 | 205 | 5010 | 0.705 | 0.00 | 5.89 | 4.29 | 1.54 | 1.75 | 13.72 | 453.97 | 5.26 | 57.88 | 1.41 | 2164.00 | 40.2 | 7.71 | 0.00 | 2104.50 | 1201.80 | 1998.90 | 63.30 | 42.30 | 1.51 | 19.18 | 1.81 | 0.27 | 136.06 | 7.23 | 0.00116 | 0.00032 | 0.00116 | 0.00049 | 7.84 | 0.21 | 33.09 | 0.38 | 4.22 | 0.10 | 77.09 | 20.14 |
| RCC111C. braarudii | C. braarudii | 0.29 | 0.13 | 205 | 4920 | 0.714 | 0.01 | 4.89 | 3.21 | 1.54 | 1.75 | 14.29 | 282.56 | 129.96 | 63.52 | 3.59 | 2095.75 | 8.4 | 7.70 | 0.03 | 2040.10 | 1193.80 | 1938.20 | 59.90 | 42.00 | 1.43 | 19.18 | 1.81 | NA | NA | 0.00087 | 0.00029 | 0.00087 | 0.00048 | 4.45 | 2.06 | 19.78 | 9.10 | 4.45 | 0.25 | 57.74 | 32.15 |

# References

**Adams RLP**. **1995**. Eukaryotic DNA methyltransferases – structure and function. *BioEssays* **17**: 139–145.

**Adkins JF, Boyle EA, Curry WB, Lutringer A**. **2003**. Stable isotopes in deep-sea corals and a new mechanism for "vital effects". *Geochimica et Cosmochimica Acta* **67**: 1129–1143.

**Agnini C, Fornaciari E, Rio D, Raffi I, Catanzariti R, Pälike H, Backman J**. **2014**. A New Low-to Middle-Latitude Biozonation and Revised Biochronology of Palaeogene Calcareous Nannofossils Biozonation and biochronology of Paleogene calcareous nannofossils from low and middle latitudes. *Newsletters on Stratigraphy* **47**: 131–181.

**Al-Bassam J, Chang F**. **2011**. Regulation of microtubule dynamics by TOG-domain proteins XMAP215/Dis1 and CLASP. *Trends in Cell Biology* **21**: 604–614.

**Allison N, Finch AA**. **2010**. δ11B, Sr, Mg and B in a modern Porites coral: the relationship between calcification site pH and skeletal chemistry. *Geochimica et Cosmochimica Acta* **74**: 1790–1800.

**Ambrose JC, Shoji T, Kotzer AM, Pighin JA, Wasteneys GO**. **2007**. The Arabidopsis CLASP Gene Encodes a Microtubule-Associated Protein Involved in Cell Expansion and Division. *The Plant Cell* **19**: 2763–2775.

**Amici SA, Osman W, Guerau-de-Arellano M**. **2021**. PRMT5 Promotes Cyclin E1 and Cell Cycle Progression in CD4 Th1 Cells and Correlates With EAE Severity. *Frontiers in immunology* **12**.

**Andersen R**. **2005**. *Algal culturing techniques*. Elsevier.

**Anning T, Nimer N, Merrett MJ, Brownlee C**. **1996**. Costs and benefits of calcification in coccolithophorids. *Journal of Marine Systems* **9**: 45–56.

**Archontikis OA, Probert I, Beaufort L, Rickaby REM, Filatov DA, Bendif EM, Bendif M**. **2023**. Taxonomic and nomenclatural notes on the coccolithophore Gephyrocapsa huxleyi (Noelaerhabdaceae, Haptophyta) and related species. *Notulae Algarum*.

**Arnoux P, Morosinotto T, Saga G, Bassi R, Pignol D**. **2009**. A Structural Basis for the pH-Dependent Xanthophyll Cycle in Arabidopsis thaliana. *The Plant Cell* **21**: 2036–2044.

**Asada K**. **2003**. THE WATER-WATER CYCLE IN CHLOROPLASTS: Scavenging of Active Oxygens and Dissipation of Excess Photons. *https://doi.org/10.1146/annurev.arplant.50.1.601* **50**: 601–639.

**Auguères AS, Loreau M**. **2015**. Regulation of Redfield ratios in the deep ocean. *Global Biogeochemical Cycles* **29**: 254–266.

**Avrahami EM, Eyal Z, Varsano N, Zagoriy I, Mahamid J, Gal A**. **2023**. Transport-Limited Growth of Coccolith Crystals. *Advanced Materials*: 2309547.

**Avrahami EM, Houben L, Aram L, Gal A**. **2022**. Complex morphologies of biogenic crystals emerge from anisotropic growth of symmetry-related facets. *Science* **376**: 312–316.

**Avram VF, Merce AP, Hâncu IM, Bătrân AD, Kennedy G, Rosca MG, Muntean DM**. **2022**. Impairment of Mitochondrial Respiration in Metabolic Diseases: An Overview. *International Journal of Molecular Sciences* **23**.

**Azad HS, Borchardt JA**. **1970**. Variations in Phosphorus Uptake by Algae Total phosphorus determinations were carried out using. *Current Research* **4**: 21.

**Bach LT, Gill SJ, Rickaby REM, Gore S, Renforth P**. **2019**. CO2 Removal With Enhanced Weathering and Ocean Alkalinity Enhancement: Potential Risks and Co-benefits for Marine Pelagic Ecosystems. *Frontiers in Climate* **1**: 476698.

**Bach LT, MacKinder LCM, Schulz KG, Wheeler G, Schroeder DC, Brownlee C, Riebesell U. 2013**. Dissecting the impact of CO2 and pH on the mechanisms of photosynthesis and calcification in the coccolithophore Emiliania huxleyi. *New Phytologist* **199**: 121–134.

**Bach L, Riebesell U, and KS-L, 2011 undefined. 2011a**. Distinguishing between the effects of ocean acidification and ocean carbonation in the coccolithophore Emiliania huxleyi. *Wiley Online Library* **56**: 2040–2050.

**Bach L, Riebesell U, Gutowska MA, Federwisch L, Schulz KG. 2015**. A unifying concept of coccolithophore sensitivity to changing carbonate chemistry embedded in an ecological framework. *Progress in Oceanography* **135**: 125–138.

**Bach LT, Riebesell U, Schulz KG. 2011b**. Distinguishing between the effects of ocean acidification and ocean carbonation in the coccolithophore Emiliania huxleyi. *Limnology and Oceanography* **56**: 2040–2050.

**Backman J. 1980**. Miocene-Pliocene nannofossils and sedimentation rates in the Hatton-Rockall Basin, NE Atlantic Ocean.

**Badger MR, Andrews TJ, Whitney SM, Ludwig M, Yellowlees DC, Leggat W, Price GD. 1998**. The diversity and coevolution of Rubisco, plastids, pyrenoids, and chloroplast-based CO2-concentrating mechanisms in algae. *Canadian Journal of Botany* **76**: 1052–1071.

**Badger MR, Kaplan A, Carnegie JAB, St P, Stanford C. 1980**. Internal Inorganic Carbon Pool of Chlamydomonas reinhardtiiEVIDENCE FOR A CARBON DIOXIDE-CONCENTRATING MECHANISM. *Plant Physiology* **66**: 407–413.

**Badger MR, Palmqvist K, Yu J -W. 1994**. Measurement of CO2 and HCO3− fluxes in cyanobacteria and microalgae during steady-state photosynthesis. *Physiologia Plantarum* **90**: 529–536.

**Balch WM. 2018**. The ecology, biogeochemistry, and optical properties of coccolithophores. *Annual Review of Marine Science* **10**: 71–98.

**Balch WM, Holligan PM, Kilpatrick KA. 1992**. Calcification, photosynthesis and growth of the bloom-forming coccolithophore, Emiliania huxleyi. *Continental Shelf Research* **12**: 1353–1374.

**Balch WM, Kilpatrick K, Holligan PM, Cucci T. 1993**. Coccolith Production and Detachment By Emiliania huxleyi (prymnesiophyceae)1. *Journal of Phycology* **29**: 566–575.

**Barcelos E Ramos J, Uller MNM, Riebesell U. 2010**. Short-term response of the coccolithophore Emiliania huxleyi to an abrupt change in seawater carbon dioxide concentrations. *Biogeosciences* **7**: 177–186.

**Barton S, Jenkins J, Buckling A, Schaum CE, Smirnoff N, Raven JA, Yvon-Durocher G. 2020**. Evolutionary temperature compensation of carbon fixation in marine phytoplankton. *Ecology Letters* **23**: 722–733.

**Barton S, Yang M, Chen H, Batchelor-McAuley C, Compton RG, Bouman HA, Rickaby REM. 2023**. A novel fluoro-electrochemical technique for classifying diverse marine nanophytoplankton. *Limnology and Oceanography: Methods* **21**: 656–672.

**Barton S, Yvon-Durocher G. 2019**. Quantifying the temperature dependence of growth rate in marine phytoplankton within and across species. *Limnology and Oceanography* **64**: 2081–2091.

**Bateman A, Martin MJ, O'Donovan C, Magrane M, Apweiler R, Alpi E, Antunes R, Arganiska J, Bely B, Bingley M, *et al.* 2015**. UniProt: a hub for protein information. *Nucleic Acids Research* **43**: D204–D212.

**Beaufort L, Probert I, De Garidel-Thoron T, Bendif EM, Ruiz-Pino D, Metzl N, Goyet C, Buchet N, Coupel P, Grelaud M, *et al.* 2011**. Sensitivity of coccolithophores to carbonate chemistry and ocean acidification. *Nature* **476**: 80–83.

**Behrenfeld MJ, Halsey KH, Milligan AJ. 2008**. Evolved physiological responses of phytoplankton to their integrated growth environment. *Philosophical Transactions of the Royal Society B: Biological Sciences* **363**: 2687.

**BeMiller JN. 2019**. Polysaccharides: Properties. *Carbohydrate Chemistry for Food Scientists*: 103–157.

**Bendif EM, Nevado B, Wong ELY, Hagino K, Probert I, Young JR, Rickaby REM, Filatov DA. 2019**. Repeated species radiations in the recent evolution of the key marine phytoplankton lineage Gephyrocapsa. *Nature Communications 2019 10:1* **10**: 1–9.

**Ben-Joseph O, Haan D de, Rechav K, Shimoni E, Levin-Zaidman S, Langer G, Probert I, Wheeler GL, Gal A. 2023**. Crystallization of Coccolith Calcite at Different Life-Cycle Phases Exhibits Distinct Degrees of Cellular Confinement. *Small Structures* **4**: 2200353.

**Benner I, Diner RE, Lefebvre SC, Li D, Komada T, Carpenter EJ, Stillman JH. 2013**. Emiliania huxleyi increases calcification but not expression of calcification-related genes in long-term exposure to elevated temperature and pCO2. *Philosophical Transactions of the Royal Society B: Biological Sciences* **368**.

**Berg JM, Tymoczko JL, Gatto GJ, Stryer L. 2015**. *Biochemistry*. New York: Freeman, WH.

**Berman-Frank I, Erez J. 1996**. Inorganic carbon pools in the bloom-forming dinoflagellate Peridinium gatunense. *Limnology and Oceanography* **41**: 1780–1789.

**Berry L, Taylor AR, Lucken U, Ryan KP, Brownlee C. 2002**. Calcification and inorganic carbon acquisition in coccolithophores. *Functional Plant Biology* **29**: 289–299.

**Billard C, Inouye I. 2004**. What is new in coccolithophore biology? *Coccolithophores*: 1–29.

**Bindoff NL, Willebrand J, Artale V, Cazenave A, Gregory JM, Gulev S, Hanawa K, Le Quere C, Levitus S, Nojiri Y, *et al.* 2007**. Observations: oceanic climate change and sea level. *An African savanna: synthesis of the Nylsvley study.*

**Blanco-Ameijeiras S, Lebrato M, Stoll HM, Iglesias-Rodriguez D, Müller MN, Méndez-Vicente A, Oschlies A. 2016**. Phenotypic Variability in the Coccolithophore Emiliania huxleyi. *PLOS ONE* **11**: e0157697.

**Blum M, Chang HY, Chuguransky S, Grego T, Kandasaamy S, Mitchell A, Nuka G, Paysan-Lafosse T, Qureshi M, Raj S, *et al.* 2021**. The InterPro protein families and domains database: 20 years on. *Nucleic Acids Research* **49**: D344–D354.

**De Bodt C, Van Oostende N, Harlay J, Sabbe K, Chou L. 2010**. Individual and interacting effects of pCO2 and temperature on Emiliania huxleyi calcification: Study of the calcite production, the coccolith morphology and the coccosphere size. *Biogeosciences* **7**: 1401–1412.

**Boller AJ, Thomas PJ, Cavanaugh CM, Scott KM. 2011**. Low stable carbon isotope fractionation by coccolithophore RubisCO. *Geochimica et Cosmochimica Acta* **75**: 7200–7207.

**Bolton CT, Hernández-Sánchez MT, Fuertes MÁ, González-Lemos S, Abrevaya L, Mendez-Vicente A, Flores JA, Probert I, Giosan L, Johnson J, *et al.* 2016**. Decrease in coccolithophore calcification and CO2 since the middle Miocene. *Nature Communications 2016 7:1* **7**: 1–13.

**Bolton CT, Stoll HM. 2013**. Late Miocene threshold response of marine algae to carbon dioxide limitation. *Nature 2013 500:7464* **500**: 558–562.

**Bolton CT, Stoll HM, Mendez-Vicente A. 2012**. Vital effects in coccolith calcite: Cenozoic climate-pCO2 drove the diversity of carbon acquisition strategies in coccolithophores? *Paleoceanography* **27**.

**Boron WF. 2004**. Regulation of intracellular pH. *American Journal of Physiology - Advances in Physiology Education* **28**: 160–179.

**Bown PR, Lees JA, Young JR. 2004**. Calcareous nannoplankton evolution and diversity through time. *Coccolithophores*: 481–508.

**Boyd PW, Strzepek R, Fu F, Hutchins DA. 2010**. Environmental control of open-ocean phytoplankton groups: Now and in the future. *Limnology and Oceanography* **55**: 1353–1376.

**Brand MD, Nicholls DG. 2011**. Assessing mitochondrial dysfunction in cells. *Biochemical Journal* **435**: 297–312.

**Bricker TM, Roose JL, Zhang P, Frankel LK. 2013**. The PsbP family of proteins. *Photosynthesis Research* **116**: 235–250.

**Broecker W, Clark E. 2009**. Ratio of coccolith CaCO3 to foraminifera CaCO3 in late Holocene deep sea sediments. *Paleoceanography* **24**.

**Brown RM. 1969**. Observations on the relationship of the golgi apparatus to wall formation in the marine chrysophycean alga Pleurochrysis scherffelii Pringsheim. *The Journal of cell biology* **41**: 109–123.

**Brown RM, Franke WW, Kleinig H, Falk H, Sitte P. 1970**. SCALE FORMATION IN CHRYSOPHYCEAN ALGAE I. Cellulosic and Noncellulosic Wall Components Made by the Golgi Apparatus. *Journal of Cell Biology* **45**: 246–271.

**Brown MR, Herth W, Franke W. W., Romanovicz D. 1973**. The role of the golgi apparatus in the biosynthesis and secretion of a cellulosic glycoprotein in pleurochrysis: A model system for the synthesis of structural polysaccharides. In: Loewus F, ed. Biogenesis of Plant cell wall Polysaccharides. Elsevier, 207–287.

**Brownlee C, Langer G, Wheeler GL. 2021**. Coccolithophore calcification: Changing paradigms in changing oceans. *Acta Biomaterialia* **120**: 4–11.

**Brownlee C, Wheeler GL, Taylor AR. 2015**. Coccolithophore biomineralization: New questions, new answers. *Seminars in Cell & Developmental Biology* **46**: 11–16.

**Buitenhuis ET, De Baar HJW, Veldhuis MJW. 1999**. Photosynthesis and calcification by Emiliania huxleyi (Prymnesiophyceae) as a function of inorganic carbon species. *Journal of Phycology* **35**: 949–959.

**Burkhardt S, Riebesell U, Zondervan I. 1999a**. Stable carbon isotope fractionation by marine phytoplankton in response to daylength, growth rate, and CO2 availability. *Marine Ecology Progress Series* **184**: 31–41.

**Burkhardt S, Riebesell U, Zondervan I. 1999b**. Effects of growth rate, CO2 concentration, and cell size on the stable carbon isotope fractionation in marine phytoplankton. *Geochimica et Cosmochimica Acta* **63**: 3729–3741.

**Burkhardt S, Zondervan I, Riebesell U. 1999c**. Effect of CO2 concentration on C:N:P ratio in marine phytoplankton: A species comparison. *Limnology and Oceanography* **44**: 683–690.

**Burns BD, Beardall J. 1987**. Utilization of inorganic carbon by marine microalgae. *Journal of Experimental Marine Biology and Ecology* **107**: 75–86.

**Byrnes AE, Slep KC. 2017**. TOG–tubulin binding specificity promotes microtubule dynamics and mitotic spindle formation. *The Journal of Cell Biology* **216**: 1641.

**Carbon S, Douglass E, Dunn N, Good B, Harris NL, Lewis SE, Mungall CJ, Basu S, Chisholm RL, Dodson RJ, *et al.* 2019**. The Gene Ontology Resource: 20 years and still GOing strong. *Nucleic Acids Research* **47**: D330–D338.

**Casareto B, Niraula M, Fujimura H, Biology YS-A, 2009 undefined**. **2009**. Effects of carbon dioxide on the coccolithophorid Pleurochrysis carterae in incubation experiments. *int-res.com*.

**Casey JR, Grinstein S, Orlowski J**. **2009**. Sensors and regulators of intracellular pH. *Nature Reviews Molecular Cell Biology 2009 11:1* **11**: 50–61.

**Catalá A**. **2009**. Lipid peroxidation of membrane phospholipids generates hydroxy-alkenals and oxidized phospholipids active in physiological and/or pathological conditions. *Chemistry and Physics of Lipids* **157**: 1–11.

**Chandel NS**. **2021**. Glycolysis. *Cold Spring Harbor Perspectives in Biology* **13**.

**Chauhan N, Rickaby REM**. **2024**. Size-dependent dynamics of the internal carbon pool drive isotopic vital effects in calcifying phytoplankton. *Geochimica et Cosmochimica Acta* **373**: 35–51.

**Chavez FP, Bertrand A, Guevara-Carrasco R, Soler P, Csirke J**. **2008**. The northern Humboldt Current System: Brief history, present status and a view towards the future. *Progress in Oceanography* **79**: 95–105.

**Chen S, Gagnon AC, Adkins JF**. **2018**. Carbonic anhydrase, coral calcification and a new model of stable isotope vital effects. *Geochimica et Cosmochimica Acta* **236**: 179–197.

**Chen L, Zhang Z, Hoshino A, Zheng HD, Morley M, Arany Z, Rabinowitz JD**. **2019**. NADPH production by the oxidative pentose-phosphate pathway supports folate metabolism. *Nature metabolism* **1**: 404.

**Chisholm SW**. **1992**. Phytoplankton Size. *Primary Productivity and Biogeochemical Cycles in the Sea*: 213–237.

**Chondrogianni N, Petropoulos I, Grimm S, Georgila K, Catalgol B, Friguet B, Grune T, Gonos ES**. **2014**. Protein damage, repair and proteolysis. *Molecular Aspects of Medicine* **35**: 1–71.

**Chrachri A, Hopkinson BM, Flynn K, Brownlee C, Wheeler GL**. **2018**. Dynamic changes in carbonate chemistry in the microenvironment around single marine phytoplankton cells. *Nature Communications 2017 9:1* **9**: 1–12.

**Claxton L**. **2022**. Exploring the carbon isotopic ratio and chemistry of coccoliths and coccolith associated polysaccharides as a proxy for $CO_2$.

**Claxton LM, McClelland HLO, Hermoso M, Rickaby REM**. **2022**. Eocene emergence of highly calcifying coccolithophores despite declining atmospheric CO2. *Nature Geoscience 2022 15:10* **15**: 826–831.

**Cobbe N, Heck MMS**. **2000**. Review: SMCs in the World of Chromosome Biology— From Prokaryotes to Higher Eukaryotes. *Journal of Structural Biology* **129**: 123–143.

**Cros L, Estrada M**. **2013**. Holo-heterococcolithophore life cycles: ecological implications. *Marine Ecology Progress Series* **492**: 57–68.

**Crowley TJ**. **2000**. Causes of climate change over the past 1000 years. *Science* **289**: 270–277.

**Cunha SR, Mohler PJ**. **2009**. Ankyrin protein networks in membrane formation and stabilization. *Journal of Cellular and Molecular Medicine* **13**: 4364–4376.

**Daines SJ, Clark JR, Lenton TM**. **2014**. Multiple environmental controls on phytoplankton growth strategies determine adaptive responses of the N : P ratio. *Ecology Letters* **17**: 414–425.

**Dalle-Donne I, Rossi R, Milzani A, Di Simplicio P, Colombo R**. **2001**. The actin cytoskeleton response to oxidants: from small heat shock protein phosphorylation to changes in the redox state of actin itself. *Free Radical Biology and Medicine* **31**: 1624–1632.

**Daniels C, Poulton A, Young J, Esposito M, Humphreys MP, Ribas-Ribas M, Tynan E, Tyrrell T. 2016**. Species-specific calcite production reveals Coccolithus pelagicus as the key calcifier in the Arctic Ocean. *Marine Ecology Progress Series* **555**: 29–47.

**Daniels CJ, Sheward RM, Poulton AJ. 2014**. Biogeochemical implications of comparative growth rates of Emiliania huxleyi and Coccolithus species. *Biogeosciences* **11**: 6915–6925.

**Von Dassow P, Montresor M. 2011**. Unveiling the mysteries of phytoplankton life cycles: patterns and opportunities behind complexity. *Journal of Plankton Research* **33**: 3–12.

**Daumann M, Hickl D, Zimmer D, DeTar RA, Kunz HH, Möhlmann T. 2018**. Characterization of filament-forming CTP synthases from Arabidopsis thaliana. *The Plant journal : for cell and molecular biology* **96**: 316.

**Dawes IW; 2000**. Responses of Eukaryotic Cells to Oxidative Stress. *Journal of Applied Biological Chemistry* **43**: 211–217.

**Dedman CJ, Barton S, Fournier M, Rickaby REM. 2023a**. The cellular response to ocean warming in Emiliania huxleyi. *Frontiers in Microbiology* **14**: 1177349.

**Deng Y, Ye J, Mi H. 2003**. Effects of Low CO2 on NAD(P)H Dehydrogenase, a Mediator of Cyclic Electron Transport Around Photosystem I in the Cyanobacterium Synechocystis PCC6803. *Plant and Cell Physiology* **44**: 534–540.

**Deutscher MP. 2006**. Degradation of RNA in bacteria: comparison of mRNA and stable RNA. *Nucleic Acids Research* **34**: 659–666.

**Dickson AG, Millero FJ. 1987**. A comparison of the equilibrium constants for the dissociation of carbonic acid in seawater media. *Deep Sea Research Part A. Oceanographic Research Papers* **34**: 1733–1743.

**Dickson AG, Sabine CL, Christian JR. 2007**. Guide to Best Practices for Ocean CO2 measurements. PICES Special Publication. *Guide to Best Practices for Ocean CO2 measurements. PICES Special Publication* **3**: 191 pp.

**Dixon GK, Brownlee C, Merrett MJ. 1989**. Measurement of internal pH in the coccolithophoreEmiliania huxleyi using 2',7'-bis-(2-carboxyethyl)-5(and-6)carboxyfluorescein acetoxymethylester and digital imaging microscopy. *Planta* **178**: 443–449.

**Dolan SK, Welch M. 2018**. The Glyoxylate Shunt, 60 Years On. *Annual Review of Microbiology* **72**: 309–330.

**Doney SC, Fabry VJ, Feely RA, Kleypas JA. 2009**. Ocean acidification: The other CO2 problem. *Annual Review of Marine Science* **1**: 169–192.

**Dudley WC, Blackwelder P, Brand L, Duplessy JC. 1986**. Stable isotopic composition of coccoliths. *Marine Micropaleontology* **10**: 1–8.

**Durak GM, Brownlee C, Wheeler GL. 2017**. The role of the cytoskeleton in biomineralisation in haptophyte algae. *Scientific Reports* **7**.

**Eberhard S, Finazzi G, Wollman FA. 2008**. The Dynamics of Photosynthesis. *https://doi.org/10.1146/annurev.genet.42.110807.091452* **42**: 463–515.

**Eikrem W, Medlin LK, Henderiks J, Rokitta S, Rost B, Probert I, Throndsen J, Edvardsen B. 2016**. Haptophyta. *Handbook of the Protists*: 1–61.

**Eiler JM. 2007**. "Clumped-isotope" geochemistry—The study of naturally-occurring, multiply-substituted isotopologues. *Earth and Planetary Science Letters* **262**: 309–327.

**Elser JJ. 2012**. Phosphorus: a limiting nutrient for humanity? *Current Opinion in Biotechnology* **23**: 833–838.

**Elser JJ, Acharya K, Kyle M, Cotner J, Makino W, Markow T, Watts T, Hobbie S, Fagan W, Schade J, *et al.* 2003**. Growth rate–stoichiometry couplings in diverse biota. *Ecology Letters* **6**: 936–943.

**Elzenga JTM, Prins HBA, Stefels J. 2000**. The role of extracellular carbonic anhydrase activity in inorganic carbon utilization of Phaeocystis globosa (Prymnesiophyceae): A comparison with other marine algae using the isotopic disequilibrium technique. *Limnology and Oceanography* **45**: 372–380.

**Emeis K, Eggert A, Flohr A, Lahajnar N, Nausch G, Neumann A, Rixen T, Schmidt M, Van der Plas A, Wasmund N. 2018**. Biogeochemical processes and turnover rates in the Northern Benguela Upwelling System. *Journal of Marine Systems* **188**: 63–80.

**Engel A, Abramson L, Szlosek J, Liu Z, Stewart G, Hirschberg D, Lee C. 2009**. Investigating the effect of ballasting by CaCO3 in Emiliania huxleyi, II: Decomposition of particulate organic matter. *Deep Sea Research Part II: Topical Studies in Oceanography* **56**: 1408–1419.

**Engel A, Novoa CC, Wurst M, Endres S, Tang T, Schartau M, Lee C. 2014**. No detectable effect of CO2 on elemental stoichiometry of Emiliania huxleyi in nutrient-limited, acclimated continuous cultures. *Marine Ecology Progress Series* **507**: 15–30.

**Falkowski PG. 2000**. Rationalising elemental ratios in unicellular algae. *J. Phycol* **36**: 3–6.

**Falkowski PG, Barber RT, Smetacek V. 1998**. Biogeochemical controls and feedbacks on ocean primary production. *Science* **281**: 200–206.

**Falkowski P, Scholes RJ, Boyle E, Canadell J, Canfield D, Elser J, Gruber N, Hibbard K, Hogberg P, Linder S, *et al.* 2000**. The global carbon cycle: A test of our knowledge of earth as a system. *Science* **290**: 291–296.

**Faucher G, Riebesell U, Thomas Bach L. 2020**. Can morphological features of coccolithophores serve as a reliable proxy to reconstruct environmental conditions of the past? *Climate of the Past* **16**: 1007–1025.

**Feng Y, Roleda MY, Armstrong E, Boyd PW, Hurd CL. 2017**. Environmental controls on the growth, photosynthetic and calcification rates of a Southern Hemisphere strain of the coccolithophore Emiliania huxleyi. *Limnology and Oceanography* **62**: 519–540.

**Feng Y, Roleda MY, Armstrong E, Law CS, Boyd PW, Hurd CL. 2018**. Environmental controls on the elemental composition of a Southern Hemisphere strain of the coccolithophore Emiliania huxleyi. *Biogeosciences* **15**: 581–595.

**Feng Y, Warner ME, Zhang Y, Sun J, Fu FX, Rose JM, Hutchins DA. 2008**. Interactive effects of increased pCO2, temperature and irradiance on the marine coccolithophore Emiliania huxleyi (Prymnesiophyceae). *European Journal of Phycology* **43**: 87–98.

**Fichtinger-Schepman AM, Kamerling J, Versluis C, Vliegenthart JFG. 1980**. STRUCTURAL ANALYSIS OF ACIDIC OLIGOSACCHARIDES DERIVED FROM THE METHYLATED, ACIDIC POLYSACCHARIDE ASSOCIATED WITH COCCOLITHS OF Emiliania huxleyi (LOHMANN) KAMPTNER. *Carbohydrate Research* **86**: 215–225.

**Fidelman ML, Seeholzer SH, Walsh KB, Moore RD. 1982**. Intracellular pH mediates action of insulin on glycolysis in frog skeletal muscle. *https://doi.org/10.1152/ajpcell.1982.242.1.C87* **11**.

**Field CB, Behrenfeld MJ, Randerson JT, Falkowski P. 1998**. Primary production of the biosphere: Integrating terrestrial and oceanic components. *Science* **281**: 237–240.

**Fiorini S, Middelburg J, Phycology JG-J of, 2011 undefined. 2011**. Testing the effects of elevated Pco2 on coccolithophores (Prymnesiophyceae): Comparison between haploid and diploid life stages 1. *Wiley Online Library* **47**: 1281–1291.

**Frada M, Bendif E, Keuter S, Probert I. 2018**. The private life of coccolithophores. *Perspectives in Phycology*.

**Fritz KS, Petersen DR. 2013**. An overview of the chemistry and biology of reactive aldehydes. *Free Radical Biology and Medicine* **59**: 85–91.

**Fukuda SY, Suzuki Y, Shiraiwa Y. 2014**. Difference in physiological responses of growth, photosynthesis and calcification of the coccolithophore Emiliania huxleyi to acidification by acid and CO2 enrichment. *Photosynthesis Research* **121**: 299–309.

**Gafar NA, Eyre BD, Schulz KG. 2019a**. A comparison of species specific sensitivities to changing light and carbonate chemistry in calcifying marine phytoplankton. *Scientific Reports 2019 9:1* **9**: 1–12.

**Gafar NA, Eyre BD, Schulz KG. 2019c**. Particulate inorganic to organic carbon production as a predictor for coccolithophorid sensitivity to ongoing ocean acidification. *Limnology and Oceanography Letters* **4**: 62–70.

**Gal A, Sviben S, Wirth R, Schreiber A, Lassalle-Kaiser B, Faivre D, Scheffel A, Gal A, Sviben S, Scheffel A, *et al.* 2017**. Trace-Element Incorporation into Intracellular Pools Uncovers Calcium-Pathways in a Coccolithophore. *Advanced Science* **4**: 1700088.

**Gal A, Wirth R, Kopka J, Fratzl P, Faivre D, Scheffel A. 2016**. Macromolecular recognition directs calcium ions to coccolith mineralization sites. *Science* **353**: 590–593.

**Gao K, Aruga Y, Asada K, Ishihara T, Akano T, Kiyohara M. 1991**. Enhanced growth of the red algaPorphyra yezoensis Ueda in high CO2 concentrations. *Journal of Applied Phycology 1991 3:4* **3**: 355–362.

**Gao K, Zheng Y. 2010**. Combined effects of ocean acidification and solar UV radiation on photosynthesis, growth, pigmentation and calcification of the coralline alga Corallina sessilis (Rhodophyta). *Global Change Biology* **16**: 2388–2398.

**Garcia NS, Bonachela JA, Martiny AC. 2016**. Interactions between growth-dependent changes in cell size, nutrient supply and cellular elemental stoichiometry of marine Synechococcus. *The ISME Journal* **10**: 2715–2724.

**Gately JA, Kim SM, Jin B, Brzezinski MA, Iglesias-Rodriguez MD. 2023**. Coccolithophores and diatoms resilient to ocean alkalinity enhancement: A glimpse of hope? *Science Advances* **9**.

**Geider RJ. 1987**. Light and Temperature Dependence of the Carbon to Chlorophyll a Ratio in Microalgae and Cyanobacteria: Implications for Physiology and Growth of Phytoplankton on JSTOR. *The New Phytologist* **106**: 1–34.

**Geider RJ, Mooreb CM, Rossc ON. 2009**. The role of cost–benefit analysis in models of phytoplankton growth and acclimation. *Plant Ecology & Diversity* **2**: 165–178.

**Geider RJ, La Roche J. 2002**. Redfield revisited: Variability of C:N:P in marine microalgae and its biochemical basis. *European Journal of Phycology* **37**: 1–17.

**Geisen M, Billard C, Broerse ATC, Cros L, Probert I, Young JR. 2002**. Life-cycle associations involving pairs of holococcolithophorid species: intraspecific variation or cryptic speciation? *European Journal of Phycology* **37**: 531–550.

**Geisen M, Young JR, Probert I, Sáez AG, Baumann K-H, Sprengel C, Bollmann J, Cros L, de Vargas C, Medlin LK. 2004**. Species level variation in coccolithophores. *Coccolithophores*: 327–366.

**Gerecht AC, Šupraha L, Edvardsen B, Probert I, Henderiks J. 2014**. High temperature decreases the PIC / POC ratio and increases phosphorus requirements in Coccolithus pelagicus (Haptophyta). *Biogeosciences* **11**: 3531–3545.

**Giuffre AJ, Hamm LM, Han N, De Yoreo JJ, Dove PM. 2013**. Polysaccharide chemistry regulates kinetics of calcite nucleation through competition of interfacial energies. *Proceedings of the National Academy of Sciences of the United States of America* **110**: 9261–9266.

**Godrijan J, Drapeau D, Balch WM. 2020**. Mixotrophic uptake of organic compounds by coccolithophores. *Limnology and Oceanography* **65**: 1410–1421.

**Golda-VanEeckhoutte RL, Roof LT, Needoba JA, Peterson TD. 2018**. Determination of intracellular pH in phytoplankton using the fluorescent probe, SNARF, with detection by fluorescence spectroscopy. *Journal of Microbiological Methods* **152**: 109–118.

**Gómez I, López-Figueroa F, Ulloa N, Morales V, Lovengreen C, Huovinen P, Hess S. 2004**. Patterns of photosynthesis in 18 species of intertidal macroalgae from southern Chile. *Marine Ecology Progress Series* **270**: 103–116.

**Gong S, Jin X, Xiao Y, Li Z. 2020**. Ocean Acidification and Warming Lead to Increased Growth and Altered Chloroplast Morphology in the Thermo-Tolerant Alga Symbiochlorum hainanensis. *Frontiers in Plant Science* **11**.

**González-Lanchas A, Hernández-Almeida I, Flores JA, Sierro FJ, Guitian J, Stoll HM. 2021**. Carbon Isotopic Fractionation of Alkenones and Gephyrocapsa Coccoliths Over the Late Quaternary (Marine Isotope Stages 12–9) Glacial-Interglacial Cycles at the Western Tropical Atlantic. *Paleoceanography and Paleoclimatology* **36**.

**Gore S, Renforth P, Perkins R. 2019**. The potential environmental response to increasing ocean alkalinity for negative emissions. *Mitigation and Adaptation Strategies for Global Change* **24**: 1191–1211.

**Green JC, Hori T. 1986**. The ultrastructure of the flagellar root system of Imantonia rotunda (Prymnesiophyceae). *British Phycological Journal* **21**: 5–18.

**Griffiths MJ, Garcin C, van Hille RP, Harrison STL. 2011**. Interference by pigment in the estimation of microalgal biomass concentration by optical density. *Journal of Microbiological Methods* **85**: 119–123.

**Gruber N. 2008**. The Marine Nitrogen Cycle: Overview and Challenges. In: Nitrogen in the marine environment 2. 1–50.

**Guillard RR, Ryther JH. 1962**. Studies of marine planktonic diatoms: I. Cyclotella nana Hustedt, and Detonula confervacea (Cleve) Gran. *Canadian journal of microbiology* **8**: 229–239.

**Gussone N, Langer G, Thoms S, Nehrke G, Eisenhauer A, Riebesell U, Wefer G. 2006**. Cellular calcium pathways and isotope fractionation in Emiliania huxleyi. *Geology* **34**: 625–628.

**Guy RD, Fogel ML, Berry JA. 1993**. Photosynthetic Fractionation of the Stable Isotopes of Oxygen and Carbon. *Plant Physiology* **101**: 37–47.

**Hahn A, Vonck J, Mills DJ, Meier T, Kühlbrandt W. 2018**. Structure, mechanism, and regulation of the chloroplast ATP synthase. *Science* **360**.

**Halevy I, Bachan A. 2017**. The geologic history of seawater pH. *Science* **355**: 1069–1071.

**Halloran PR, Hall IR, Colmenero-Hidalgo E, M. Rickaby RE. 2008**. Evidence for a multi-species coccolith volume change over the past two centuries: Understanding a potential ocean acidification response. *Biogeosciences* **5**: 1651–1655.

**Hawkins EK, Lee JJ. 2001**. Architecture of the Golgi apparatus of a scale-forming alga: Biogenesis and transport of scales. *Protoplasma* **216**: 227–238.

**Hay WW. 2004**. Carbonate fluxes and calcareous nannoplankton. *Coccolithophores*: 509–528.

**He S, Crans VL, Jonikas MC. 2023**. The pyrenoid: the eukaryotic CO2-concentrating organelle. *The Plant Cell* **35**: 3236.

**Healey FP. 1978**. Physiological indicators of nutrient deficiency in algae. *SIL Communications, 1953-1996* **21**: 34–41.

**Heidenreich E, Wördenweber R, Kirschhöfer F, Nusser M, Friedrich F, Fahl K, Kruse O, Rost B, Franzreb M, Brenner-Weiß G, *et al.* 2019**. Ocean acidification has little effect on the biochemical composition of the coccolithophore Emiliania huxleyi. *PLOS ONE* **14**: e0218564.

**Heinze I, Dau H. 1996**. The pH-dependence of the photosystem II fluorescence: Cooperative transition to a quenching state. *Berichte der Bunsengesellschaft/Physical Chemistry Chemical Physics* **100**: 2008–2013.

**Henderiks J, Pagani M. 2008**. Coccolithophore cell size and the Paleogene decline in atmospheric CO2. *Earth and Planetary Science Letters* **269**: 576–584.

**Henderiks J, Rickaby REM. 2007**. A coccolithophore concept for constraining the Cenozoic carbon cycle. *Biogeosciences* **4**: 323–329.

**Henriksen K, Stipp SLS. 2009**. Controlling biomineralization: The effect of solution composition on coccolith polysaccharide functionality. *Crystal Growth and Design* **9**: 2088–2097.

**Henriksen K, Stipp SLS, Young JR, Marsh ME. 2004**. Biological control on calcite crystallization: AFM investigation of coccolith polysaccharide function. *American Mineralogist* **89**: 1709–1716.

**Herfort L, Loste E, Meldrum F, Thake B. 2004**. Structural and physiological effects of calcium and magnesium in Emiliania huxleyi (Lohmann) Hay and Mohler. *Journal of Structural Biology* **148**: 307–314.

**Herfort L, Thake B, Roberts J. 2002**. Acquisition and use of bicarbonate by Emiliania huxleyi. *New Phytologist* **156**: 427–436.

**Hermoso M. 2014**. Coccolith-Derived Isotopic Proxies in Palaeoceanography: Where Geologists Need Biologists. *Cryptogamie, Algologie* **35**: 323–351.

**Hermoso M. 2015**. Control of ambient pH on growth and stable isotopes in phytoplanktonic calcifying algae. *Paleoceanography* **30**: 1100–1112.

**Hermoso M, Candelier Y, Browning TJ, Minoletti F. 2015**. Environmental control of the isotopic composition of subfossil coccolith calcite: Are laboratory culture data transferable to the natural environment? *GeoResJ* **7**: 35–42.

**Hermoso M, Chan IZX, McClelland HLO, Heureux AMC, Rickaby REM. 2016a**. Vanishing coccolith vital effects with alleviated carbon limitation. *Biogeosciences* **13**: 301–312.

**Hermoso M, Horner TJ, Minoletti F, Rickaby REM. 2014**. Constraints on the vital effect in coccolithophore and dinoflagellate calcite by oxygen isotopic modification of seawater. *Geochimica et Cosmochimica Acta* **141**: 612–627.

**Hermoso M, McClelland HLO, Hirst JS, Minoletti F, Bonifacie M, Rickaby REM. 2020**. Towards the use of the coccolith vital effects in palaeoceanography: A field investigation during the middle Miocene in the SW Pacific Ocean. *Deep Sea Research Part I: Oceanographic Research Papers* **160**: 103262.

**Hermoso M, Minoletti F, Aloisi G, Bonifacie M, Mcclelland HLO, Labourdette N, Renforth P, Chaduteau C, Rickaby REM. 2016b**. An explanation for the 18 O excess in Noelaerhabdaceae coccolith calcite. *Geochimica et Cosmochimica Acta* **189**: 132–142.

**Heureux A. 2016**. Carbon fixation in eukaryotic marine algae: Evolution of photosynthetic machinery and isotopic footprints [PhD Thesis].

**Hirooka S, Hirose Y, Kanesaki Y, Higuchi S, Fujiwara T, Onuma R, Era A, Ohbayashi R, Uzuka A, Nozaki H, *et al.* 2017**. Acidophilic green algal genome provides insights into adaptation to an acidic environment. *Proceedings of the National Academy of Sciences of the United States of America* **114**: E8304–E8313.

**Holtz LM, Wolf-Gladrow D, Thoms S. 2015**. Numerical cell model investigating cellular carbon fluxes in Emiliania huxleyi. *Journal of Theoretical Biology* **364**: 305–315.

**Holtz LM, Wolf-Gladrow D, Thoms S. 2017**. Stable carbon isotope signals in particulate organic and inorganic carbon of coccolithophores – A numerical model study for Emiliania huxleyi. *Journal of Theoretical Biology* **420**: 117–127.

**Hönisch B, Ridgwell A, Schmidt DN, Thomas E, Gibbs SJ, Sluijs A, Zeebe R, Kump L, Martindale RC, Greene SE, *et al.* 2012**. The geological record of ocean acidification. *Science* **335**: 1058–1063.

**Hoppe CJM, Langer G, Rost B. 2011**. Emiliania huxleyi shows identical responses to elevated pCO2 in TA and DIC manipulations. *Journal of Experimental Marine Biology and Ecology* **406**: 54–62.

**Houdan A, Bonnard A, Fresnel J, Fouchard S, Billard C, Probert I. 2004**. Toxicity of coastal coccolithophores (Prymnesiophyceae, Haptophyta). *Journal of Plankton Research* **26**: 875–883.

**Houdan A, Probert I, Zatylny C, Véron B, Billard C. 2006**. Ecology of oceanic coccolithophores. I. Nutritional preferences of the two stages in the life cycle of Coccolithus braarudii and Calcidiscus leptoporus. *Aquatic Microbial Ecology* **44**: 291–301.

**Iglesias-Rodriguez MD, Buitenhuis ET, Raven JA, Schofield O, Poulton AJ, Gibbs S, Halloran PR, De Baar HJW. 2008a**. Response to comment on 'Phytoplankton calcification in a high-CO 2 world'. *Science* **322**.

**Iglesias-Rodriguez MD, Halloran PR, Rickaby REM, Hall IR, Colmenero-Hidalgo E, Gittins JR, Green DRH, Tyrrell T, Gibbs SJ, Von Dassow P, *et al.* 2008b**. Phytoplankton calcification in a high-CO2 world. *Science* **320**: 336–340.

**Inzé D, Montagu M Van. 1995**. Oxidative stress in plants. *Current Opinion in Biotechnology* **6**: 153–158.

**Isensee K, Erez J, Stoll HM. 2014**. Detection of a variable intracellular acid-labile carbon pool in Thalassiosira weissflogii (Heterokontophyta) and Emiliania huxleyi (Haptophyta) in response to changes in the seawater carbon system. *Physiologia Plantarum* **150**: 321–338.

**Jähne B, Heinz G, Dietrich W. 1987**. Measurement of the diffusion coefficients of sparingly soluble gases in water. *Journal of Geophysical Research: Oceans* **92**: 10767–10776.

**Jin P, Gao K, Beardall J. 2013**. EVOLUTIONARY RESPONSES OF A COCCOLITHOPHORID GEPHYROCAPSA OCEANICA TO OCEAN ACIDIFICATION. *Evolution* **67**: 1869–1878.

**Johnson R, Langer G, Rossi S, Probert I, Mammone M, Ziveri P. 2022**. Nutritional response of a coccolithophore to changing pH and temperature. *Limnology and Oceanography* **67**: 2309–2324.

**Jones BM, Iglesias-Rodriguez MD, Skipp PJ, Edwards RJ, Greaves MJ, Young JR, Elderfield H, O'Connor CD. 2013**. Responses of the Emiliania huxleyi Proteome to Ocean Acidification. *PLOS ONE* **8**: e61868.

**Jordan RW. 2009**. Protists: Coccolithophores. In: Encyclopedia of Microbiology. 593–605.

**Juan CA, de la Lastra JMP, Plou FJ, Pérez-Lebeña E. 2021**. The Chemistry of Reactive Oxygen Species (ROS) Revisited: Outlining Their Role in Biological Macromolecules (DNA, Lipids and Proteins) and Induced Pathologies. *International Journal of Molecular Sciences 2021, Vol. 22, Page 4642* **22**: 4642.

**Kadner RJ, Murphy GP, Stephens CM. 1992**. Two mechanisms for growth inhibition by elevated transport of sugar phosphates in Escherichia coli. *Journal of general microbiology* **138**: 2007–2014.

**Kang L, Kim HS, Kwon YS, Ke Q, Ji CY, Park SC, Lee HS, Deng X, Kwak SS. 2017**. IbOr regulates photosynthesis under heat stress by stabilizing ibpsbp in sweetpotato. *Frontiers in Plant Science* **8**: 267421.

**Kaplan A, Badger MR, Berry JA. 1980**. Photosynthesis and the intracellular inorganic carbon pool in the bluegreen alga Anabaena variabilis: Response to external CO2 concentration. *Planta* **149**: 219–226.

**Kaplan A, Reinhold L. 2003**. CO2 Concentrating Mechanisms in photosynthetic microorganisms. *Annual Review of Plant Physiology and Plant Molecular Biology* **50**: 539–570.

**Käse L, Geuer JK. 2018**. Phytoplankton Responses to Marine Climate Change – An Introduction. *YOUMARES 8 – Oceans Across Boundaries: Learning from each other*: 55–71.

**Kawachi M, Inouye I. 1994**. Observations on the flagellar apparatus of a coccolithophorid, Cruciplacolithus neohelis (Prymnesiophyceae). *Journal of Plant Research* **107**: 53–62.

**Kawachi M, Inouye I, Maeda O, Chihara M. 1991**. The haptonema as a food-capturing device: observations on Chrysochromulina hirta (Prymnesiophyceae). *Phycologia* **30**: 563–573.

**Keller MD, Guillard RRL. 1985**. *Factors significant to marine dinoflagellate culture* (DM Anderson, Ed.). New York: Elsevier.

**Keller K, Morel FMM. 1999**. A model of carbon isotopic fractionation and active carbon uptake in phytoplankton. *Marine Ecology Progress Series* **182**: 295–298.

**Keller MD, Selvin RC, Claus W, Guillard RR. 1987**. Media for the culture of oceanic ultraphytoplankton . *Journal of phycology* **23**: 633–638.

**Kideys AE, Soydemir N, Eker E, Vladymyrov V, Soloviev D, Melin F. 2005**. Phytoplankton distribution in the Caspian Sea during March 2001. *Hydrobiologia* **543**: 159–168.

**Kim ST, O'Neil JR. 1997**. Equilibrium and nonequilibrium oxygen isotope effects in synthetic carbonates. *Geochimica et Cosmochimica Acta* **61**: 3461–3475.

**Kistner F, Grossmann JL, Sinn LR, Demichev V. 2023**. QuantUMS: uncertainty minimisation enables confident quantification in proteomics. *bioRxiv*: 2023.06.20.545604.

**Kitidis V, Hardman-Mountford NJ, Litt E, Brown I, Cummings D, Hartman S, Hydes D, Fishwick JR, Harris C, Martinez-Vicente V, *et al.* 2012**. Seasonal dynamics of the carbonate system in the Western English Channel. *Continental Shelf Research* **42**: 30–40.

**Klaas C, Archer DE. 2002**. Association of sinking organic matter with various types of mineral ballast in the deep sea: Implications for the rain ratio. *Global Biogeochemical Cycles* **16**: 63–1.

**Kleijne A. 1990**. Distribution and malformation of extant calcareous nannoplankton in the Indonesian Seas. *Marine Micropaleontology* **16**: 293–316.

**Koppelle S, López-Escardó D, Brussaard CPD, Huisman J, Philippart CJM, Massana R, Wilken S. 2022**. Mixotrophy in the bloom-forming genus Phaeocystis and other haptophytes. *Harmful Algae* **117**: 102292.

**Korenbaum E, Rivero F. 2002**. Calponin homology domains at a glance. *Journal of Cell Science* **115**: 3543–3545.

**Kottmeier DM, Chrachri A, Langer G, Helliwell KE, Wheeler GL, Brownlee C. 2022**. Reduced H+ channel activity disrupts pH homeostasis and calcification in coccolithophores at low ocean pH. *Proceedings of the National Academy of Sciences of the United States of America* **119**: e2118009119.

**Kottmeier D, Rokitta S, Phytologist BR-N, 2016 undefined. 2016a**. Acidification, not carbonation, is the major regulator of carbon fluxes in the coccolithophore Emiliania huxleyi. *Wiley Online Library* **211**: 126–137.

**Kottmeier DM, Rokitta SD, Rost B. 2016b**. Acidification, not carbonation, is the major regulator of carbon fluxes in the coccolithophore Emiliania huxleyi. *New Phytologist* **211**: 126–137.

**Kottmeier DM, Rokitta SD, Rost B. 2016c**. H+-driven increase in CO2 uptake and decrease in HCO3− uptake explain coccolithophores' acclimation responses to ocean acidification. *Limnology and Oceanography* **61**: 2045–2057.

**Kottmeier D, Rokitta SD, Tortell PD, Rost B. 2014**. Strong shift from HCO3- To CO2 uptake in Emiliania huxleyi with acidification: New approach unravels acclimation versus short-term pH effects. *Photosynthesis Research* **121**: 265–275.

**Krajewska B. 2009**. Ureases I. Functional, catalytic and kinetic properties: A review. *Journal of Molecular Catalysis B: Enzymatic* **59**: 9–21.

**Krueger-Hadfield SA, Balestreri C, Schroeder J, Highfield A, Helaouët P, Allum J, Moate R, Lohbeck KT, Miller PI, Riebesell U, *et al.* 2014**. Genotyping an Emiliania huxleyi (prymnesiophyceae) bloom event in the North Sea reveals evidence of asexual reproduction. *Biogeosciences* **11**: 5215–5234.

**Krug S, Schulz K, Biogeosciences UR-, 2011 undefined. 2011**. Effects of changes in carbonate chemistry speciation on Coccolithus braarudii: a discussion of coccolithophorid sensitivities. *bg.copernicus.org* **8**: 771–777.

**Krumhardt KM, Lovenduski NS, Iglesias-Rodriguez MD, Kleypas JA. 2017**. Coccolithophore growth and calcification in a changing ocean. *Progress in Oceanography* **159**: 276–295.

**ter Kuile B, Erez J. 1988**. The size and function of the internal inorganic carbon pool of the foraminifer Amphistegina lobifera. *Marine Biology* **99**: 481–487.

**Kültz D. 2004**. MOLECULAR AND EVOLUTIONARY BASIS OF THE CELLULAR STRESS RESPONSE. *https://doi.org/10.1146/annurev.physiol.67.040403.103635* **67**: 225–257.

**Kwon EY, Dunne JP, Lee K. 2024**. Biological export production controls upper ocean calcium carbonate dissolution and $CO_2$ buffer capacity. *Science Advances* **10**: 779.

**Langer G, Bode M. 2011**. CO2 mediation of adverse effects of seawater acidification in Calcidiscus leptoporus. *Geochemistry, Geophysics, Geosystems* **12**: n/a-n/a.

**Langer G, Geisen M, Baumann KH, Kläs J, Riebesell U, Thoms S, Young JR. 2006**. Species-specific responses of calcifying algae to changing seawater carbonate chemistry. *Geochemistry, Geophysics, Geosystems* **7**.

**Langer G, Jie VW, Kottmeier D, Flori S, Sturm D, de Vries J, Harper GM, Brownlee C, Wheeler G. 2023a**. Distinct physiological responses of Coccolithus braarudii life cycle phases to light intensity and nutrient availability. *European Journal of Phycology* **58**: 58–71.

**Langer G, Nehrke G, Probert I, Ly J, Ziveri P. 2009**. Strain-specific responses of Emiliania huxleyi to changing seawater carbonate chemistry. *Biogeosciences* **6**: 2637–2646.

**Langer G, Probert I, Cox MB, Taylor A, Harper GM, Brownlee C, Wheeler G. 2023b**. The Effect of cytoskeleton inhibitors on coccolith morphology in Coccolithus braarudii and Scyphosphaera apsteinii. *Journal of Phycology* **59**: 87–96.

**Langer G, Taylor AR, Walker CE, Meyer EM, Ben Joseph O, Gal A, Harper GM, Probert I, Brownlee C, Wheeler GL. 2021**. Role of silicon in the development of complex crystal shapes in coccolithophores. *New Phytologist* **231**: 1845–1857.

**LaRoche J, Rost B, Engel A. 2010**. Bioassays, batch culture and chemostat experimentation. *In Approaches and tools to manipulate the carbonate chemistry., Guide for Best Practices in Ocean Acidification Research and Data Reporting.*: 81–94.

**Laws EA, Popp BN, Bidigare RR, Kennicutt MC, Macko SA. 1995**. Dependence of phytoplankton carbon isotopic composition on growth rate and [CO2)aq: Theoretical considerations and experimental results. *Geochimica et Cosmochimica Acta* **59**: 1131–1138.

**Laws EA, Popp BN, Cassar N, Tanimoto J. 2002**. 13C discrimination patterns in oceanic phytoplankton: likely influence of CO2 concentrating mechanisms, and implications for palaeoreconstructions. *Functional Plant Biology* **29**: 323–333.

**Laws EA, Thompson PA, Popp BN, Bidigare RR. 1998**. Sources of inorganic carbon for marine microalgal photosynthesis: A reassessment of δ13C data from batch culture studies of Thalassiosira pseudonana and Emiliania huxleyi. *Limnology and Oceanography* **43**: 136–142.

**Lee RBY, Mavridou DAI, Papadakos G, McClelland HLO, Rickaby REM. 2016**. The uronic acid content of coccolith-associated polysaccharides provides insight into coccolithogenesis and past climate. *Nature Communications* **7**.

**Lefebvre SC, Harris G, Webster R, Leonardos N, Geider RJ, Raines CA, Read BA, Garrido JL. 2010**. Characterization and expression analysis of the LHCF gene family in emiliania huxleyi (haptophyta) reveals differential responses to light and co2. *Journal of Phycology* **46**: 123–134.

**Lenning K Van, Probert I, Latasa M, Estrada M, Young JR. 2004**. Pigment diversity of coccolithophores in relation to taxonomy, phylogeny and ecological preferences. *Coccolithophores*: 51–73.

**Leonardos N, Read B, Thake B, Young JR. 2009**. NO MECHANISTIC DEPENDENCE OF PHOTOSYNTHESIS ON CALCIFICATION IN THE COCCOLITHOPHORID EMILIANIA HUXLEYI (HAPTOPHYTA)1. *Journal of Phycology* **45**: 1046–1051.

**Lewis E, Wallace D, Allison L. 1998**. Program developed for CO {sub 2} system calculations.

**Li Y, Tran Q, Shrestha R, Piao L, Park S, Park J, Park J. 2019**. LETM1 is required for mitochondrial homeostasis and cellular viability. *Molecular Medicine Reports* **19**: 3367.

**Liang M, Wang Z, Li H, Cai L, Pan J, He H, Wu Q, Tang Y, Ma J, Yang L. 2018**. l-Arginine induces antioxidant response to prevent oxidative stress via stimulation of glutathione synthesis and activation of Nrf2 pathway. *Food and Chemical Toxicology* **115**: 315–328.

**Lichtenthaler HK, Buschmann C, Knapp M. 2005**. How to correctly determine the different chlorophyll fluorescence parameters and the chlorophyll fluorescence decrease ratio R Fd of leaves with the PAM fluorometer. *PHOTOSYNTHETICA* **43**: 379–393.

**Lim YA, Khong NMH, Priyawardana SD, Ooi KR, Ilankoon IMSK, Chong MN, Foo SC. 2022**. Distinctive correlations between cell concentration and cell size to microalgae biomass under increasing carbon dioxide. *Bioresource Technology* **347**: 126733.

**Liu YW, Eagle RA, Aciego SM, Gilmore RE, Ries JB. 2018**. A coastal coccolithophore maintains pH homeostasis and switches carbon sources in response to ocean acidification. *Nature Communications* **9**.

**Liu YW, Rokitta SD, Rost B, Eagle RA. 2021**. Constraints on coccolithophores under ocean acidification obtained from boron and carbon geochemical approaches. *Geochimica et Cosmochimica Acta* **315**: 317–332.

**Lohbeck K, Riebesell U. 2012**. Adaptive evolution of a key phytoplankton species to ocean acidification. *Nature Geoscience*.

**Lohbeck KT, Riebesell U, Reusch TBH. 2012**. Adaptive evolution of a key phytoplankton species to ocean acidification. *Nature Geoscience* **5**: 346–351.

**Lohbeck KT, Riebesell U, Reusch TBH. 2014**. Gene expression changes in the coccolithophore Emiliania huxleyi after 500 generations of selection to ocean acidification. *Proceedings of the Royal Society B: Biological Sciences* **281**.

**Loschen G, Azzi A, Richter C, Flohé L. 1974**. Superoxide radicals as precursors of mitochondrial hydrogen peroxide. *FEBS Letters* **42**: 68–72.

**Lu J, Holmgren A. 2014**. The thioredoxin antioxidant system. *Free Radical Biology and Medicine* **66**: 75–87.

**Ma J, Wang W, Liu X, Wang Z, Gao G, Wu H, Li X, Xu J. 2020**. Zinc toxicity alters the photosynthetic response of red alga Pyropia yezoensis to ocean acidification. *Environmental Science and Pollution Research* **27**: 3202–3212.

**Mackey KRM, Morris JJ, Morel FMM, Kranz SA. 2015**. Response of photosynthesis to ocean acidification. *Oceanography* **28**: 74–91.

**Mackinder L, Wheeler G, Schroeder D, Riebesell U, Brownlee C. 2010**. Molecular mechanisms underlying calcification in coccolithophores. *Geomicrobiology Journal* **27**: 585–595.

**Manton I, Peterfi LS. 1969**. Observations on the tine structure of coccoliths, scales and the protoplast of a freshwater coccolithophorid, Hymenomonas roseola Stein, with supplementary observations on the protoplast of Cricosphaera carterae. *Proceedings of the Royal Society of London. Series B. Biological Sciences* **172**: 1–15.

**Marañón E. 2008**. Inter-specific scaling of phytoplankton production and cell size in the field. *Journal of Plankton Research* **30**: 157–163.

**Marcus F, Gontero B, Harrsch PB, Rittenhouse J. 1986**. Amino acid sequence homology among fructose-1,6-bisphosphatases. *Biochemical and Biophysical Research Communications* **135**: 374–381.

**Marsh ME. 1994**. *Polyanion-mediated mineralization-assembly and reorganization of acidic polysaccharides in the Golgi system of a coccolithophorid alga during mineral deposition*. Springer-Verlag.

**Marsh ME. 1996**. *PROI'ON.ASMA Polyanion-mediated mineralization-a kinetic analysis of the calcium-carrier hypothesis in the phytoflagellate Pleurochrysis carterae*.

**Marsh ME. 2003**. Regulation of CaCO3 formation in coccolithophores. *Comparative Biochemistry and Physiology - B Biochemistry and Molecular Biology* **136**: 743–754.

**Marsh ME, Chang DK, King GC. 1992**. Isolation and characterization of a novel acidic polysaccharide containing tartrate and glyoxylate residues from the mineralized scales of a unicellular coccolithophorid alga Pleurochrysis carterae. *Journal of Biological Chemistry* **267**: 20507–20512.

**Martin CL, Tortell PD. 2008**. Bicarbonate transport and extracellular carbonic anhydrase in marine diatoms. *Physiologia Plantarum* **133**: 106–116.

**Marzec B, Walker JM, Panagopoulou M, Jhons Y, Clare D, Wheeler A, Shaver MP, Nudelman F. 2019**. Three-dimensional architecture and surface functionality of coccolith base plates. *Journal of Structural Biology* **208**: 127–136.

**McCarthy A, Rogers SP, Duffy SJ, Campbell DA. 2012**. ELEVATED CARBON DIOXIDE DIFFERENTIALLY ALTERS THE PHOTOPHYSIOLOGY OF THALASSIOSIRA PSEUDONANA (BACILLARIOPHYCEAE) AND EMILIANIA HUXLEYI (HAPTOPHYTA)1. *Journal of Phycology* **48**: 635–646.

**McClelland HLO, Bruggeman J, Hermoso M, Rickaby REM. 2017**. The origin of carbon isotope vital effects in coccolith calcite. *Nature Communications 2017 8:1* **8**: 1–16.

**McConnaughey T. 1989a**. 13C and 18O isotopic disequilibrium in biological carbonates: I. Patterns. *Geochimica et Cosmochimica Acta* **53**: 151–162.

**McConnaughey T. 1989b**. 13C and 18O isotopic disequilibrium in biological carbonates: II. In vitro simulation of kinetic isotope effects. *Geochimica et Cosmochimica Acta* **53**: 163–171.

**McConnaughey TA. 2003**. Sub-equilibrium oxygen-18 and carbon-13 levels in biological carbonates: Carbonate and kinetic models. *Coral Reefs* **22**: 316–327.

**McCrea JM. 1950**. On the Isotopic Chemistry of Carbonates and a Paleotemperature Scale. *The Journal of Chemical Physics* **18**: 849–857.

**Mehrbach C, Culberson C, … JH-L and, 1973 undefined. 1973**. Measurement of the apparent dissociation constants of carbonic acid in seawater at atmospheric pressure 1. *Wiley Online Library* **18**: 897–907.

**Meyer J, Riebesell U. 2015**. Reviews and syntheses: Responses of coccolithophores to ocean acidification: A meta-analysis. *Biogeosciences* **12**: 1671–1682.

**Millo C, Dupraz S, Ader M, Guyot F, Thaler C, Foy E, Ménez B. 2012**. Carbon isotope fractionation during calcium carbonate precipitation induced by ureolytic bacteria. *Geochimica et Cosmochimica Acta* **98**: 107–124.

**Miyake C. 2020**. Molecular Mechanism of Oxidation of P700 and Suppression of ROS Production in Photosystem I in Response to Electron-Sink Limitations in C3 Plants. *Antioxidants* **9**.

**Monteiro FM, Bach LT, Brownlee C, Bown P, Rickaby REM, Poulton AJ, Tyrrell T, Beaufort L, Dutkiewicz S, Gibbs S, *et al.* 2016**. Why marine phytoplankton calcify. *Science Advances* **2**.

**Mook WG, Bommerson JC, Staverman WH. 1974**. Carbon isotope fractionation between dissolved bicarbonate and gaseous carbon dioxide. *Earth and Planetary Science Letters* **22**: 169–176.

**Moore TS, Dowell MD, Franz BA. 2012**. Detection of coccolithophore blooms in ocean color satellite imagery: A generalized approach for use with multiple sensors. *Remote Sensing of Environment* **117**: 249–263.

**Morabito G, Oggioni A, Caravati E, Panzani P. 2007**. Seasonal morphological plasticity of phytoplankton in Lago Maggiore (N. Italy). *Hydrobiologia* **578**: 47–57.

**Morel FMM, Rueter JG, Anderson DM, Guillard RRL. 1979**. AQUIL: A chemically defined phytoplankton culture medium for trace metal studies. *Journal of Phycology* **15**: 135–141.

**Moreno AR, Martiny AC. 2018**. Ecological stoichiometry of ocean plankton. *Annual Review of Marine Science* **10**: 43–69.

**Moutot Fran, Huet J, Morot-gaudry J, Pernollet J. 1986**. Relationship between Photosynthesis and Protein Synthesis in Maize I. KINETICS OF TRANSLOCATION OF THE PHOTOASSIMILATED CARBON FROM THE EAR LEAF TO THE SEED. *Plant Physiol* **80**: 211–215.

**Müller MN. 2019**. On the genesis and function of coccolithophore calcification. *Frontiers in Marine Science* **6**: 438482.

**Muramatsu M, Hihara Y. 2011**. Acclimation to high-light conditions in cyanobacteria: from gene expression to physiological responses. *Journal of Plant Research 2011 125:1* **125**: 11–39.

**Murata N, Takahashi S, Nishiyama Y, Allakhverdiev SI. 2007**. Photoinhibition of photosystem II under environmental stress. *Biochimica et Biophysica Acta (BBA) - Bioenergetics* **1767**: 414–421.

**Murphy J, Riley JP. 1962**. A modified single solution method for the determination of phosphate in natural waters. *Analytica Chimica Acta* **27**: 31–36.

**Nagao R, Yokono M, Ueno Y, Shen JR, Akimoto S. 2019**. PH-Sensing Machinery of Excitation Energy Transfer in Diatom PSI-FCPI Complexes. *Journal of Physical Chemistry Letters* **10**: 3531–3535.

**Nakao LS, Olson MF, Vázquez-Medina JP, Valdivia A. 2023**. Editorial: Reactive oxygen species (ROS) signaling during cytoskeleton dynamics. *Frontiers in Cell and Developmental Biology* **11**: 1295263.

**Nakata E, Nazumi Y, Yukimachi Y, Uto Y, Maezawa H, Hashimoto T, Okamoto Y, Hori H. 2011**. Synthesis and photophysical properties of new SNARF derivatives as dual emission pH sensors. *Bioorganic and Medicinal Chemistry Letters* **21**: 1663–1666.

**Nanninga HJ, Tyrrell T. 1996**. Importance of light for the formation of algal blooms by Emiliania huxleyi. *Marine Ecology Progress Series* **136**: 195–203.

**Nebert DW, Vasiliou V. 2004**. Analysis of the glutathione S-transferase (GST) gene family. *Human genomics* **1**: 460–464.

**Nicholls K, gesamten PD-IR der, 1978 undefined. 1978**. An evaluation of phosphorus-chlorophyll-phytoplankton relationships for lakes. *Wiley Online Library* **1**: 141.

**Nielsen M V. 1995**. Photosynthetic Characteristics of the Coccolithophorid Emiliania huxleyi (Prymnesiophyceae) exposed to elevated concentrations of dissolved inorganic carbon. *Journal of Phycology* **31**: 715–719.

**Nimer NA, Brownlee C, Merrett MJ. 1994a**. *Carbon dioxide availability, intracellular pH and growth rate of the coccolithophore Emiliania huxleyi*.

**Nimer NA, Guan Q, Merrett MJ. 1994b**. Extra- and intra-cellular carbonic anhydrase in relation to culture age in a high-calcifying strain of Emiliania huxleyi Lohmann. *New Phytologist* **126**: 601–607.

**Nimer NA, Iglesias-Rodriguez MD, Merrett MJ. 1997**. BICARBONATE UTILIZATION BY MARINE PHYTOPLANKTON SPECIES. *Journal of Phycology* **33**: 625–631.

**Nimer NA, Merrett MJ. 1992**. Calcification and utilization of inorganic carbon by the coccolithophorid Emiliania huxleyi Lohmann. *New Phytologist* **121**: 173–177.

**Nowicki M, DeVries T, Siegel DA. 2022**. Quantifying the Carbon Export and Sequestration Pathways of the Ocean's Biological Carbon Pump. *Global Biogeochemical Cycles* **36**: e2021GB007083.

**O'Leary MH. 1984**. Measurement of the isotope fractionation associated with diffusion of carbon dioxide in aqueous solution. *Journal of Physical Chemistry* **88**: 823–825.

**O'Leary BM, Asao S, Millar AH, Atkin OK. 2019**. Core principles which explain variation in respiration across biological scales. *New Phytologist* **222**: 670–686.

**O'Leary MH, Madhavan S, Paneth P. 1992**. Physical and chemical basis of carbon isotope fractionation in plants. *Plant, Cell & Environment* **15**: 1099–1104.

**Olson M, Wuori T, Love B, Marine SS. 2017**. Ocean acidification effects on haploid and diploid Emiliania huxleyi strains: Why changes in cell size matter. *Journal of Experimental Marine Biology and Ecology* **488**: 72–82.

**Ouellet C, Benson AA. 1952**. The Path of Carbon in Photosynthesis: XIII. pH EFFECTS IN C14O2 FIXATION BY SCENEDESMUS. *Journal of Experimental Botany* **3**: 237–245.

**Paasche E. 1964**. A tracer study of the inorganic carbon uptake during coccolith formation and photosynthesis in the coccolithophorid Coccolithus huxleyi. *Physiol Plant Suppl* **0**: 5–82.

**Paasche E. 2001**. A review of the coccolithophorid Emiliania huxleyi (Prymnesiophyceae), with particular reference to growth, coccolith formation, and calcification-photosynthesis interactions. *Phycologica* **40**: 503–529.

**Pagani M**. **2002**. The alkenone-CO2 proxy and ancient atmospheric carbon dioxide. *Philosophical Transactions of the Royal Society of London. Series A: Mathematical, Physical and Engineering Sciences* **360**: 609–632.

**Palenik B, Henson SE**. **1997**. The use of amides and other organic nitrogen sources by the phytoplankton Emiliania huxleyi. *Limnology and Oceanography* **42**: 1544–1551.

**Paleoceanography MH-, 2015 undefined**. **2015**. Control of ambient pH on growth and stable isotopes in phytoplanktonic calcifying algae. *Wiley Online Library* **30**: 1100–1112.

**Parente A, Cachão M, Baumann KH, de Abreu L, Ferreira J**. **2004**. Morphometry of Coccolithus pelagicus s.l. (Coccolithophore, Haptophyta) from offshore Portugal, during the last 200 kyr. *Micropaleontology* **50**: 107–120.

**Pedraza-González L, Cignoni E, D'Ascenzi J, Cupellini L, Mennucci B**. **2023**. How the pH Controls Photoprotection in the Light-Harvesting Complex of Mosses. *Journal of the American Chemical Society* **145**: 7482–7494.

**Peled-Zehavi H, Gal A**. **2021**. Exploring Intracellular Ion Pools in Coccolithophores Using Live-Cell Imaging. *Advanced Biology* **5**: 2000296.

**Petit JR, Jouzel J, Raynaud D, Barkov NI, Barnola JM, Basile I, Bender M, Chappellaz J, Davis M, Delaygue G, *et al.* 1999**. Climate and atmospheric history of the past 420,000 years from the Vostok ice core, Antarctica. *Nature 1999 399:6735* **399**: 429–436.

**Pienaar RN**. **1971**. Coccolith production in Hymenomonas carterae. *Protoplasma* **73**: 217–224.

**Pierrot D, Lewis E, Wallace DWR**. **2006**. MS Excel program developed for CO2 system calculations. ORNL/CDIAC-105a.

**Poulton AJ, Adey TR, Balch WM, Holligan PM**. **2007**. Relating coccolithophore calcification rates to phytoplankton community dynamics: Regional differences and implications for carbon export. *Deep Sea Research Part II: Topical Studies in Oceanography* **54**: 538–557.

**Price NM, Harrison GI, Hering JG, Hudson RJ, Nirel PM V., Palenik B, Morel FMM**. **1989**. Preparation and Chemistry of the Artificial Algal Culture Medium Aquil. *Biological Oceanography* **6**: 443–461.

**Probert I, Houdan A**. **2004**. The Laboratory Culture of Coccolithophores. *Coccolithophores*: 217–249.

**Qi F, Zhang F**. **2019**. Cell Cycle Regulation in the Plant Response to Stress. *Frontiers in Plant Science* **10**.

**Quinn P, Profile S, Sáez AG, Baumann K-H, Sprengel C, Wegener A**. **2004**. Coccolithophorid biodiversity: evidence from the cosmopolitan species Calcidiscus leptoporus. *SpringerPS Quinn, AG Sáez, KH Baumann, BA Steel, C Sprengel, LK MedlinCoccolithophores: from molecular processes to global impact, 2004 · Springer*: 299–326.

**Raimbault P, Diaz F, Pouvesle W, Boudjellal B**. **1999**. Simultaneous determination of particulate organic carbon, nitrogen and phosphorus collected on filters, using a semi-automatic wet-oxidation method. *Marine Ecology Progress Series* **180**: 289–295.

**Rau GH, Riebesell U, Wolf-Gladrow D**. **1996**. A model of photosynthetic 13C fractionation by marine phytoplankton based on diffusive molecular CO2 uptake. *Marine Ecology Progress Series* **133**: 275–285.

**Raven JA**. **1984**. A COST-BENEFIT ANALYSIS OF PHOTON ABSORPTION BY PHOTOSYNTHETIC UNICELLS. *New Phytologist* **98**: 593–625.

**Raven JA**. **1997**. CO2-concentrating mechanisms: a direct role for thylakoid lumen acidification? *Plant, Cell & Environment* **20**: 147–154.

**Raven JA, Crawfurd K**. **2012**. Environmental controls on coccolithophore calcification. *Marine Ecology Progress Series* **470**: 137–166.

**Ray PD, Huang BW, Tsuji Y**. **2012**. Reactive oxygen species (ROS) homeostasis and redox regulation in cellular signaling. *Cellular signalling* **24**: 981.

**Read BA, Kegel J, Klute MJ, Kuo A, Lefebvre SC, Maumus F, Mayer C, Miller J, Monier A, Salamov A, *et al.* 2013**. Pan genome of the phytoplankton Emiliania underpins its global distribution. *Nature* **499**: 209–213.

**Reichheld JP, Vernoux T, Lardon F, Van Montagu M, Inzé D**. **1999**. Specific checkpoints regulate plant cell cycle progression in response to oxidative stress. *The Plant Journal* **17**: 647–656.

**Reinfelder JR**. **2010**. Carbon Concentrating Mechanisms in Eukaryotic Marine Phytoplankton. *Annual Review of Marine Science* **3**: 291–315.

**Relvas P, Barton ED, Dubert J, Oliveira PB, Peliz Á, da Silva JCB, Santos AMP**. **2007**. Physical oceanography of the western Iberia ecosystem: Latest views and challenges. *Progress in Oceanography* **74**: 149–173.

**Richier S, Fiorini S, Kerros ME, von Dassow P, Gattuso JP**. **2011**. Response of the calcifying coccolithophore Emiliania huxleyi to low pH/high pCO2: From physiology to molecular level. *Marine Biology* **158**: 551–560.

**Rickaby R, Henderiks J, Past JY-C of the, 2010 undefined**. **2010**. Perturbing phytoplankton: response and isotopic fractionation with changing carbonate chemistry in two coccolithophore species. *cp.copernicus.org* **6**: 771–785.

**Rickaby REM, Hermoso M, Lee RBY, Rae BD, Heureux AMC, Balestreri C, Chakravarti L, Schroeder DC, Brownlee C**. **2016**. Environmental carbonate chemistry selects for phenotype of recently isolated strains of Emiliania huxleyi. *Deep Sea Research Part II: Topical Studies in Oceanography* **127**: 28–40.

**Ridgwell A**. **2005**. A Mid Mesozoic Revolution in the regulation of ocean chemistry. *Marine Geology* **217**: 339–357.

**Ridgwell A, Zeebe RE**. **2005**. The role of the global carbonate cycle in the regulation and evolution of the Earth system. *Earth and Planetary Science Letters* **234**: 299–315.

**Riebesell U, Bellerby RGJ, Engel A, Fabry VJ, Hutchins DA, Reusch TBH, Schulz KG, Morel FMM**. **2008**. Comment on 'Phytoplankton calcification in a high-CO2 world'. *Science* **322**.

**Riebesell U, Zondervan I, Rost B, Tortell PD, Zeebe RE, Morel FMM**. **2000**. Reduced calcification of marine plankton in response to increased atmospheric CO2. *Nature 2000 407:6802* **407**: 364–367.

**Riegman R, Stolte W, … AN-J of, 2000 undefined**. **2000a**. Nutrient uptake and alkaline phosphatase (ec 3:1:3:1) activity of emiliania huxleyi (PRYMNESIOPHYCEAE) during growth under n and p limitation in continuous. *Wiley Online Library* **36**: 87–96.

**Ries JB**. **2011**. A physicochemical framework for interpreting the biological calcification response to CO2-induced ocean acidification. *Geochimica et Cosmochimica Acta* **75**: 4053–4064.

**Rikhvanov EG, Fedoseeva I V., Pyatrikas D V., Borovskii GB, Voinikov VK**. **2014**. Role of mitochondria in the operation of calcium signaling system in heat-stressed plants. *Russian Journal of Plant Physiology* **61**: 141–153.

**RIS H, PLAUT W**. **1962**. ULTRASTRUCTURE OF DNA-CONTAINING AREAS IN THE CHLOROPLAST OF CHLAMYDOMONAS. *The Journal of Cell Biology* **13**: 383.

**Ritchie RJ**. **2006**. Consistent sets of spectrophotometric chlorophyll equations for acetone, methanol and ethanol solvents. *Photosynthesis Research* **89**: 27–41.

**Rokitta SD, John U, Rost B. 2012a**. Ocean Acidification Affects Redox-Balance and Ion-Homeostasis in the Life-Cycle Stages of Emiliania huxleyi. *PLOS ONE* **7**: e52212.

**Rokitta SD, Rost B. 2012a**. Effects of CO 2 and their modulation by light in the life-cycle stages of the coccolithophore Emiliania huxleyi. *Limnology and Oceanography* **57**: 607–618.

**Rokitta SD, Rost B. 2012b**. Effects of CO2 and their modulation by light in the life-cycle stages of the coccolithophore Emiliania huxleyi. *Limnology and Oceanography* **57**: 607–618.

**Romanek CS, Grossman EL, Morse JW. 1992**. Carbon isotopic fractionation in synthetic aragonite and calcite: Effects of temperature and precipitation rate. *Geochimica et Cosmochimica Acta* **56**: 419–430.

**Rost B, Riebesell U. 2004a**. Coccolithophores and the biological pump: responses to environmental changes. *Coccolithophores*: 99–125.

**Rost B, Riebesell U, Burkhardt S, Sültemeyer D. 2003**. Carbon acquisition of bloom-forming marine phytoplankton. *Limnology and Oceanography* **48**: 55–67.

**Rost B, Riebesell U, Sültemeyer D. 2006**. Carbon acquisition of marine phytoplankton: Effect of photoperiod length. *Limnology and Oceanography* **51**: 12–20.

**Rost B, Zondervan I, Riebesell U. 2002**. Light-dependent carbon isotope fractionation in the coccolithophorid Emiliania huxleyi. *Limnology and Oceanography* **47**: 120–128.

**Sáez AG, Engel H, Medlin LK, Huss VAR. 2001**. Plastid genome size and heterogeneous base composition of nuclear DNA from Ochrosphaera neapolitana (Prymnesiophyta). *Phycologia* **40**: 147–152.

**Sakurada S, Fujiwara S, Suzuki M, Kogure T, Uchida T, Umemura T, Tsuzuki M. 2018**. Involvement of Acidic Polysaccharide Ph-PS-2 and Protein in Initiation of Coccolith Mineralization, as Demonstrated by In Vitro Calcification on the Base Plate. *Marine Biotechnology* **20**: 304–312.

**Salbreux G, Charras G, Paluch E. 2012**. Actin cortex mechanics and cellular morphogenesis. *Trends in Cell Biology* **22**: 536–545.

**Sas KN, Haldrup A, Hemmingsen L, Danielsen E, Øgendal LH. 2006**. pH-dependent structural change of reduced spinach plastocyanin studied by perturbed angular correlation of γ-rays and dynamic light scattering. *Journal of Biological Inorganic Chemistry* **11**: 409–418.

**Schauble EA. 2004**. Applying Stable Isotope Fractionation Theory to New Systems. *Reviews in Mineralogy and Geochemistry* **55**: 65–111.

**Schlüter L, Lohbeck K, … MG-NC, 2014 undefined. 2014**. Adaptation of a globally important coccolithophore to ocean warming and acidification. *Nature Climate*.

**Schlüter L, Lohbeck KT, Gröger JP, Riebesell U, Reusch TBH. 2016**. Long-term dynamics of adaptive evolution in a globally important phytoplankton species to ocean acidification. *Science Advances* **2**.

**Schroer TA. 2004**. DYNACTIN. *Annual Review of Cell and Developmental Biology* **20**: 759–779.

**Sciandra A, Harlay J, Lefèvre D, Lemée R, Rimmelin P, Denis M, Gattuso JP. 2003**. Response of coccolithophorid Emiliania huxleyi to elevated partial pressure of CO2 under nitrogen limitation. *Marine Ecology Progress Series* **261**: 111–122.

**Seidel T, Scholl S, Krebs M, Rienmüller F, Marten I, Hedrich R, Hanitzsch M, Janetzki P, Dietz KJ, Schumacher K. 2012**. Regulation of the V-type ATPase by redox modulation. *The Biochemical journal* **448**: 243–251.

**Sekino K, Shiraiwa Y. 1994**. Accumulation and Utilization of Dissolved Inorganic Carbon by a Marine Unicellular Coccolithophorid, Emiliania huxleyi. *Plant and Cell Physiology* **35**: 353–361.

**Sekino K, Shiraiwa Y. 1996**. Evidence for the Involvement of Mitochondrial Respiration in Calcification in a Marine Coccolithophorid, Emiliania huxleyi. *Plant and Cell Physiology* **37**: 1030–1033.

**Sena LA, Chandel NS. 2012**. Physiological Roles of Mitochondrial Reactive Oxygen Species. *Molecular Cell* **48**: 158–167.

**SenGupta D. 2013**. RNA-Binding Domains in Proteins. *Brenner's Encyclopedia of Genetics: Second Edition*: 274–276.

**Sett S, Bach LT, Schulz KG, Koch-Klavsen S, Lebrato M, Riebesell U. 2014**. Temperature modulates coccolithophorid sensitivity of growth, photosynthesis and calcification to increasing seawater pCO2. *PLoS ONE* **9**.

**Shetye S, Gazi S, Manglavil A, Shenoy D, Kurian S, Pratihary A, Shirodkar G, Mohan R, Dias A, Naik H, *et al.* 2023**. Malformation in coccolithophores in low pH waters: evidences from the eastern Arabian Sea. *Environmental Science and Pollution Research* **30**: 42351–42366.

**Sheward RM. 2022**. Cycling carbon with coccolithophores. *Nature Geoscience 2022 15:10* **15**: 758–759.

**Sheward RM, Liefer JD, Irwin AJ, Finkel Z V. 2023**. Elemental stoichiometry of the key calcifying marine phytoplankton Emiliania huxleyi under ocean climate change: A meta-analysis. *Global Change Biology* **29**: 4259–4278.

**Sheyn U, Rosenwasser S, Ben-Dor S, Porat Z, Vardi A. 2016**. Modulation of host ROS metabolism is essential for viral infection of a bloom-forming coccolithophore in the ocean. *The ISME Journal 2016 10:7* **10**: 1742–1754.

**Shi D, Xu Y, More FMM. 2009**. Effects of the pH/pCO2 control method on medium chemistry and phytoplankton growth. *Biogeosciences* **6**: 1199–1207.

**Shuler ML. 1992**. Bioprocess engineering. *Prentice-Hall*: 412–420.

**Sikes CS, Roer RD, Wilbur KM. 1980**. Photosynthesis and coccolith formation: Inorganic carbon sources and net inorganic reaction of deposition1. *Limnology and Oceanography* **25**: 248–261.

**Sikes CS, Wheeler AP. 1982**. CARBONIC ANHYDRASE AND CARBON FIXATION IN COCCOLITHOPHORIDS1. *Journal of Phycology* **18**: 423–426.

**Silkin VA, Pautova LA, Pakhomova S V., Lifanchuk A V., Yakushev E V., Chasovnikov VK. 2014**. Environmental control on phytoplankton community structure in the NE Black Sea. *Journal of Experimental Marine Biology and Ecology* **461**: 267–274.

**Singh S, Brocker C, Koppaka V, Chen Y, Jackson BC, Matsumoto A, Thompson DC, Vasiliou V. 2013**. Aldehyde dehydrogenases in cellular responses to oxidative/electrophilic stress. *Free radical biology & medicine* **56**: 89–101.

**Skeffington A, Fischer A, Sviben S, Brzezinka M, Górka M, Bertinetti L, Woehle C, Huettel B, Graf A, Scheffel A. 2023**. A joint proteomic and genomic investigation provides insights into the mechanism of calcification in coccolithophores. *Nature Communications 2023 14:1* **14**: 1–15.

**Smith FA, Reid RJ. 1991**. Biophysical and Biochemical Regulation of Cytoplasmic pH in Chara corallina during Acid Loads. *Journal of Experimental Botany* **42**: 173–182.

**Spero HJ, Bijma J, Lea DW, Bernis BE. 1997**. Effect of seawater carbonate concentration on foraminiferal carbon and oxygen isotopes. *Nature 1997 390:6659* **390**: 497–500.

**Spinelli JB, Haigis MC. 2018**. The multifaceted contributions of mitochondria to cellular metabolism. *Nature Cell Biology 2018 20:7* **20**: 745–754.

**Steinacher M, Joos F, Frölicher TL, Bopp L, Cadule P, Cocco V, Doney SC, Gehlen M, Lindsay K, Moore JK, *et al.* 2010**. Projected 21st century decrease in marine productivity: A multi-model analysis. *Biogeosciences* **7**: 979–1005.

**Sterner RW, Elser JJ. 2003**. Ecological Stoichiometry. *Ecological Stoichiometry*.

**Stojkovic S, Beardall J, Matear R. 2013**. CO2-concentrating mechanisms in three southern hemisphere strains of Emiliania huxleyi. *Journal of Phycology* **49**: 670–679.

**Stoll HM, Guitian J, Hernandez-Almeida I, Mejia LM, Phelps S, Polissar P, Rosenthal Y, Zhang H, Ziveri P. 2019**. Upregulation of phytoplankton carbon concentrating mechanisms during low CO2 glacial periods and implications for the phytoplankton pCO2 proxy. *Quaternary Science Reviews* **208**: 1–20.

**Suffrian K, Schulz KG, Gutowska MA, Riebesell U, Bleich M. 2011a**. Cellular pH measurements in Emiliania huxleyi reveal pronounced membrane proton permeability. *New Phytologist* **190**: 595–608.

**Suffrian K, Schulz KG, Gutowska MA, Riebesell U, Bleich M. 2011b**. Cellular pH measurements in Emiliania huxleyi reveal pronounced membrane proton permeability. *New Phytologist* **190**: 595–608.

**Suggett DJ, Le Floc'H E, Harris GN, Leonardos N, Geider RJ. 2007**. Different strategies of photoacclimation by two strains of Emiliania huxleyi (Haptophyta)1. *Journal of Phycology* **43**: 1209–1222.

**Sugiyama T, Murao N, Kadowaki H, Takao K, Miyakawa T, Matsushita Y, Katagiri T, Futatsugi A, Shinmyo Y, Kawasaki H, *et al.* 2021**. ERAD components Derlin-1 and Derlin-2 are essential for postnatal brain development and motor function. *iScience* **24**: 102758.

**Sviben S, Gal A, Hood M, Bertinetti L, Y Politi. 2016**. A vacuole-like compartment concentrates a disordered calcium phase in a key coccolithophorid alga. *Nature*.

**Takahashi S, Murata N. 2008**. How do environmental stresses accelerate photoinhibition? *Trends in Plant Science* **13**: 178–182.

**Tanhua T, Bates NR, Körtzinger A. 2013**. The Marine Carbon Cycle and Ocean Carbon Inventories. *International Geophysics* **103**: 787–815.

**Taylor AR, Brownlee C, Wheeler G. 2017**. Coccolithophore Cell Biology: Chalking Up Progress. *https://doi.org/10.1146/annurev-marine-122414-034032* **9**: 283–310.

**Taylor AR, Chrachri A, Wheeler G, Goddard H, Brownlee C. 2011**. A voltage-gated H+ channel underlying pH homeostasis in calcifying Coccolithophores. *PLoS Biology* **9**.

**Tcherkez GGB, Farquhar GD, Andrews TJ. 2006**. Despite slow catalysis and confused substrate specificity, all ribulose bisphosphate carboxylases may be nearly perfectly optimized. *Proceedings of the National Academy of Sciences of the United States of America* **103**: 7246–7251.

**Tchernov D, Gruber DF, Irwin A. 2014**. Isotopic fractionation of carbon in the coccolithophorid Emiliania huxleyi. *Marine Ecology Progress Series* **508**: 53–66.

**Tchernov D, Helman Y, Keren N, Luz B, Ohad I, Reinhold L, Ogawa T, Kaplan A. 2001**. Passive Entry of CO2 and Its Energy-dependent Intracellular Conversion to HCO3- in Cyanobacteria Are Driven by a Photosystem I-generated ΔμH+. *Journal of Biological Chemistry* **276**: 23450–23455.

**Terrats L, Claustre H, Briggs N, Poteau A, Briat B, Lacour L, Ricour F, Mangin A, Neukermans G. 2023**. BioGeoChemical-Argo Floats Reveal Stark Latitudinal Gradient in the Southern Ocean Deep Carbon Flux Driven by Phytoplankton Community Composition. *Global Biogeochemical Cycles* **37**: e2022GB007624.

**Thangaraj S, Liu H, Guo Y, Ding C, Kim IN, Sun J. 2023**. Transitional traits determine the acclimation characteristics of the coccolithophore Chrysotila dentata to ocean warming and acidification. *Environmental Microbiology* **25**: 1099–1117.

**Thiagarajan N, Adkins J, Eiler J. 2011**. Carbonate clumped isotope thermometry of deep-sea corals and implications for vital effects. *Geochimica et Cosmochimica Acta* **75**: 4416–4425.

**Thierstein HR, Geitzenauer KR, Molfino B, Shackleton NJ. 1977**. Global synchroneity of late Quaternary coccolith datum levels Validation by oxygen isotopes. *Geology* **5**: 400–404.

**Thomas H, Prowe AEF, van Heuven S, Bozec Y, de Baar HJW, Schiettecatte LS, Suykens K, Koné M, Borges A V., Lima ID, *et al.* 2007**. Rapid decline of the CO2 buffering capacity in the North Sea and implications for the North Atlantic Ocean. *Global Biogeochemical Cycles* **21**: 4001.

**Thomasen H, Heldal M, Ostergaard J. 2015**. Coccolithophores in Polar Waters: Papposphaera arctica HET and HOL revisited. *Micropaleontology* **61**: 419–427.

**Tillmann U. 1998**. Phagotrophy by a plastidic haptophyte, Prymnesium patelliferum. *Aquatic Microbial Ecology* **14**: 155–160.

**Toennies G, Gallant D. 1949**. The relation between photometric turbidity and bacterial concentration. *Growth* **13**: 7–20.

**Tomanek L. 2010**. Environmental Proteomics: Changes in the Proteome of Marine Organisms in Response to Environmental Stress, Pollutants, Infection, Symbiosis, and Development. *https://doi.org/10.1146/annurev-marine-120709-142729* **3**: 373–399.

**Tong S, Gao K, Biology DH-GC, 2018 undefined. 2018**. Adaptive evolution in the coccolithophore Gephyrocapsa oceanica following 1,000 generations of selection under elevated CO2. *Wiley Online Library* **24**: 3055–3064.

**Tortell PD. 2000**. Evolutionary and ecological perspectives on carbon acquisition in phytoplankton. *Limnology and Oceanography* **45**: 744–750.

**Trimborn S, Langer G, Rost B. 2007**. Effect of varying calcium concentrations and light intensities on calcification and photosynthesis in Emiliania huxleyi. *Limnology and Oceanography* **52**: 2285–2293.

**Trimborn S, Wolf-Gladrow D, Richter KU, Rost B. 2009**. The effect of pCO2 on carbon acquisition and intracellular assimilation in four marine diatoms. *Journal of Experimental Marine Biology and Ecology* **376**: 26–36.

**Trinh MDL, Masuda S. 2022**. Chloroplast pH Homeostasis for the Regulation of Photosynthesis. *Frontiers in Plant Science* **13**: 919896.

**Trotter J, Montagna P, McCulloch M, Silenzi S, Reynaud S, Mortimer G, Martin S, Ferrier-Pagès C, Gattuso JP, Rodolfo-Metalpa R. 2011**. Quantifying the pH 'vital effect' in the temperate zooxanthellate coral Cladocora caespitosa: Validation of the boron seawater pH proxy. *Earth and Planetary Science Letters* **303**: 163–173.

**Tyrrell T, Merico A. 2004**. Emiliania huxleyi: bloom observations and the conditions that induce them. *Coccolithophores*: 75–97.

**Tyrrell T, Schneider B, Charalampopoulou A, Riebesell U. 2008**. Coccolithophores and calcite saturation state in the Baltic and Black Seas. *Biogeosciences* **5**: 485–494.

**Tyrrell T, Young JR. 2009**. Coccolithophores. *Encyclopedia of Ocean Sciences*: 606–614.

**Uchikawa J, Zeebe RE. 2012**. The effect of carbonic anhydrase on the kinetics and equilibrium of the oxygen isotope exchange in the CO2–H2O system: Implications for δ18O vital effects in biogenic carbonates. *Geochimica et Cosmochimica Acta* **95**: 15–34.

**Ui M. 1966**. A role of phosphofructokinase in pH-dependent regulation of glycolysis. *Biochimica et Biophysica Acta (BBA) - General Subjects* **124**: 310–322.

**Urey H. 1947**. The thermodynamic properties of isotopic substances. *Journal of the Chemical Society*: 562–581.

**Vázquez V, León P, Gordillo FJL, Jiménez C, Concepción I, Mackenzie K, Bresnan E, Segovia M. 2023**. High-CO2 Levels Rather than Acidification Restrict Emiliania huxleyi Growth and Performance. *Microbial Ecology* **86**: 127–143.

**Venn A, Tambutté E, Holcomb M, Allemand D, Tambutté S. 2011**. Live Tissue Imaging Shows Reef Corals Elevate pH under Their Calcifying Tissue Relative to Seawater. *PLOS ONE* **6**: e20013.

**Vohwinkel CU, Lecuona E, Sun H, Sommer N, Vadász I, Chandel NS, Sznajder JI. 2011**. Elevated CO 2 Levels Cause Mitochondrial Dysfunction and Impair Cell Proliferation * □ S. *Journal of Biological Chemistry* **286**: 37067–37076.

**De Vries J, Monteiro F, Wheeler G, Poulton A, Godrijan J, Cerino F, Malinverno E, Langer G, Brownlee C. 2021**. Haplo-diplontic life cycle expands coccolithophore niche. *Biogeosciences* **18**: 1161–1184.

**Wakatsuki T, Schwab B, Thompson NC, Elson EL. 2001**. Effects of cytochalasin D and latrunculin B on mechanical properties of cells. *Journal of Cell Science* **114**: 1025–1036.

**van der Wal P, de Jong EW, Westbroek P, de Bruijn WC, Mulder-Stapel AA. 1983**. Polysaccharide localization, coccolith formation, and golgi dynamics in the coccolithophorid Hymenomonas carterae. *Journal of Ultrastructure Research* **85**: 139–158.

**van der Wal P, Leunissen-Bijvelt JJM, Verkleij AJ. 1985**. Ultrastructure of the membranous layers enveloping the cell of the coccolithophoridEmiliania huxleyi. *Journal of Ultrastructure Research* **91**: 24–29.

**Walker JM, Marzec B, Ozaki N, Clare D, Nudelman F. 2020**. Morphological development of Pleurochrysis carterae coccoliths examined by cryo-electron tomography. *Journal of Structural Biology* **210**: 107476.

**Walker CE, Taylor AR, Langer G, Durak GM, Heath S, Probert I, Tyrrell T, Brownlee C, Wheeler GL. 2018**. The requirement for calcification differs between ecologically important coccolithophore species. *New Phytologist* **220**: 147–162.

**Wang GF, Dong Q, Bai Y, Yuan J, Xu Q, Cao C, Liu X. 2017**. Oxidative stress induces mitotic arrest by inhibiting Aurora A-involved mitotic spindle formation. *Free Radical Biology and Medicine* **103**: 177–187.

**Wang J, Hua H, Ran Y, Zhang H, Liu W, Yang Z, Jiang Y. 2008**. Derlin-1 is overexpressed in human breast carcinoma and protects cancer cells from endoplasmic reticulum stress-induced apoptosis. *Breast Cancer Research : BCR* **10**: R7.

**Wanner P, Hunkeler D. 2019**. Isotope fractionation due to aqueous phase diffusion – What do diffusion models and experiments tell? – A review. *Chemosphere* **219**: 1032–1043.

**Warren CR. 2008**. Rapid Measurement of Chlorophylls with a Microplate Reader. *Journal of Plant Nutrition* **31**: 1321–1332.

**Watkins JM, Nielsen LC, Ryerson FJ, DePaolo DJ. 2013**. The influence of kinetics on the oxygen isotope composition of calcium carbonate. *Earth and Planetary Science Letters* **375**: 349–360.

**Werdan K, Heldt HW, Milovancev M. 1975**. The role of pH in the regulation of carbon fixation in the chloroplast stroma. Studies on CO2 fixation in the light and dark. *Biochimica et Biophysica Acta (BBA) - Bioenergetics* **396**: 276–292.

**Westberry T, Behrenfeld MJ, Siegel DA, Boss E. 2008**. Carbon-based primary productivity modeling with vertically resolved photoacclimation. *Global Biogeochemical Cycles* **22**: 2024.

**Westbroek P, Brown CW, Bleijswijk J van, Brownlee C, Brummer GJ, Conte M, Egge J, Fernández E, Jordan R, Knappertsbusch M, *et al.* 1993**. A model system approach to biological climate forcing. The example of Emiliania huxleyi. *Global and Planetary Change* **8**: 27–46.

**Whatley JM, Whatley FR. 1981**. Chloroplast Evolution. *New Phytologist* **87**: 233–247.

**Wheeler GL, Sturm D, Langer G. 2023**. Gephyrocapsa huxleyi (Emiliania huxleyi) as a model system for coccolithophore biology. *Journal of Phycology* **59**: 1123–1129.

**White MM, Drapeau DT, Lubelczyk LC, Abel VC, Bowler BC, Balch WM. 2018**. Calcification of an estuarine coccolithophore increases with ocean acidification when subjected to diurnally fluctuating carbonate chemistry. *Marine Ecology Progress Series* **601**: 59–76.

**Whitten ST, García-Moreno E. B, Hilser VJ. 2005**. Local conformational fluctuations can modulate the coupling between proton binding and global structural transitions in proteins. *Proceedings of the National Academy of Sciences* **102**: 4282–4287.

**Wilkes EB, Lee RBY, McClelland HLO, Rickaby REM, Pearson A. 2018**. Carbon isotope ratios of coccolith–associated polysaccharides of Emiliania huxleyi as a function of growth rate and CO2 concentration. *Organic Geochemistry* **119**: 1–10.

**Winter A, Henderiks J, Beaufort L, Rickaby REM, Brown CW. 2014**. Poleward expansion of the coccolithophore Emiliania huxleyi. *Journal of Plankton Research* **36**: 316–325.

**Wu F, Guo J, Duan H, Li T, Wang Y, Wang Y, Wang S, Feng Y. 2023**. Ocean Acidification Affects the Response of the Coastal Coccolithophore Pleurochrysis carterae to Irradiance. *Biology* **12**: 1249.

**Wurtmann EJ, Wolin SL. 2009**. RNA under attack: Cellular handling of RNA damage. *Critical Reviews in Biochemistry and Molecular Biology* **44**: 34–49.

**Xie Y, Chen L, Sun T, Jiang J, Tian L, Cui J, Zhang W. 2021**. A transporter Slr1512 involved in bicarbonate and pH-dependent acclimation mechanism to high light stress in Synechocystis sp. PCC 6803. *Biochimica et Biophysica Acta (BBA) - Bioenergetics* **1862**: 148336.

**Yan LL, Zaher HS. 2019**. How do cells cope with RNA damage and its consequences? *Journal of Biological Chemistry* **294**: 15158–15171.

**Yang TN, Wei KY, Chen M pen, Ji SJ, Gong GC, Lin FJ, Lee TQ. 2004**. Summer and winter distribution and malformation of coccolithophores in the East China Sea. *Micropaleontology* **50**: 157–170.

**Young JR. 1998**. Neogene. In: Bown PR, ed. Calcareous nannofosssil biostrarigraphy. British Micropalaeontological Society Publication Series, 225–265.

**Young JR, Davis SA, Bown PR, Mann S. 1999**. Coccolith Ultrastructure and Biomineralisation. *Journal of Structural Biology* **126**: 195–215.

**Yu EPK, Reinhold J, Yu H, Starks L, Uryga AK, Foote K, Finigan A, Figg N, Pung YF, Logan A, *et al.* 2017**. Mitochondrial Respiration Is Reduced in Atherosclerosis, Promoting Necrotic Core Formation and Reducing Relative Fibrous Cap Thickness. *Arteriosclerosis, thrombosis, and vascular biology* **37**: 2322–2332.

**Zeebe RE. 1999**. An explanation of the effect of seawater carbonate concentration on foraminiferal oxygen isotopes. *Geochimica et Cosmochimica Acta* **63**: 2001–2007.

**Zeebe RE, Wolf-Gladrow DA. 2001**. *CO2 in seawater: equilibrium, kinetics, isotopes*. Oceanography, Elsevier.

**Zhang Q, Bendif EM, Zhou Y, Nevado B, Shafiee R, Rickaby REM. 2022**. Declining metal availability in the Mesozoic seawater reflected in phytoplankton succession. *Nature Geoscience 2022 15:11* **15**: 932–941.

**Zhang H, Blanco-Ameijeiras S, Hopkinson BM, Bernasconi SM, Mejia LM, Liu C, Stoll H. 2021a**. An isotope label method for empirical detection of carbonic anhydrase in the calcification pathway of the coccolithophore Emiliania huxleyi. *Geochimica et Cosmochimica Acta* **292**: 78–93.

**Zhang Y, Gao K. 2021**. Photosynthesis and calcification of the coccolithophore Emiliania huxleyi are more sensitive to changed levels of light and CO2 under nutrient limitation. *Journal of Photochemistry and Photobiology B: Biology* **217**.

**Zhang L, Li M, Chan AK, Liu Q, Kang H, Pokharel SP, Mattson N, Singh P, Yang L, Chen C-WD. 2023**. COX4I1 Controls Mitochondrial Electron Transport Chain Complex IV Assembly and Leukemia Progression in Acute Myeloid Leukemia. *Blood* **142**: 581–581.

**Zhang Y, Li Z, Schulz KG, Hu Y, Irwin AJ, Finkel Z V. 2021b**. Growth-dependent changes in elemental stoichiometry and macromolecular allocation in the coccolithophore Emiliania huxleyi under different environmental conditions. *Limnology and Oceanography* **66**: 2999–3009.

**Zhang H, Stoll H, Bolton C, Jin X, Liu C. 2018**. Technical note: A refinement of coccolith separation methods: Measuring the sinking characteristics of coccoliths. *Biogeosciences* **15**: 4759–4775.

**Zhou C, Luo J, Ye Y, Yan X, Liu B, Wen X. 2016**. The metabolite profiling of coastal coccolithophorid species Pleurochrysis carterae (Haptophyta). *Chinese Journal of Oceanology and Limnology* **34**: 749–756.

**Ziveri P, Passaro M, Incarbona A, Milazzo M, Rodolfo-Metalpa R, Hall-Spencer JM. 2014**. Decline in coccolithophore diversity and impact on coccolith morphogenesis along a natural CO2 gradient. *Biological Bulletin* **226**: 282–290.

**Ziveri P, Stoll H, Probert I, Klaas C, Geisen M, Ganssen G, Young J. 2003**. Stable isotope 'vital effects' in coccolith calcite. *Earth and Planetary Science Letters* **210**: 137–149.

**Ziveri P, Thoms S, Probert I, Geisen M, Langer G. 2012**. A universal carbonate ion effect on stable oxygen isotope ratios in unicellular planktonic calcifying organisms. *Biogeosciences* **9**: 1025–1032.

**Zondervan I, Rost B, Riebesell U. 2002**. Effect of CO2 concentration on the PIC/POC ratio in the coccolithophore Emiliania huxleyi grown under light-limiting conditions and different daylengths. *Journal of Experimental Marine Biology and Ecology* **272**: 55–70.

**Zou D. 2005**. Effects of elevated atmospheric CO2 on growth, photosynthesis and nitrogen metabolism in the economic brown seaweed, Hizikia fusiforme (Sargassaceae, Phaeophyta). *Aquaculture* **250**: 726–735.